Internal frost damage in concrete - experimental studies of destruction mechanisms

Fridh, Katja

2005

LUND INSTITUTE OF TECHNOLOGY
LUND UNIVERSITY

Division of Building Materials

INTERNAL FROST DAMAGE IN CONCRETE

Experimental studies of destruction mechanisms

Katja Fridh

Report TVBM-1023 Doctoral thesis

Lund 2005

ISRN LUTVDG/TVBM--05/1023--SE(1-276)
ISSN 0348-7911 TVBM
ISBN 91-628-6558-7

Lund Institute of Technology
Division of Building Materials
Box 118
SE-221 00 Lund, Sweden

Telephone: 46-46-2227415
Telefax: 46-46-2224427
www.byggnadsmaterial.lth.se

Preface

The work presented here was carried out at the Division of Building Materials at the Lund Institute of Technology. It was financed by Cementa AB and the Swedish Agency for Innovation Systems (Vinnova) as a part of the research consortium Road /Bridge/Tunnel. The support received is gratefully acknowledged. Being part of this large research group, which provided opportunities to meet with representatives of the building industry and with PhD students from all parts of Sweden on regular basis, was highly stimulating.

I would like to express my gratitude to my supervisor Professor Göran Fagerlund who initiated the project and introduced me to the fascinating topic of ice in concrete and for his effort during finalisation of this thesis.

I would also like to thank my assistant supervisor Dr. Björn Johannesson for introducing to me the world of thermodynamics and for valuable discussions we had concerning science and the evaluation of measurements.

Dr. Lars Wadsö provided great inspiration through the passion he showed for calorimetry and applied science and sharing it with me.

Many thanks to Dr. Sture Lindmark for his support and encouragement and the valuable discussions we had at the beginning of the project.

I would also like to thank my friend and colleague Peter Utgenannt for his support and encouragement and for the discussions we have had throughout the project.

To the boys in the laboratory, Bosse, Ingemar, Bengt och Stefan - without you, this day would have been a reality only in some distant future. Thank you for your patience and your good spirits.

My sincere gratitude to all my colleges at the Division of Building Materials for being able to share with you all the very enjoyable and the less enjoyable episodes of my life during my time at the Division, especially since you never had the choice not to…..

I would like to thank my dad and granddad for introducing me to the world of buildings and I hope you forgive me for approaching it theoretically.

To all the intelligent and strong women in my life, especially Mum, Rita, Cecilia, Eva-Lena, Vicky, Ullis, Gunilla, Ulrika, Åse and Kaisa, each for inspiring me in your own very special way.

Finally, my deepest gratitude to my family, my parents for always encouraging me to be the best I could ever be and for never once doubting my ability, and the two loves of my life, Christian and Josefine, who give me more than they will ever understand.

At last, Malmö May 2005

Katja Fridh

Summary

Chapter 1 presents the *background* to the project. There are two different types of attack; surface scaling and internal damage. Only internal frost attack is dealt with in the report. This type of attack, is often very severe, since big reduction in strength and stiffness can occur. After wide introduction of air-entrainment internal frost damage has become less frequent. Much phenomenological research on internal frost damage has been performed, but little research aiming at understanding the destruction mechanism. Understanding of frost destruction is stated to be important for many reasons; e.g. for safe use of new types of concrete, for development of realistic freeze/thaw test methods, for development of durable surface treatments and repair. Understanding internal frost damage might also contribute to understanding of the surface scaling mechanism. Surface scaling which is a phenomenon of big economical importance is still unsatisfactorily clarified.

Chapter 2 briefly describes the three most frequently stated *frost destruction mechanisms*; (i) the hydraulic pressure mechanism, (ii) the closed container mechanism, (iii) the ice lens growth mechanism. A fourth mechanism, based on different thermal expansion coefficient of ice and concrete, acting during thawing, is presented, but shown to be of no importance. Each destruction mechanism depends both on *internal* factors, like degree of saturation, water-cement ratio, permeability, air content, air-pore size distribution, and on *external* factors like freezing temperature, rate of cooling, duration of cooling, wetness. Possible effects of each factor are discussed for each mechanism.

A literature review concentrated upon research at which the effect of the different factors mentioned above is performed. Results obtained in different studies are not unambiguous. For example, some studies show that increased cooling rate is negative for frost resistance, other that it is positive. The reason is that, at changing one parameter -like cooling rate-, also other parameters are changed, most often the degree of saturation. The latter often overshadows the other variations.
A literature review is also made of previous low temperature calorimeter studies of ice formation and melting in cement paste and concrete. Work in which combined measurements of ice formation and length changes have been made are presented.

Chapter 3 presents the *aim* and general *layout* of the work. The aim was to try to identify the destruction mechanism behind internal frost damage. This should be done by selected experimental work in which one parameter at a time was varied. A main characteristic of the work is that the moisture content is held constant when

variation is made by some other factor, like rate of cooling. Investigated internal variables are; (i) water-cement ratio, (ii) air content, (iii) degree of saturation, (iv) moisture /drying history, (v) salt concentration of pore water. Investigated external variables are; (i) rate of cooling and warming, (ii) duration of constant low temperature, (iii) lowest temperature level. The experimental work was divided in three different types of study:

Study 1: Length change measurements during moisture-isolated freeze/thaw.
Study 2: Calorimeter investigations of ice formation and ice melting.
Study 3: Simultaneous measurements of ice formation/melting and length changes.

In *APPENDIX to Chapter 3* experimental variables and characteristics of the concretes are presented.

Chapter 4 describes the *experimental procedure* for length change measurements presented in Chapters 5-8. Definition of different 'damage parameters' is made. Technique for moisture pre-conditioning of samples before length change measurements are presented.

Chapter 5 presents an investigation of the *effect of cooling and warming rate* on length changes during single cycle freeze/thaw. Two cooling/warming rates were studied; 'normal rate' 3.6°C/h, and 'rapid rate' 7.8°C/h. Tests were made with concrete preconditioned in different ways; (i) natural water content after 4 years water storage, (ii) vacuum-saturated, (iii) a number of adjusted degrees of saturation, between natural and complete saturation. The main result is that that the rate of cooling has no, or marginal, effect on the observed length change at each given temperature. Another result, that was also confirmed in the studies in Chapter 6-7, is that non-air-entrained concrete expands during freezing at all degrees of saturation investigated, while air-entrained concrete with natural water content contracts more than the normal thermal contraction, except concrete with w/c-ratio 0.40 for which a small expansion was observed. At high degrees of saturation air-entrained concrete behaves like nonair-entrained. No destruction was seen during the thawing phase in any concrete at any warming rate.

In *APPENDIX to Chapter 5* results for all samples are presented.

Chapter 6 presents the results of an investigation of the *level of the lowest temperature* on length changes during single cycle freeze/thaw. Two temperature levels were investigated; -15°C and -30°C. For non-air-entrained concrete, and for air-entrained concrete with high degree of saturation, damage (expansion) was found to be directly

proportional to the minimum temperature; i.e. –30°C gave twice as big expansion as –15°C.

Air-entrained concrete with natural water content contracted more than normal thermal contraction over the entire temperature range. Contraction was not dependent of the minimum temperature.

Temperature was held constant for 3 hours at the two levels -15°C and -30°C. As soon as temperature change was stopped all specimens almost immediately stopped to expand or contract, except for some very small length changes.

In *APPENDIX to Chapter 6* results for all samples are presented.

Chapter 7 presents the results of an investigation of the *duration of the lowest temperature* on length changes during single cycle freeze/thaw. In the tests in Chapter 6 temperature had been kept constant for 3 hours at -15°C and -30°C. In Chapter 7 these periods were extended to 12 hours. No effect of these longer halts in periods of constant temperature could be observed. As for the samples in Chapter 6, length changes stopped almost totally as soon as temperature lowering or warming was stopped.

In *APPENDIX to Chapter 6* results for all samples are presented.

Chapter 8 describes the results of an investigation of the *salt concentration* of the pore water on length changes during single cycle freeze/thaw. The samples had been prestored for 4 years in NaCl-solutions with concentration 2%, 4.5% and 11%. Companion specimens were stored in ordinary water. For non-air-entrained concrete with w/c-ratio 0.60, the concentrations 4.5% gave considerably bigger expansion than pure water, or the other concentrations. For non-air-entrained concrete with w/c-ratio 0.40, pure water gave biggest expansion, while 2% and 4.5% gave no expansion.

For air-entrained concrete very big expansion occurred at salt concentrations 4.5% and 11%, while, as expected, the specimens with pure water contracted. Thus, it actually seems as if high air content could be a detrimental factor in internal frost destruction when the pore water is saline. This was an unexpected result, which could not be explained.

Chapter 9 presents the results of a study of *ice formation and melting*. The chapter starts with an analysis of the relation between pore structure and freezing point. Supercooling phenomena are described, and are claimed to be the cause behind the always observed hysteresis between freezing and melting. A method of calculating freezable water versus temperature from the low-temperature calorimeter results is described.

Ice formation/ice melting curves for the same materials, as were used for studies in Chapters 4-8, are presented. The effects of water-cement ratio, air content, water content, pre-drying procedure, and saline pore water are presented and discussed. Big hysteresis between ice formation and melting was observed for all samples. Freezing occurred within three temperature regions, the most dominant at some degrees below 0°C, when super-cooled water freezes, and the second big freezing at about -40°C when locally super-cooled water freezes. Melting always occurred gradually from -40°C upwards, but most rapidly around –5°C to 0°C.

It is shown that the amount of non-freezable water is fairly constant, which means that the amount of freezable water depends on the total water content (degree of saturation). The non-freezable water content is used for calculating the sorption isotherms. Comparison between calculated and measured sorption isotherms is made. The agreement is low.

Chapter 10 summarizes the findings from the length change measurements and the ice formation measurements. The two types of measurements are combined in order to draw conclusions on the destruction mechanism. No safe conclusions could be drawn. It seems as if the cause of expansion when the first ice is formed by nucleation of super-cooled water is a combination of the hydraulic pressure and the closed container mechanisms. In the small specimens used in the present study, this expansion sometimes caused considerable damage. Continued expansion from about -10°C occurring in non-air-entrained concrete might be explained by hydraulic pressure since it was found that there is direct proportionality between expansion rate and ice formation rate; a doubling of ice formation rate gives a doubling of the expansion rate.

Air-entrained samples contract, which indicates that ice lens growth is also an active mechanism. To what extent it gives bigger internal stresses in nonairentrained concrete than hydraulic pressure could not be judged from the experimental results.

Chapter 11 describes a new promising equipment (combined calorimeterdilatometer) by which the length change and the ice formation can be determined simultaneously on the same specimen. Some results are presented. They are similar to results found by the separate determinations discussed in Chapter 10.

The equipment is presented in more detail in *APPENDIX to Chapter 11*.

Chapter 12 presents some conclusions from the work. Subjects for future research are suggested.

Contents

1 Introduction

1.1 The problem

In countries with cold climate, like Scandinavia, USA, Canada, Russia, Japan, frost attack on building structures is a major problem. Frost attacks not only concrete but almost all types of porous mineral-based building materials, like clay brick, natural stone, mortar, etc. In Sweden severe frost attack on concrete was observed already in the beginning of the last century, especially in hydraulic structures like dams, spillways, water reservoirs, but also on structures in seawater, like quays and bridge pillars.

A major reason for these early damage cases was that one was not aware of the very big importance of using 'watertight' concrete, i.e. concrete with low enough water-cement ratio. There was also shortage of cement in those days that led to the use of low cement contents, especially in massive structures like dams. These therefore suffered both from leaching and from frost damage, the latter being aggravated by the first.

In the 1930´s it was found in USA that air bubbles, at the beginning unintentionally entrained, gave big increase in frost resistance; the history of air-entrainment is described in Klieger (1980). This observation rapidly led to the development of surface-active air-entraining admixtures, and even to the development of airentraining cements containing the admixture is solid form. Air-entrained concrete found wide application in USA already during the 1930´s and 1940´s. In Sweden, requirement for air entrainment was not introduced until 1966, and then only in the most exposed structures. This means that a considerable fraction of all Swedish concrete structures is built with non-air-entrained concrete, and with fairly high water-cement ratio, which means that they have low potential frost resistance.

After the introduction of watertight concrete and air-entrainment in 1966, frost damage in hydraulic structures and other structures exposed to ordinary water has been less frequent in Sweden. Also structures where no air is required and used, like facades, have had high frost resistance, which might depend on the use of fairly low water-cement ratio combined with low moisture load. In other countries, though, facades have been much more vulnerable to frost damage.

However, even after introduction of air entrainment, concrete bridges have suffered big frost damage. Partly, this can be blamed on the use of de-icing salts, which have caused surface scaling on edge beams and other unprotected parts of the superstructure of the bridge. The main reason for this type of damage is that unsuitable combinations of admixture and cement created low quality air-pore systems. Never-

theless, in a considerable fraction of all Swedish bridges, even protected parts of the bridge, particularly the bridge deck beneath the bituminous membrane and pavement, have suffered from frost damage. The damage is often blamed on ageing of the membrane, making salt water penetrate to the concrete. Thus, the reason is normally claimed to be normal salt-frost scaling. However, it is just as likely, or maybe more likely, that the damage is of type internal frost damage of the same type as in hydraulic structures; viz. it depends on a transgression of a critical moisture condition. It can be shown, both theoretically and by measurements, that moisture can easily penetrate cracks in a membrane by capillary action, but that it cannot easily escape. Thus, moisture tends to accumulate under dense surface layers containing defects; RE-HABCON (2004). Both non-air-entrained and air-entrained bridge decks were harmed.

The fact that frequent frost damage appeared also after the introduction of air-entrainment, which was highly unexpected, led to research in order to find the reason why air did seemingly not function. This research was purely empirical, but indicated that there is an intricate interaction between the cement and the combination of air-entraining and water reducing agents used. For some cements, robust air pore systems tends to form for many admixture combinations. For other cements, the quality of the air-pore system, and its stability, is highly dependent on the actual admixture combination.

Since it is not possible to theoretically design a concrete mix, which has high probability of being frost resistant, e.g. a mix with a given minimum air content, or a mix with a defined air-pore system as determined by optical analysis, the best possibility is to use some sort of functional test of frost resistance. Only mixes that stand the frost test are allowed to be used. Such a pre-testing system has been in use in Sweden for more than 15 years and has turned out to be very successful. The test method (Swedish Standard, SS 13 72 44) is primarily aimed at the resistance to surface scaling in NaCl-solution. There is no well-established functional frost test for freezing without salt.

1.2 Types of frost damage

As shortly touched upon above, there are two types of frost damage:

1. Freezing in the presence of *pure water* (no salt present). Damage is *internal* while the surface is often intact. Internal frost damage is very serious since the cohesion and integrity of the concrete can be lost more or less completely. This means that the tensile strength, the bond strength, and the E-modulus can by seriously reduced. Effects of internal frost damage on the

mechanical properties of concrete and on the structural stability of the structure are described in CONTECVET (2001).

2. Freezing in the presence of *saline water*, de-icing salt or seawater. The visible attack is *scaling* of the surface. Possibly, also internal damage occurs, but it is seldom noticed, maybe because the surface attack is so much more apparent. Salt frost scaling can lead (in the worst scenario) to a total loss of the cover over the reinforcement. Also, if only part of the cover is lost, the protection of the reinforcement is reduced which might lead to early corrosion of the reinforcement.

The *pure water* frost attack has been subject to numerous studies, both experimental and theoretical. Important work was done by Powers (1949), Powers and Helmuth (1953), Verbeck and Klieger (1958), Warris (1964), Vuorinen (1969) and others. Destruction mechanisms have been suggested and quantified. The most important of these are described briefly in Chapter 2. Test methods have been suggested and are used, but the most frequent of these are neither based on understanding of the destruction mechanism, nor related to the practical application of the material. A theory for the service life estimation of structures exposed to internal frost attack has been suggested, but has not been verified, partly due to limitations in the understanding of the destruction mechanism; Fagerlund (2004). The research on internal frost was as most intense during the 1950's to 1970's when many important studies were made, particularly in USA, Sweden, Finland and Germany.

The first to report on the sometimes devastating effect of frost and *de-icing salts* on concrete surfaces was Arnfelt (1943). During the 1950's, as salts became used more and more on concrete roads, the problem was also experienced in the USA. Important early experimental work was done by Verbeck and Klieger (1957), Bergström (1955) and others.

During the last decades the problem of salt frost scaling has become more and more into focus and much experimental work has been made, and test methods have been developed. A considerable part of this research was carried out within the committee RILEM TC 117 FDC 'Freeze Thaw and De-icing Salt Resistance'. Most work has been experimental and aimed at investigating phenomena taking place during an open salt-frost test in which the specimen is repeatedly frozen and thawed in salt solution. Jacobsen (1995) performed such experimental research on ordinary Portland cement concrete and on concrete containing silica fume. Petersson (1975) investigated relations between field exposure and laboratory salt frost tests. Rønning (2001) carried out an extensive investigation of moisture uptake during freezing and thawing, and of the extent to which laboratory tests and field exposure are related. Ut-

genannt (2004) performed tests on slag cement concrete in order to investigate the effect of natural ageing on salt frost resistance. Ageing effects were also studied by Vesikari (1988), Kaufmann (1999) discussed qualitative aspects of destruction mechanisms on the basis of extensive studies of freezing and thawing of concrete. There are many more studies performed that are not mentioned here.

Damage hypotheses for salt frost scaling have been presented by Powers (1965), Lindmark (1998), Tange Jepsen (2002), Setzer (2002) and others. In all cases the hypothesis is supported by experiments. An overview of the frost resistance problems can be found in Pigeon and Pleau (1995). Conference proceedings on frost resistance problems, are Setzer and Auberg (1997) and Setzer et al. (2002).

Despite all this work on salt frost scaling, the destruction mechanism is still not fully clarified. There is a hypothesis, sometimes put forward, that the same mechanism is responsible for both internal frost damage and salt frost scaling. Therefore, if the internal frost damage mechanism is understood, maybe also the salt scaling mechanism has got its explanation.

1.3 Required research on internal frost damage

Use of air-entrainment, and application of well-tried methods for function testing of concrete exposed to salt and frost have solved much of the frost damage problems, that were so frequent earlier. It is a fact, however, that the destruction mechanism behind frost damage has not been fully clarified and that will have negative practical and principal implications. Examples are:

1. The exact mechanism by which entrained air protects concrete against internal frost damage is not understood. It can be shown theoretically and experimentally that some of the air pore system -it is unknown which part- is inactivated by water absorption, but this is normally not recognized in existing theories. Some air pores might be active at rapid freezing, other pores at slow freezing, it is unknown which.
2. The requirements as regards the air pore structure for obtaining high resistance to internal frost damage might be different for concrete with different w/c-ratio, or for concrete containing mineral admixtures. The requirements are probably a function both of ice formation and of the permeability of the concrete in unfrozen and frozen condition.
3. Some researchers claim that thawing is more harmful than freezing; most researchers are of the opposite opinion. No systematic investigations have been made.

4. One of the main destruction mechanisms – hydraulic pressure – predicts that rapid freezing is more harmful than slow freezing. The other main mechanism – ice lens growth – predicts the opposite. No systematic investigations have been made.
5. According to existing theories, low water-cement ratio and high air content should be positive factors, both for salt frost scaling, and for internal frost damage. There are experimental indications, however, that this is not necessarily true, since very dense concrete with low w/c-ratio has in some tests turned out to have low internal frost resistance in laboratory freeze/thaw, but very high salt frost resistance. The theoretical background to these observations is unknown.
6. The interaction between a concrete and a surface layer (porous or non-porous) during freeze/thaw, and the frost resistance of the combined materials is not understood, but depends on the destruction mechanism.

It is unsatisfactory, from an intellectual point of view, that the mechanism behind such an important destruction of concrete structures as internal frost is not fully understood.

Increased knowledge of why, and how, frost destruction takes place will have practical importance. Examples are:

1. Design of realistic freeze/thaw test methods that predict the real frost resistance in the real structure in a fair manner.
2. Safe use of new types of concrete with new type of binders that do not jeopardize internal frost resistance. Examples are composite cements containing two or more mineral admixtures, and dense, high performance concretes.
3. Safe use of new types of air-entraining admixtures, that gives higher and safer frost resistance.
4. Safe use of repair systems that will not negatively affect the frost resistance of the base concrete. This can often be assumed to have inferior internal frost resistance, and is therefore sensitive to changes that alter the moisture content.

1.4 This research work

The aim of the present work was to increase the knowledge of frost destruction by systematic studies of how concrete responds to freezing. This was done by experimental studies of the freezing and thawing process of pore water, and the corresponding response in terms of length changes. A main characteristic of the investigation is that all tests were made with moisture sealed specimens. This was done because it is known from previous research that the effect of the moisture content, and changes in moisture content during the test, will overshadow all other influencing factors.

The whole study was made with quite small specimens, which means that moisture or temperature gradients will not influence the result, which facilitates the interpretation of these. Thus, the investigation is valid for what can be called a 'unit representative cell' located somewhere inside a structure. If the destruction mechanism in the unit cell is understood, and the moisture content within the cell is known, the response of the cell to frost can be predicted.

Theoretically, the result for the unit cell can be extrapolated to the real structure. This is composed of a large number of unit cells. Each cell will respond in its own way to frost action because the moisture content and the temperature-time field is different in each cell. Therefore, principally, also the response to frost of the entire structure, like its structural stability, can be predicted. The concept 'unit cell' has previously been used in Fagerlund (1997), (2004).

2 Frost damage mechanisms

2.1 Introduction

The primary aim of this chapter is to present important existing theories of frost deterioration, and to discuss their consequences. The theories presented are, (i) hydraulic pressure, (ii) closed container, (iii) ice lens growth.

Implications of the theories are discussed in terms of main external and internal parameters that might be of importance in each theory; freezing rate, lowest temperature, duration of the lowest temperature, w/c-ratio, air content, salt concentration. The chapter also contains a short literature survey of experimental studies at which the effect of the parameters mentioned above have been investigated.

Ice formation is a primary parameter in frost destruction. Important previous calorimeter studies of ice formation and melting are reviewed.

Finally, the chapter presents some interesting studies of simultaneously occurring length change and ice formation.

2.2 The hydraulic pressure theory

2.2.1 The mechanism

Powers (1945) observed in laboratory testing two types of damage to concrete specimens caused by freezing; (i) continuous scaling of the surface but small or no changes in strength and strain, (ii) small changes of weight and appearance, but large decrease in strength and elasticity. Powers' experiments showed that at high w/c-ratio, the degree of scaling was high, but that the degree of expansion and the drop in elasticity were low. Materials with lower w/c-ratio showed the opposite. In his paper from 1945 Powers presented a destruction mechanism, the hydraulic pressure mechanism that might explain both types of damage.

Loss of strength and elasticity, *internal frost damage*, was supposed to be caused by hydraulic pressure arising when excess water, produced by the 9% increase in volume at ice formation, was expelled out of the capillary pores into the surrounding cement paste.

Surface frost damage was explained by an increase in the degree of saturation of the surface part of the concrete, when this was thawed in water as it was in Powers´ experiments. Also this causes a hydraulic pressure when excess water has to be forced inwards towards an unsaturated part of the material.

A theoretical analysis showed that the hydraulic pressure was dependent on the following factors; permeability of the material, rate of ice formation and effective degree of saturation. The latter describes the space available for expelled water:

$$S_f = \frac{w_f}{w_f + a} \qquad \text{Eq. 2.2.1}$$

w_f is the amount of freezable water (m^3/m^3), and a is the air-filled pore volume (m^3/m^3). According to the theory, hydraulic pressure can only arise when S_f>0.917; i.e. when the air volume is smaller than the volume expansion at freezing. If S_f<0.917 all excess water is taken care of in the freezing pore itself without causing pressure.

The hydraulic pressure theory predicts the existence of a *critical size* of a completely saturated piece of a material (S_f=1). As illustration of the critical size Powers (1956) used a slice with thickness D of the material, and with open surfaces to the surrounding air; Figure 2.2.1. The effective degree of saturation is above 0.917 which means that some water has to be forced out of the slice, through the surface. This causes pressure that can be described by Darcy's law, Eq. 2.2.3. Maximum pressure appears at the centre of the slice. The slice fractures when the pressure (P) exceeds the tensile strength of the material (P=f_t), see Eq. 2.2.2.

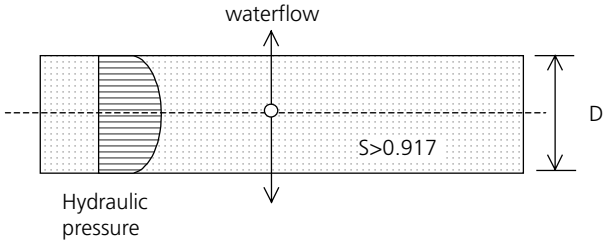

Figure 2.2.1. The critical thickness, Powers (1956).

The analysis is quite simple and leads to the following value of the *critical thickness:*

$$D_{CR} = \left(\frac{8K}{\eta}\right)\left(\frac{f_t}{\left(1.09 - \frac{1}{S_f}\right)\frac{dw_f}{dt}}\right)^{1/2} \qquad \text{Eq. 2.2.2}$$

where the permeability K (m^2) is defined by Darcy's law:

$$\frac{dw}{dt} = \frac{K}{\eta} A \frac{dP}{dx} \qquad \text{Eq. 2.2.3}$$

where dw/dt is the rate of generation of excess water flow (m^3/s), A is the cross-section of water flow (m^2), η is the viscosity of the flow (Ns/m^2), and dP/dx is the hydraulic pressure gradient (Pa/m).

The rate of ice formation, dw_f/dt (m^3/m^{3}s) is a function of the cooling rate, dθ/dt (K/s), and of the amount of water freezing in the concrete for one degree temperature lowering, dw_f/dθ (m^3/m^{3}K):

$$\frac{dw_f}{dt} = \frac{dw_f}{d\theta}\frac{d\theta}{dt} \qquad \text{Eq. 2.2.4}$$

Eq. 2.2.2 shows that maximum pressure appears when S_f=1. No pressure appears when $S_f \leq 0.917$. A consequence of the hydraulic theory is that pressure increases in proportion to the square of the flow distance.

Powers (1949) initially applied the hydraulic pressure theory to a more realistic material model than the simple slice, viz. an air-filled pore surrounded by a cement paste shell containing freezable water. This hollow sphere has an outer boundary that is impermeable. The permeability is assumed to be constant independently of temperature and amount of ice formed. The flow can only be in one direction, to the air void, which is big enough to take care of all displaced water at all times, see Figure 2.2.2.

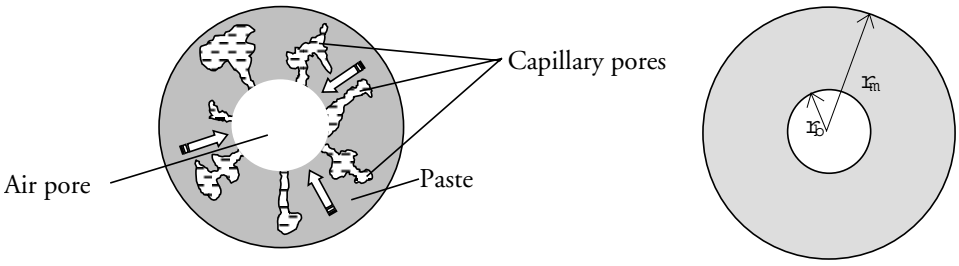

Figure 2.2.2. The Powers model of a freezing cement paste.

At the periphery to the air pore (r=r_b), pressure is zero, p=0. Maximum pressure appears at the outer boundary of the hole-sphere, r=r_m. Powers (1949) derived the following expression for the maximum pressure:

$$p(r=r_m) = \frac{\eta}{K}\left(1.09 - \frac{1}{S_f}\right)\frac{d\theta}{dt}\frac{dw_f}{d\theta}\frac{1}{3}\left(\frac{r_m^3}{r_b} + \frac{r_b^2}{2} - \frac{3r_m^2}{2}\right) \qquad \text{Eq. 2.2.5}$$

where K is the permeability if the cement paste (m^2), η is the viscosity of water (Ns/m^2), $d\theta/dt$ is the rate of temperature change (°C/s), $dw_f/d\theta$ is the amount of

freezable water per volume of paste caused by a temperature change of dθ ($m^3/m^3°C$), S_f is the effective degree of saturation of the cement paste *outside* the air-pore, and r_m *and* r_b (m) are defined in Figure 2.2.2.

A real cement paste is not a single hole-sphere, but consists of a big number of cement paste 'shells' of different shape and size, surrounding air-pores of different size. Powers used the model in Figure 2.2.3 for defining a spacing factor *L*. The calculation is based on the following assumptions; (i) all air pores are of equal size which is based on the assumption that its specific surface is the same as that of entire air pore system, (ii) every air pore is surrounded by a cube of cement paste, the volume relationship between the paste and the air pore is the same as the relationship between all cement paste and all air pores in the entire material. The distance L (the spacing factor) is the distance from a corner of the paste cube to the circumference of the pore.

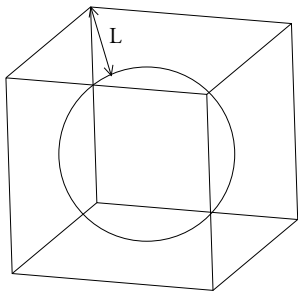

Figure 2.2.3. Definition of Powers' spacing factor.

In Eq. 2.2.5 the following replacements are made*: (i)* $r_m=L+r_b$, (ii) $(dw_f/d\theta)\cdot(d\theta/dt)=dw_f/dt$ which is the rate of ice formation, see Eq. 2.2.4.

$$p(r=r_m)=\frac{\eta}{K}\left(1.09-\frac{1}{S_f}\right)\frac{dw_f}{dt}\frac{1}{3}\left(\frac{L^3}{r_b}+\frac{3}{2}L^2\right) \qquad \text{Eq. 2.2.6}$$

If the tensile strength f_t is introduced as the highest pressure the paste can withstand, one can calculate the maximum thickness of the shell L_{max}

$$L^2{}_{\max}\left(\frac{L_{\max}}{r_b}+\frac{3}{2}\right)=\frac{3Kf_t}{\eta\left(1.09-\frac{1}{S_f}\right)\frac{dw_f}{dt}} \qquad \text{Eq. 2.2.7}$$

Powers (1949) used experimental data for air-pore structure (r_b), tensile strength (f_t), permeability of unfrozen cement paste (K/η), and rate of ice formation (dw_f/dt) to calculate a value of the maximum tolerable (critical) value of L for saturated cement paste (S_f=1). The values he found were of the order 0.25 mm, rather independently of the water-cement ratio. Similar calculations based on the hydraulic pressure theory have later been performed by Fagerlund (2004) indicating a certain effect of the water-cement ratio. Furthermore, the values were found to be of the order 0.37 à 0.43 mm, i.e. considerably higher than the Powers critical spacing factor, but in fair agreement with experimentally observed values calculated from critical water contents at freezing. The main reason between the different results is that Powers wrongly assumed that all air pores were actually air-filled during freezing, which means that the value of r_b for a given pore system used in the equation becomes too small. This leads to an underestimation of L. Furthermore, in Fagerlund (2004) consideration is taken to a gradual reduction of permeability as more and more ice is formed. Powers assumed that permeability is constant.

A way of testing the hydraulic pressure theory is to compare the measured expansion curves with calculated ones based on the hydraulic pressure model using realistic data for the air-filled fraction of the air pore system and for permeability changes. The results of such attempts are presented in Fagerlund (1973b), (1997).

Note: Hydraulic pressure can only occur when ice is formed and not when ice melts. Therefore damage, possible caused by thawing, cannot be explained by hydraulic pressure.

2.2.2 Implications of the hydraulic pressure theory

Below, a short discussion is performed on 'climatic' and material parameters that might influence hydraulic pressure.

Rate of freezing

As can be seen from the equations above, the hydraulic pressure theory predicts a strong influence of the freezing rate on the destructive forces, A higher rate of temperature lowering gives a higher rate of ice formation and therefore bigger internal tensile stress. If all other material properties are kept constant, an increase in the freezing rate by a factor two, should generate twice as high pressure and dilation. This will be tested in the present work.

The highest ice formation rate during a freeze-thaw cycle in the laboratory is often taking place when supercooling is overcome. Thus, the highest hydraulic pressure during a freeze/thaw cycle could be expected in connection with nucleation of supercooled water. However, ice forms continuously during the gradual decrease in temperature, and this ice might obstruct the flow of the expelled water. The consequence

could be that the hydraulic pressure is not always largest when the ice formation rate is highest but when the ratio between ice formation rate and permeability is largest; see Eq. 2.2.5.

Halts in cooling

If cooling is stopped, the hydraulic pressure should, according to the theory, immediately become zero, since no water flow is generated. Therefore, the material should contract elastically to its original size. In reality, however, ice formed before cooling is stopped, might have caused so big destruction of the material (e.g. due to excessive hydraulic pressure) that no relaxation of tensile strain is possible. The contraction can also be 'mechanically' obstructed by ice in the pores. In a damaged concrete ice is occupying bigger volume than the initial volume of the pores containing water before freezing, and this hinders contraction. This feature of the hydraulic pressure mechanism will be studied in the present work.

Freezing temperature

Ice formation increases with decrease in temperature. In the hydraulic pressure theory this is expressed by the parameter $dw_f/d\theta$ in Eq. 2.2.5. There are indications that this parameter can be high at low temperature. Therefore, the lowest temperature is an interesting parameter in the hydraulic pressure theory. Tests of this are made in the present work

Duration of freezing temperature

The duration of the lowest temperature should have no influence since, according to the hydraulic pressure theory, when the freezing rate is zero no hydraulic pressure, nor any damage should occur, and this is independent of the duration of constant freezing temperature. The effect of duration is tested in the present work.

Degree of saturation

In Powers derivation of hydraulic pressure, this will only appear when the *effective* degree of saturation, S_f, of the cement paste shell *outside the air pore* (see Figure 2.2.2) is above 0.917. In a real outdoor concrete structure this is always the case. According to Powers, a concrete should be frost resistant in all types of environment as long as the spacing factor does not exceed the critical value calculated by Eq. 2.2.7 for S_f=1.

In reality, however, also part of the air-pore system becomes water-filled which makes the value of r_b in Eq. 2.2.7 a function of the 'wetness' of the environment. Also the aggregate might contain pores that can become more or less water-filled. Cracks and defects in the concrete can contain water. Therefore, Powers' definition of degree of saturation is unsuitable as a measure of frost resistance. It is more feasible to use a degree of saturation, S, based on the total water content in the concrete.

$$S = \frac{w_e}{V_p} \qquad \text{Eq. 2.2.8}$$

where w_e is the total evaporable water in the concrete (m^3/m^3) and V_p is the total pore volume in the concrete (including air pores and all other pore space) (m^3/m^3).

Powers definition of spacing factor corresponds to the case when only the cement paste is porous, and when all pores, except all air pores, are water-filled. Under these conditions S is:

$$S = 1 - \frac{a}{V_p} \qquad \text{Eq. 2.2.9}$$

where a is the total air content (m^3/m^3). The value of S will always be higher than S_f since only a fraction of all pore water is freezable. Besides, the relation between S and S_f depends on temperature, since more water freezes the lower the temperature.[1].

By experiments it can be shown that a considerable fraction of the air-pore system can be water-filled, and still the concrete be frost resistant. Each concrete has its own critical degree of saturation corresponding to a 'true' critical spacing factor, which is higher than the Powers critical spacing factor, since it excludes water-filled 'air pores'. This 'true' critical spacing factor might also be a consequence of hydraulic pressure. The only difference from Powers definition of spacing factor is that his hole-sphere model, and the equation based on that, is not exactly valid. The discrepancy between the Powers way of defining a critical spacing factor for cement paste assuming no water-filled air pores, and the 'true' spacing factor for cement paste (or concrete) with some part of the air-pore system water-filled, and the consequences of this discrepancy, is discussed in Fagerlund (2004).

Increased degree of saturation causes increased flow distance from the ice formation site and the nearest air-filled space. This will, according to the theory, increase the hydraulic pressure, provided the critical degree of saturation is transgressed. In order to investigate if this is the case, concrete with different degrees of saturation were tested.

[1]) The relation between the two definitions of degree of saturation is:
$S=S_f \cdot a/(1-S_f)V_p + K$. Where $K=w_{nf}/V_p$. Thus the non-freezable water (w_{nf}) is expressed as a constant (but temperature-dependent) fraction of the pore volume.

Water-cement ratio

The *water-cement ratio* might have an effect on the hydraulic pressure. A high w/c-ratio results in high permeability, but also high rate of ice formation. A low w/c-ratio gives the opposite effects. The net effect of w/c-ratio on the hydraulic pressure is difficult to predict. Tests of the effect of w/c-ratio on dilation during freezing were therefore performed.

Air content

The spacing between air pores, and consequently the flow distance for expelled water, will increase with decreased air content. Therefore, hydraulic pressure will increase with decreased air content. The effect of air on behaviour during freezing was investigated in the present work

2.3 The closed container theory

2.3.1 The mechanism

The '*closed container*' is a special case of the hydraulic pressure mechanism, applied to the case where the permeability is zero, and the ductility of the material is zero. The mechanism was suggested by Fagerlund (1997) for describing the maximum allowable amount of freezable water, and the maximum pressure in very dense saturated cement paste, or in very dense concrete containing embedded saturated coarse porous aggregate particles. In such cases water flow from the freezing site is practically impossible due to low permeability. Therefore, the 9% increase in volume at ice formation creates huge stresses in the material when this is 100% saturated. No porous material can withstand these stresses, unless the porosity is very low. This is shown by the calculations below.

Ice can be formed without causing stress if the effective degree of saturation in the container (the closed pore), defined by Eq. 2.2.1 is below 0.917. Then, all volume expansion can be taken care of within the container (neglecting air pressure formed when ice expands).

If the container is saturated to a level above 0.917, and water freezes, expansion will occur and the container might burst. The higher the degree of saturation, the bigger is the expansion.

Ice formation can be hindered if the pressure in the water is sufficiently high. Thus, ice formation in a closed stiff container, or in a closed pore inside a very stiff material, can be hindered if the container (pore) walls can resist the volume expansion that should have occurred at ice formation, had the material been infinitely ductile. The pressure needed for hindering ice formation (the depressed freezing point)

can be calculated by the Clapeyron equation applied to the equilibrium between ice and water:

$$\frac{dp}{dT} = \frac{\Delta H^{fus}}{T\Delta V^{l-s}} \qquad \text{Eq. 2.3.1}$$

where ΔH_m^{fus} is the change in enthalpy at freezing (the heat of fusion) (J/mol), ΔV^{l-s} is the change in molar volume of water at ice formation (m^3/mol) and T (K) is the temperature of phase transition. The following values are valid:

$\Delta H^{fus} = 6009$ J/mole at 0°C (5300 J/mole at –20°C)
$\Delta V^{l-s} = -1.61 \cdot 10^{-6}$ m³/mole
$T = 273.15$ K

Inserting these values in Eq. 2.3.1 shows that the walls need to exert a pressure of 13.7 MPa on the ice for each degree of decrease in temperature, in order to hinder ice formation.

This stress can be taken up if the container walls are extremely strong, or if the water volume is very small compared to the volume of the container itself. A simplified calculation is made based on the model in Figure 2.3.1. The hole-sphere contains water that should be freezable, had the over-pressure been zero. The freezable water content is $w_f=(4/3)\pi r^3$ (m^3). The total volume is (4/3) πR^3 (m^3). The volume fraction of freezable water is $w_f=(r/R)^3$ (m^3/m^3).

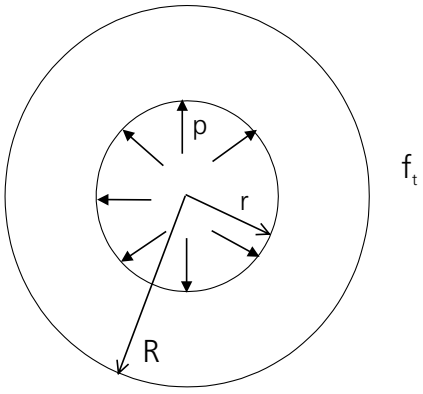

Figure 2.3.1. Hole-sphere containing water with depressed freezing point due to hindered freezing.

To simplify the analysis the stress in the walls is supposed to be the same over the entire cross-section. The internal pressure acting against the wall is 13.6·θ MPa where θ (°C) is the temperature of the water (θ<0°C). The tensile stress (f_t, MPa) in the wall becomes:

$$f_t = -\frac{13.6\theta w_f^{3/3}}{1 - w_f^{3/3}} \qquad \text{Eq. 2.3.2}$$

Concrete has a maximum tensile strength of about 6 MPa. Thus, according to Eq. 2.3.2, ice formation might be hindered at temperature -10°C, provided the amount of freezable water is less than about 10 litre/m^3. This is a very small water content that is hardly found in concrete. The calculation also indicates that the maximum tolerable porosity in aggregate that can become saturated when embedded in dense concrete is of the order 1%. This has also been confirmed in tests, Cady (1969).

2.3.2 Implications of the closed container theory

In Fagerlund (1997) a number of cases are presented when this mechanism can be active in concrete, such as saturated porous coarse aggregate grains surrounded by cement paste, freezing of water in porous interfaces between aggregate and cement paste, freezing of water in high performance concrete with extremely low w/c-ratio, freezing of insufficiently self-desiccated young concrete, freezing of water in cracks, and freezing of water absorbed in air pores.

The mechanism can maybe also explain the big expansion sometimes observed in non-air-entrained ordinary concrete at low temperature. In such concrete a big amount of ice is formed at low temperature. This late freezing therefore might occur more or less as in a closed container.

The closed container cannot explain all the features observed in materials during freezing, especially not the shrinkage often observed in concrete with air-entrainment.

2.4 The ice lens growth theory

2.4.1 Macroscopic ice lens growth – frost heave

Taber (1930) presented a hypothesis to explain the phenomenon of frost heave in soils. Another classical theoretical work on frost heave is Beskow (1935). The frost heave could not be explained only by the volume expansion caused by freezing of water already present in the soil at the freezing zone. In laboratory tests of clays, Taber found ice lenses to be able to grow by the suction of water from the warm side of the specimen. This caused the soil specimen to heave. He also found that not all the pore water in the soil was freezable, and suggested that this could be caused by

surface interactions between solid grains and water. He also pointed out the big difference between freezing of open and closed system, the latter type being without access to external water, and therefore having much smaller frost heave.

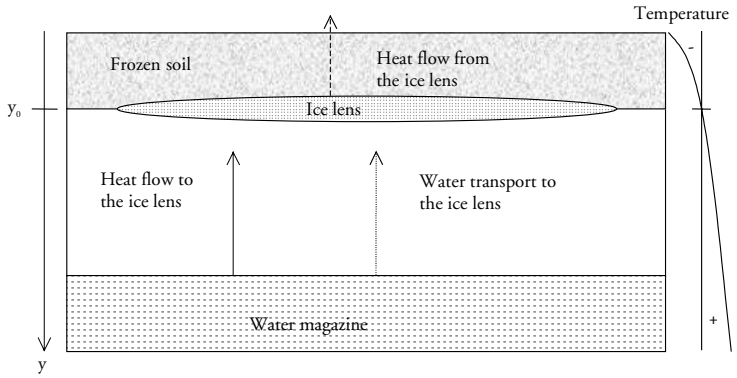

Figure 2.4.1. Principles of frost heave in soil.

The difference in free energy between the cold ice lens and the warmer water creates the driving force for water flow to the ice lens. If equilibrium between the heat flow *to* the ice lens caused by (i) the temperature gradient itself, (ii) the water flow upwards, and (iii) heat generated at freezing of this water, and heat flow *from* the ice lens caused by cooling to the outside air, can be established, the ice lens will for a long time remain on depth y_0 from the surface, and continue to grow there. If the soil is very impermeable, the water and, therefore, the heat flow to the ice will be so low that ice lens growth becomes impossible. Instead freezing continues further down into the soil. If the soil is coarse-grained, the water transport will be hindered because the 'water-path' between the ice lens and the water magazine further down in the soil is interrupted. No ice lens growth will occur. Frost heave can also be stopped if an external pressure is applied to the soil. The required pressure has to be increased with increased fineness of the soil. One way of creating pressure is that arising by cohesion in the soil (or solid) when the ice lens tries to grow.

Collins (1944) found evidence that the mechanism might be active also in concrete under certain circumstances, like in concrete of poor quality, and in contact with unfrozen water, e.g. in old concrete dams and foundations near the waterline. He meant that these types of structures, besides availability to unfrozen water, might have a combination of high permeability and low cohesion (tensile strength) that made destructive macroscopic ice lens growth possible. Maybe macroscopic ice lens growth is responsible for frost damage observed also in Swedish dams. The real significance of the mechanism for concrete structures has never been established.

Air-entrainment cannot stop macroscopic ice lens growth.

2.4.2 Microscopic ice lens growth

Experimental work performed by the American researcher Powers gave results, which could not be explained by the hydraulic pressure mechanism. Instead of expansion, as could be expected, considerable contraction was sometimes found, particularly in samples containing air-entrainment. Non-air-entrained concrete normally expanded. Typical results are shown in Figure 2.4.2. The smaller the spacing factor between air pores the bigger is the contraction. For very small spacing factors (high air contents) the contraction was considerably bigger than the normal thermal contraction evaluated from the contraction of the unfrozen concrete.

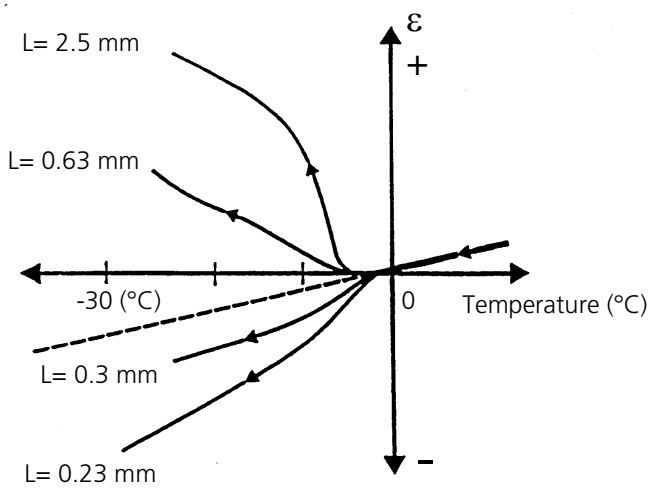

Figure 2.4.2. Effect of the spacing factor on length changes of cement paste (w/c-ratio 0.60) during freezing, cooling rate 0.25°C/hour. Powers and Helmuth (1953).

An even more unexpected result was that some non-air-entrained cement pastes with low w/c-ratio (0.45) continued to expand for many hours when temperature was kept constant, while cement pastes with high w/c-ratio (0.60) immediately stopped expanding but continued to expand when cooling was resumed; see Figure 2.4.3.

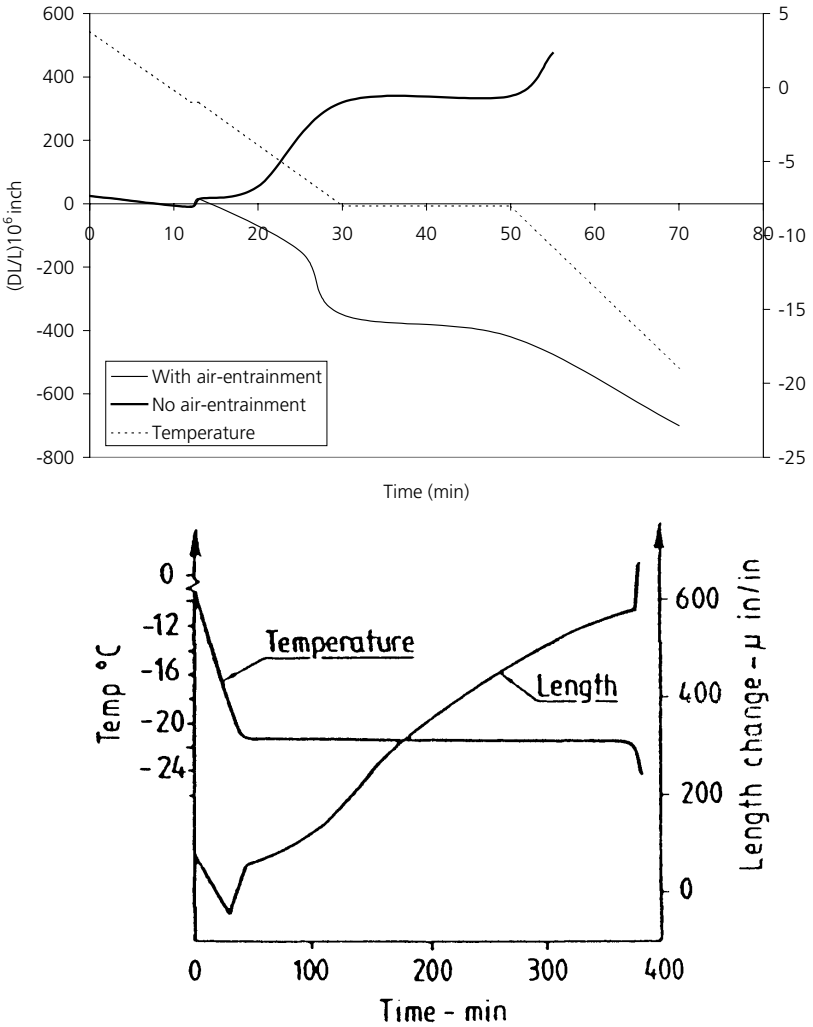

Figure 2.4.3. Length change versus temperature for non-air-entrained cement paste. (a) w/c-ratio 0.60. (b) w/c-ratio 0.45. Powers and Helmuth (1953).

In order to explain these findings, Powers and Helmuth (1953) suggested the theory of microscopic ice lens growth. It is briefly described below.

The mechanism is based on the work presented in Powers and Brownyard (1948) according to which the hardened cement paste was found to have a structure consisting of very small gel particles, separated by very narrow 'gel-pores', containing water unable to freeze at normal freezing temperatures. Besides the gel pores the cement paste also contains coarser so-called 'capillary pores'. Water in these is freezable, water in coarse capillary pores freeze close to 0°C, water in finer pores might not freeze

until -40°C or lower. This means that at each given freezing temperature the cement paste contains unfrozen water in gel pores and in finer capillary pores, and ice in coarser capillary pores. In addition, some ice is present in the air pores. This is formed by freezing of water that was expelled from capillaries at early freezing in these. Unfrozen, supercooled, water might also exist in isolated coarser capillaries, since ice nucleation of this is obstructed by narrow entrances (neck-pores); see Chapter 9.

When equilibrium prevails between ice and all unfrozen water, no water transfer is possible, and no expansion or contraction occurs. If temperature is quickly dropped by $\Delta\theta$ the equilibrium is disturbed. The free energy of ice already formed will be reduced more than the free energy of unfrozen water. This creates diffusion potential between the water and the ice. Water from fine capillaries containing unfrozen water, and water from isolated pores containing supercooled water moves towards the capillary ice, and towards ice in the air pores, see Figure 2.4.4. Possibly also outer layers of gel-pore water, that is less firmly bound, can be transported to the ice. The transport takes place from the fine pores through the liquid like adsorbed layer between the ice body and the pore wall.

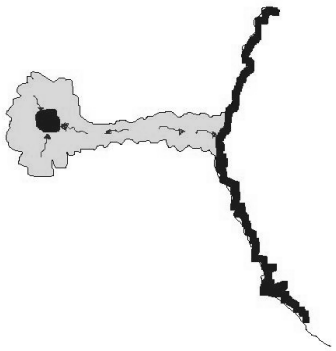

Figure 2.4.4. Ice in the capillary and the air pore attracts un-frozen water.

The water transport causes a drying out of the cement paste, a sort of freeze-drying effect, see Figure 2.4.5. Drying creates shrinkage.

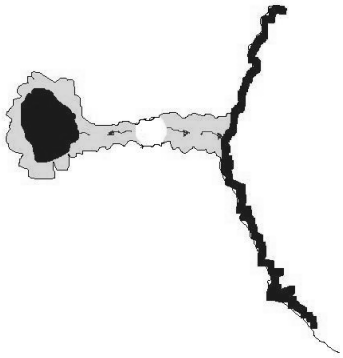

Figure 2.4.5. The movement of the un-frozen water dries out the gel and the small capillaries, creating shrinkage.

Consequently, the cement paste might shrink, both from temperature lowering and from drying. Water arriving at the ice body will freeze, however. Therefore, the ice body will grow. Shrinkage might therefore be obstructed by expansion of the growing ice, as described below. The net effect on the length change depends on the relative effects of shrinkage and expansion. If ice growth dominates, the cement paste will expand, as shown in Figure 2.4.2 for cement pastes with big spacing factor. If shrinkage dominates, the net effect will be contraction as shown in Figure 2.4.2 for cement pastes with low spacing factor.

A growing ice body in a *capillary pore* will excite pressure against the pore wall. The pressure is transferred over an adsorbed unfrozen water layer. Increased pressure increases the free energy of the ice, while drying decreases the free energy of unfrozen water. Both these effects contribute to reduce the driving force for water diffusion. When free energy balance has been restored, water movement stops, which means that both expansion and shrinkage stops. Before that happens, considerable expansion and destruction could have taken place.

A growing ice body in an *air pore* will grow without obstruction from the pore walls. Thus its growth will not be stopped until drying has reduced the free energy of unfrozen water to the same level as that of stress-less air pore ice.

When the spacing between air pores is low, making air pore ice easily reachable, water will primarily move to this stress-less ice, since this has lower free energy than growing capillary ice. Thus, the growth of capillary pore ice will be reduced. At a certain critical spacing, expansion caused by ice lens growth in capillaries equals the shrinkage caused by water transport to capillary and air pore ice. At lower spacing, shrinkage dominates, which according to Powers and Helmuth (1953) explain the results in Figure 2.4.2.

The microscopic ice lens growth mechanism should therefore also predict the existence of a critical spacing factor.

Water flow and ice lens growth continues as long as there is energy unbalance between ice and water. This is the case as long as temperature is gradually lowered. When temperature comes to a halt, ice lens growth can continue as long as equilibrium has not been restored. According to Powers and Helmuth (1953) this could explain the long-term continued expansion at constant temperature noticed for cement paste with low w/c-ratio, Figure 2.4.3b. Such cement paste contains a big amount of non-freezable water available for ice growth. Cement paste with high w/c-ratio stopped expanding immediately, which was explained by the low amount of non-freezable water in such paste. Continued expansion for a long period at constant temperature requires that local equilibrium between capillary ice and unfrozen water is not established until long time after temperature lowering has been stopped.

Another factor, possibly contributing to moisture movement, ice growth and pressure, is that the pore water contains dissolved ions, mainly from alkali hydroxide. When ice forms in the capillary, the ion concentration in the remaining pore water increases and becomes higher than the concentration of unfrozen water in finer pores, or locally supercooled water. In order to even out the concentration difference, ions have to move into unfrozen water and unfrozen water move into the capillaries containing ice. It is possible that the cement gel acts as a sort of semi-permeable membrane that retards diffusion of ions more than diffusion of water. In such case an *osmotic pressure* could be built up. It can contribute to expansion and destruction.

The possibility of osmotic pressure as a destructive force was recognised in the article by Power and Helmuth (1953), but was not treated further for the sake of simplicity. The osmotic pressure theory was further discussed in Powers (1955), (1956) and was considered to be of major importance in salt frost scaling.

The presentation of the ice growth mechanism made by Powers and Helmuth (1953) is, like the one above, purely qualitative. A quantitative discussion of principally the same mechanism, based on thermodynamic reasoning, is performed by Everett (1961).

2.4.3 Implications of the theory of microscopic ice lens growth theory

Rate of freezing (cooling)

Increased cooling rate creates bigger free energy unbalance between ice and water. This increases the diffusion rate of water and thus the rate of ice lens growth. On the other hand, the time available for diffusion is reduced. The net effect is uncertain. The effect of freezing rate is investigated in the present work.

Freezing temperature

The influence of the lowest temperature on pressure caused by ice lens growth is not clear. On the one hand, lower temperature increases the amount of ice, and therefore creates a bigger number of ice lenses that can grow. On the other hand the amount of non-freezable water, feeding ice growth, is reduced in the same proportion. The net effect cannot be predicted. A lower temperature must not in itself cause bigger driving force for ice lens growth, since both unfrozen water and ice has the same low temperature. The total water flow from locally supercooled water will however be increased since its free energy is always high. The effect of freezing temperature is studied in the present work.

Duration of freezing temperature and halts in cooling

The influence of the duration of freezing and of halts in the cooling process might be considerable as illustrated by Figure 2.4.3(b). According to this result a longer duration of constant low temperature gives the mechanism more time to work and to build up pressure. The pre-requisite for this is that local equilibrium is not rapidly established when temperature is held constant. The effect of temperature and duration are studied in this work.

Degree of saturation

The degree of saturation might be just as important for ice lens growth as for hydraulic pressure. Increased degree of saturation above a certain level causes water absorption in air pores which means reduction of the spacing between pores that are still air-filled. Thus, it has the same effect as reducing the air content. This means that capillary ice growth will increase. When the degree of saturation exceeds a critical value corresponding to a critical spacing expansion due to ice lens growth will dominate over contraction caused by drying and the concrete will be damaged. The effect of degree of saturation is studied in this work.

Water-cement ratio

Decreased water-cement ratio means increased fraction of non-freezable water. Thus, more water becomes available for ice lens growth. On the other hand, the number of ice lenses decreases in about the same proportion. According to Powers and Helmuth (1953) the negative effect, i.e. increased ice lens growth, dominates as illustrated by Figure 2.4.3b. The effect of w/c-ratio is studied in this work.

Air content

Low air content favours expansive ice lens growth since it means increased air pore spacing. This must be low enough for air pore ice to be able to 'compete' favourably with capillary ice. The effect of the air content is investigated in this work.

2.5 The theory of ice expansion during thawing

The melting process is a continuous process, but most of the ice melts close to 0°C; see Chapter 9. This means that, during the main part of warming from the lowest temperature (-20°C or lower during a freeze/thaw test), the system consists of 'solid' concrete, ice and un-frozen water. The thermal coefficient of expansion of ice is about five times as large as that of concrete. This means that, theoretically, ice might exert so big pressure by its thermal expansion that the concrete fractures.

This is a very unlikely mechanism however, which can be shown by a simple calculation, using the following expression for the thermal expansion coefficient of a composite material. Only the cement paste phase is considered, Cahn (1966).

$$\alpha = \frac{\alpha_i K_i V_i + \alpha_s K_s V_s}{K_i V_i + K_s V_s} \qquad \text{Eq. 2.5.1}$$

α is the thermal expansivity (m/mK), K is the bulk modulus (Pa), V is the volume fraction (-). The subscript i is valid for ice, and s for unfrozen cement paste.

According to Fletcher (1970) the E-modulus of ice at -16°C is of the order $9 \cdot 10^9$ Pa, and Poisson's ratio of the order 0.40. This gives $K_i = 1.5 \cdot 10^{10}$ Pa. For dry cement paste K_s depends on the porosity. For w/c-ratio 0.60, $K_s \approx 5 \cdot 10^9$ Pa. For w/c-ratio 0.40, $K_s \approx 1 \cdot 10^{10}$ Pa. The coefficients of thermal expansion are about $5 \cdot 10^{-5}$ for ice and 10^{-5} for cement paste (this is a low value, more valid for concrete). The maximum amount of ice at low temperature is equal to the capillary porosity. Thus $V_{i,max} \approx 0.33$ for w/c-ratio 0.60 and $V_{i,max} \approx 0.18$ for w/c-ratio 0.40.

The thermal expansion of frozen concrete becomes:

w/c-ratio 0.60: $\alpha_{max} = 3.4 \cdot 10^{-5} = 0.034$ ‰
w/c-ratio 0.40: $\alpha_{max} = 2.0 \cdot 10^{-5} = 0.02$ ‰

Thus, since the expansion of concrete without ice is $1 \cdot 10^{-5} = 0.01$ ‰, the extra expansion caused by ice is maximum 0.01 ‰ to 0.024 ‰. This is only a fraction of the fracture tensile strain (≈ 0.15‰). Consequently damage cannot occur.

2.6 Literature survey

The literature survey focuses on the same three areas as the experimental work presented in this report.

1. Studies of how different changes in the environment around the specimen in a freeze/thaw test (freezing rate, lowest temperature, duration of freezing temperature) affects the specimen with regard to internal damage (loss in strength and stiffness, dilation). Investigations dealing with surface deterioration were not included in the survey.
2. Studies of ice formation by low-temperature calorimetry.
3. Combined measurements of ice formation and length change.

All studies reviewed relate to different types of cementitious material; cement paste, concrete, cement mortar.

2.6.1 Influence of freezing rate

Freezing rate can be defined as the rate of change of temperature in the surrounding air or liquid, or as the rate of temperature change in the material itself. The latter is preferable, since then, no consideration has to be taken to the time lag between the temperature in the surrounding and in the material. The freezing rate should not be confused with the rate of ice formation, but there is of course a relationship between the two.

Valore (1950) investigated how different freeze-thaw cycles influenced the volume of moisture sealed concrete cylinders (ϕ= 49 mm, l= 183 mm) containing different amounts of water and entrained air. He considered a slow freezing to have a cooling rate of 5.5°C/h, and a rapid freezing to be the cooling rate of a sample of temperature +4.5°C being immersed in a bath at a temperature of -29°C. The following materials were tested; (1) w/c-ratio 0.53 with 5.3% of entrained air, (2) w/c-ratio 0.56 with no entrained air but with natural air content 2.5%.

Water-saturated specimens were, as could be expected, destroyed after one freeze-thaw cycle regardless of the freezing rate. The loss of dynamic E-modulus was 60% or more. Dried samples showed no damage regardless of the freezing rate. For the partially saturated specimen the expansions were much smaller and were found to be dependant of the freezing/thawing rate. The combination of different freezing and thawing tested that gave the longest time of freezing temperature, gave also the largest damage, i.e. fast freezing and slow thawing. This makes it difficult to interpret whether it is the actual rate of freezing/heating or the duration of the freezing temperature that increases the damage.

Vuorinen (1969) argued that no influence of freezing rate could be found on the 'dilation factor', which was defined as the difference between the relative length change of the specimen over the temperature range +20°C to 0°C and the final relative change of the same specimen over the temperature range 0°C to-20°C.

In evaluating a round-robin test of the critical degree of saturation method, Fagerlund (1977) found that the rate of freezing (~ 1.8°C/h to ~ 6°C/h) had almost no effect on the critical degree of saturation (S_{crit}) of concrete. There was a certain effect of freezing rate on the sensitivity of transgressing the critical value. At high freezing rates the concrete obtained somewhat more damage, but this is of no big importance, since the concrete is damaged anyhow; see Figure 2.6.1. The tested concretes were; (1) w/c-ratio 0.50, non-air-entrained, (2) w/c-ratio 0.57, air content 7.6%. The test was performed with moisture isolated specimens, which is required in a test aiming at determination of S_{crit}.

In Fagerlund (1992) these results are discussed, together with a comprehensive analysis of other tests in which the effect of freezing rate on frost damage has been investigated. It was shown, based on a theoretical calculation of S_{crit} for the actual air pore systems, that even if the hydraulic pressure mechanism was the active destruction mechanism, an increased freezing rate from 1.8 to 6°C/h should only have small effect on S_{crit}. Thus, the experimental findings were theoretically verified. In this report he also showed that the degree of saturation will outdo most of the other factors involved, including the freezing rate. He argued that the influence of the freezing rate should be studied in terms of its influence on S_{crit} and that testing of the effect of freezing rate should be done on moisture-sealed specimens. As an example of the big effect of degree of saturation Fagerlund (1980) found that adding further water in very small amounts (3 l/m³) when the saturation was close to S_{crit} could have extraordinary effects on frost damage of concrete, much bigger effect than increasing freezing rate.

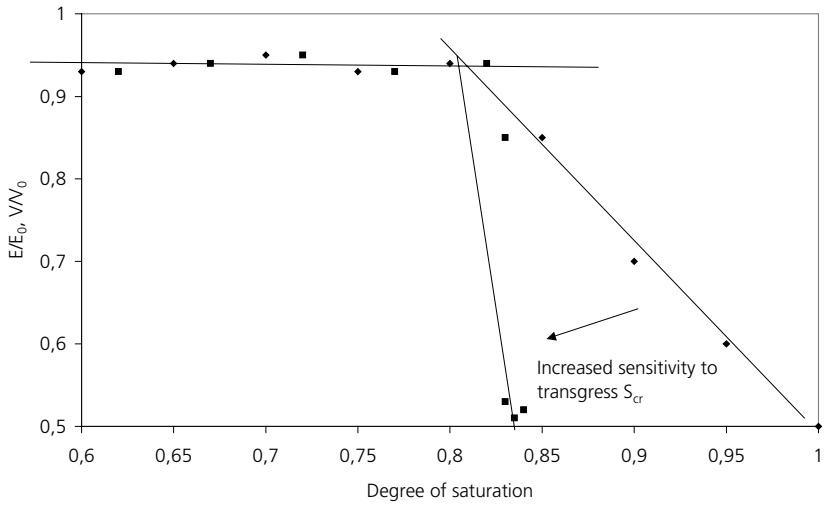

Figure 2.6.1. Effect of the cooling rate on change in dynamic E-modulus. Principal results from Fagerlund (1977).

Pigeon and Lachance (1981) investigated how a slow freezing rate of 2°C/h influenced the critical spacing factor (L_{crit}) as compared to the more rapid ASTM 666-method (12°C/h). Samples (w/c-ratio 0.50 and 0.60) were tested at 300 cycles and a relative humidity (RH) of 100% (but not in water). The length change and ultra sonic pulse velocity were used as indication of damage. The authors found $L_{crit} \sim 600$ μm by their own slow 'dry' method, which is much higher than the usual limit of 200 à 250 μm obtained by the rapid 'wet' ASTM 666-method The authors concluded that the large difference in L_{crit} was due mainly to the difference in freezing rate, just as Powers (1945) theory of hydraulic pressure states. The markedly different moisture condition at the ASTM test and the Pigeon/Lachance test was not commented upon.

In a comment on Pigeon and Lachance's paper, Mather (1982) argued that it was not the freezing rate that caused the change in the spacing factor but the difference in degree of saturation.

Pigeon, Prévost and Simard (1985) continued the study described above by introducing two higher freezing rates, 4 and 6 °C/h, keeping all other parameters as before. They found a relationship for the critical spacing factor and the freezing rate, the L_{crit} being lower when the freezing rate was higher, see Figure 2.6.2.

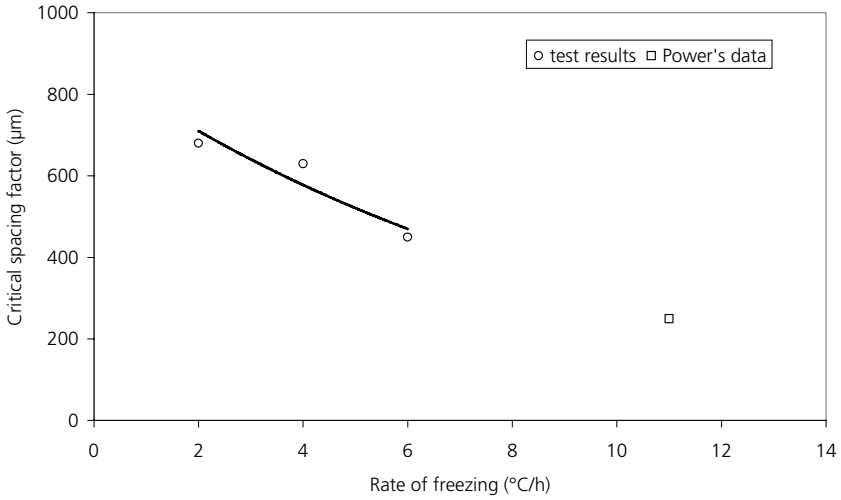

Figure 2.6.2. The influence of freezing rate on the critical spacing factor; Pigeon, Prévost and Simard (1985).

Marchand, Pleau and Gagné (1995) concluded in a literature study that there is a relationship between the critical spacing factor and the freezing rate. When the very 'moist' ASTM 666 is employed, it seems as if the critical spacing factor decreases with increasing rate, but this is not necessarily the case if some other test method is employed. They argued that the results of laboratory freeze/thaw tests involve a safety margin since the freezing rate used is normally considerably higher than in natural freeze/thaw.

The comment made by Mather (1982), mentioned above, is very relevant to all tests performed on the effect of freezing rate on damage. In the Pigeon/Lachance test, which is performed with un-isolated specimens in air, the moisture content was much lower than in the ASTM test performed in water at which the specimens gradually increase its moisture content. Probably the moisture content was also different for the different freezing rates in Pigeon/Lachance and Pigeon/Prévost/ Simard tests. Pigeon and colleagues base their calculation of the critical spacing on the entire air pore system assuming all air pores being empty. In reality, air-pores always take up some water, the wetter the test, the bigger portion of the air pore system is water-filled. The comparison of spacing factors, as was done, is therefore not correct. This is further discussed in Fagerlund (1992) where it is shown that in the case of non-moisture isolated tests all types of influence of the freezing rate have been reported; some authors claim that increased freezing rate is favourable, other researchers claim the opposite. This is because of the fact that different freeze-thaw cycles give different

possibility for the specimen to absorb or desorb water during the test. A freeze-thaw cycle, which makes big water absorption possible will generate large damage, while a 'drier' freeze-thaw cycle applied to the same material will generate little or no damage. The most important parameters for damage to occur were found to be the time in water during the cycle and the relation, time in water/time in air.

Jacobsen (1995) studied how the freezing rate influences salt frost scaling and the resonance frequency. He used the CDF-method in which the specimens had free access to sodium chloride solution during the entire test. He detected a slight tendency for a higher freezing rate to result in a larger decrease in the resonance frequency than a lower freezing rate. He agreed that the results are very much dependent on whether the specimens have been able, or not able to absorb the solution during testing.

This short literature review can be summarized as follows: Different tests performed of the effect of freezing rate on frost damage have given opposing results. The most plausible reason for this is that a change in the freezing rate normally also give a change in the moisture conditions during the test. Thus, the observed effect of freezing rate is instead mainly an effect of changed moisture condition. Most of the investigations indicate that increased freezing rate creates more damage. This can be explained by Powers' theory of hydraulic pressure but hardly by the other mechanisms. However, as said above, the observations might be incorrect. If so, the hydraulic pressure mechanism was not confirmed.

The importance of controlling the water content during studies of the effect of different characteristics of freeze-thaw cycles is clearly demonstrated.

2.6.2 Influence of lowest temperature and duration of freezing temperature

The influence of the lowest temperature on internal frost damage appears to have been little investigated. Marchand et al. (1995) point to a lack of relevant data but do not regard the lowest temperature reached to have any significant influence on the internal frost damage.

Pigeon and Pleau (1995) argue that, although the influence of the lowest temperature is debated, damage increases with decreased freezing temperature.

Schulson (1998) considers the kinetics of freezing to be more important than the magnitude of the temperature.

The influence of duration of the lowest temperature has gained little interest in research.

2.6.3 Low temperature calorimeter studies on ice formation and melting in cementitious materials

Low temperature calorimeter is a powerful tool for studies of ice formation and melting in materials, and therefore to obtain information of the destruction process when the material freezes. The amount of water melted at different temperature also makes it possible to determine the pore size distribution.

Pioneers in the field of studying cement-based materials with a low temperature scanning calorimeter were Bager, le Sage de Fontenay and Sellevold. A brief account of some of their work follows.

Le Sage de Fontenay and Sellevold (1980) tested saturated mature HCP (hardened cement paste) cured at room temperature and having w/c-ratio between 0.40 and 0.70, using a Calvet micro-calorimeter. The calorimeter is of type DSC (Differential Scanning Calorimeter). The authors found that insignificant amount of ice formed below -55°C. They observed three peaks in the heat flow curve during the freezing part of the experiments, namely at about -8°C, -23°C and -40°C, the magnitude of the peaks being a function of the w/c-ratio, see Figure 2.6.3. With an increase in the w/c-ratio, the last peak increased and the second peak decreased. They also found a change in freezing behaviour for w/c ratio equal to and below 0.50, the first peak did not appear for w/c-ratio 0.40 and were found to be small for w/c-ratio 0.50. This result was explained in terms of an inkbottle effect. A material with low w/c-ratio contains pores with narrow openings making ice nucleation impossible. Water in these pores will therefore freeze at lower temperature than that corresponding to their size. A material with higher w/c-ratio was believed to contain few or no such pores. It was found that melting occurred continuously from -55°C upwards, but that the larger part took place close to 0°C. The part of the evaporable water that froze ranged from 20% to 57% (w/c-ratio 0.40-0.70). The authors also tested the influence of different cooling rates, finding the amount of ice formed at a given temperature to not vary much. They also concluded that the Powers and Brownyard (1948) indirect method of determine the amount of freezable water by studies of volume increase in saturated specimens, could overestimate the ice quantity.

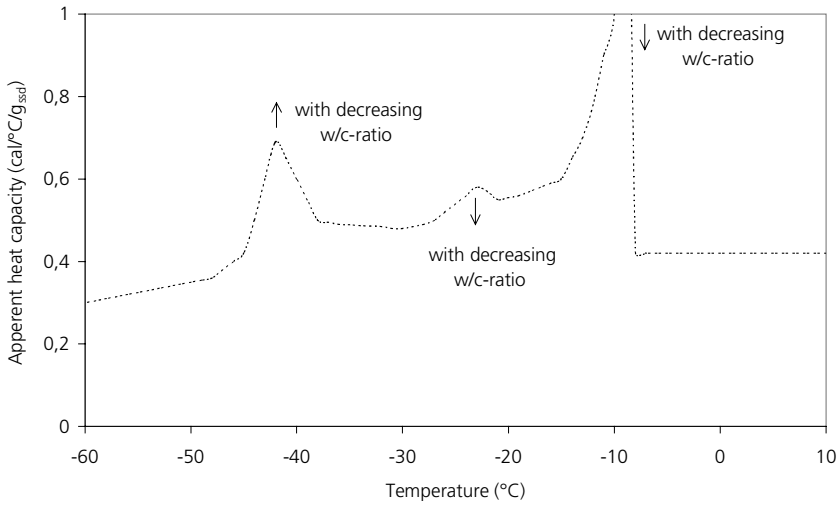

Figure 2.6.3. Typical heat flow from a saturated cement paste during freezing found by le Sage de Fontenay and Sellevold (1980).

Bager and Sellevold (1980a) extended the investigation to include steam-cured hardened cement pastes (HCP). Steam curing is known to create a coarser pore structure. This was confirmed since they found that 60 to 80% of the evaporable water was freezable and that most of it froze when the first ice formation was nucleated at a few degrees below 0°C, an expected result for a material with coarse pore structure. The non-frozen water content (g/g_{dry}) at a temperature of -55°C was found to be independent of the w/c-ratio which differed from the results from the former study when the amount of non-freezable water (g/g_{dry}) increased slightly with increasing w/c-ratio. In the same study the authors conditioned samples to different relative humidity (RH) and thereafter determined the amount of freezable water. The content of non-frozen water was found to decrease with a decrease in initial moisture content, no ice forming when the moisture content was below a 60% relative vapour pressure at 20°C.

Continuing their calorimetric experiments on cement paste, this time cured at room temperature with variable moisture content in the samples, Bager and Sellevold (1986a) found the initial freezing temperature to increase with an increase in moisture content. They also found that a moisture content corresponding to three monolayers was not freezable even at –55°C. For specimen containing freezable water, there was a slight increase in the amount of non-freezable water as the water content increased, as was found also for the steam cured specimens. There was also a slight increase in the content (g/g_{dry}) of non-freezable water with an increase in the

w/c-ratio for specimens conditioned at the same RH. On the basis of these findings the authors postulated that frost problems could not be expected in specimens containing less water than that corresponding to a relative vapour pressure of about 0.9.

In drying and re-saturating hardened cement pastes, Bager and Sellevold (1986b) found that drying caused a coarsening of the pore structure. Their explanation was collapse of pore walls caused by drying.

In a third work, Bager and Sellevold (1987) studied the effect of a much slower re-saturation of the HPC after pre-desorption to different vapour pressures (RH). They did not obtain any large differences in ice formation for differences in the rates of re-saturation. They also showed that the moisture history as a whole had a very large effect on the ice formation. The amount of non-freezable water in a specimen was found to decrease as the degree of previous drying increased. This had previously been observed by Vuorinen (1973) who tested big concrete specimens in a conduction calorimeter.

Bager and Sellevold (1980b) calculated the pore size distribution from the melting curve. The melting curve was used since it is free from supercooling. The method is principally the same as that described in Chapter 9 below, and which had also been used previously by other researchers. It is important to note that the calculation involves a considerable number of simplifications. Nevertheless this method of determination of pore size distribution is not inferior to other methods available. When pore size distributions based on the calorimeter test was compared with results of a mercury penetration test, the correlation between the two was found to be larger when the specimens were pre-treated in the same way.

Kaufmann (1999) constructed a DSC, which could be used to test four specimens (ϕ= 18 mm, l= 10 mm) simultaneously. The samples were placed with a flat side against the heat flow sensor, which was connected with a calorimetric block made of copper. The entire calorimeter was submerged in ethanol during the tests. The ethanol was gradually cooled and heated between –49°C and + 10°C. Cholesterol was successfully used as ice-nucleating agent, supercooling being almost absent. He found no peak at -25°C, and concluded that when this peak is found it is caused by supercooling, but it seems unlikely that the cholesterol should be able to seed that small pores. He also found no hysteresis between freezing and thawing, and almost no effect of drying. For specimens in which cholesterol was used, the freezing rate was found to have no influence on the supercooling, whereas without use of cholesterol an increase in supercooling was found as the freezing rate increased.

2.6.4 Studies using combined low temperature calorimeter and dilatometer

Verbeck and Klieger (1958) were the first to suggest and develop an instrument that made it possible to simultaneously measure ice formation and length change. An instrument of this type is excellent for studies of frost destruction mechanisms. Therefore, others have adopted the idea. Fagerlund (1973b) built an instrument according to the same principles. Later, the same type of measurements has been made by Kaufmann (1999), and Penttala, (1998, 1999). A condensed description of their work follows.

Verbeck and Klieger (1958) developed an equipment that could use quite large concrete specimens. It consisted of a liquid-tight metal container inside which there was a smaller metal container holding the sample. Between the two containers was heat insulation. Heat flow over the insulation, being proportional to the temperature difference over the insulation, was measured by thermocouples. Length changes were measured by strain gauges.

The instrument was placed in a brine bath at a temperature of -30°F (~-34°C). 10 cycles were performed. For thawing between each cycle, the specimen was placed in a water bath. Measurements were made during the first and tenth cycle. The authors found that the higher the water/cement-ratio was, the higher were the water absorption in the bath and the expansion during the test. They also found that specimens that had smaller increase in freezable water at thawing in the bath also had smaller increase in expansion. They also found the amount of freezable water decreasing with increasing age of the sample.

The authors also let a specimen absorb calcium chloride for seven days, measuring the effect this had on the amount of freezable water. The decrease in freezable water that occurred was proposed to be due to two factors; water moving from the specimen to the more concentrated outer solution during the pre-storage in salt water before the test, and at the same time calcium chloride diffusing into the specimen. Both factors were claimed to increase the concentration of the pore water, and thereby decrease the freezing point and the amount of freezable water.

Measurement of expansion (water stored samples) showed that specimens without air-entrainment continued to expand during the entire cooling, but that specimens in which there was air-entrainment showed contraction.

Fagerlund (1973b) used a combined calorimeter/dilatometer built on the same priciples as the Verbeck and Klieger equipment. It made use of smaller specimens (3·3·12 cm) and was applied not only to cement-based material like mortar and cement paste, but also to other types of building materials; clay brick, cellular concrete, ceramics. Many degrees of saturation were investigated for each material. Attempts were made to verify the hydraulic pressure theory by using measured data for degree

of saturation, expansion rate (m/m·s), and ice formation rate ($m^3/m^3 \cdot s$) in the expression for hydraulic pressure, Eq. 2.2.6. The author claimed that he could find some indications that hydraulic pressure might be the reason for expansion. It was, however pointed out that the verification is difficult since it is unknown how permeability changes with the amount of ice formed.

Penttala (1998) derived a theory based on thermodynamics in which it was possible to calculate the pore pressure by simply measuring the relative humidity and the temperature in the specimen chamber during freezing. The theory was then tested by measuring ice-formation, RH, and strain simultaneously, using a low temperature calorimeter of the same type as used by Bager and his colleagues, and used in the work presented in Chapter 9. Length changes were measured by strain gauges mounted on the small specimen. Special humidity gauges measured RH in the calorimeter cell. The experiments were conducted on mortar, which had been designed as normal concrete but without the 2-16 mm fraction.

When the first expansion occurred, the relative humidity (RH) rose due to the over-pressure caused by ice pressing water out of the specimen. When the temperature decreased ice-bodies formed in the specimen drew the water back into the specimen, RH thus decreasing. Penttala found the measurements to agree with the thermodynamic theory down to a temperature of -15-(-20)°C. Deviations below that temperature could be due to ice that had left the specimen causing RH in the sample holder not to reflect the state of ice and water pressure in the specimen.

After the first expansion, the length change in the air-entrained and the non-air-entrained specimens differed, a non-air-entrained specimen continuing to expand, whereas an air-entrained specimen continuing to contract. This contraction was attributed to the under-pressure in the smaller pores, caused by suction from the larger ice-filled pores, which the calculation of the pore pressure from the RH-measurements also showed. The contribution to shrinkage by water movement from the gel pores was found to increase as the temperature decreased.

Penttala (1999) also studied the influence of chlorides in the pore water on the thermodynamic theory both theoretically and by measurements. The theory was only applied to temperatures down to approximately -15°C, since no consideration was taken of the surface forces involved. Among other things, he found large dilation of the mortar, which had been exposed to sodium chloride. This was thought to depend on the larger amount of evaporable water in these specimens.

2.7 Conclusions

Many destruction mechanisms for internal frost damage have been suggested. None of these has actually been satisfactory verified. When studies have been made of factors that might affect destruction, like freezing rate or minimum temperature, other factors that also might have an effect, like the moisture content, have also varied. Therefore, it is not possible to tell which parameter has had the biggest influence. Verification of destruction mechanisms ought to be based on systematic investigations, at which one parameter at a time is investigated. A promising approach is to combine measurements of ice formation and melting with measurements of the specimen response in terms of expansion and contraction. Preferably these measurements should be made simultaneously.

3 Aim and layout of the study

3.1 Aim

The aim of the study was to identify mechanisms acting at internal frost destruction of concrete. By 'internal frost destruction' is meant damage caused inside concrete that is moisture insulated from the surroundings, i.e. when no moisture exchange with the surroundings is possible during freeze-thaw. Thus, the aim was *not* to investigate destruction processes (scaling) taking place at the surface of a concrete exposed to water or salt solution.

The aim should be reached by *experimental work* at which different parameters, that are supposed to influence destruction, such as concrete quality, moisture content, freezing rate, and duration of freezing temperature were varied independently of each other. The effect of these parameters on formation of ice, and on the behaviour of the concrete during freeze-thaw should be monitored. In this way it was imagined that the individual effect of each fundamental parameter could be identified.

The aim was to use the experimental results to test different existing destruction theories like the hydraulic pressure theory and the microscopic ice lens theory. The aim was not to build a quantitative model for internal frost destruction.

3.2 Layout of the experimental work

Three types of experimental studies were performed:

3.2.1 Study 1: Single-cycle freeze-thaw of moisture insulated specimens; Chapter 4-8

The primary aim of this study was to measure the response of moisture preconditioned specimens when exposed to single freeze-thaw of varying type as regards rate of freezing, deepest freezing temperature, and duration of freezing temperatures. By 'response' is meant length change versus temperature (contraction or dilation), and change in dynamic E-modulus.

The study is based on the assumption that one single freeze-thaw is sufficient to damage concrete provided the moisture content is above a critical value, which is individual for each concrete.

A secondary aim was to see if destruction changes when the pores contain salt solution. Therefore, in a limited study, the effect of long-term storage in NaCl-solution was investigated by the same method as in the main study.

3.2.2 Study 2: Investigation of freezable and non-freezable water; Chapter 9

In this study the freezing-melting process of pore water was investigated. The specimens were subjected to the same moisture pre-conditioning as was used in Study 1, and exposed to about the same freeze-thaw cycles as in Study 1.

The aim was to obtain information on the destruction process by combining the length change temperature curves from Study 1, with the ice formation and ice melting curves from Study 2. For example, if freezing temperature is kept constant, and as a consequence of this length change has stopped, this does not necessarily mean that ice formation does not take place, since heat might leave the specimen at the same rate as heat is generated by freezing. But combined with calorimeter determination, showing that no ice is formed, this possibility could be rejected.

Theoretically there exist relationships between the water sorption isotherms (desorption, adsorption and scanning) at a given relative humidity and the amount of non-freezable water at a corresponding temperature. This relationship is not unambiguous, however, since it depends on the equilibrium between the different phases in frozen concrete, ice, liquid water, water vapour. This equilibrium cannot be easily predicted due to the very complex arrangement of the different phases inside the pore system of concrete, and due to pressures developing in these phases when water freezes.

In order to find out how the relationships between sorption and freezing look like, determinations were made of sorption isotherms. They were compared with calculated isotherms from the calorimeter experiments.

3.2.3 Combined dilatometry and calorimetry: Chapter 11

A drawback when combining dilation measurements in Study 1 with measurements of freezing and thawing of water in Study 2 is that one cannot be sure that the specimens used for the two determinations are identical. The water content might differ somewhat, and so might the air-pore distribution and the supercooling. In order to overcome these problems, measurements were also performed in a combined dilatometer-calorimeter designed by Lindmark and further developed and investigated by Fridh, Lindmark, Wadsö (2003). In this ice formation is measured simultaneously with measurement of length change. Therefore it is an excellent instrument for studying frost destruction mechanisms. Due to limited time it was not possible to make a full study of all variables used in Study 1. A number of representative tests were made.

3.3 Concrete types and specimens

3.3.1 Concrete

Ten 'micro-concretes' were produced and used for all studies. A micro-concrete is defined as a concrete in which the sieve curve of aggregate, although having the same shape as a normal sieve curve, is displaced in the direction of smaller size. The stone/sand fractions used were 50% 0-3 mm (natural gravel) and 50% 4-8 mm (granite & diabase).

Concrete with three water-cement ratio (0.60, 0.45 and 0.40) and three air-content levels, no air entrainment, nominal 4% and nominal 6% air content, were produced. For w/c-ratio 0.45, an additional concrete with 10% air was made. The reason was that this high air content might represent a concrete with a collapsed air-pore system forming continuous water absorbing air-pore 'channels'. This type of pore system was not achieved, however. The real air contents differed somewhat from the nominal aimed at, see APPENDIX to Chapter 3.

The cement was a low-alkali ($K_2O+Na_2O\approx0.6\%$) sulphate-resistant ($C_3A\approx2\%$) Portland cement. Neutralized vinsol-resin was used as air-entraining agent. The mix compositions, sieve curves, strength levels and air contents are shown in APPENDIX to Chapter 3.

3.3.2 Production of specimens

After cement and aggregate had been mixed, water and air-entraining agent were added and were mixed with the other ingredients for about 3 minutes. For each concrete type, three cubes (100x100x100 mm) and three large blocks (400x400x150 mm) were cast. The air content and the slump were determined for each mix. The cubes were used for determining the strength after 28 days. During the first twenty-four hours prior to de-moulding the top surface of the cubes and moulds were covered with wet cloths and plastic foil. After being de-moulded the blocks were stored in water for a week, after which all the specimens for freeze-thaw testing or determination of freezable water were sawn or drilled out from the blocks. Specimens of three different kinds were produced; (1) prisms 20x20x170 mm used for dilation testing and sorption isotherms determinations (Chapter 4-9), (2) cylinders diameter 11 mm, length 60 mm used for freezable water (Chapter 9).

Before sawing or drilling was begun, the outer part (2 cm) of the block was sawn off to prevent the mould surface from having any influence. All the samples were taken in a direction perpendicular to the casting direction so as to avoid any important differences within the samples caused by possible separation of the fresh concrete.

The specimens were then stored in water for 2-3 months, after which they were placed in their respective storing liquid; either lime-saturated water or a 2%, a 4.5% or an 11% sodium chloride solution.

3.3.3 Overview of all experiments

The aim described in paragraph 3.1 is very wide. Therefore, a large experimental program had to be performed. An overall view of the experimental work is presented in APPENDIX to Chapter 3.

4 Freezing and thawing experiments - methods, variables and materials

4.1 Background and aim

The details in the destructive mechanisms acting during freeze/thaw have to be clarified in order that one shall understand how different material characteristics influence frost resistance. Such understanding is needed in order to make it possible to design materials with a sufficiently high probability of withstanding the actual external climatic conditions.

As described in the literature review of frost damage mechanisms presented in Chapter 2, there are two groups of factors of importance for internal frost damage; those connected with the *characteristics of the environment* in which the material is situated, and those connected with the *characteristics of the material itself*. The characteristics of the *environment* include such parameters as the freezing rate, the lowest temperature, the duration of freezing temperatures, and the moisture conditions of the surroundings. All these parameters affect the inner moisture-temperature field before and during freeze/thaw in the material. *Material parameters* that are of interest are the degree of saturation, the porosity and pore size distribution, the air pore structure and air content, the strength, and the permeability.

The aim of the studies presented in Chapters 5-8 was to obtain results that make it possible to better understand frost destruction mechanisms in different types of concrete. Therefore, freeze-thaw experiments were performed in which a number of different environmental and material characteristics were varied *independently of each other*. The impact of frost on the concrete was characterised in terms of changes in length and resonance frequency (a measure of the dynamic E-modulus) of the specimens.

In order to avoid influence from varying moisture conditions during the tests, all of these were performed with moisture sealed specimens that had been adjusted to different moisture levels before the test started, but not changed during the test.

The aim was also to combine the observed length change curves with supplementary calorimeter studies of ice formation and melting in order to get a better understanding of destruction mechanisms. These calorimeter studies are presented in Chapter 9.

Additional tests aiming at understanding the destruction mechanisms are presented in Chapter 11. In these experiments, length change curves were combined with *calorimeter* studies of ice formation and melting.

NOTE: The same materials, and the same moisture conditions, were used in these calorimeter experiments as in the length change experiments presented in Chapter 5-8. The temperature conditions during freeze/thaw differ somewhat, however.

4.2 Test variables

4.2.1 Concrete types

All 10 concrete types described in Chapter 3 and in APPENDIX to Chapter 3 were used for the experiments described in Chapters 4-9. Normally, two separate specimens of each concrete quality were used for each variation in moisture and temperature cycle. For more detailed information of specimens used for different tests, see APPENDIX to Chapter 3, paragraph A3.1.

The concrete had water-cement ratio within the span 0.40 to 0.60 and air contents within the following span: natural air (about 2.5%) to 10%. Therefore, most concrete types that are used in practice for structures exposed to internal frost attack were utilized in the investigations.

4.2.2 Moisture level in specimens

As described in Chapter 2, the moisture content in the concrete seems to be the most fundamental parameter affecting internal frost resistance. Therefore, for each concrete type, 3 different types of moisture level were investigated. These were achieved by different techniques for moisture pre-conditioning:

- *'Natural' or 'virgin'.*
  Moisture level obtained after very long time of water storage of never-dried specimens (3-4 years).
- *Vacuum saturated.*
  Moisture level obtained after vacuum saturation of pre-dried, previously long-term water-stored specimens (this caused big damage and was therefore only used in one test series – No 2).
- *'Adjusted degree of saturation'*
  Moisture level adjusted to be below or above the expected critical water content. The water content was so high that always a certain fraction of the air-pore system was water-filled. The moisture content was obtained by drying specimens that had been saturated as described above for 'vacuum saturated' specimens.

The pre-conditioning is further described in paragraph 4.5 and in Chapters 5-8 describing the individual Test series.

4.2.3 Temperature cycles

Different destruction mechanisms predict different effects of the shape of the temperature cycle; like effects of the rate of freezing, and the effect of the temperature level at which temperature is kept constant for varying length of time. For each moisture level described above the following alternative temperature cycles were therefore employed.

- *Different freezing-thawing rates*: Two different freezing-thawing rates down to -23°C were used (by "freezing-thawing rate" is meant the rate of temperature change of air in the climate chamber).
  (1) 'normal cycle', 3.6°C/h
  (2) 'rapid cycle', 7.8°C/h
- *Different lowest freezing temperature*: Temperature of air in the climate chamber during freezing and during thawing (normal freezing rate) was kept constant for 3 hours, either at –15°C, or at –30°C. Thus, besides the effect of the temperature level itself; also the effect of duration of freezing temperatures was studied.
- *Different lowest freezing temperature combined with long duration of this*: During the freezing part of the cycle, the temperature of air in the climate chamber (normal freezing rate) was held constant for 12 hours, either at –15°C, or at –30°C.

The temperature cycles are further described in paragraphs 5.2, 6.2 and 7.2.

4.2.4 Salt concentration of pore water

The primary aim of this research work was to study internal frost damage of moisture sealed concrete, and not to study salt-frost scaling occurring when the concrete is frozen in contact with an outer salt solution, conditions during which it can also gradually absorb solution. Therefore, the main studies were made with concrete containing ordinary salt-free water in its pore system as described in 'Moisture levels in specimens' above. For understanding internal frost damage it is of interest, however, to find out if a sealed concrete behaves differently when it contains salt solution in the pores. Therefore, besides the long-term storage in pure water, some specimens were also stored for 4 years in 2%, 4.5% and 11% NaCl-solution. The thin specimens combined with the long storage made the concentration of pore solution to be about the same as in the outer solution.

4.3 Test series

8 Test series were performed.

Test series 1-3: Investigations of the effect of freezing rate. The results are presented in Chapter 5.

- *Test series 1:* Specimens with natural water content; paragraph 5.3.
- *Test series 2:* Vacuum saturated specimens; paragraph 5.4.
- *Test series 3:* Specimens with adjusted moisture content between natural and saturation; paragraph 5.5.

Test series 4-5: Investigations of the effect of lowest freezing temperature. The results are presented in Chapter 6.

- *Test series 4:* Specimens with natural water content; paragraph 6.3.
- *Test series 5:* Specimens with adjusted moisture content between natural and saturation; paragraph 6.4.

Test series 6-7: Investigations of the effect of lowest freezing temperature combined with long duration of low temperature. The results are presented in Chapter 7.

- *Test series 6:* Specimens with natural water content; paragraph 7.3.
- *Test series 7:* Specimens with adjusted moisture content between natural and saturation; paragraph 7.4.

Test series 8: Investigations of the effect of salt concentration of pore water. The results are presented in Chapter 8.

- *Test series 8:* Specimens with natural content of NaCl-solutions of different concentrations; paragraph 8.3.

4.4 Experimental technique

4.4.1 Freeze-thaw

The response of specimens to internal frost damage was studied by exposing moisture insulated specimens to single freeze-thaw cycles of different characteristics as regards freezing rate, lowest temperature, and duration of lowest temperature.

The specimen size was 20x20x170 mm. The specimens were sawn from bigger blocks as described in Chapter 3. A metal stud -see Figure 4.4.1- was glued at each end for holding the specimen in the measuring frame. The stud was designed so that only a very small contact area between specimen and support in the frame was obtained.

Before freeze-thaw, the specimen was pre-conditioned so that a certain moisture condition (or a certain salt concentration of pore water) was reached. The exact pre-conditioning method was different for different Test series and specimens. The pre-conditioning techniques are described below in paragraph 4.5 and in connection with presentation of results from the different Test series. During the freeze-thaw cycle the specimen was wrapped in polyethylene foil in order to keep the moisture content constant during the cycle.

Before moisture insulation and freeze-thaw, the specimen was weighed, and the resonance frequency at transverse vibration was determined. The weight and resonance frequency were also determined after terminated freeze-thaw.

A thermocouple (type T9) was placed against an outer specimen surface. The thermocouple was heat insulated from the surrounding air. It would have been better to place the thermocouple in the centre of the specimen in a drilled hole. For practical reasons, due to the risk of fracturing the thin specimen, this was not possible. The difference between the measured temperature and the centre temperature was estimated to be about 0.4°C.

The specimen was placed in vertical position in a measuring frame made of INVAR which is a metal with very low thermal movement. The studs were used for supporting the specimen on the bottom plate of the frame and for connecting the specimen to the LVDT gauge (Linear Variable Differential Transformer) used for monitoring the length changes of the specimen during the freeze-thaw cycle.
The frame had room for 6 specimens. It is shown in Figure 4.4.1.

The frame was placed in a climate chamber. The air temperature cycle in the chamber is very precise and could be pre-determined within a wide range. The actual temperature cycle was different in different Test series. The cycles used are shown in Figure 5.2.4, Figure 6.2.2 and Figure 7.2.2.

Figure 4.4.1. The test set-up for measurement of changes in length.

The length and temperature changes in the specimens during the freeze-thaw test were continuously monitored and stored for further analysis. The length change curves shown below in Chapter 5-8 are directly taken from the LVDT-gauges without any corrections for thermal movements of the frame and other components in the device. Thus, they give the total length change of the frame, the studs, the LVDT-sensor and the specimen. It was sufficient to verify that the test set-up itself had a linear length change-temperature curve, so that if any non-linear movements were detected, they would emanate from the specimen. In Figure 4.4.2 and Figure 4.4.3 length change measurements made in the test frame on metal samples are shown. It can be seen that the thermal movement of the frame is quite linear.

Since the specimen was thin, and the temperature gradient therefore small, freeze-thaw took place almost simultaneously within the entire specimen volume. Thus, the length change monitored, being an average for the whole specimen, can be assumed to be representative for all parts of the specimen.

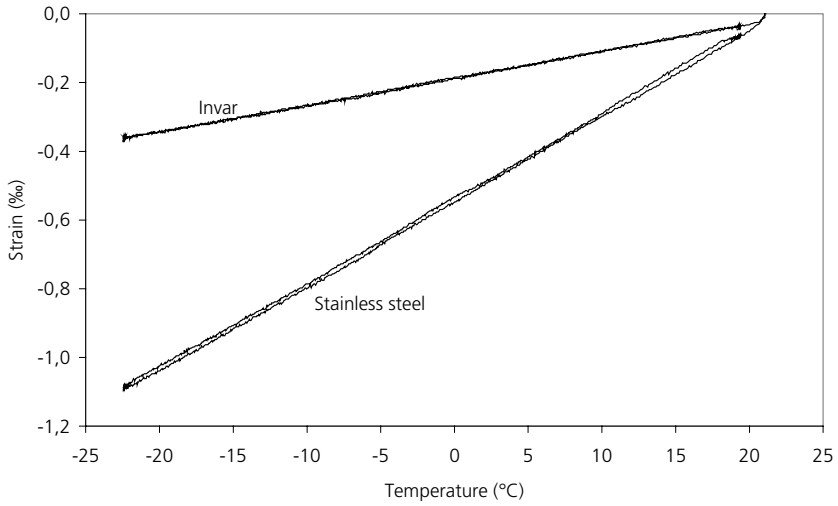

Figure 4.4.2. Results of length change versus temperature of stainless steel and Invar samples during the 'normal' cycle (3,6 °C/h) investigated in the test frame used in Test series 1-3 and 8.

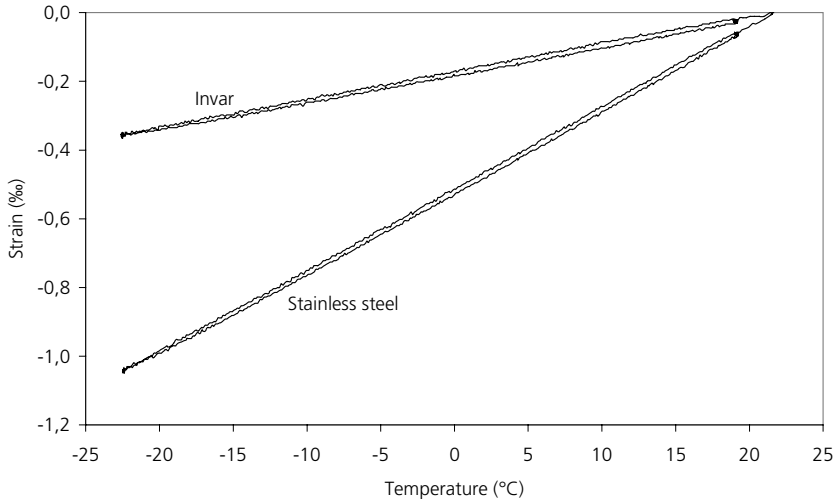

Figure 4.4.3. Results of length change versus temperature of stainless steel and Invar samples during the 'rapid' cycle (7.8 °C/h) investigated in the test frame used in Test series 1 and 3.

4.4.2 Interpretation of length change curves. Detection of damage.

The length-temperature curves obtained during the freeze-thaw cycle reflect processes that are going on inside the concrete during freeze-thaw. Sometimes -at low moisture contents or high air contents- specimens contract. In other cases -at moisture contents above the critical- the specimens expand. The shape of the curves might also depend on the temperature cycle. The curves might be used for analyses of the destruction mechanism. Qualitative analyses are made below in Chapter 5-8 for each Test series.

Damage was detected by two methods; (1) measurement of dilation (expansion), (2) measurement of change in resonance frequency at transverse vibration. The methods are described below.

(1) Dilation

Three types of dilation were used in the evaluation: Definitions of these are shown in Figure 4.4.4.

(i) Permanent dilation after thawing to +5°C.

(ii) Rapid dilation when supercooling terminates at some degrees below 0°C, whereby a considerable amount of ice is formed almost instantaneously.

(iii) Dilation at -20°C. This is defined as the specimen length at -20°C minus the thermal contraction at that temperature had no ice formation taken place. The thermal contraction is defined by an extrapolated contraction of the unfrozen specimen within the range +10°C to 0°C.

Permanent dilation indicates substantial internal micro-cracking, and loss of cohesion of the concrete. Rapid dilation when supercooling terminates indicates the occurrence of hydraulic pressure as a consequence of big and rapid ice formation. Dilation of the frozen concrete at -20°C indicates that internal pressure is built up as a consequence of ice formation by some mechanism. 'Negative dilation', i.e. contraction, of the frozen concrete indicates the presence of shrinkage stresses, probably as a consequence of drying out by transport of unfrozen water to ice in capillaries or air pores, causing microscopic ice lens formation.

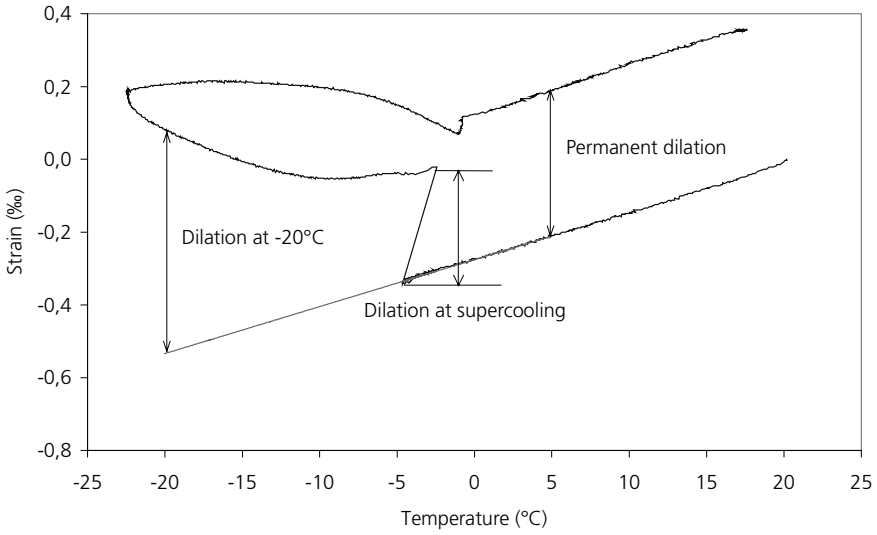

Figure 4.4.4 Definition of dilation.

(2) Change in resonance frequency at transverse vibration

The resonance frequency at transverse vibration of a specimen is very sensitive to loss in cohesion and micro-cracking. Therefore, this method was used for detecting damage caused by freeze-thaw. Theoretically, if there is no mass loss during freezing, as in the case at moisture sealed freeze-thaw, the dynamic E-modulus is proportional to the resonance frequency in square.

The resonance frequency was determined before and after a test in the length measurement frame. The measuring equipment employed was of type Grindosonic. The specimen is tapped by a hammer which makes the specimen vibrate freely by its natural frequency. This is recorded by an accelerometer; Figure 4.4.5. The sample was placed on a thick foam-rubber slab to ensure free oscillation. In this report the result is presented as the squared ratio of the resonance frequency after freeze-thaw, to that before freeze-thaw.

Immediately before each measurement the weight of the specimen was determined.

Figure 4.4.5 Equipment for measuring the resonance frequency.

4.5 Moisture preconditioning of the samples

4.5.1 Specimens and pre-storage before freeze-thaw

The specimens used for freeze-thaw testing (20x20x170 mm prisms) were sawn out of larger blocks a week after casting, and were thereafter placed in lime-saturated water. Before freeze-thaw testing started the samples had been stored in lime-saturated water for 3 to 4 years.

The specimens used in Test series 8 were long-term stored in NaCl-solution of different concentration.

4.5.2 Definition of moisture content

The moisture content is defined both as degree of saturation (S, m^3/m^3), and as moisture ratio (u, kg/kg). They are defined by the following equations:

$$S = \frac{w_e}{V_p} \qquad \text{Eq. 4.5.1}$$

$$u = \frac{(Q_{test} - Q_d)}{Q_d} \qquad \text{Eq. 4.5.2}$$

Where w_e (m^3) is the total amount of evaporable water leaving the specimen when it is dried at +105 ºC, or over silica gel at room temperature, V_p (m^3) is the total pore volume including all air pores, Q_{test} (kg) is the weight of the wet specimen during the freeze-thaw test (kg), Q_d (kg) is the weight of the completely dry specimen, dried at +105°C or at room temperature over silica gel, see below (kg). The values of S and u will be somewhat different depending on the drying procedure. This is discussed below.

Different water contents were used at different freeze-thaw test. The method of pre-conditioning the specimens to these moisture contents varied in the way shown below.

4.5.3 Pre-conditioning procedure and moisture content

A: Specimens with natural moisture content (virgin specimens); Test series 1, 4 and 6

For each type of temperature cycle, two specimens of the same concrete were taken out of the bath and weighed just prior to the first freeze-thaw test, $Q_{test,1}$ (kg). No further moisture conditioning was made.

After terminated freeze-thaw cycle the specimen was either damaged or undamaged as judged by dilation and resonance frequency. All specimens with natural air

content suffered so much damage already after the first test that they could not be used for further experiments.

Damaged specimens

A *damaged* specimen was dried at +105°C and weighed, $Q_{d,105}$ (kg). Then, it was vacuum-saturated and weighed, $Q_{s,105}$, in order to obtain the pore volume V_p (including some pore volume change caused by freezing.) Degree of saturation is calculated by:

$$S_A = \frac{Q_{test,1} - Q_{d,105}}{Q_{s,105} - Q_{d,105}} \qquad \text{Eq. 4.5.3}$$

The symbol S_A is used for degrees of saturation based on the weights obtained after drying at +105°C.

Note 1: The weight Q_{test} could be a bit different after terminated test than before due to some small losses of water during the test by condensation on the plastic foil in which the specimen is wrapped during the test. The weight before the test was considered most relevant, and it was therefore used in the calculations.

Note 2: In some cases, for specimens containing only natural air, the specimen weight during the test $Q_{test,1}$ was higher than the saturated weight, $Q_{s,105}$, resulting in the calculated degree of saturation being higher than 1, which is impossible. The reason is that it was not possible to completely re-saturate all pores in specimens that had been dried at +105°C before it was vacuum-saturated. This problem is further discussed below.

Damaged specimen tested at the low freezing rate (specimens with natural air) were used to investigate the carbonation depth since it was suspected that some carbonation might have taken place, despite the fact that the specimens had been stored in lime-saturated water. The carbonation depth was measured by splitting the specimens and thereafter spraying phenolphthalein on the fracture surface. Hence, the samples were destroyed and unfortunately, dry weights could not be obtained beforehand. Therefore, the exact degree of saturation could not be obtained for these specimens. There is good reason to believe, however, that it was very similar to companion specimens of the same concrete quality tested at rapid freezing. No sign of carbonation was found in any of the investigated specimens.

The moisture ratio of the specimen is calculated by Eq. 4.5.2.

Undamaged specimens

An *undamaged* specimen was normally used for further testing in another Test series. Therefore, it was not dried at +105°C after the first test, but instead dried at room temperature over silica gel and carbon dioxide absorbent in the manner described below. After it had been freeze-thaw tested once again in one of Test series 2, 3, 5 or 7, the specimen was finally dried at +105°C, followed by vacuum saturation. Thus, both the values $Q_{d,105}$ and $Q_{s,105}$ were finally obtained. Thereafter, the degree of saturation S_A during the first test could be calculated by Eq. 4.5.3.

It is also possible to calculate a value of the degree of saturation S_B according to Eq. 4.5.5 for these specimens. The two values of S often differ somewhat, S_A often being a bit higher. The reason is described below.

B: Specimens with 'adjusted degree of saturation'; Test series 3, 5 and 7

If a specimen was clearly undamaged after the test in Test series 1, 4 or 6 with natural water content, it was normally used again in a *second test* in Test series 3, 5 or 7 with the same temperature cycle, although with an adjusted degree of saturation higher than natural saturation. For specified degrees of saturation to be achieved, samples were first dried for two months in a box containing silica gel and a carbon dioxide absorbent, so that the dry weight $Q_{d,sg}$ (kg) could be obtained. The drying climate corresponds to a relative humidity of 6%. This type of drying was used in efforts to avoid destruction of the internal structure due to heating of the material. After drying, samples were vacuum-saturated with water and were weighed, to obtain the saturated weight $Q_{s,sg}$ (kg).

The specimen weight to be used during the new freeze-thaw test depends on the degree of saturation, S, aimed at. This weight $Q_{test,2}$ was calculated by the following approximate equation:

$$Q_{test,2} = S\left(Q_{s,sg} - Q_{d,sg}\right) + Q_{d,sg} \qquad \text{Eq. 4.5.4}$$

For adjusting the saturated specimen to the desired degree of saturation it was dried at +50°C to obtain the desired weight. When drying was completed, the specimen was wrapped in plastic foil that was sealed by tape. Thereafter it was placed in a plastic bag sealed to be airtight. To achieve as homogenous moisture content as possible the specimens were stored for at least a week before the new freeze-thaw test.

The temporarily unsealed specimen was weighed prior to the new test. This weight, $Q_{test,2,a}$ (kg), might be a bit different from the desired value according to Eq. 4.5.4. It was used to calculate the actual degree of saturation during the second freeze-thaw test.

After terminated freeze-thaw testing, the specimen was first dried at +105°C, $Q_{d,105}$ (kg) and thereafter vacuum-saturated with water and weighed, $Q_{s,105}$ (kg). The degree of saturation S_A was calculated by Eq. 4.5.3.

The value S_A is often a bit too high, however, for the following reason. The vacuum-saturated weight obtained after drying over silica gel $Q_{s,sg}$ was normally found to be somewhat higher than the value obtained after drying at +105°C, $Q_{s,105}$. The reason for this has not been clarified. One possible explanation is that drying at +105°C creates micro-structural changes ('structural collapse') that makes it difficult, or even impossible, to re-saturate the material completely also when vacuum is used.

This means that the pore volume is underestimated and the degree of saturation therefore overestimated when calculation is made by Eq. 4.5.3. An alternative, which probably gives a more correct value, is to base the calculation of degree of saturation on the silica gel dried weight. This value is called S_B.

$$S_B = \frac{Q_{test} - Q_{d,105}}{Q_{s,sg} - Q_{d,105}} \qquad \text{Eq. 4.5.5}$$

In the presentation of test results the value S_B is normally used.

C: Vacuum saturated specimens; Test series 2

One Test series (Nr 2) was performed with vacuum saturated specimens. Before vacuum treatment the specimens were pre-dried at +105°C. By definition S=1.

D: Salt water stored specimens; Test series 8

The specimens were taken directly from the saline bath in which they had been stored for 4 years. They were treated in exactly the same manner as the specimens for Test series 1. The degree of saturation S_A was calculated by Eq. 4.5.3. This involves a certain error since the density of the saline pore water is somewhat higher than for pure water, which gives a certain overestimation of the volume of pore solution. Besides, when the specimen is dried in order to obtain the dry weight some salt is deposited in the pores increasing the dry weight. This gives an underestimation of the pore volume. These errors are neglected in calculation of S_A.

5 Freezing and thawing experiments - Influence of the freezing rate

5.1 Introduction

The hydraulic pressure theory, Powers (1945), (1949) (see Chapter 2), explains internal frost destruction in terms of water pressure (hydraulic pressure) arising when ice is formed in the capillaries, and excess water is expelled from these into the surrounding cement paste. The reason is that when water is transformed into ice, there is insufficient space in the pores where freezing takes place, due to the 9% volume expansion that occurs. When the hydraulic pressure exceeds the tensile strength of the material, damage to the material takes place.

The magnitude of the hydraulic pressure depends upon the degree of saturation, the permeability of the material, and the rate of ice formation. The latter increases with increasing rate of lowering the concrete temperature. The rate of temperature lowering is called the 'freezing rate'. According to Powers' theory, a rapid freezing rate, is more dangerous than a slow, since it leads to a higher rate of ice formation.

Also the other major destruction mechanism suggested, the microscopic ice lens growth mechanism, Powers and Helmuth (1953), is theoretically depending on the freezing rate, a slower rate providing a longer time for ice lens growth to occur. This is further discussed in Chapter 2 and 7.

The effect of freezing rate has been investigated previously, but as pointed out in Fagerlund (1992), most of these experiments have been made by 'open' freeze-thaw where the specimen has had the possibility to absorb or desorb water during the test. Therefore, no unambiguous results have been found. Some researchers, using very 'moist' tests, have found that a slow freezing is more harmful, other researchers, using 'dry' tests, have found the opposite. The reason is that the degree of saturation reached during the test depends on the way this is performed. Tests giving high moisture levels, like when the specimen is slowly frozen and thawed in water, give big destruction, while tests in which the specimen is rapidly frozen in air and rapidly thawed in air or water give small water uptake and small destruction. In a few tests performed with specimen that were moisture isolated the freezing rate is of marginal importance. No systematic investigations of the freezing rate has however been made.

In order to find out how the freezing rate itself, uninfluenced by other factors, affects the destruction, moisture isolated specimens of different concrete qualities, i.e. with different permeability and strength, and with different moisture content were exposed to different freezing rates.

5.2 Experimental technique and variables

Two freezing rates of air in the freezing cabinet were used, 3.6°C/h and 7.8°C/h. The lowest temperature was -23°C, that temperature being maintained for a duration of three hours before thawing started with the same rate of temperature change as for freezing. The freeze-thaw cycle for air in the climate chamber is shown in Figure 5.2.4.

It was a certain disadvantage that the two cycles necessarily differed in the duration of the sub-zero temperature involved (9h 15 min for 7.8°C/h and 15h 35 min for 3.6°C/h), see Figure 5.2.4. The damage which a subzero temperature produces is probably a combination of both the freezing rate and the duration of the sub-zero temperature. This could not be avoided, however. The isolated effect of duration of freezing could be judged by comparing results from Test series 4 with Test series 6, or Test series 5 with Test series 7; these Test series are described in Chapters 6 and 7.

All tests were performed in the test rig described in paragraph 4.4.1 and shown in Figure 4.4.1.

The pre-treatment of specimens in the Test series 1, 2 and 3 is shown graphically in Figure 5.2.1-5.2.3. The pre-treatment is also described in detail in paragraph 4.5.3.

In *Test* series *1* (natural moisture content) 20 specimens were tested for each rate of freezing.

In *Test series 3* (adjusted degree of saturation) 12 undamaged specimens from test series 1 were used for testing with the 'normal cycle'. Besides, 12 previously untested specimens were used for rapid freezing.

Two specimens for each intended degree of saturation were tested. The real degree of saturation differed a bit from the intended, which is of no significance since the absolute value of this is not important in this investigation. The degrees of saturation reached in the specimens are shown in Table A5.1, A5.3 and A5.4 in APPENDIX to Chapter 5.

In *Test series 2* (vacuum-saturated specimens) 12 undamaged specimens from test series 1 were used.

Air contents for different concrete types given below in tables and figures refer to the 'nominal' air content. The real air content of the fresh concrete is given in APPENDIX to Chapter 3.

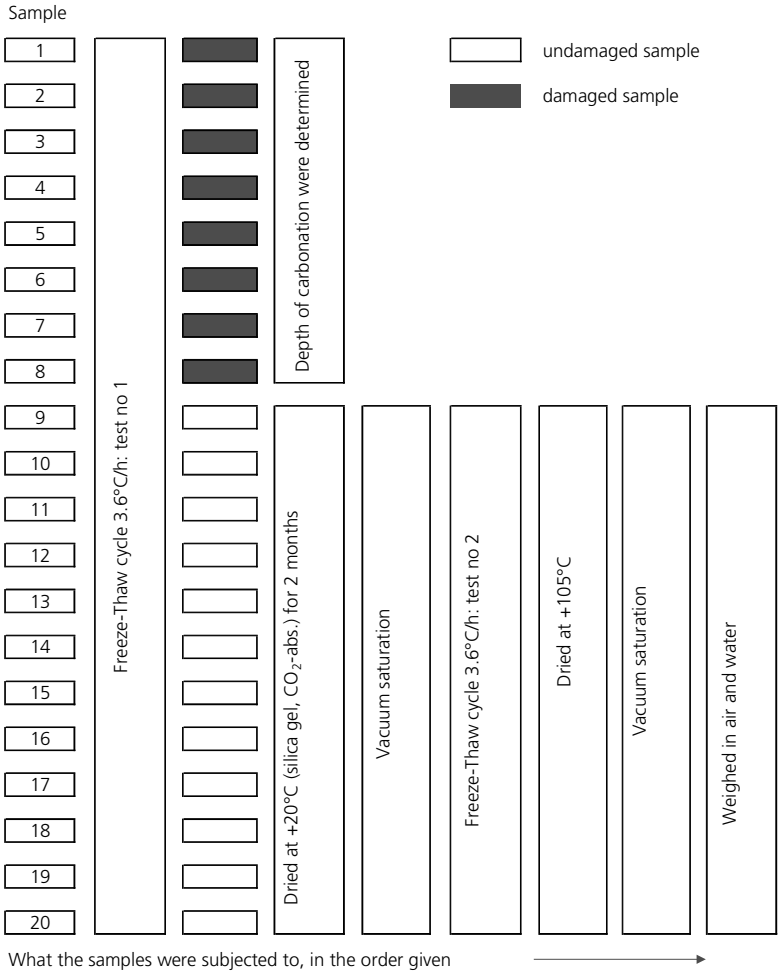

Figure 5.2.1. Test series 1 and 2; effect of the freezing rate. Specimens and test procedure for the 'normal' freeze/thaw cycle.

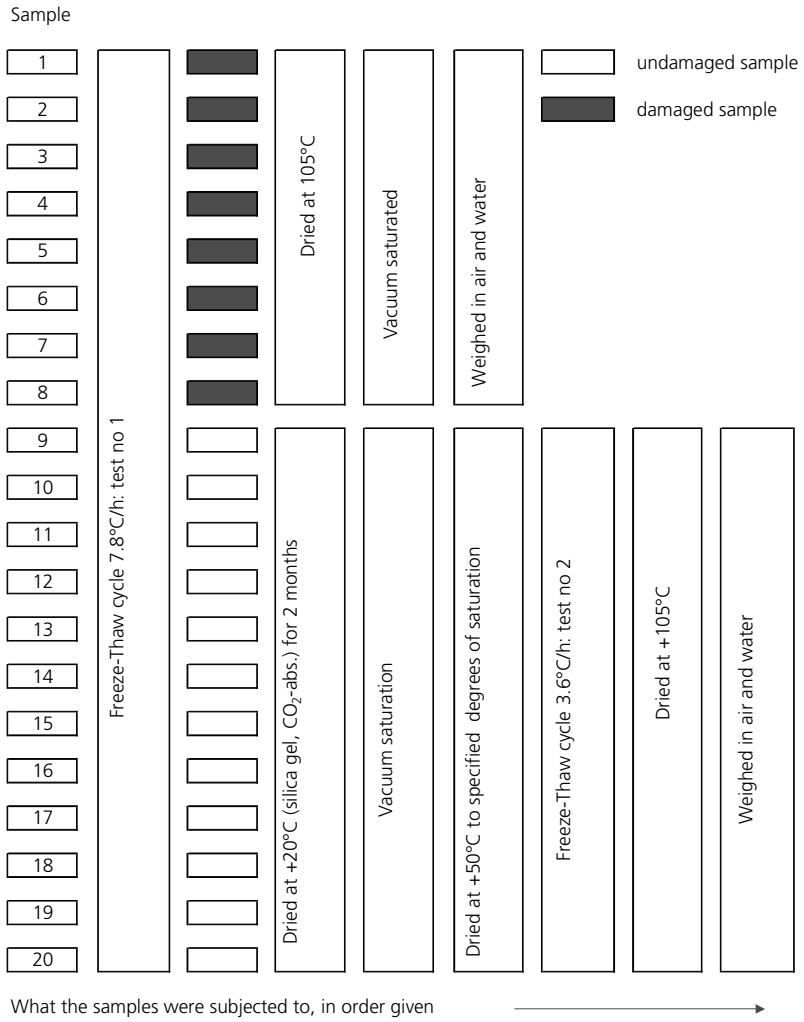

Figure 5.2.2. Test series 1 and 3; effect of the freezing rate. Specimens and test procedure for the 'rapid' and 'normal' freeze/thaw cycle.

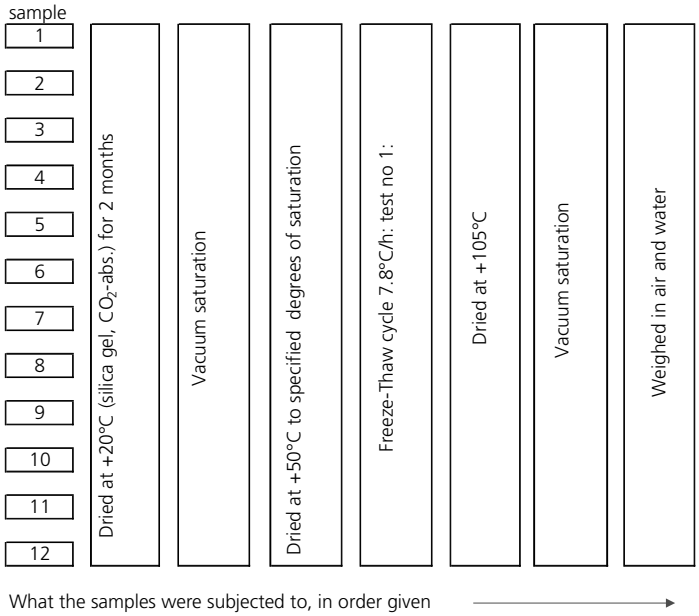

Figure 5.2.3. Test series 3; effect of the freezing rate. Additional specimens and test procedure for the 'rapid' freeze/thaw cycle.

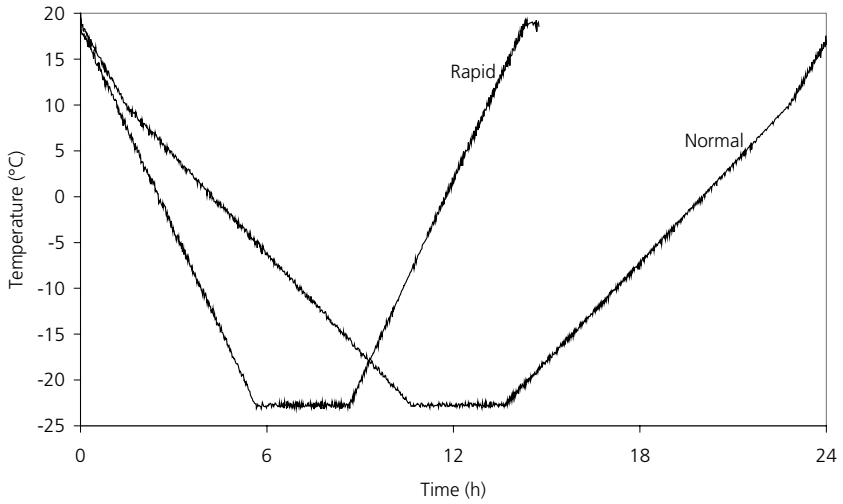

Figure 5.2.4. Test series 1,2 and 3. Temperature cycles of air in the climate chamber.

5.3 Test series 1: Never-dried specimen with 'natural' water content

5.3.1 Introduction

Test series 1 represents a situation where the structure has been exposed to water for long time, like a hydraulic structure. In such a situation one can assume that the whole capillary pore system is water-filled, and also part of the air pore system. The actual water storage time before the test was almost 4 years.

All specimens were 'virgin' which means that they were taken directly out of the lime saturated water bath without been dried. Drying is a sort of destructive process that will cause a certain change of the finer pore system. The effect of drying on the frost resistance can be both positive and negative:

Positive: Drying removes water from coarse pores in aggregate, water in cracks, and water in separation pockets under coarse aggregate. When the concrete is once again stored in water these defects will not be able to fill by water again, since the fine-porous cement paste encloses them. The positive effect of drying has been observed many times, e.g. Klieger (1956), Wong et al (1973).

Negative: The amount of freezable water increases considerably by a drying-resaturation procedure. This has been found in many studies, e.g. Vuorinen (1973), Sellevold et al (1982) and also in paragraph 9.9.

Most experimental results indicate that the positive effect of drying dominates. Therefore Test series 1 might represent a 'worst scenario', although the moisture content in a real structure might be still higher than that corresponding to 4 years in water.

5.3.2 Results in general

Typical results from the freeze-thaw experiments are shown in Figure 5.3.1. In the upper part of the figure specimen temperature and length change are plotted versus *time*. In the lower part of the figure length change is plotted versus *temperature*. The two diagrams supplement each other, since both duration of freezing temperature and the temperature itself influences the behaviour of the specimen.

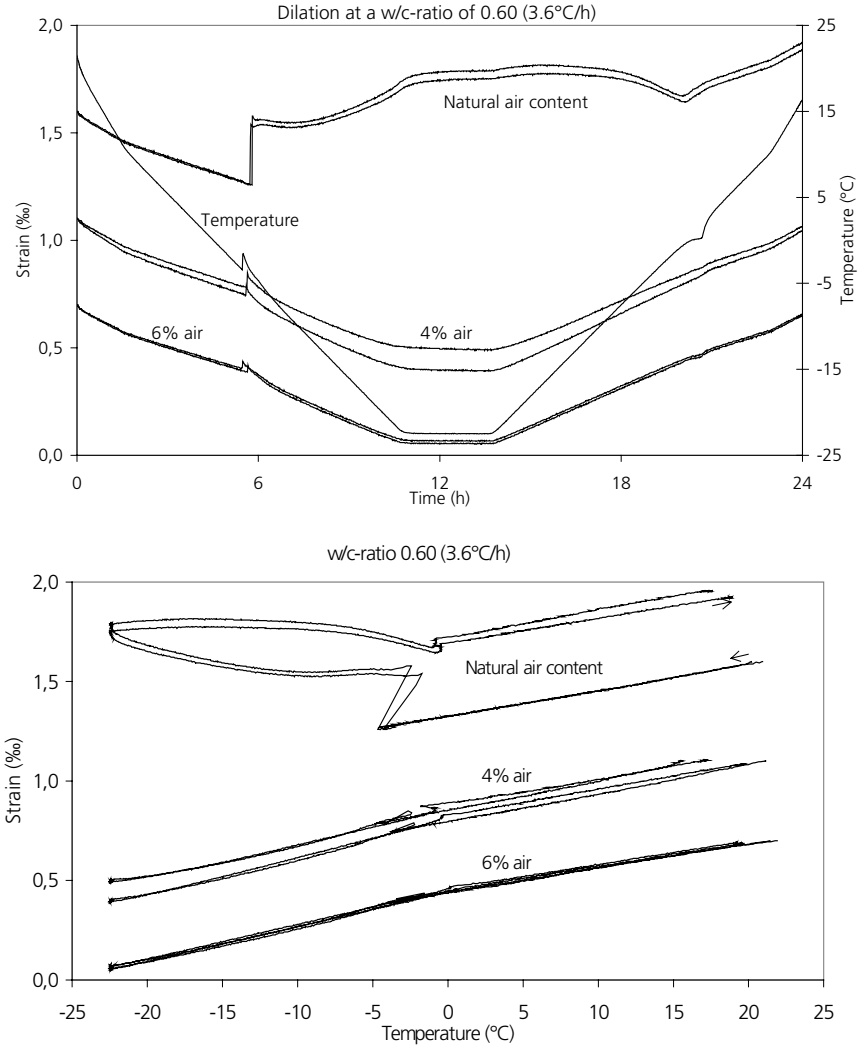

Figure 5.3.1. Freeze-thaw results for concrete with w/c-ratio 0.60 containing either natural air, 4% air, or 6% air when exposed to 'normal' freezing rate. Natural water contents.

(Note: The position of a test on the Strain scale is arbitrarily chosen in order to make the result more clear)

The results in Figure 5.3.1 are typical for all concrete types and for both freezing rates. Major results are:

- Non-air entrained concrete expands during freezing. Part of this expansion is permanent after thawing, indicating that the concrete is damaged.
- Air-entrained concrete contract more at freezing temperature than the normal thermal contraction. There is no, or negligible, permanent dilation indicating that no damage has occurred.
- 4% is a high enough air content to protect the concrete from frost damage when the water content is 'natural', i.e. corresponding to natural absorption during almost 4 years.
- When the first water is nucleated at about –5°C the specimen temperature is momentarily raised a few degrees simultaneous with a rapid expansion.
- When temperature is held constant at -23°C there is almost no length change of the specimen indicating that neither a release of internal pressure occurs or an increase in this.
- Repeated tests, using two different specimens give, almost the same result.

A length change curve for a specimen can be divided in 8 different stages; see Figure 5.3.2. Different stages appear in different specimens depending on air content, w/c-ratio and freezing/thawing conditions.

Stage 1: Thermal contraction before nucleation of super-cooled water.
Stage 2: Rapid expansion caused by nucleation of super-cooled water sometimes followed by contraction when 'rapid' stresses are relieved.
Stage 3: Contraction (or expansion) with no or low rate of ice formation.
Stage 4: Expansion (or contraction) caused by ice formation.
Stage 5: Expansion (or contraction) before major melting of ice.
Stage 6: Thermal contraction and contraction caused by melting of ice.
Stage 7: Expansion immediately before all ice is melted.
Stage 8: Thermal expansion of the thawed specimen.

In the discussion below reference is made to these different stages.

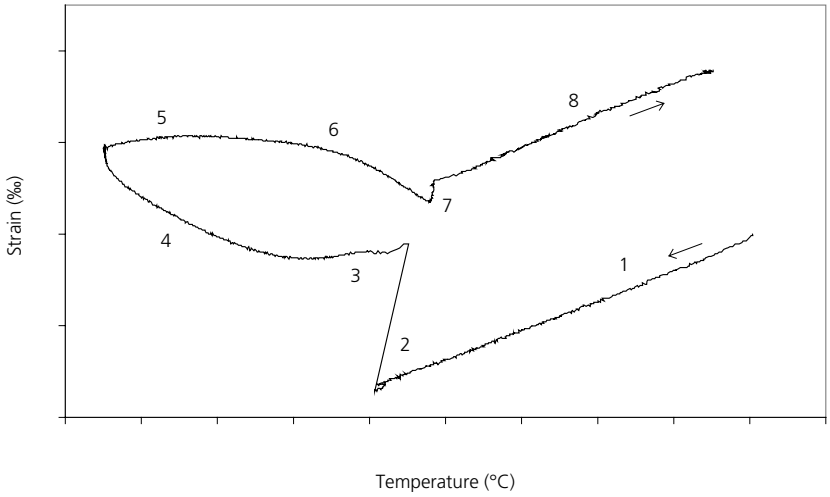

Figure 5.3.2: Different stages in a length change curve.

5.3.3 Non-air-entrained concrete

Results for non-air-entrained concrete with w/c-ratio 0.40 and 0.60 are discussed below. The discussion is performed for each w/c-ratio individually. Data for w/c-ratio 0.45 are found in APPENDIX to Chapter 5.

w/c-ratio 0.60

Expansion-temperature curves for non-air-entrained concrete with w/c-ratio 0.60 exposed to the two freezing rates are shown in Figure 5.3.3. *Expansion-time curves* for the normal freezing rate are shown in Figure 5.3.4.

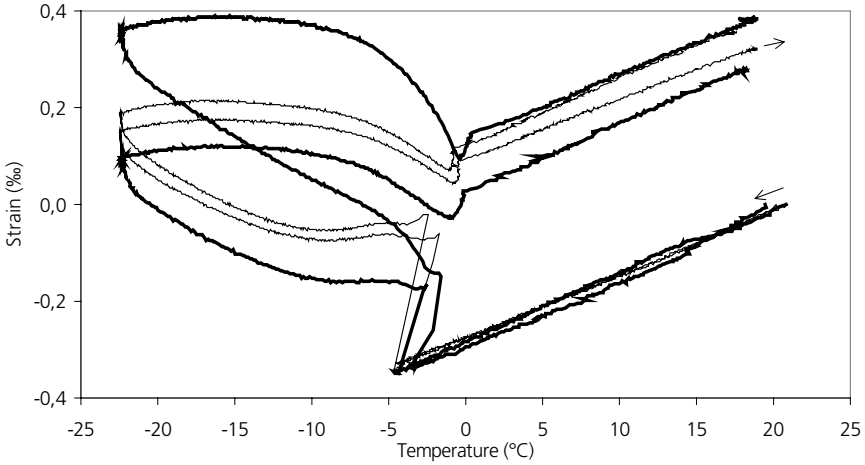

Figure 5.3.3. Length change versus temperature. Test series 1. w/c-ratio 0.60. No air-entrainment. The thin line shows results from the 'normal' freeze-thaw cycle and the thick line from the 'rapid'.

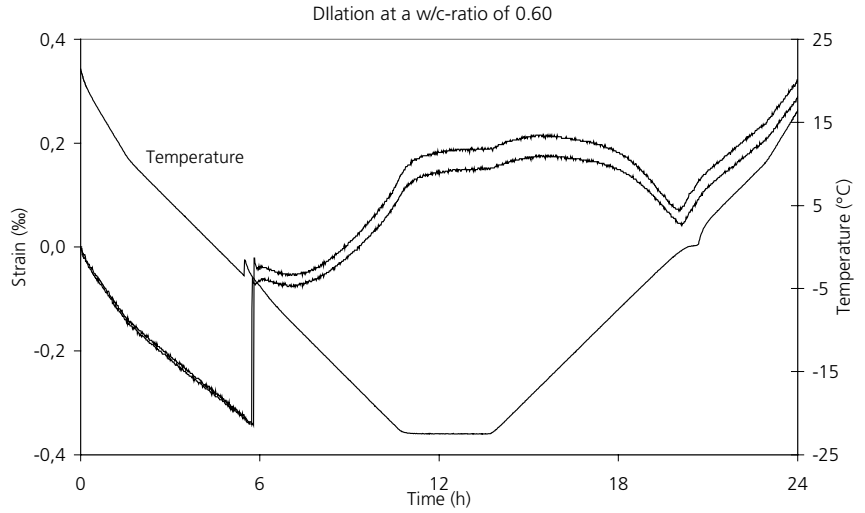

Figure 5.3.4. Length change versus time. Test series 1. w/c-ratio 0.60. No air-entrainment. 'Normal' freeze-thaw cycle.

Stage 1: Before any ice formation has taken place, the length change curves are linear and almost identical regardless of the freezing rate, which was also expected. There are some earlier experimental observations that cement paste might have a certain non-linear thermal contraction/expansion, and that the rate of temperature change

might influence this, Helmuth (1961). This could not be confirmed by the actual experiments.

Stage 2: The temperature at which the ice starts to form by nucleation of supercooled water is about the same for both freezing rates; -4 à -5°C. There is a slight tendency that the 'rapid' freeze-thaw cycle initiates the ice formation at a higher temperature than the 'normal' freeze-thaw cycle. The difference is however very small.

When ice is nucleated, temperature rises momentarily by a few degrees due to heat developed at ice formation. A rough value of the amount of ice formed can be calculated from this temperature rise (assuming adiabatic conditions):

$$Q_{ice} = \frac{Q_s c_s \Delta\theta}{\Delta H^{fus}} \qquad \text{Eq. 5.3.1}$$

where Q_{ice} is the amount of ice formed [g], Q_s is the weight of the specimen [g], c_s is the heat capacity of the specimen [J/g,K], $\Delta\theta$ is the temperature rise [K], ΔH^{fus} is the heat of fusion of water [333 J/g]. *Example vct 0.60 natural air content:* $\Delta\theta$=2.3 Figure 5.3.4, c_s=1, Q_s=158 g. Then, the ice formed will be 1.1 g. This is about 18 % of all freezable water in the specimen (Figure 9.6.1 and a cement content of the specimen of 25 g).

The ice formation when supercooling ceases gives rise to a rapid expansion. This is probably caused by pressure generated when a big amount of ice is formed in short time. The smaller supercooling at the higher freezing rate, and therefore the somewhat smaller amount of ice formed, leads to the observed somewhat smaller expansions in those samples. The observation, therefore, supports the hypothesis that the hydraulic pressure mechanism is active in Stage 2.

Directly after terminated rapid ice formation one might have expected that the concrete should contract momentarily, since the 'pumping' effect, caused by hydraulic pressure when excess water has to be expelled, should vanish. The expansion maintains on the same level, however, which indicates that in fact only some water has been expelled and that, therefore, much of the ice has formed in situ in the pore. The reason is certainly that the concrete lacks entrained pores and therefore that the spacing between air-filled spaces is too big for the stresses to be relieved.

The observed rapid expansion can be compared with the expansion of water when this is transformed into ice. According to the example above 1.1 g water was frozen. The volume increase is 0.09·1.1=0.099 cm^3. The specimen volume is 71.2 cm^3. Thus the maximum possible volume expansion of the specimen if all ice is formed in situ in each individual pore is (0.099/71.2)·1000= 1.4‰. The measured length expansion is about 0.3‰ that gives the volume expansion 0.9‰. This calculation shows

that about 35% of the excess water caused by freezing has been able to escape to air pores where it was transformed to ice.

The length expansion 0.3‰ at Stage 2 is somewhat higher than the tensile fracture strain of concrete, which is normally about 0.15‰. Therefore, it is reasonable to believe that the concrete becomes damaged already in connection with the nucleation of super-cooled water. This destruction is most probably caused by hydraulic pressure.

Stage 3: When the temperature continues to decrease, three of the four samples showed contractions for a period of about one and a half hour (corresponding to a decrease in temperature of 5°C). The contraction is a bit smaller than the normal thermal contraction, which indicates that there is ice formation going on, causing some internal stresses. These might originate from hydraulic pressure, but they can also be caused by microscopic ice lens formation, since the concrete still contains much unfrozen water; see Chapter 9. A contributing reason for contraction is that water that is freezable in the range 0 to -4 à -5°C became frozen already when super-cooled water was nucleated.

One of the samples exposed to rapid freeze-thaw has much smaller contraction than the other three samples. This can depend on a somewhat different air-pore system, making it more difficult for water to escape from the site of ice formation. It is hardly caused by ice lens formation, since this is not promoted by rapid freezing, but it can be explained by the hydraulic pressure theory.

Stage 4: After the 'relaxation period' in Stage 3 the samples begin to expand again when temperature is lowered, which certainly depends on continued ice formation. The reason for the expansion can be that ice formation occurs in a pore system that becomes more and more blocked by ice, for which reason water cannot be easily displaced from the freezing site. Thus, there might be big expansion also in a case where the ice formation is slow, simply because much of the ice has to be accommodated in the pore where it is formed without being able to displace the surplus water. This will create hydraulic pressure, which might therefore be the main reason for the expansion.

One cannot exclude that microscopic ice lens growth is the main, or an additional, cause of the expansion. All prerequisites for this are at hand, big amount of unfrozen water, big amount of ice (Chapter 9), big spacing between air-pores, gradually lowered temperature.

Except for the one specimen described above, there is no marked difference in behaviour between the samples tested with the 'normal' freeze-thaw cycle and the sam-

ples tested with the 'rapid' freeze-thaw cycle. This effect is difficult to explain by the main destruction mechanisms.

The theory of hydraulic pressure predicts larger dilations when the freezing rate is higher (due to larger rate of ice formation), but that effect could not bee seen in Stage 4. The theory of ice lens growth does not predict any major influence of the freezing rate on the growth of the lenses. Theoretically, a more rapid temperature change could cause a bigger difference in free energy between ice bodies and unfrozen water, provided bigger temperature differences appear between these phases. This should lead to a bigger driving potential for water migration to the ice bodies. This type of water transport occurs only very locally in the specimen, however, and one can therefore assume that there is almost local equilibrium between the phases, even when the freezing rate is doubled as in the actual case. Besides, a more rapid freezing means a shorter freezing time counteracting the effect described above. A decreased freezing rate automatically causes a longer duration of temperature change. This ought to promote the ice lens growth mechanism since water has longer time to migrate to ice bodies.

Maybe, the fact that no effect of freezing rate could be observed is that the increased hydraulic pressure caused by increased freezing rate is counteracted by reduced pressure caused by ice lens growth.

The observed volume expansion during stage 3+4 is of the order 1.6 ‰ (counted from the extrapolated linear contraction), an expansion which can be caused by freezing of only about 1.2 g water, provided freezing occurs as in a 'closed container' (Note: 1.2 g in the specimen corresponds to about 20 kg in 1 m^3 of concrete). Thus expansion occurring during Stage 3+4 is about twice the expansion following the nucleation of super-cooled water. In Figure 9.6.1 about 0.15 g ice is formed per g cement at -20°C. In specimen used here in Test series 1, this corresponds to 3.75 g ice.

Directly after onset of the isothermal period at –23°C, all the samples continued to expand for about an hour before the length became constant. This dilation could be explained by small temperature differences between the air and the sample making some ice formation possible despite the fact that the specimen temperature was almost constant.

Stage 5: When warming started from –23°C, some small expansion could be observed. The expansion is smaller than the expected thermal expansion of a stress-free specimen, indicating that internal pressure in the concrete caused by ice is relieved when temperature is raised.
The rate of warming has no marked effect on the length changes in Stage 5.

Stage 6: Melting of ice occurs at a considerably higher temperature than ice formation. Thus, at -5°C more ice is present in a specimen during thawing than in the same specimen during freezing. This is also seen in the calorimeter experiments in Chapter 9. When the specimen is approaching 0°C most of the ice melts, which makes the specimen contract. The most obvious explanation for this is that internal pressure is released when ice melts. Melting will also cause 'suction' inside the concrete since water occupies less volume than ice. Therefore, water is sucked back from air-pores to which it was displaced during freezing. This suction, or under-pressure in the pore-water, can give shrinkage stresses contributing to the contraction in Stage 6 at temperature close to 0 °C. Another explanation is the moisture migration mechanism described in Stage 7. This will also cause contraction. The rate of warming has no marked effect on the contraction in Stage 6.

Stage 7: Immediately before all ice has melted there is a small expansion. The expansion is about the same at both warming rates. There are at least two explanations for the expansion:

1) The suction described above vanishes when all ice is melted and the pore system is once again 'saturated' and stress-less.
2) During the last stage in thawing, the surface part of the specimen is completely thawed while the interior still contains some ice and therefore is a bit colder. Therefore, there will be a free energy difference between the water at the surface and the ice in the interior. This causes moisture movement as described by the microscopic ice lens theory. The surface part dries which leads to shrinkage as that observed in the last part of Stage 6. When all ice is thawed, moisture transport is reversed and the surface part is once again saturated causing the specimen to expand to a stress-less condition

Stage 8: When warming continues after the specimen has become completely thawed there is linear expansion with the same heat expansion coefficient as the heat contraction coefficient during the cooling phase. There is a permanent expansion of about 0.4 ‰ (in length) in all specimens, which indicates considerable damage. The fracture strain of concrete at tension is only about 0.15 ‰. Damage was also noticed at the determination of dynamic E-modulus. This was reduced by about 20% for both freezing rates; see Table A5.1 in APPENDIX to Chapter 5.

w/c-ratio 0.40

Expansion-temperature curves for non-air-entrained concrete exposed to the two freezing rates are shown in Figure 5.3.5. *Expansion-time curves* for normal the freezing rate are shown in Figure 5.3.6.

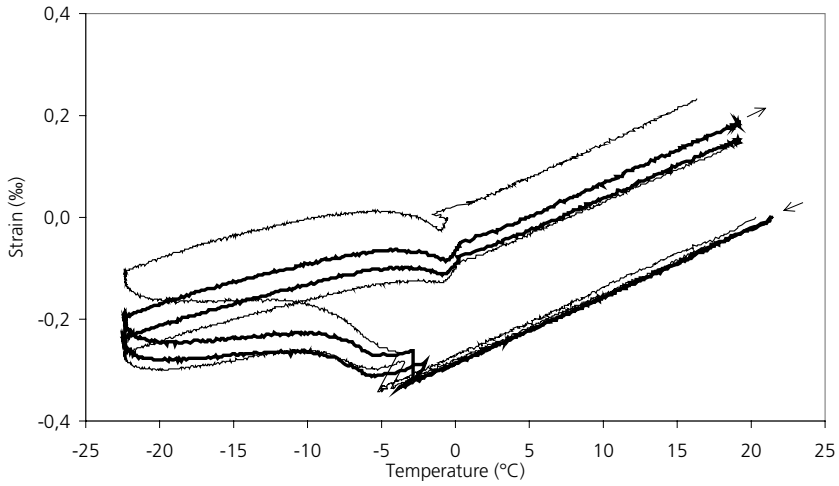

Figure 5.3.5. Length change versus temperature. Test series 1. w/c-ratio 0.40. No air-entrainment. The thin line shows results from the 'normal' freeze-thaw cycle and the thick line from the 'rapid'.
(Note: The scale on the y-axis is the same as in Figure 5.3.3.)

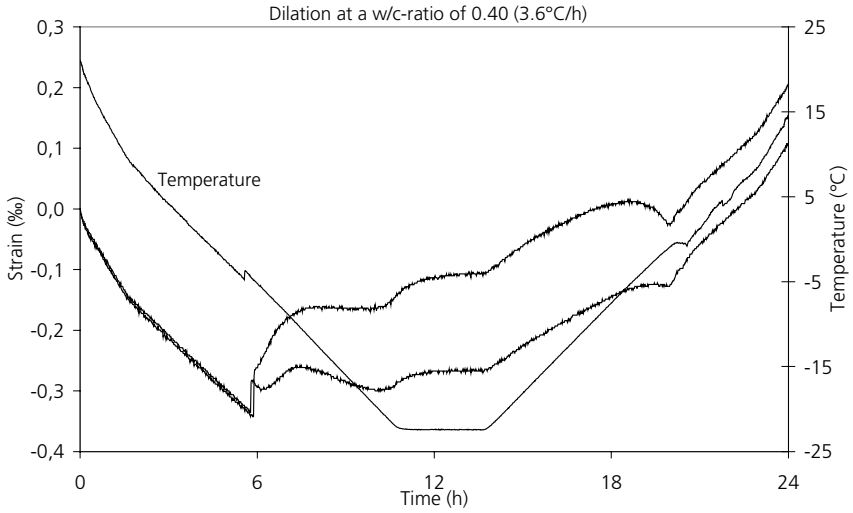

Figure 5.3.6. Length change versus time. Test series 1. w/c-ratio 0.40. No air-entrainment. Normal freeze-thaw cycle.

The behaviour is very much the same as for w/c-ratio 0.60. The main difference is that the expansion both during the different freezing stages and after thawing is smaller. Some comments will be made below:

Stage 2: The nucleation temperature is about the same as for w/c-ratio 0.60 (-3 à -5°C). A lower temperature might have been expected due to the finer pore system in concrete with w/c-ratio 0.40. Probably, however, nucleation occurs at the surface of the specimen, and then the pore size plays minor role. The temperature rise and expansion is much smaller than for w/c-ratio 0.60, which means that the amount of water able to freeze at temperature above the nucleation temperature is smaller for w/c-ratio 0.40. The expansion is not big enough to cause damage. It is less than 0.1‰. This means that the damage registered for the specimen after thawing occurs during Stage 3 and particularly during Stage 4.

As for w/c-ratio 0.60 there is no recovery of expansion when the first rapid ice formation has taken place. This indicates that a big portion of this initial ice formation takes place in situ without much transport of excess water created by ice formation. The reason is the same as for w/c-ratio 0.60, namely too big distance to air-filled pores in the non-air-entrained concrete. There is no marked effect of the freezing rate in Stage 2.

Stage 3: For both specimens in the rapid test and for one in the normal test there is a rather long period with contraction (down to about –7°C). This indicates that a small amount of water is freezing in this temperature range.

Stage 4: A gradual expansion occurs with lowered temperature, but the expansion is much smaller than for w/c-ratio 0.60. The total expansion during stage 3+4 (counted from the extrapolated linear thermal contraction) is about 0.3 ‰ (in length) compared with about 0.6‰ for w/c-ratio 0.60. A strain of 0.3‰ is however more than needed to fracture the concrete, which is also seen by the big permanent expansion of the thawed specimen.

The effect of the freezing rate is small. There are some differences between the four specimens, but there is no tendency that the more rapid test gives the biggest expansion. One specimen tested by the 'normal' cycle has considerably bigger expansion than the other three. The most plausible explanation is that the natural air-pore system is a bit more unfavourable in this specimen. This is strengthened by the fact that the other specimen tested by the same 'normal' cycle has the lowest expansion.

As for w/c-ratio 0.60 one cannot state whether the hydraulic pressure or the ice lens growth mechanism is dominant. Theoretically both will cause big stresses in a concrete without air.

When temperature lowering is stopped at –23°C length changes immediately stops.

Stage 5: Warming the specimen from –23°C to about –5°C causes considerable expansion, which makes w/c-ratio 0.40 differ from w/c-ratio 0.60. Expansion is to be expected in a heated body and can be explained by normal thermal expansion, in this case strengthened by the presence of ice. The thermal expansion coefficient of ice is higher than that of unfrozen concrete. The expected expansion in a stress-less concrete is, however, bigger than that observed, which indicates that there are internal stresses in the frozen concrete, that are gradually relieved when the concrete thaws. There is no marked effect of the warming rate.

Stage 6: The contraction during stage 6, starting at about –5°C, is much smaller than for w/c-ratio 0.60 which probably depends on the fact that much less ice was formed.

Stage 7: Even for w/c 0.40 there is a small expansion immediately before all ice has melted. The size of this is however somewhat smaller than for w/c-ratio 0.60. This is reasonable according to the theoretical background to the expansion. Lower ice formation should lead to smaller flow of water between the thawed surface part and the interior ice and between air pores and capillary pores.

Stage 8: There is a big permanent expansion. This is independent of the freezing rate (except for one specimen which also had the biggest expansion during the freezing part). The expansion is about 0.2‰, which is smaller than for w/c-ratio 0.60 (0.4‰). This can be explained by the smaller ice formation; see Chapter 9. The loss in dynamic E-modulus is about 12% for both freezing rates; see Table A5.1 in APPENDIX to Chapter 5.

5.3.4 Air-entrained concrete

Results for air-entrained concrete with w/c-ratio 0.40 and 0.60 and 6% air (nominal) are discussed below. The discussion is performed for each w/c-ratio individually. Data for concrete with w/c-ratio 0.45 and for other air contents are found in Table A5.1 in APPENDIX to Chapter 5.

w/c-ratio 0.60

Expansion-temperature curves for air-entrained concrete with w/c-ratio 0.60 and 6% air (nominal value) exposed to the two freezing rates are shown in Figure 5.3.7. *Expansion-time* curves for the normal freezing rate are shown in Figure 5.3.8.

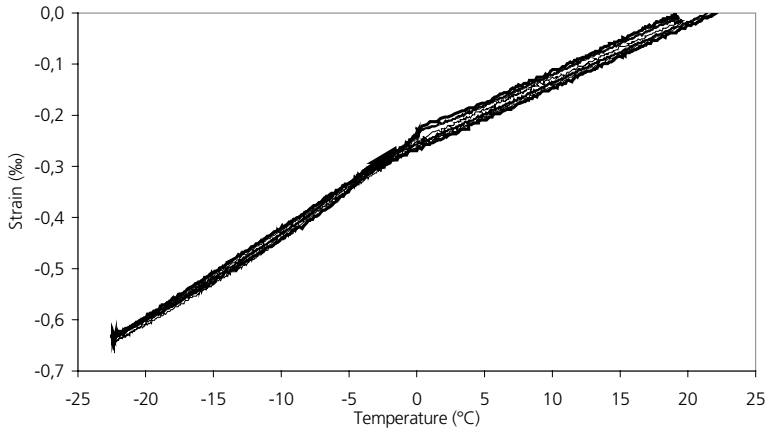

Figure 5.3.7. Length change versus temperature. Test series 1. w/c-ratio 0.60. 6% air. The thin line shows results from the 'normal' freeze-thaw cycle and the thick line from the 'rapid'.

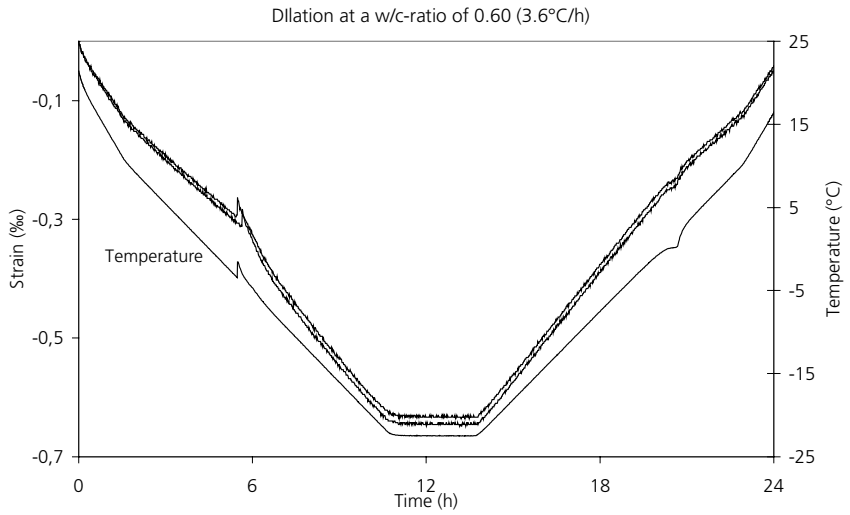

Figure 5.3.8. Length change versus time. Test series 1. w/c-ratio 0.60. 6% air. 'Normal' freeze-thaw cycle.

As expected, air-entrainment changes the behaviour drastically. Some comments to the curves in the figures above will be given. The different stages in the curves are defined in Figure 5.3.2.

Stage 2: Supercooling to a few degrees below zero occurs. The expansion when ice formation is nucleated is very small and can therefore not cause any damage. Besides, the expansion is recovered by an immediate contraction, which means that the specimen is stress-less after this first ice formation. This behaviour is quite different from the non-air-entrained concrete. There is no effect of the freezing rate

Stages 3+4: The specimen contracts more than the normal thermal contraction being defined by the extrapolated contraction of the unfrozen concrete. This phenomenon has been observed in many previous studies, e.g. Powers and Helmuth (1953). One can assume that about the same amount of ice is formed as in the non-air-entrained concrete with w/c-ratio 0.60. Therefore, the contraction shows that this ice is formed without causing any destructive forces. Excess water generated by the 9% increase in volume when water is transformed into ice can therefore be easily forced away from the freezing site to the adjacent air-pores. A hydraulic pressure will appear due to this transport, but this is evidently very small, and/or counteracted by a contractive force, the net effect being contraction. As described by the hydraulic pressure theory, only small hydraulic pressure appears when there is a small distance between a pore where freezing occurs and the nearby air-filled pore. This is evidently the case in the actual concrete. The Powers spacing factor is 0.16 mm, which is a low value, see APPENDIX to Chapter 3.

The contractive force is probably caused by internal drying appearing as a result of transfer of unfrozen water from very small capillary pores and gel pores to ice-bodies in the larger capillaries and air pores. This transfer depends on the difference in free energy between the two phases when temperature is gradually decreased. According to this so-called 'microscopic ice lens growth theory' pressure should theoretically appear, since the water freezes when it reaches the ice body, which therefore grows. In a concrete with high amount of air, and short spacing between the air pores, water will, however, primarily move to ice in the air pores, and there it can freeze without causing stresses. (ice in the air pores emanates from water displaced from capillary pores when freezing occurs in these.)

One should not exclude that the contraction is of purely thermal nature, i.e. that the thermal expansivity is a bit bigger in a frozen concrete than in an unfrozen, simply because ice has a bigger thermal expansivity than unfrozen concrete. The contraction seems to be too big however to support this hypothesis; c.f. Chapter 10. No effect of the freezing rate could be observed.

When temperature is kept constant at –23°C no length changes occur. Length changes stop and start directly when temperature change is stopped or started.

Stages 5+6: During warming the specimens expand along almost the same path as they contracted during freezing. This supports the hypothesis that the movement is purely thermal, and that no internal forces are acting. The effect might however also be obtained if the previously dried fine capillary pores and gel pores become re-saturated when ice in the capillaries gradually melts.

Stage 7: Immediately before all ice has melted there is a slight expansion, which is much smaller than for non-air-entrained concrete. The most probable reason is the 'suction' caused when ice contracts during melting.

Stage 8: Almost no permanent expansion (0.03‰) and only very small reduction in E-modulus (5%) could be observed. This indicates that the specimen is unharmed.

w/c-ratio 0.40

Expansion-temperature curves for air-entrained concrete with w/c-ratio 0.40 and 6% air (nominal value) exposed to the two freezing rates are shown in Figure 5.3.9. *Expansion-time* curves for the 'normal' freezing rate are shown in Figure 5.3.10.

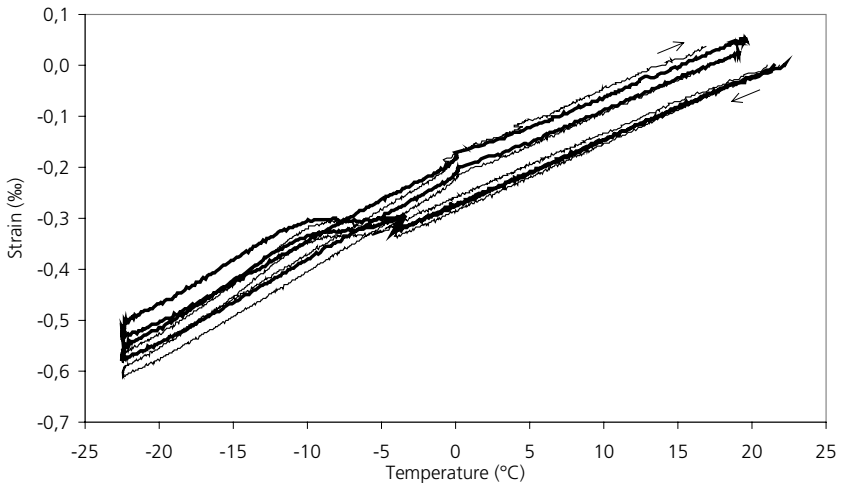

Figure 5.3.9. Length change versus temperature. Test series 1. w/c-ratio 0.40 6% air. The thin line shows results from the 'normal' freeze-thaw cycle and the thick line from the 'rapid'.

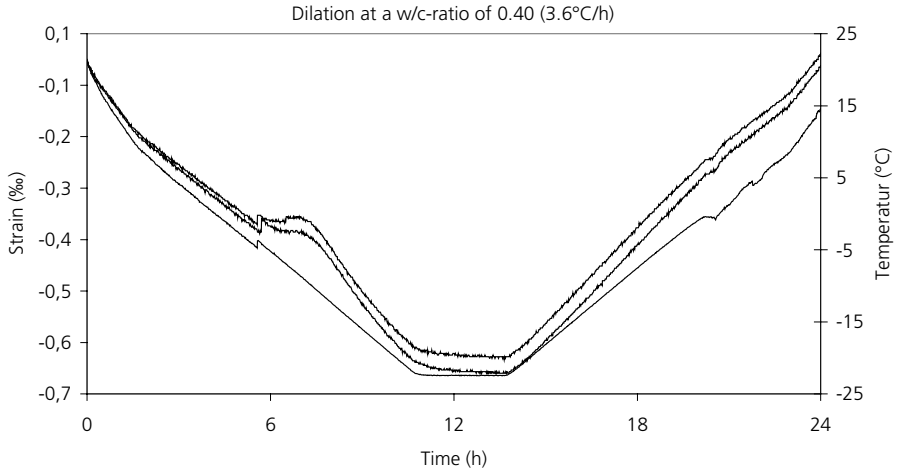

Figure 5.3.10. Length change versus time. Test series 1. w/c-ratio 0.40 6% air. 'Normal' freeze-thaw cycle.

Also for w/c-ratio 0.40 air-entrainment decreases the dilation occurring during freezing. There is a marked difference in the length change curves from the air-entrained concrete with w/c-ratio 0.60.This will be commented upon.

Stage 2: The expansion when the first ice is nucleated at about –4°C is very small as it was for w/c-ratio 0.60, but in contrast to w/c-ratio 0.60 expansion is not reversed but maintains, indicating that ice formation has created some internal permanent stresses. This is not big enough to cause any damage. No effect on Stage 2 of the freezing rate could be seen.

Stage 3+4: Instead of the contraction observed for w/c-ratio 0.60 there is a small expansion down to about –10°C. Thereafter, the specimens contract thermally. Both freezing rates give about the same expansion and contraction. The expansion is small however, less than 0.06‰, and could therefore not cause damage.

The reason for the observed behaviour must be that the air-pore structure is not of high enough quality in this very dense concrete (spacing factor 0.13 mm, specific surface 44.7 mm^{-1}). The low w/c-ratio certainly gives lower amount of freezable water (see Chapter 9), but despite this the stresses are higher than for the higher w/c-ratio. There are two possibilities for this:

1. The hydraulic pressure is higher since the permeability is lower. A reduced rate of ice formation is therefore more than counteracted by the lower permeability.

2. The concrete contains much more non-freezable water (see Chapter 9). Therefore, the possibility of microscopic ice lens growth might increase.

The fact that a more dense concrete can become more vulnerable to internal frost damage has been demonstrated in other research, e.g. Malhotra et al (1987), Kukko (1995).

As for the other concrete types virtually all length change stopped immediately when temperature change was stopped at –23°C.

Stage 5+6: When warming starts all specimens directly respond by a small contraction, which is a bit higher for the most rapid warming rate. One explanation is that the equilibrium between unfrozen water and ice, which was reached when temperature was kept constant during 3 hours, is momentarily changed when temperature starts to rise. In this case, moisture movement should rather go towards the partly dried capillaries and gel pores and not towards the ice, which ought to cause expansion and not contraction.

After this immediate contraction at almost constant temperature, the specimens expand almost linearly with increased temperature. This expansion is very similar to w/c-ratio 0.60.

Stage 7: A very small expansion immediately before all ice is melted is observed.

Stage 8: A certain permanent dilation of the thawed specimen is observed. It is 0.06 to 0.09‰ for both freezing rates, which indicates that the freeze/thaw cycle has had a certain damaging effect. This is very small however. The dynamic E-modulus is decreased by only about 5% for both freezing rates.

5.3.5 Concrete with other w/c-ratio and air contents

Detailed results and detailed discussion were presented in paragraphs 5.3.3 and 5.3.4 above for concrete with w/c-ratio 0.60 and 0.40, and for concrete without air-entrainment and with 6% air (nominal). Results for concrete with w/c-ratio 0.45 and for all concrete types with 4% air (nominal) are presented without discussion in APPENDIX to Chapter 5.

For w/c-ratio 0.40 containing 4% nominal air content one sample behaves uncharacteristic. Very large expansions occur when supercooling is overcome and these expansions do hardly decrease at all when temperature is increased. Since the change in resonance frequency is very small indicating no damage it is believed that the LVDT-sensor malfunctioned for some reason and thus this result is disregarded.

5.3.6 Test series 1: Summary and discussion of results

All results from Test series 1 are presented in APPENDIX to Chapter 5. In Table A5.1 an overview of dilation at different stages (defined by Figure 4.4.4) during the freeze/thaw cycle is given. Furthermore, values of the change in resonance frequency caused by freeze/thaw, and the degree of saturation during freeze/thaw are listed.

Length change curves both versus temperature and versus time for all specimens are also shown in APPENDIX to Chapter 5, Figures A5.1-A5.12.

The question to be answered in Test series 1 was how an increase in the freezing rate (and warming rate) by a factor of two influences damage caused by freeze/thaw for concrete that had a 'natural' water content reached after many years of water absorption. Damage is measured as dilation and change in resonance frequency of the specimen. It should be noticed that the two freezing rates were applied to different specimens, so an influence of differences in the air-pore system of the specimen, and maybe of the moisture content, cannot be excluded. The difference in behaviour between repeated freeze/thaw at the same freezing rate using two different specimens is small for almost all concrete types, which indicates that the differences between the specimens are small. This is reasonable since specimens were taken out of the same block, and the water storage time and conditions were exactly the same.

The effect of the freezing rate on the damage parameters dilation and change in E-modulus was found to be very small if any, see Figure 5.3.11. There are some differences, but then in most cases it is the more rapid freezing that gives less damage. Thus, Test series 1 clearly shows that the freezing rate *in itself* all other parameters held constant, does not influence the frost resistance of concrete.

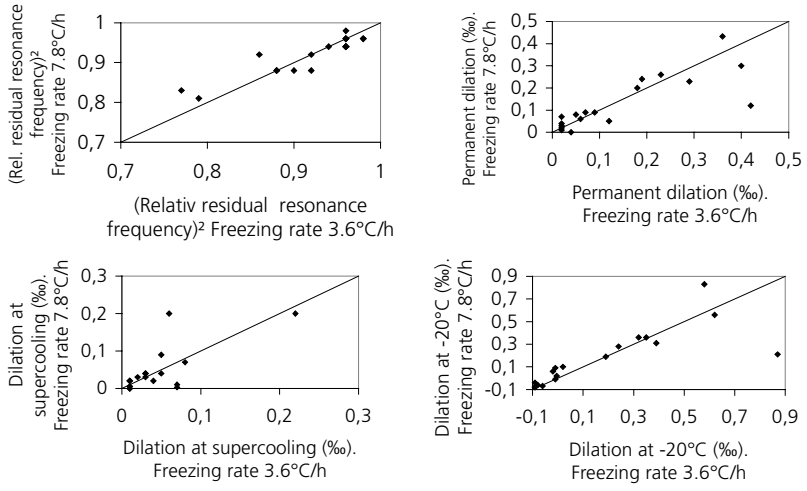

Figure 5.3.11. The influence of freezing rate on the damage parameters in Test series 1. Data from APPENDIX to Chapter 5, Table A5.1.

In Figure 5.3.12 the relation between observed dilations or change in E-modulus for all specimens is plotted versus w/c-ratio and air content. As expected, a low water cement ratio alone is not enough to give high frost resistance. Air-entrainment is needed in such concrete. On the other hand, a fairly high w/c-ratio (0.60) can give high frost resistance, provided the air content is high enough. For the actual mix constituents, it seems as if 5-6% air is needed if the limit for undamaged concrete is set to 5% reduction in E and 0.1‰ in permanent dilation.

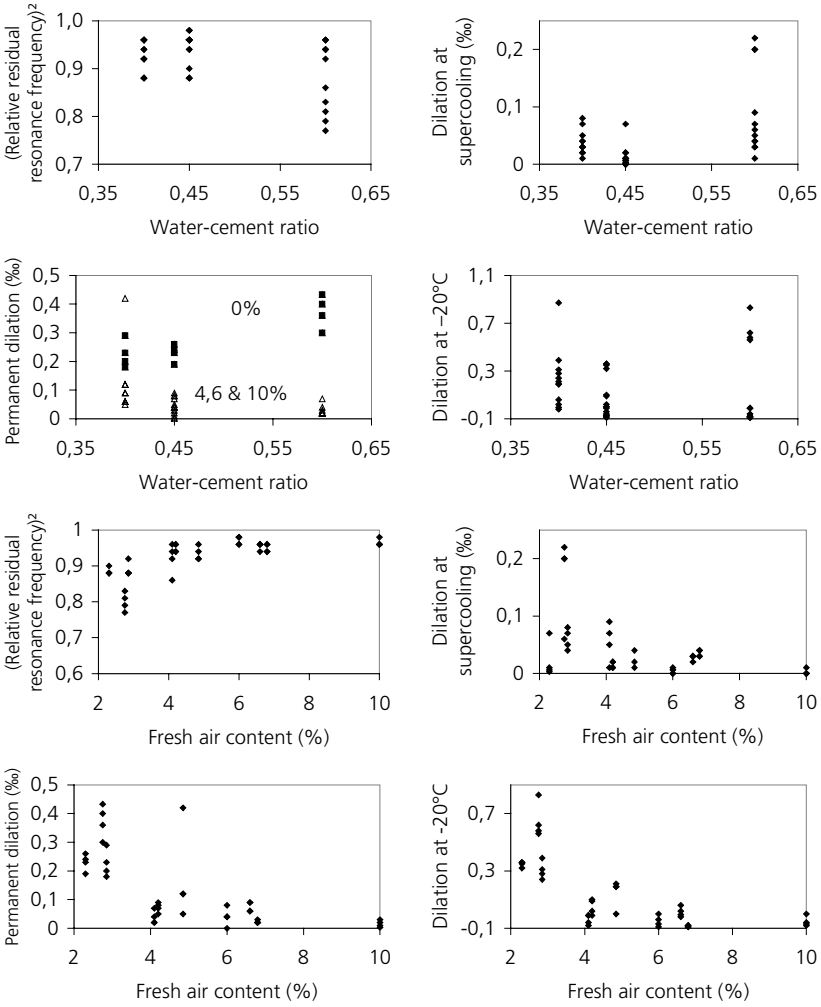

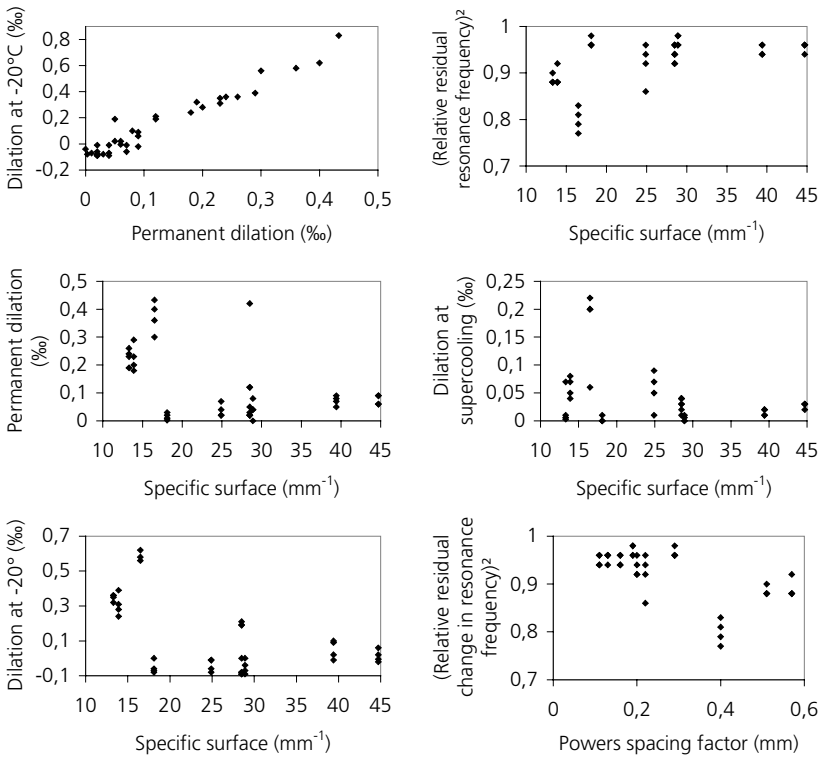

Figure 5.3.12. Influence of w/c-ratio and air content on E-modulus and dilation Data from APPENDIX to Chapter 5, Table A5.1

5.3.7 Test series 1: Conclusions

The results of Test series 1 can be summarized as follows.

1. A doubling of the freezing/warming rate from 3.6°C/h to 7.8°C/h has no, or marginal, effect on damage occurring during freeze/thaw. It is unlikely that a freezing rate higher than 7.8°C/h will ever occur in a real structure. 3.6°C/h is a fast freezing rate that can sometimes appear in the surface part of a concrete structure.
2. Non-air-entrained concrete cannot sustain water absorption for long time without becoming frost damaged. This is true for w/c-ratio as low as 0.40.
3. Air-entrained concrete with w/c-ratio as high as 0.60 can sustain 4 years of continuous water absorption before freezing.
4. The rapid ice formation occurring when supercooled water is nucleated some degrees below zero can in *non-air-entrained* concrete be high enough to cause

damage, since water cannot be expelled to air spaces fast enough not to cause damage.

5. The amount of supercooling was uninfluenced by the freezing rate and was about the same for all w/c-ratios. It was always lower than 5°C. Probably ice formation was nucleated in water condensed on the plastic foil in which the specimens were wrapped.
6. The expansion occurring when supercooled water is nucleated is most probably caused by hydraulic pressure when excess water is expelled from the freezing site.
7. Big expansion occurs in *non-air-entrained* concrete when temperature is gradually lowered to –23°C. No effect of the freezing rate on the expansion can be observed. Thus neither the hydraulic pressure theory, nor the microscopic ice lens growth theory could be verified. One possibility is that the negative effect of an increased freezing rate on hydraulic pressure is evened out by a positive effect on ice lens growth.
8. *Air-entrained* concrete contracts more than the normal contraction when temperature is lowered to –23°C. Concrete with w/c-ratio 0.40 and 0.45 have lower contraction (even slight expansion) than concrete with w/c-ratio 0.60. No effect of the freezing rate on the contraction could be observed.
9. When temperature lowering is stopped at –23°C expansion or contraction stops almost immediately in all specimens irrespectively of the w/c-ratio.
10. When warming starts *non-air-entrained* specimens start to expand slightly to about –10°C. The expansion is lower than calculated from the thermal expansion coefficient, indicating that some relieve of stresses occur, possibly since ice melts gradually. Big contraction occurs in the range –10°C à –5°C until 0°C. This indicates that the main melting of ice takes place at higher temperature than ice formation. This is also verified in the calorimeter experiments in Chapter 9. No effect of the warming rate could be observed.
11. Warming of air-entrained concrete proceeds along the same path as freezing.
12. Immediately before all ice is melted the specimens expand slightly. This is explained by two mechanisms: (1) water is sucked back from air pores to which it was expelled during freezing, (2) liquid water at the surface, that has migrated to ice-bodies in the interior at a few degrees below zero, is re-sucked to the surface.

13. After complete thawing all specimens expand thermally by the same thermal coefficient as they contracted before freezing.
14. A big expansion during freezing corresponds directly to a big reduction in E-modulus, and a big permanent dilation.
15. The test clearly shows that one single freeze/thaw cycle is enough to determine the frost resistance of concrete.

5.4 Test series 2: Pre-dried, vacuum-saturated specimens

5.4.1 Introduction. Preparation of samples

In Test series 1, the specimens had been stored continuously in lime-saturated water for almost 4 years before freeze/thaw, which is a very high moisture exposure. The objective of Test series 2 was to investigate how concrete responds to an even higher moisture load in a worst possible scenario, using saturated specimens.

The specimens that were undamaged after Test series 1, i.e. all air-entrained samples, except one damaged air-entrained specimen with w/c-ratio 0.40 and 4% nominal air content, were dried over silica gel and carbon dioxide absorbent at room temperature for two months. Thereafter, they were water saturated using vacuum treatment for 24 hours at 1-3 mbar followed by water absorption. Since Test series 1 had shown that the freezing rate had no influence on the behaviour during freeze/thaw only the 'normal' freeze-thaw cycle was used in Test series 2.

5.4.2 Test series 2: Examples of results

Typical results are shown below. All results can be found in APPENDIX to Chapter 5.

w/c-ratio 0.60 and 0.45: 4% air

Expansion-temperature curves for air-entrained concrete with w/c-ratio 0.60 and 0.45, and with 4% air (nominal value) are shown in Figure 5.4.1. *Expansion-time curves* for the same samples are shown in Figure 5.4.2. Length change curves both versus temperature and versus time for all specimens are also shown in APPENDIX to Chapter 5, Figures A5.17-A5.22.

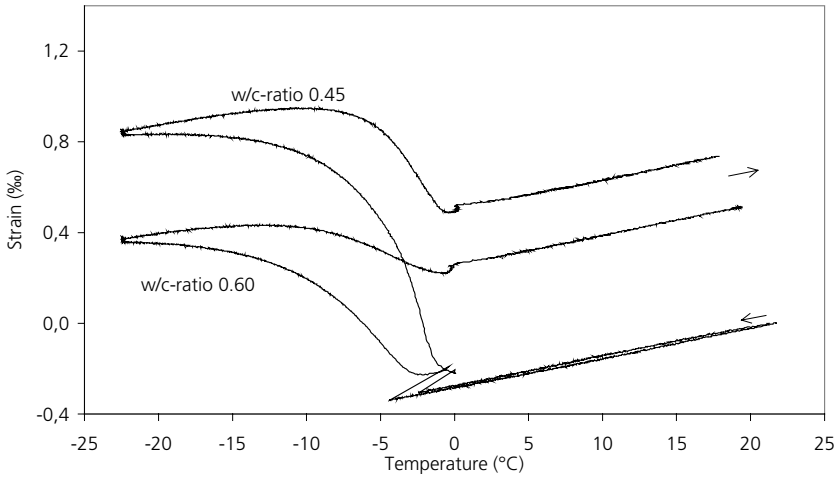

Figure 5.4.1. Strain versus temperature for vacuum saturated samples of w/c-ratio 0.60 and 0.45 with 4% of entrained air (4.1% for w/c-ratio 0.60 and 4.2% for w/c-ratio 0.45).

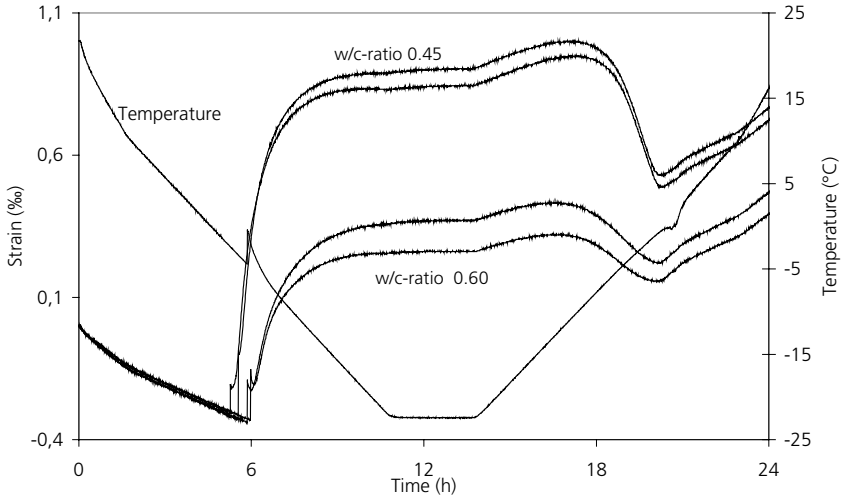

Figure 5.4.2 Length change and temperature versus time for vacuum-saturated samples of w/c-ratio 0.60 and 0.45 with 4% of entrained air (4.1% for w/c-ratio 0.60 and 4.2% for w/c-ratio 0.45).

The samples that showed little or none dilation when tested with natural degree of saturation in Test series 1 now showed huge expansions and suffered large permanent dilations when the freeze-thaw cycle was finished. The reason is of course that all, or

most, of the air pores had become water-filled during the vacuum saturation procedure. An observation that is astonishing is that the concrete with w/c-ratio 0.45 had bigger expansion than the concrete with w/c-ratio 0.60. One might have expected that the amount of freezable water should have been bigger for w/c-ratio 0.60 and therefore the expansion bigger.

Other results of similar type can be found in APPENDIX to Chapter 5, where it is seen that some concretes with high air content expands less than concrete with lower air content and the same w/c-ratio. In all these cases one can suspect that the vacuum saturation procedure was more or less successful for different specimens. If a specimen had unexpectedly small expansions it can be concluded that the vacuum saturation had been unsuccessful for that specimen.

Some comments to the figures above will be made. Concerning the different stages in the freeze/thaw curve, see Figure 5.3.2.

Stage 2: Supercooling is 2.5°C for w/c-ratio 0.45 and 5°C for w/c-ratio 0.60. These values are of the same order as in Test series 1. Thus, the fact that air-pores contain water does not change supercooling. The expansion occurring when supercooled water freezes were not recovered which is explained by lack of space for expelled water. The expansion is somewhat bigger for w/c-ratio 0.60 indication somewhat more ice formed, which is reasonable since supercooling is bigger.

Stage 3: For w/c-ratio 0.60 there is a short period of contraction within the temperature range 0- to –3°C. This can be explained by the fact that water that is freezable in this range has already been frozen when supercooled water was nucleated.

Stage 4: For both concretes big expansion occurs. This is bigger for w/c-ratio 0.45 which is unexpected as mentioned above. One possibility is that the preparation procedure had a larger impact on this material. The drying and re-saturation might have caused microcracking, opening smaller, previously isolated, pores for early ice formation by nucleation from ice in adjacent coarser pores.

The expansion is biggest in the beginning and continues to about –15°C, indicating that most ice is formed within this range. The expansion can be explained by the so-called 'closed container theory', which is a special case of the hydraulic pressure theory; see Chapter 2. The expansion when water is transformed to ice must be accommodated inside the pore space since there is no air-filled pore space in a saturated concrete to which water can be forced away. Thus, if the concrete is completely saturated one can expect a volume expansion that is $0.09 \cdot w_f$ where w_f is the amount of frozen water (provided no water can escape from the specimen surface).

For w/c-ratio 0.60 the volume expansion is about 2.6‰ or 0.185 cm^3 in a specimen with volume 71.2 cm^3. This corresponds to only 2.1 g frozen water. For w/c-ratio 0.45 the corresponding figures are 4‰, 0.25 cm^3 and 3.2 g. The expected amount of freezable water in a saturated concrete is about 8 g for w/c-ratio 0.60 and 6.5 g for w/c-ratio 0.45, Fagerlund and Johannesson (2005). The discrepancy between the theoretical amount of frozen water and the experimental can have two explanations:

1. The concrete was not completely saturated. Only a very small residual air space (0.75% air for the w/c-ratio 0.60 and 0.42% for the w/c-ratio 0.45) can explain the low expansion.
2. Water is expelled through the surface of the specimen. The total surface is 144 cm^2. If the critical thickness with regard to frost damage is 1 mm Fagerlund (2004), a specimen volume of $144 \cdot 0.05 = 7$ cm^3 can be 'protected' by the surface. There is still 61 cm^3 that is not protected. Maybe the critical thickness is a bit higher for w/c-ratio 0.60 but that could not explain the lower expansion for this concrete.

The calculation shows that the first explanation is the most plausible one.

When temperature lowering is stopped at –23°C the specimen expansion immediately stops. Thus, as for Test series 1, there is no sign of internal migration of unfrozen water accompanied by microscopic ice lens growth.

Stage 5: When warming starts, the concretes immediately start to expand. This depends on the normal thermal expansion. In this case this is strengthened by a thermal coefficient of expansion of ice being about five times as large as that of the material itself. The expansion is however lower than the thermal expansion of the completely thawed concrete, which indicates that there is some relaxation of internal stresses due to some melting of ice.

Stage 6: From about –10°C the concretes contract until all ice is melted at about -1°C. This indicates that some of the tensile stresses in the concrete caused by freezing are elastic, while other had led to fracture and permanent dilation.

Stage 7: The small recovery (expansion) in the range -1°C to 0°C was observed in both concrete types. The explanation is discussed in paragraph 5.3.3.

Stage 8: After complete thawing there is a big permanent dilation, about 0.5‰ for w/c-ratio 0.60 and about 0.8‰ for w/c-ratio 0.45. This is more than 3 or 5 times the fracture tensile strain. The reduction in dynamic E-modulus is about 40% for w/c-ratio 0.60 and about 60% for w/c-ratio 0.45.

w/c-ratio 0.40: 6% air

The concrete with w/c-ratio 0.40 and high air content (nominal 6%) behaved differently from the two concrete types described above. See Figure 5.4.3 and Figure 5.4.4.

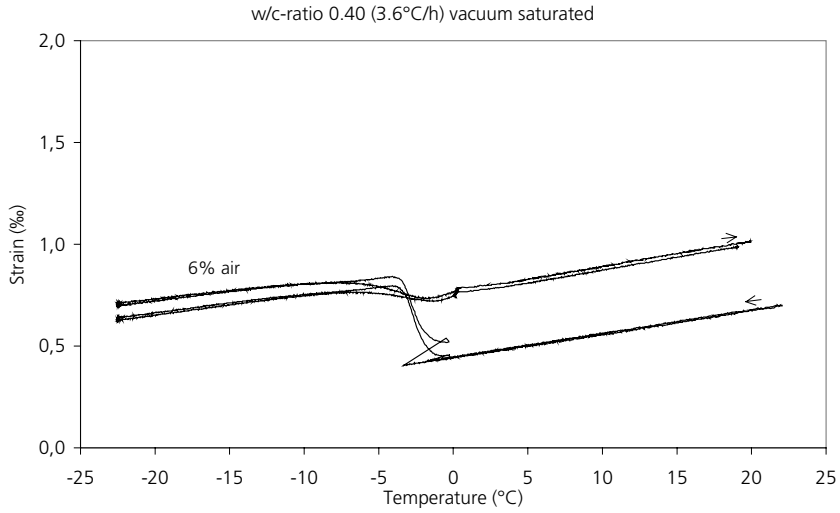

Figure 5.4.3. Strain versus temperature for vacuum saturated samples of w/c-ratio 0.40 and with 6 % of entrained air (nominal value, real value 6.6%).

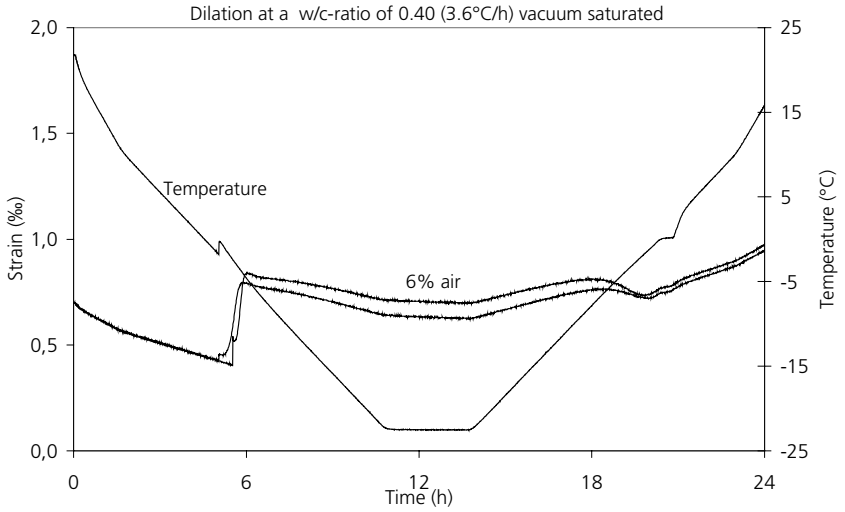

Figure 5.4.4. Length change and temperature versus time for vacuum-saturated specimens with a w/c-ratio of 0.40 containing 6% air (nominal).

Nucleation of supercooled water at about –4°C creates a big expansion of about 0.5‰ which is three times the fracture strain. This early expansion is probably to big extent caused by freezing of water in the air pores. Thereafter, when temperature is lowered, no expansion occurs. The specimens contract linearly with lowered temperature by almost the same contraction coefficient as that of the unfrozen concrete. This indicates that no, or very little, ice is formed in the region –5°C to -23°C.

In Test series 1 the same concrete had a certain, although small, expansion down to –10°C. The reason why this expansion is lacking in Test series 2 could be that water that was locally supercooled in isolated capillaries in the virgin, non-dried concrete in Test series 1 is now nucleated due to micro-cracking occurring during the pre-drying procedure before Test series 2.

The damage after thawing was considerable, the E-modulus was reduced by about 25% and the permanent dilation was about 0.3‰, which is twice the fracture strain. This result shows that the nucleation of supercooled water can cause severe frost damaged in a concrete with high degree of saturation.

5.4.3 Test series 2: Summary and discussion of results

All results from Test series 2 are presented in APPENDIX to Chapter 5. In Table A5.3 an overview of dilation at different stages (defined by Figure 4.4.4) during the freeze/thaw cycle is given. Furthermore, values of the change in resonance frequency caused by freeze/thaw, and the degree of saturation during freeze/thaw are listed.

Length change curves versus temperature and versus time for all specimens are also shown in APPENDIX to Chapter 5, Figures A5.17-A5.22.

By the vacuum saturation procedure the effect of air pore structure, like specific surface and spacing factor, should be neutralized. The major parameter supposed to possibly affect damage should be the amount of freezable water, which for a constant air content, is only a function of the water-cement ratio. For that reason only the influence of the w/c-ratio on dilation and resonance frequency is shown in Figure 5.4.5. It can be seen that all the damage parameters have been significantly changed since Test series 1.

There is no unique relation between the w/c-ratio and damage. The reason could be that the saturation was more or less complete in different specimens. It has previously been found in numerous studies that the degree of damage can vary quite much for concrete in which the critical degree of saturation has been transgressed, Fagerlund (1977).

The mean value of damage is about the same for w/c-ratio 0.40 and 0.60. Concrete with w/c-ratio 0.45 suffers considerably more damage. Both the dilations and the reduction in resonance frequency are bigger than for the two other w/c-ratios.

The reason for this is unclear. One possibility is that the saturation was more complete at this w/c-ratio.

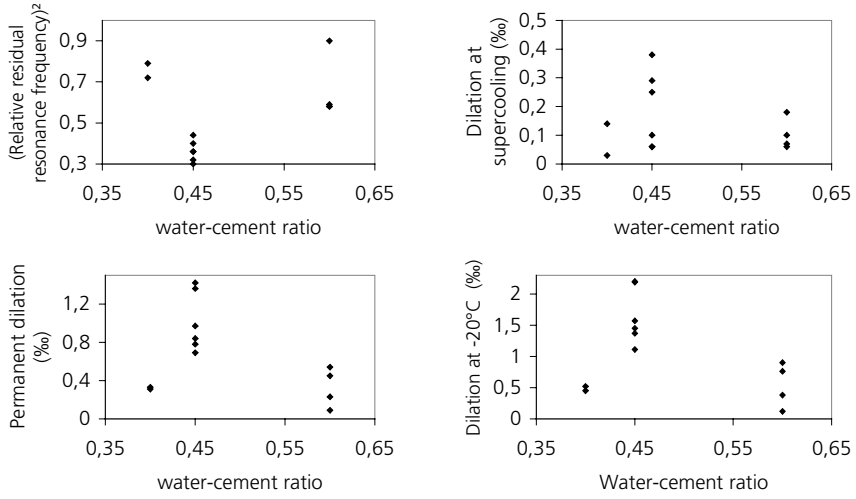

Figure 5.4.5. The influence of the water-cement ratio on the damage parameters in Test series 2. Data from APPENDIX to Chapter 5, Table A5.3.

5.4.4 Test series 2: Conclusions

As expected, all the specimens expanded considerably, and therefore obtained considerable damage. Most expansion occurred in the temperature region 0°C to -10°C, but the specimens continued to expand to the lowest temperature used, -23°C. When temperature change was stopped at that temperature also expansion stopped. One can suspect that the expansion curve is more or less affine with the ice formation curve.

The expansion during freezing was lower than expected, since the 9% increase in volume when water is transformed into ice ought to cause the same expansion of the concrete, considering the closed container model of destruction, which ought to be valid. Part of this discrepancy can be explained by escape of 'excess' water from the periphery of the specimens. The most plausible explanation is however that it was found to be quite difficult to completely saturate concrete with high air content. That this explanation is reasonable is strengthened by the fact that concrete of a given w/c-ratio sometimes has lower expansion during freezing the higher the air content is. The reverse ought to have been the case had the whole air-pore system been fully saturated.

The discrepancy between air content and dilation at –20°C is shown in Table 5.4.1. The table also illustrates the differences between the two specimens of the same

type, which indicates that somewhat different degrees of saturation had been reached in the two specimens.

Table 5.4.1. Relation between nominal air content and dilation at –20°C.

w/c-ratio	Air content %	Dilation at –20°C ‰	
		Specimen 1	Specimen 2
0.60	4	0.90	0.76
	6	0.38	0.12
0.45	4	1.45	1.37
	6	0.45	0.52
	10	1.57	1.11

5.5 Test series 3: Pre-dried, re-saturated samples with adjusted degree of saturation

5.5.1 Introduction. Preparation of samples

Natural water absorption for almost 4 years into virgin specimens was not high enough to cause frost damage in air-entrained concrete (with one exception, w/c-ratio 0.40 with 4% air, see Figure A5.5.9). Vacuum saturation – although not complete – caused severe frost damage in all concretes irrespectively of the air content. In Test series 1 only a small portion of the air pore system can be assumed to be water-filled. In test series 2 almost all air pore space was supposed to be water filled. In previous research it has been proven that damage occurs when a certain fraction of the air pore system is water-filled, Warris (1964), Fagerlund (1980), Klamrowski et al (1984). This means that a certain individual critical degree of saturation exists for each concrete.

The aim of Test series 3 was to investigate how different freezing rates affected concrete with degrees of saturation between the natural and full saturation, on the other hand to investigate how the critical moisture content might be affected by the freezing rate.

To study this, undamaged specimens from Test series 1 were given a degree of saturation lower than 1 and were then tested with use of the 'normal' cycle. New virgin samples were also prepared in the same manner and were tested with use of the 'rapid' cycle.

For adjustment of the moisture content the samples were first pre-dried in a closed box together with silica gel and a carbon dioxide absorbent for two months, and were then vacuum saturated with water, see paragraph 4.5. The weights obtained after drying and water saturation enabled the target weights to be calculated (see Eq. 4.5.4). The samples were dried at +50°C in order for these targets weights to be reached. In some cases it occurred that the specimens to be compared with regard to response to the freezing rate did not receive exactly the same degree of saturation,

although the aim was to achieve this. Since the degree of saturation is the most fundamental parameter for internal frost damage the difference in this will unfortunately obscure the effect of different freezing rates.

In contrast to Test series 1 the specimens were not 'virgin', but hade been subjected to a drying-re-saturation procedure. As described in paragraph 5.3.1, this procedure will have an effect that might be negative due to increase in freezable water, but that might also be positive due to drying out of defects like cracks. Thus, in Test series 3 both the effects of the drying-re-saturation procedure and the effect of the degree of saturation will be revealed.

5.5.2 Test series 3: Examples of results

All results from Test series 3 are presented in APPENDIX to Chapter 5. In Table A5.4 an overview of dilation at different stages (defined by Figure 4.4.4) during the freeze/thaw cycle is given. Furthermore, values of the change residual resonance frequency caused by freeze/thaw, and the degree of saturation during freeze/thaw are listed.

Length change versus temperature curves for w/c-ratio 0.60 and 0.40 are shown in this paragraph. The curves for w/c-ratio 0.45 can be found in APPENDIX to Chapter 5, Figure A5.23-A5.25.

The degrees of saturation given in the figures for each curve are rather uncertain depending on difficulties to define the total pore volume and real dry weight, c.f. paragraph 4.5.

w/c-ratio 0.60

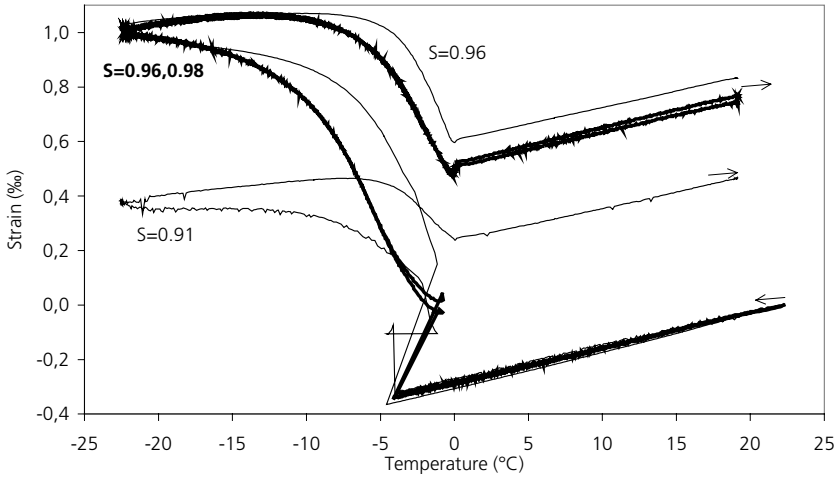

Figure 5.5.1. The influence of freezing rate on samples of w/c-ratio 0.60 with 4% nom. air content given different degrees of saturation. The thick lines belong to samples tested with the 'normal freeze-thaw cycle. The thin lines belong to samples tested with the 'rapid' freeze-thaw cycle.

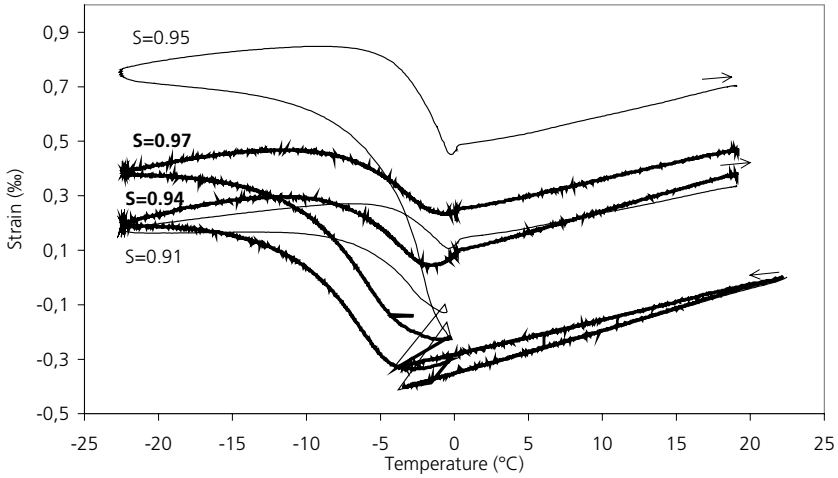

Figure 5.5.2. The influence of freezing rate on samples of w/c-ratio 0.60 with 6% nom. air content given different degrees of saturation. The thick lines belong to samples tested with the 'normal freeze-thaw cycle. The thin lines belong to samples tested with the 'rapid' freeze-thaw cycle.

w/c-ratio 0.40

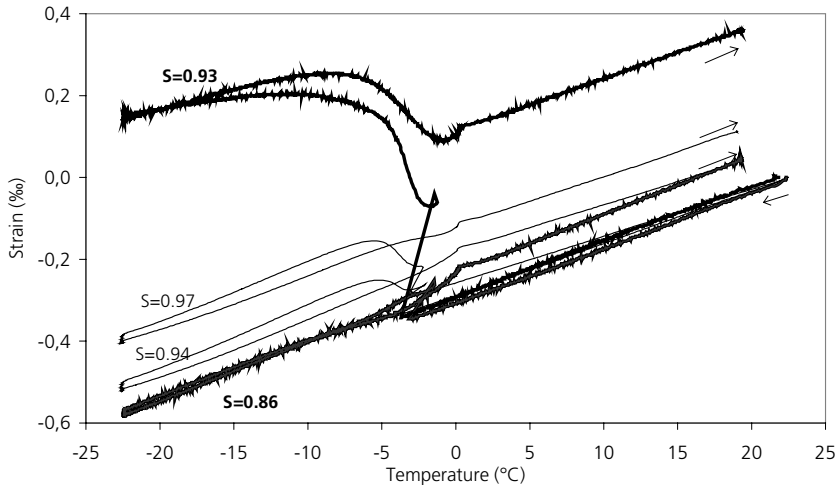

Figure 5.5.3. The influence of freezing rate on samples of w/c-ratio 0.40 with 6% nom. air content given different degrees of saturation. The thick lines belong to samples tested with the 'normal freeze-thaw cycle. The thin lines belong to samples tested with the 'rapid' freeze-thaw cycle.

As shown by the figures it was only in few cases that a fair comparison of the effect of the freezing rate could be made. In most cases the degree of saturation differed too much between the specimens. The one exception is Figure 5.5.1 where three of the four specimens had almost the same degree of saturation, 0.96-0.98. The length change curves for specimens for these three specimens are remarkably alike for both freezing rates. This indicates that the freezing rate has small influence on frost resistance, if any, when the moisture content is kept unchanged during the test (moisture isolated freeze/thaw).

The general trend of all results is that the freezing rate has no distinctive effect, sometimes an increased rate seems to increase damage (Figure 5.5.2), often it decreases damage (Figure 5.5.3, A5.23). This statement is true irrespectively of the w/c-ratio or degree of saturation. Thus, the results from Test series 1 that the freezing rate has no, or marginal, effect on frost damage is strengthened.

5.5.3 Test series 3: Summary and discussion of results

All results are presented in APPENDIX to Chapter 5.

The objective of Test series 3 was to see if the influence of freezing rate was altered as the degree of saturation was changed, or in other words, to see if the critical degree of saturation was affected by the freezing rate. All data over dilation and change in residual resonance frequency for all the 24 tests are plotted in Figure 5.5.4. This figure can be used for a qualitative estimation of the effect of the freezing rate.

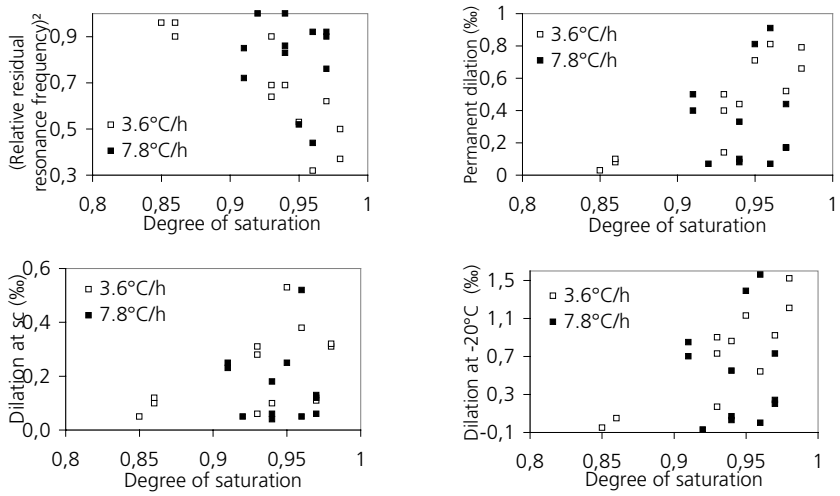

Figure 5.5.4. The influence of degree of saturation on damage parameters.

As can be seen in Figure 5.5.4, no distinct effect of the freezing rate could be observed. The major effect seen is that of the water content. For both freezing rates, destruction increases with increased degree of saturation. The maximum allowed degree of saturation seems to be about 0.85 if a maximum reduction in E of 10% and a maximum permanent dilation of 0.1‰ is accepted.

Theoretically, according to the hydraulic pressure theory, an increased freezing rate should give a reduced value of the critical spacing factor. This should cause a certain reduction in the critical degree of saturation, but as shown theoretically in Fagerlund (1992) this should be rather small, so small that it cannot be discerned in the actual tests, with its uncertainties in the true values of degree of saturation.

Note: Despite the fact that all the samples tested with the 'normal' cycle had been tested before in Test series 1, and had shown little or no expansion at that test, it cannot be excluded that the previous testing has influenced its behaviour during Test series 3.

5.5.4 Test series 3: Conclusions

Test series 1 showed that the freezing rate hade no observable effect on frost damage in specimens stored for 4 years in water. The results of Test series 3 clearly indicate that the same insensitivity to the freezing rate as was found in Test series 1 are also valid for concrete with higher moisture contents.

6 Freezing and thawing experiments - Influence of the lowest freezing temperature

6.1 Introduction

Ice can form either heterogeneously or homogeneously. Ice formed heterogeneously is nucleated on a surface, such as for example on a pore wall. According to Helmuth (1960), hardened cement paste contains no structure able to facilitate heterogeneous ice formation. In contrast, when ice is formed homogeneously, it is formed within a liquid, an ice-liquid interface being formed. Unless the ice crystal has at least a certain size, it is thermodynamically unstable and melts immediately. The possibility for an ice crystal to be of sufficient size for being stable increases with decreasing temperature. Relations between pore size and freezing temperature of water in the pores are discussed in Chapter 9. Since one might assume that the damage produced becomes more severe as the amount of ice increases, the lowest temperature that occurs during a freeze-thaw cycle is a parameter of the frost damage mechanism that should play an important role.

It must be remembered, however, that the hydraulic pressure mechanism (Chapter 2) in its original form, assuming a permeable pore system, does not necessarily predict that damage increases with increasing amount of ice but instead with increased rate of ice formation. Normally this is lower the lower the temperature. Therefore, the theory might predict smaller hydraulic pressure at lower temperature. Low temperature, however, causes more ice to form, and this might cause a big reduction in permeability of the material, so that also a slow freezing rate can generate large pressures. When the pore structure has become more or less totally blocked by ice a special case of the hydraulic pressure theory, the closed container theory (Chapter 2), might be applied.

According to the theory of microscopic ice lens growth (Chapter 2) more ice formation, for example due to lower temperature, creates more places (ice-bodies in capillary pores) to which the gel-water, and other unfrozen water, or locally supercooled water, can diffuse and freeze, creating pressure. The process is driven by the difference in free energy between the ice and the unfrozen water occurring when temperature is gradually decreased. Possibly, this driving force increases with decreasing temperature. If so, the influence of this mechanism should increase with decreased temperature.

Even if the main aim of this study was to investigate the effect of lowest temperature, it will also give information on the effect of keeping concrete temperature constant during the 3 hours periods that separates the two stages in the freezing curve,

Figure 6.2.2. Therefore, the study presented in this chapter is a complement to the investigation described in Chapter 7, in which the same minimum temperatures were used, but in which temperature was held constant for 12 hours at each minimum temperature. Results from the study presented here shall therefore be compared with results presented in Chapter 7.

When the temperature is kept constant, the hydraulic pressure should become zero, and the specimen should be expected to contract when the hydraulic pressure vanishes. On the other hand, if the ice-formation before the isothermal period has been high enough to damage the sample, this will stay in an expanded state during the period of constant temperature.

Powers and Helmuth (1953) found continued expansion of non-air-entrained concrete during many hours when temperature was held constant, Figure 2.4.3b. They explained this by a continued ice lens growth. Theoretically, however, also the microscopic ice lens growth should stop when temperature-lowering stops, provided local equilibrium is rapidly established between ice in capillaries and unfrozen water in nearby capillaries. According to the Powers/Helmuth experiments it should take long time to establish equilibrium. However, locally supercooled water in isolated capillaries is not necessarily in equilibrium with ice and might therefore migrate to ice-bodies for longer time. One objective of the test presented in this chapter (as for the test in Chapter 7) was to try to verify the Powers/Helmuth experimental findings. The technique used here, moisture isolated freeze/thaw, is possibly not the same as in the Powers/Helmuth experiments. Exactly how these were performed was not described in their article.

6.2 Experimental technique and variables

The test setup and techniques employed (dilation and resonance frequency measurements) in the investigation are described in paragraph 4.2. The damage parameters considered were the change in residual resonance frequency squared, the permanent dilation at +5°C and the maximum dilation both at -15°C and at -30°C. The definition of dilation is given in Figure 4.4.4. The temperature cycle involved a freezing rate of 3.6°C/h. Two lowest temperature levels were employed during the same cycle, -15°C and -30°C, the material being kept for 3 hours at each of the two temperature levels, see Figure 6.2.2.

Two Test series, 4 and 5, were performed and reported in this chapter. In Test series 4, the specimens used had been stored in lime-saturated water for almost four years and had never been dried. In Test series 5, specimens undamaged in Test series 4 were given (artificially) specific degrees of saturation and were then tested again

using the same temperature cycle. The procedure for adjusting the specimens to the individual degree of saturation is described in Chapter 4 paragraph 4.5.3. 20 specimens were used for Test series 4, and 14 of those specimens for Test series 5. Figure 6.2.1 provides an overview of specimens used in the two Test series.

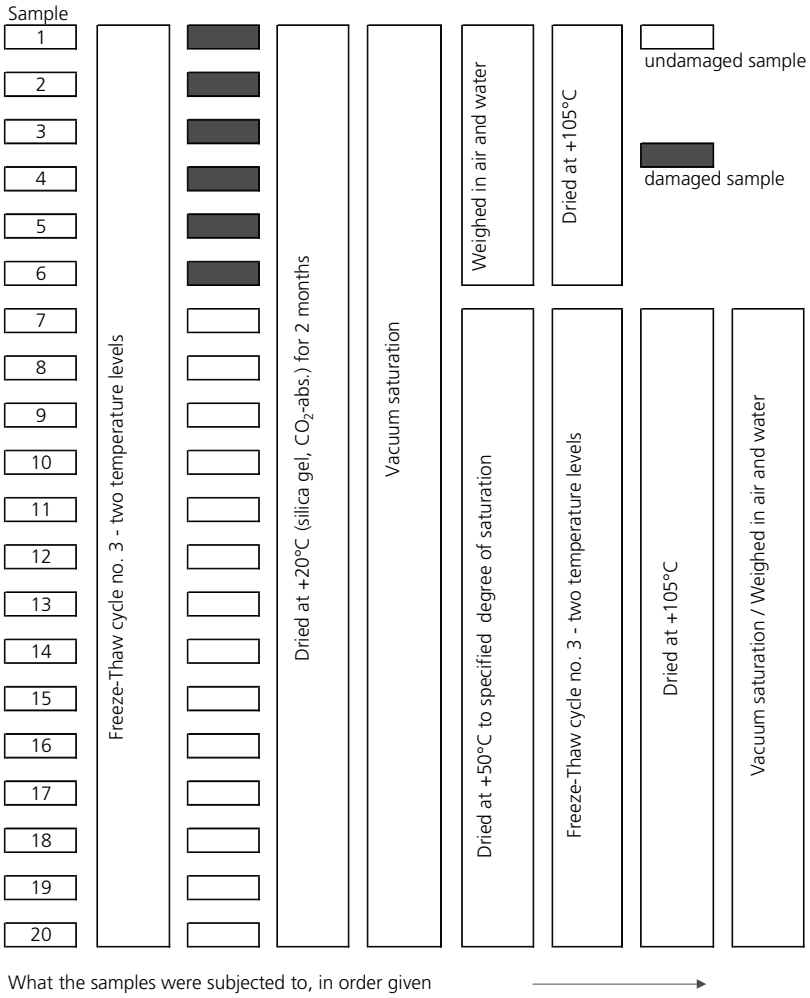

Figure 6.2.1. Test series 4 and 5; effect of lowest temperature. Specimens and test procedure.

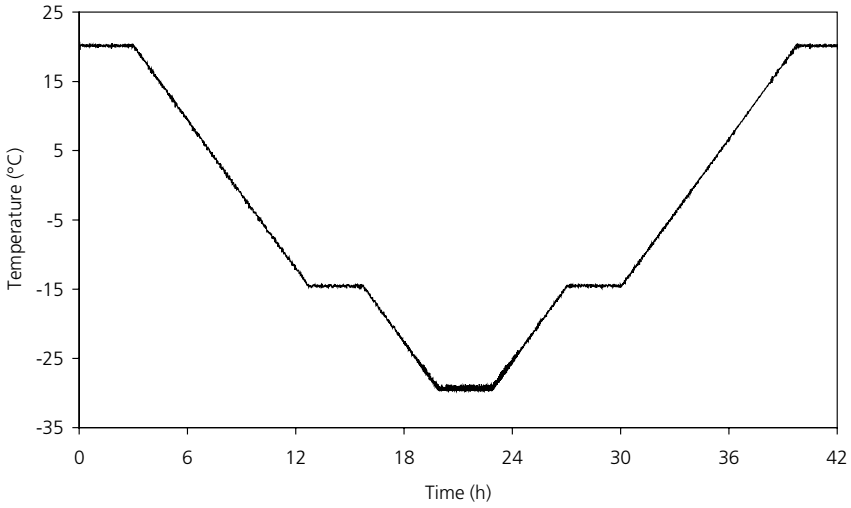

Figure 6.2.2. Test series 4 and 5. Temperature cycle of air in the climate chamber.

6.3 Test series 4: Never-dried specimen with 'natural' water content

6.3.1 Introduction

Prior to the tests the specimens had been stored in saturated lime-water for almost 4 years. The treatment and moisture content is the same as for Test series 1 (Chapter 5) and 6 (Chapter 7).

All results are shown in APPENDIX to Chapter 6. Damage parameters are dilation at different stages during the freeze/thaw cycle, and the resonance frequency. This was determined after the entire cycle.

6.3.2 Non-air-entrained concrete

Length change-time and *temperature-time* curves for non-air-entrained concrete with w/c-ratio 0.60 and 0.40 are shown in Figure 6.3.1. The corresponding *length change-temperature* curves are shown in Figure 6.3.2.

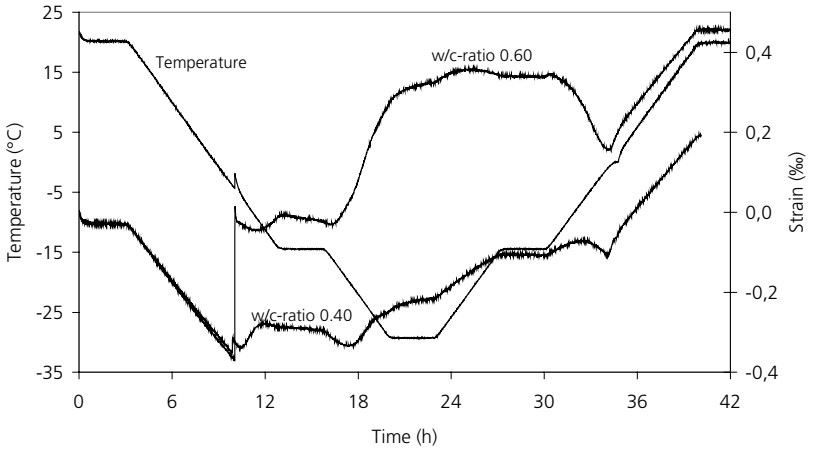

Figure 6.3.1. Length change and temperature versus time for non-air-entrained concrete with w/c-ratio 0.60 and 0.40.

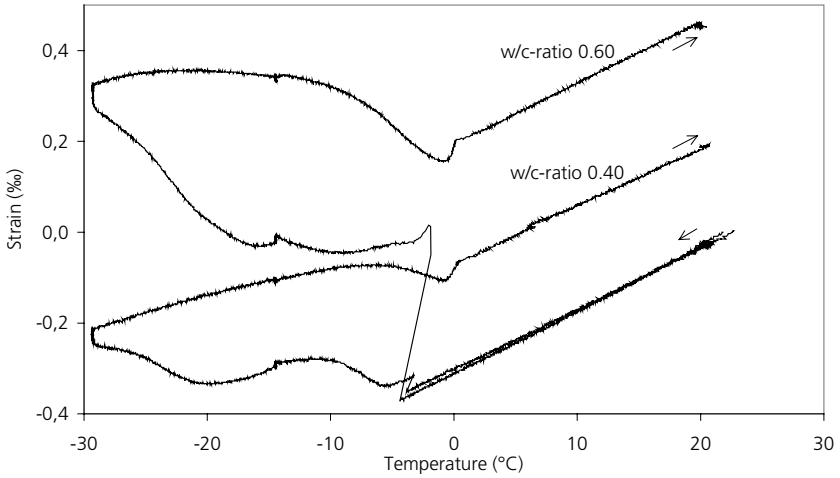

Figure 6.3.2. Length change versus temperature for non-air-entrained concrete with w/c-ratio 0.60 and 0.40.

The results are very like these obtained for non-air-entrained concrete in Test series 6, see Chapter 7, Figure 7.3.1 and Figure 7.3.2. The detailed discussion concerning mechanisms, carried out there, is therefore valid also for Test series 6. Therefore, only some comments will be made below.

- In the samples with w/c-ratio 0.60, big expansion occurs when supercooling is overcome. Expansion is almost totally non-reversible indicating that ice is formed under constrained conditions, like in a 'closed container' although certainly also hydraulic pressure is developed when excess water is expelled by high rate. At w/c-ratio 0.40 a much smaller expansion occurs indicating that less ice is formed. Expansion for w/c-ratio 0.40 is partly reversible. Exactly the same behaviour was observed for Test series 6 in Chapter 7.
- When temperature is lowered to –15°C, there is at first a certain reduction of the early expansion in all specimens, probably caused by relaxation of hydraulic pressure as the rate of ice formation is heavily reduced. Thereafter, they all expand until temperature lowering comes to a halt at -15°C. This is also the same behaviour as was found in Test series 6. The mechanism behind this expansion can be both hydraulic pressure and microscopic ice lens growth. There is no possibility to tell which of these that is dominant.
- When temperature is held constant for 3 hours at –15°C all specimens showed considerable contraction. This was about the same for both w/c-ratios. The same behaviour was observed in Test series 6 where temperature was held constant at -15°C for 12 hours. Possible reasons for the contractions are discussed in detail in paragraph 7.3.2. The most plausible explanation seems to be release of hydraulic pressure. Ice lens growth, which might occur if there is no local equilibrium established between ice and unfrozen water during the isothermal period, ought to lead to expansion and not contraction in a non-air-entrained concrete.
- During the next step in temperature lowering down to -30°C a big contraction occurred during the first hours, especially for w/c-ratio 0.40. The same behaviour was observed in Test series 6 (paragraph 7.3.2) and can be explained by the ice lens growth mechanism as is discussed in paragraph 7.3.2. After a few hours of contraction, big expansion occurred until temperature came to the next halt at –30°C. The expansion is biggest for w/c-ratio 0.60, which indicates that the main mechanism is hydraulic pressure since the amount of freezable water is higher than for w/c-ratio 0.40. This will promote hydraulic pressure but, counteract ice lens growth.
- When temperature is held constant at –30°C all specimens expanded slightly. The same was observed in Test series 6. The reasons behind the expansion are discussed in paragraph 7.3.2. Since hydraulic pressure cannot explain expansion when temperature is held constant, the most likely mechanism is contin-

ued growth of capillary ice, indicating that local equilibrium is not established between ice and unfrozen water directly when temperature change stops. Another possibility is osmotic pressure as described in paragraph 7.3.2 and 8.3.2. In the complementary calorimetric studies in Chapter 9, paragraph 9.7 and 9.8 no ice was formed during these isothermal periods.

- When temperature is gradually increased to -15°C, all samples start to expand, but after the first half of this period the samples with high w/c-ratio starts to contract. The large amounts of ice formed within these samples have expanded them to extents that have caused big internal tension. When the melting process begins, these stresses are gradually relieved, and the samples contract. The specimens with low w/c-ratio expand linearly during the entire period indicating a more continuous melting of ice.
- When the samples are kept constant for three hours at -15°C, no volume changes whatever can be seen. No hydraulic pressure can exist, since no new ice is formed. Local equilibrium between capillary ice and unfrozen water seems to be established rapidly when temperature increase is stopped, viz. no internal moisture migration in any direction seems to occur.
- During the remainder of the thawing (from -15°C to 0°C), the samples with high w/c-ratio contracts as long as they contain ice (until close to 0°C).
- After complete thawing all the samples have a permanent dilation larger than 0.20‰. In previous investigations it was found that these materials could withstand an expansion of about 0.10 à 0.15‰ before any detectable damage was measured. For w/c-ratio 0.60 the critical dilation 0.15‰ was in all cases obtained (or near to) when supercooling was overcome. The reduction in E-modulus after thawing was about:
  - 55% for w/c-ratio 0.60
  - 70% for w/c-ratio 0.45
  - 75% for w/c-ratio 0.40

Thus, a big dilation during freezing does not necessarily give the biggest damage.

All results with non-air-entrained specimens showed that the *minimum freezing temperature has big effect on frost destruction*. The following relation between the dilation at –15°C and –30°C was found (see APPENDIX to Chapter 6, Table A6.1):

w/c-ratio 0.60:	$Dil_{-30°C}/Dil_{-15°C}=2.2$
w/c-ratio 0.45:	2.5
w/c-ratio 0.40:	2.2

Thus, the expansion was more than doubled when the lowest temperature was reduced from –15°C to –30°C.

6.3.3 Air-entrained concrete

Length change-time and *temperature-time* curves for air-entrained concrete with w/c-ratio 0.60 and 0.40, and 6% air are shown in Figure 6.3.3. A *length change-temperature* curve the same samples are shown in Figure 6.3.4.

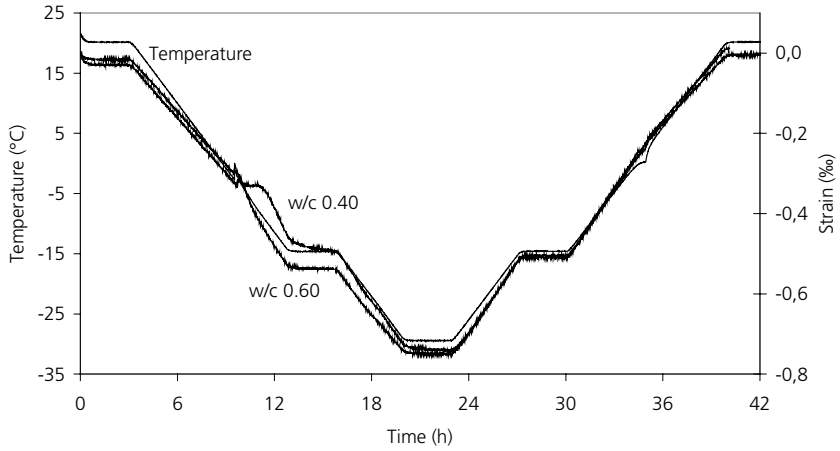

Figure 6.3.3. Length change and temperature versus time for samples with w/c-ratio 0.60 and 0.40, and with 6% air.

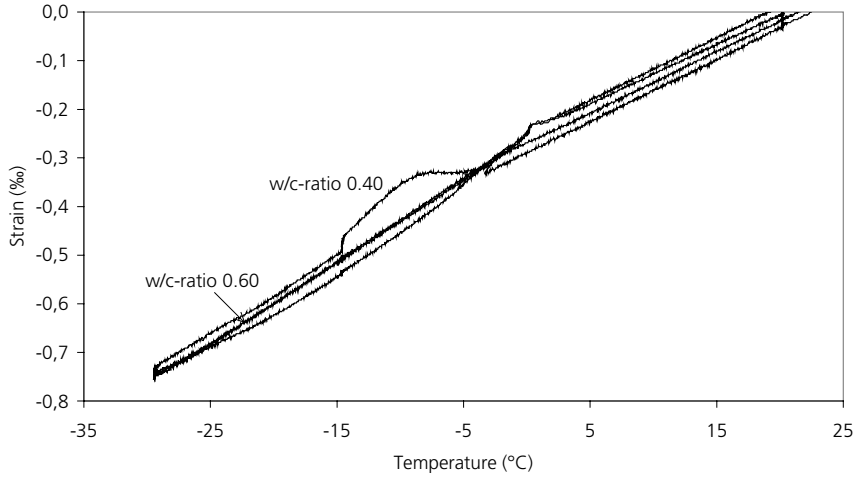

Figure 6.3.4. Length change versus temperature for samples with w/c-ratio 0.60 and 0.40 and with 6% air.

The results are very like these obtained for air-entrained concrete in Test series 6, see Chapter 7, Figure 7.3.3 and Figure 7.3.4. The detailed discussion concerning mechanisms, carried out there, is therefore valid also for Series 6. Therefore, only some comments will be made below.

- During the first constant period at –15°C the specimens with w/c-ratio 0.60 show no change in length. The specimen with w/c-ratio 0.40 contracts slightly. This is in accordance with the behaviour of the non-air-entrained concrete in this Test series (paragraph 6.3.2) and with air-entrained concrete in Test series 6 (paragraph 7.3.2).
- During the second constant period at –30°C the specimens with w/c-ratio 0.60 did not change their length, while that with w/c-ratio 0.40 contracts slightly. This is in completely accordance with what was seen in Test series 6 for air-entrained concrete.
- During the increase in temperature between -30°C and -15°C all samples show a linear expansion, which is smaller than that of a sample only containing water.
- When temperature once again reached –15°C, all specimens immediately stopped expanding. No length change occurred during the three hours long halt at –15°C.
- None of the samples had any permanent dilation after this moisture isolated single freeze-thaw cycle and were therefore used again in Test series 5.

No specimen dilated above the normal contraction at any of the two temperatures -15°C and -30°C. There is, however a certain tendency that the 'negative dilation' (contraction above the thermal) is a bit bigger at –30°C. Thus, a lower temperature does not cause bigger damage in concrete with proper air entrainment.

6.3.4 Test series 4: Summary and discussion of results

All results are presented in APPENDIX to Chapter 6.

The main object with Test series 4 was to study how the lowest temperature influences damage measured as length changes and changes in resonance frequency in the specimen. The results are best shown in Figure 6.3.5.

The *expansion part* of the figure is valid for non-air-entrained concrete. Expansion increased by a factor two when temperature was lowered from -15°C to -30°C. This shows that the internal pressure caused by hydraulic pressure, by ice formed under big constraint ('closed container' freezing), and/or by ice lens growth, increases almost in direct proportion to the minimum temperature during the cycle.

The *shrinkage part* of the figure is valid for air-entrained concrete. The effect of minimum temperature is less obvious. The fact that air-entrained concrete shrinks is in accordance with results reported by Powers and Helmuth (1953), and can be explained by the ice lens growth mechanism.

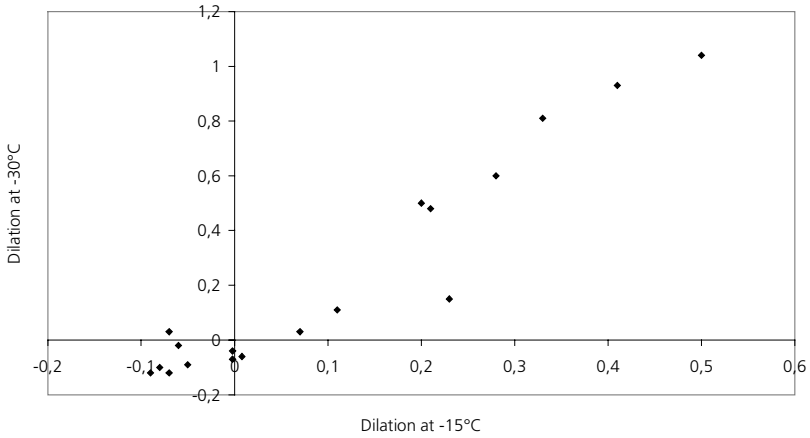

Figure 6.3.5. Relation between dilation (expansion above extrapolated thermal contraction, see Figure 4.4.4) at –15°C, and dilation at –30°C.

In Figure 6.3.6, dilation defined by Figure 4.4.4 is plotted versus degree of saturation, air content and w/c-ratio. As expected, an increase in degree of saturation tends to give an increase in both the maximum expansions, and the permanent expansion. This is valid for both temperature levels –15°C and –30°C. The deviations from a more well-defined relation between S and dilation depends on that widely different air contents and w/c-ratios are included in the same diagrams. The amount of dilation occurring when supercooling is overcome, and a large amount of ice is formed

rapidly, has not much to do with the degree of saturation but is merely depending on whether the concrete is air-entrained or not.

The influence of air content was also found to be as expected. An increase in the air content resulted in decrease in all types of dilation.

When the influence of w/c-ratio is evaluated it is necessary to separate samples containing entrained air from those without. For the specimens without entrained air the dilations were decreasing with decreasing w/c-ratio. For the specimens with entrained air very small differences in dilation were detected between the different w/c-ratios. The positive effect of air obscures the negative effect of a high w/c-ratio. For the same air content there is a tendency that a small increase in dilation occurs with decreasing w/c-ratio. The same tendency was found in Test series 1 (Chapter 5) and Test series 6 (Chapter 7). The reason might be that the resistance to flow of expelled water is higher in a concrete with lower w/c-ratio causing increased hydraulic pressure.

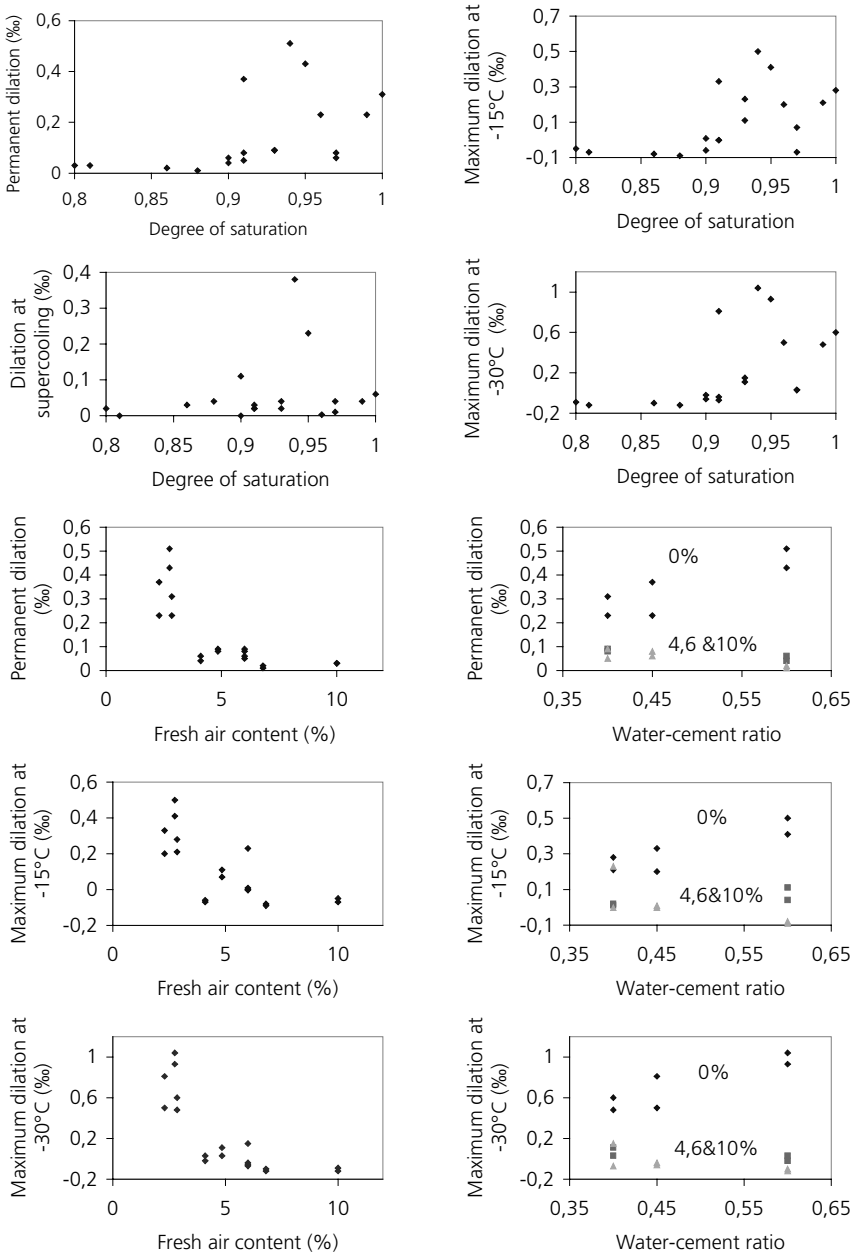

Figure 6.3.6. Different damage parameters plotted versus degree of saturation, air content of the fresh concrete and w/c-ratio.

6.3.5 Test series 4: Conclusions

For *non-air-entrained concrete* it was found that a decrease in temperature from -15°C to -30°C resulted in an increase of the dilation of the frozen concrete by a factor two. This is valid independently of the w/c-ratio.

The dilation at both -15°C and -30°C was found to be highest for w/c-ratio 0.60 and smallest for w/c-ratio 0.40:

- w/c-ratio 0.60. Average dilation at –30°C: 1.0‰
- w/c-ratio 0.45 : 0.7‰
- w/c-ratio 0.40 : 0.5%

This indicates that the *main* destruction mechanism is hydraulic pressure and/or the special case of this, the 'closed container' mechanism. The ice lens growth mechanism ought to be promoted by a high amount of non-freezable water, and this is increased with decreased w/c-ratio.

For *air-entrained concrete* it was found that the minimum temperature has no effect. All concrete types were completely undamaged after the test.

6.4 Test series 5: Pre-dried, re-saturated samples with adjusted degree of saturation

6.4.1 Introduction. Preparation of samples

Since all the samples with air entrainment were found to be undamaged, they were re-used in Test series 5.

In Test series 5 the aim was to investigate if the effect of lowest temperature observed in Test series 4, using specimens with natural water content taken up during long-term water storage, is influenced by the degree of saturation.

The same preparation procedure as described for Test series 3 was used. The samples were dried for two months at +20°C in a chamber containing silica gel and a carbon dioxide absorbent. Thereafter, they were exposed to vacuum before being saturated by water. After storage in water for several days, the samples were dried again at +50°C to varying degrees of saturation. The moisture sealed samples were subjected to the same freeze-thaw cycle as Test series 4, Figure 6.2.2.

6.4.2 Test series 5: Example of results

All results can be found in APPENDIX to Chapter 6, Table A6.2 and Figures A6.7-A6.12. Some representative results valid for concrete with w/c-ratio 0.60 are shown in Figure 6.4.1 and Figure 6.4.2.

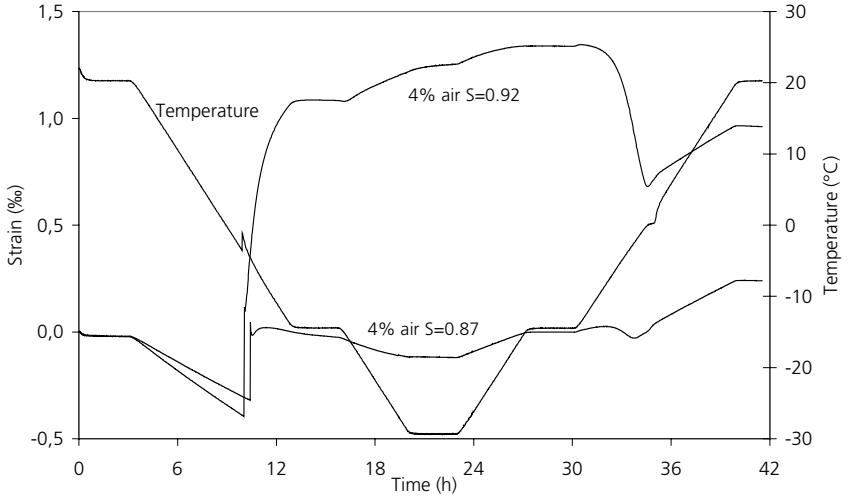

Figure 6.4.1. Length change and temperature versus time for samples with w/c-ratio 0.60 and 4% air. Two different degrees of saturation.

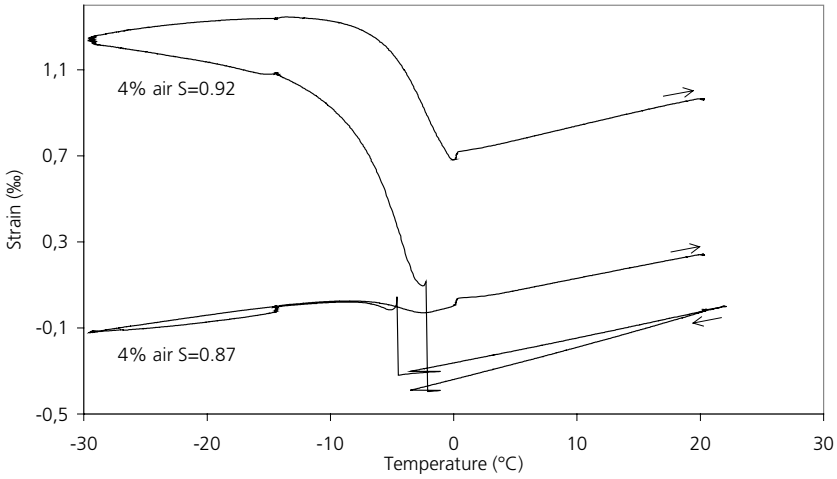

Figure 6.4.2. Length change versus temperature for samples with w/c-ratio 0.60 and 4 or 6% air. Two different degrees of saturation for each concrete type.

The big importance of the degree of saturation is very apparent. An increase in degree of saturation of 0.05 (from 0.87 to 0.92) for the specimens in Figure 6.4.1 causes a dramatic increase in dilation. This increase in degree of saturation corresponds to a difference in amount of water of only about 0.7g. Similar big effects of degree of saturation was also found for the other w/c-ratios, see APPENDIX to Chapter 6. The degree of saturation overshadows the effects of air content and w/c-ratio.

The results are similar to those obtained in Test series 7. The discussion carried out there (paragraph 7.4.2) can therefore also be applied to the results presented here. The following observations deserve some comments:

- Big expansion occurs already when supercooling is overcome, in cases where the degree of saturation is high. The higher the degree of saturation, the bigger the expansion. For the specimens in Figure 6.4.1, the expansion is big enough to cause considerable damage.
- During the decrease in temperature to -15°C the increase in degree of saturation of 0.05 leads to a four-fold increase in dilation. This is remarkable since the increase in amount of water was only 0.7 g. The reason for this big effect of a small increase in moisture content is probably that the spacing factor between pores, that are 'effective', i.e. that are not water-filled, is increased. According to the theories of frost destruction, an increased effective spacing factor will increase both hydraulic pressure and pressure caused by ice-lens

growth. The effect of water absorption on the effective spacing factor is described in detail in Fagerlund (2004).

- When temperature is held constant for three hours at -15°C specimens with both degrees of saturation contract slightly. This is in accordance with observations in Test series 7, and the possible mechanism is described in paragraph 7.4.2.
- When temperature is lowered to –30°C the samples with very high degrees of saturation continue to expand slightly (most evident for the samples with a high w/c-ratio), while the samples with lower degrees of saturation contracts.
- During the temperature halt at –30°C there is a slight tendency of expansion for concrete with w/c-ratio 0.60. This is in accordance with Test series 7 in which the temperature halt was extended to 12 hours.
- After thawing, all specimens with high degree of saturation were severely damaged as indicated by permanent dilation and loss in residual resonance frequency.

6.4.3 Test series 5: Summary and discussion of results

All results are presented in APPENDIX to Chapter 6.

All specimens obtained some expansion during freezing, also specimens with high air content. This is in contrast to the same air-entrained specimens when they were tested in Test series 4, containing water that had been sucked in under normal conditions; the 'natural' water content. The reason is certainly that the water absorption in Test series 5, after vacuum treatment (and a certain drying), was so high that the available 'effective' air content was reduced too much. Therefore the specimens behaved as if they had insufficient air content.

Lowering the temperature from –15°C to –30°C caused some increase in dilation for all tested specimens. The following average relation between the dilation at –15°C and –30°C was found (see APPENDIX to Chapter 6, Table A6.2):

w/c-ratio 0.60: $Dil_{-30°C}/Dil_{-15°C}$=1.3 (std. dev. 0.10)
w/c-ratio 0.45: 1.2 (-"- 0.03)
w/c-ratio 0.40: 1.1 (-"- 0.02)

The spread in the results is remarkably small.

When comparing the results from Test series 4 and 5 it is indicated that the lowest temperature only has an effect on damage if the degree of saturation is above the critical. The reason for this is:

1. Concrete with a degree of saturation *higher than the critical* behaves similarly to *non-air-entrained* concrete since the air pores are inactivated by water absorption. Therefore the lowest temperature has big effect. If the air content is high, and the degree of saturation not too high, the effect of lowering temperature from –15°C to –30°C seems to be of the order 30% as in this Test series. At very high degrees of saturation, the doubling of expansion observed in Test series 4 is probably valid.
2. Concrete with a degree of saturation *lower than the critical* behaves similarly to *air-entrained* concrete, since much of the air-pore space is still effective. Thus it is not at all, or only slightly, affected by the value of the lowest temperature reached during freezing.

In Figure 6.4.3 dilation and change in dynamic E-modulus are plotted versus the degree of saturation. As expected the degree of saturation is a dominant factor for frost resistance.

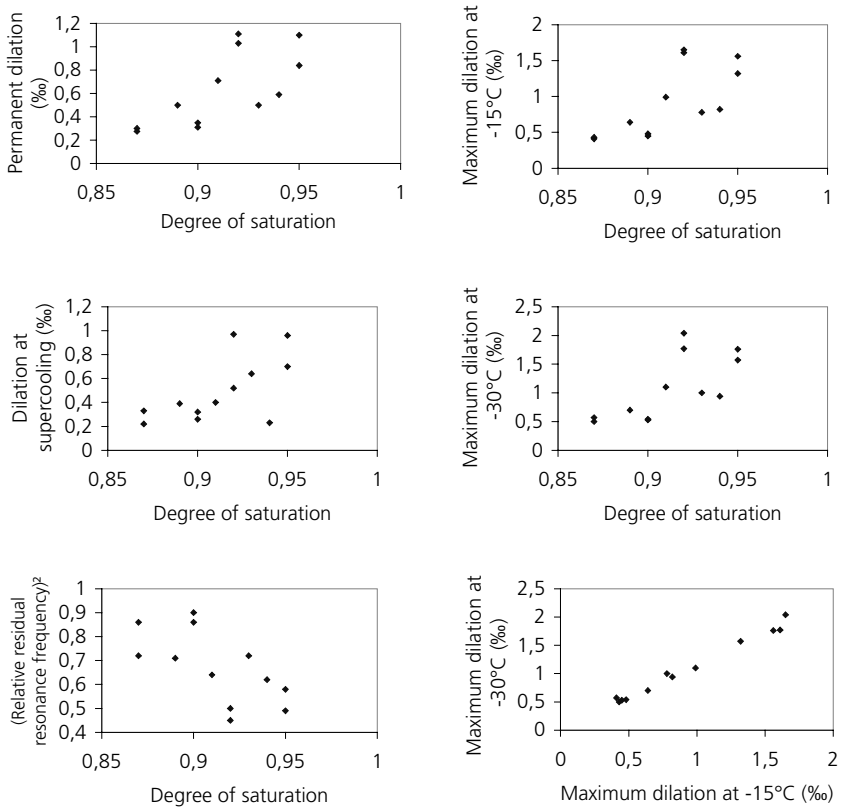

Figure 6.4.3. Different damage parameters plotted versus the degree of saturation. It must be noted that each figure contains data for all air contents (4, 6, 10%) and all w/c-ratios (0.60, 0.45, 0.40).

6.4.4 Test series 5: Conclusions

All specimens used in Test series 5 were air-entrained, but in contrast to the behaviour of the same air-entrained specimens in Test series 4, a smaller effect of the lowest temperature was found. The maximum increase in dilation when temperature was lowered from –15°C to –30°C was 30%. For non-air-entrained concrete in Test series 4, the increase was found to be 100%.

The degrees of saturation employed in Test series 5 were quite high, higher than those obtained after almost 4 years of water storage. Maybe, they correspond to the maximum possible moisture content in air-entrained structures after very long time of water uptake. If so, one might, on basis of the results in this Test series, state that the effect on frost damage of air-entrained concrete of lowering the temperature from

–15°C to –30°C is restricted to about 30%. Maybe it can in cases with low air-content be 100%. 'Damage' is then expressed in terms of dilation during freezing.

7 Freezing and thawing experiments - Influence of duration of the lowest temperature

7.1 Introduction

In Powers and Helmuth (1953), the theory called the microscopic ice lens growth theory (see Chapter 2) was presented to explain the large shrinkage, larger than the thermal shrinkage, often observed in properly air-entrained cement-based materials during freezing. The authors argued that this could be explained on the basis of water transport from the small unfrozen gel pores through the liquid-like layer surrounding the ice filled capillary pores to small bodies of stress-free ice previously formed in air voids. When arriving at the air pores the water would transform to ice and grow stress-less. The drying out of the finest pores caused by this moisture transfer pores makes the material contract. This was seen as being a process that needs some time to develop, an increase in the duration of low temperatures might thus increase the effect.

The same theory can also explain the often observed continuous expansion at freezing temperature of non-air-entrained concrete, or concrete with an air-pore system of low quality (e.g. a big spacing factor). In this case, water from the finer pores has to move to ice already present in capillary pores completely filling these. When water arrives it freezes making the ice bodies expand. Consequently, the concrete itself expands. Also this process will be promoted by a prolonged period of freezing temperatures.

Water movement of the type described requires that there is a free energy difference between ice and unfrozen water. Unfrozen water has higher free energy than ice under atmospheric pressure. In a pore system two types of unfrozen water can exist; (1) supercooled water in isolated pores that cannot for geometrical reasons (narrow entrances) be nucleated by ice in adjacent pores, (2) water in narrow pores with a freezing point depression that is bigger than the actual temperature.

Supercooled water is metastable and has higher free energy than ice at the same temperature. Thus, it will readily move to ice bodies also when the temperature is held constant. Migration will not stop until the free energy difference is evened out.

Water that is unfrozen due to freezing point depression has in itself low free energy, which might be in balance with the ice bodies when temperature is held constant, which means that local equilibrium exists. Therefore, this unfrozen water has no tendency to move. However, if temperature is suddenly lowered, the immediately occurring reduction in free energy of the ice becomes bigger than the reduction in free energy of the unfrozen water. Therefore, unfrozen water tends to migrate to-

wards the ice bodies, but only as long as the energy difference exists. After some time, that might be rather short after that temperature lowering has been once again stopped, local equilibrium will be established between the two phases. Therefore, water migration stops. As long as temperature drops water migration might proceed.

Water migration will occur both to ice-bodies in air pores and to ice-bodies in capillary spaces. Migration to ice in air pores will make the ice bodies grow stress-less which means that the free energy of air-pore ice will not be changed due to its growth. Thus, theoretically, all supercooled water might be transferred. However, migration of water causes a drying effect, which creates under-pressure in the remaining unfrozen water. This reduces the free energy of unfrozen water. Migration stops when the free energy has dropped to the same level as that of the free ice.

Ice lens growth in capillary spaces cannot take place stress-less. A pressure will be exerted on the ice from the pore walls. Consequently the free energy of ice increases steadily, at the same time as that of the unfrozen water is gradually reduced due to drying. When the energy difference has evened out water migration and ice lens growth will stop. This might happen despite a continued temperature lowering.

In air-entrained concrete migration towards air-pore ice dominates since it occurs without much hinder. Thus the drying effect makes the concrete contract. In non-air entrained concrete migration instead goes to capillary pore ice causing expansion.

Duration of freezing temperature and the level of this might have an effect on ice-lens growth, since a longer period of freezing temperature will increase the possible time for moisture transfer. To study this, an investigation of the effect of increasing the duration of the lowest temperature was performed. The test is similar to Test series 4 and 5, but duration of constant low temperature was increased to 12 hours and only one freeze/thaw rate was used, the 'normal'.

7.2 Experimental technique and variables

The test setup and the experimental techniques are described in Chapter 4. Two temperature levels were tested during each cycle, -15°C and -30°C. The freezing rate was 3.6°C/h and the isothermal periods 12 hours in length, Figure 7.2.2. Besides the damage parameters described in the previous chapters also changes in strain during 12-hour isothermal periods (-15°C and -30°C) were investigated.

Two Test series, 6 and 7, were performed. In Test series 6, the specimens used had been stored in lime-saturated water for over four years and had never been dried. In Test series 7, new specimens of the materials were given specific degrees of saturation and were then tested, using the same temperature cycle. The procedure for adjusting the specimens to the individual degree of saturation is described in paragraph

4.5. 20 specimens were used for Test series 6, and 14 specimens for Test series 7. An overview of the study and the treatment of the specimens are shown in Figure 7.2.1.

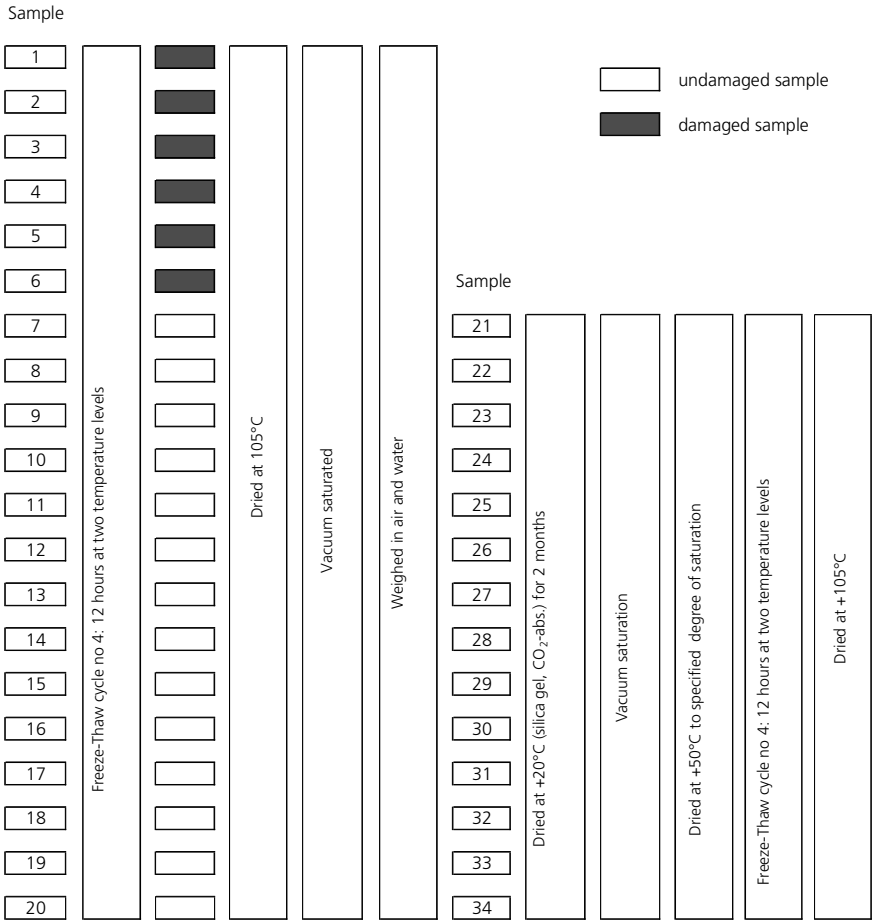

Figure 7.2.1. Test series 6 and 7; effect of duration at lowest temperature. Specimens and test procedure.

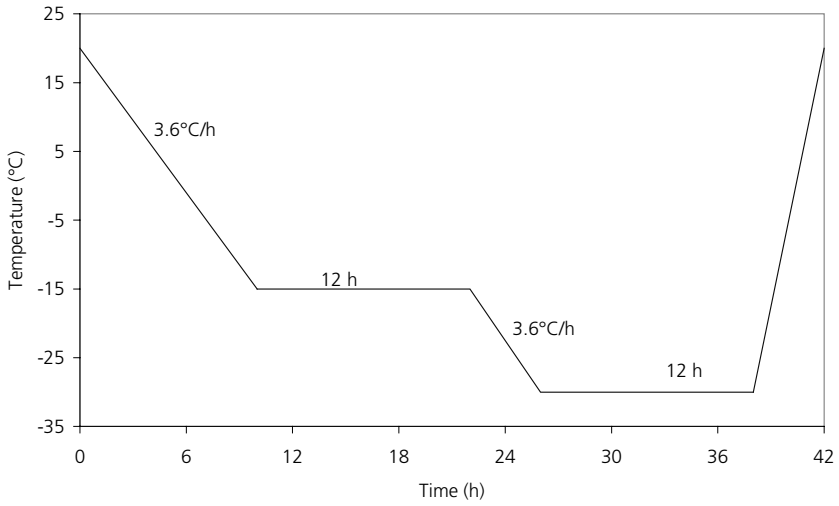

Figure 7.2.2. Temperature cycle of air in the climate chamber.

7.3 Test series 6: Never-dried samples with 'natural' water content

7.3.1 Introduction

All specimens had been stored for more than 4 years in water prior to testing. The treatment and moisture content therefore was the same as in Test series 1 (Chapter 5) and 4 (Chapter 6).

Damage parameters are dilation at different stages during the freeze/thaw cycle and resonance frequency. This was determined after the entire cycle had been completed since determination on frozen specimens is impossible to interpret in a meaningful way.

All results are shown in APPENDIX to Chapter 7.

7.3.2 Non-air-entrained concrete

Length change-time and *temperature-time* curves for non-air-entrained concrete with w/c-ratio 0.60 and 0.40 are shown in Figure 7.3.1. The corresponding *length change-temperature* curves for w/c-ratio 0.60 are shown in Figure 7.3.2. The same type of curves for w/c-ratio 0.40 is found in Figure A7.6 in APPENDIX to Chapter 7.

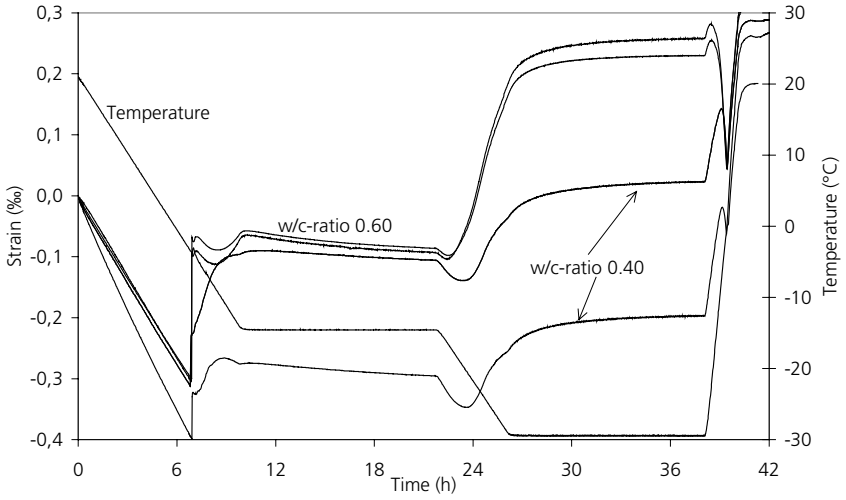

Figure 7.3.1. Length change and temperature curves for non-air-entrained concrete with w/c-ratio 0.60 and 0.40.

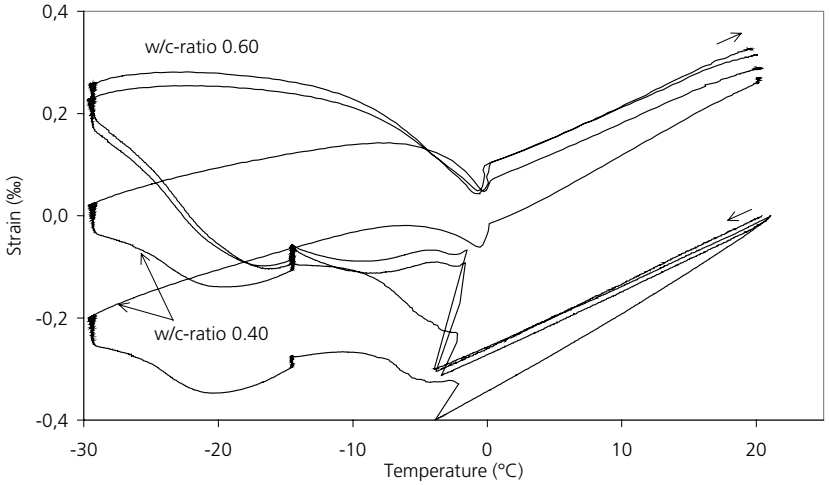

Figure 7.3.2. Length change versus temperature for non-air-entrained concrete with w/c-ratio 0.60 and 0.40.

The following observations are made (concrete with w/c-ratio 0.45 behaves much the same, see APPENDIX to Chapter 7). The results are similar to the results of Test series 4, see paragraph 6.3.2.

- When supercooled water is nucleated at about –5°C big and rapid expansion occurs in all specimens, which was also found in the other Test series. The expansion is biggest for w/c-ratio 0.60 which indicates that more water is nucleated which is reasonable due to the coarser capillary pore structure. The expansion is big enough to damage the concrete as was the case in the other Test series. The big difference in early expansion between the two specimens with w/c-ratio 0.40 is remarkable. One reason could be that more water is supercooled locally in isolated capillaries in one specimen causing less freezing. Another explanation that seems unlikely, is that there are big differences in the pore structure and the air content in the two specimens. The relaxation (contraction) immediately after the rapid ice formation had occurred is very small in both specimens indicating lack of space for expelled water in the non-air-entrained concrete.
- During the entire period (12h) when temperature was held constant at -15°C, only contraction can be observed and this is found in all materials tested. Compared to the Test series 4 in which temperature was held constant at –15°C for only 3 hours there were no signs of that an increase in duration of the lowest temperature should alter the destruction mechanism.

  The hydraulic pressure theory (Chapter 2) predicts a rapid decrease in length when the temperature is held constant, since then, theoretically, generation of water flow by ice formation should stop, and the hydraulic pressure vanishes. This will probably be hindered by ice previously formed, which obstructs contraction. The slow contraction observed does therefore not contradict the hydraulic pressure mechanism.

  The theory of microscopic ice lens growth predicts stop of ice lens growth caused by transfer of non-freezable water when temperature is held constant, provided there is local equilibrium established between ice and water, which is not necessarily the case during the first period of constant temperature. If there was no equilibrium established during the temperature halt, expansion should, however, have been expected, since the concrete was non-air-entrained, but expansion could not be seen in any specimen. This does not exclude ice lens growth from being the mechanism behind contraction. Even a concrete without air-entrainment contains some air pores. Theoretically, supercooled water in isolated capillaries could migrate to these air pores, which would lead to a contraction due to drying. It is interesting to note that the specimen w/c-ratio 0.40 with the lowest initial expansion has the biggest contraction at the temperature halt. Since this specimen might have the big-

gest amount of locally supercooled water it also ought to have the biggest moisture migration to air pore ice, thus the biggest contraction. Thus, the microscopic ice lens growth theory is not contradicted either.

- Directly after temperature is starting to decrease again all specimens contract momentarily. The contraction is biggest for w/c-ratio 0.40. According to the hydraulic pressure mechanism an expansion had been expected. Probably therefore the contraction is caused by a drying effect when unfrozen water migrates to ice lenses primarily in air pores. A change in temperature will immediately destroy the equilibrium while water starts to migrate. This causes a drying effect that gives contraction. This is reversed after short time when the expansive effect of ice formation takes over.
- When temperature continues to fall, all samples expand. The specimens with the highest w/c-ratio, containing the highest amount of freezable water, expand the most. The big expansion for both w/c-ratios depends on lack of air-pore space within easy reach from the freezing site. Both destruction mechanisms predict expansion in such a case. It is not possible from the experiment to tell which mechanism is dominant. However since the amount of freezable water is biggest for w/c-ratio 0.60, and also the expansion is biggest for this w/c-ratio, there is reason to believe that hydraulic pressure, or the special case of this, the 'closed container' freezing, is the dominant mechanism.
- During the second isothermal period at –30°C small expansion was found in all samples, a phenomenon also observed in Test series 4 and 5. The expansion occurred during the entire period but with decreasing rate.

  Since no ice formation is possible when temperature in the specimen is constant and equal to the surrounding temperature hydraulic pressure cannot exist. Therefore, expansion cannot be explained by hydraulic pressure. The relaxation of stresses, which is predicted by the hydraulic pressure theory, could not take place due to the big amount of ice in the pore system hindering contraction.

  The expansion is probably caused by ice-lens growth of capillary ice indicating that there is a certain difference in free energy between the unfrozen water and ice for some period after temperature lowering has come to a halt. This energy difference is big at the beginning but has almost been levelled out after some hours. Ice lens growth should cause heat development, which should have increased the temperature of the specimen. This could no be observed, however which indicates, that the amount of ice formed is very small.

In the calorimeter experiments presented in Chapter 9 no ice formation could be seen when temperature was kept constant.

There is another possible mechanism that might explain at least part of expansion during constant temperature, namely osmotic pressure. The mechanism is described in paragraph 8.3.2 in connection with Test series 8 in which specimens containing salt were investigated. Pore water in concrete always contains dissolved ions, primarily Na^+, K^+ and OH^-. When freezing occurs in a capillary, the concentration of the remaining solution within the same capillary increases. The concentration of non-freezable water in neighbouring finer pores is maintained on the initial level. Thus, there is a possibility for osmotic pressure to appear if dissolved ions have lower diffusivity than water. The mechanism has been suggested by Powers (1955), (1956).

- When the very rapid warming started the length change curves for all specimens showed a big expansion changing over to contraction at some higher temperature. The reason is certainly thermal expansion of the frozen specimen followed by contraction when most of the ice melts.
- As in the other test series, all non-air-entrained samples had a permanent dilation larger than the critical value 0.15‰. The reduction in residual resonance frequency varied between about 25 and 35%.

7.3.3 Air-entrained concrete

Length change-time and *temperature-time* curves for air-entrained concrete with w/c-ratio 0.60 and 0.40 are shown in Figure 7.3.3. A *length change-temperature* curves for the same samples are shown in Figure 7.3.4. The curves for the other concretes are found in APPENDIX to Chapter 7.

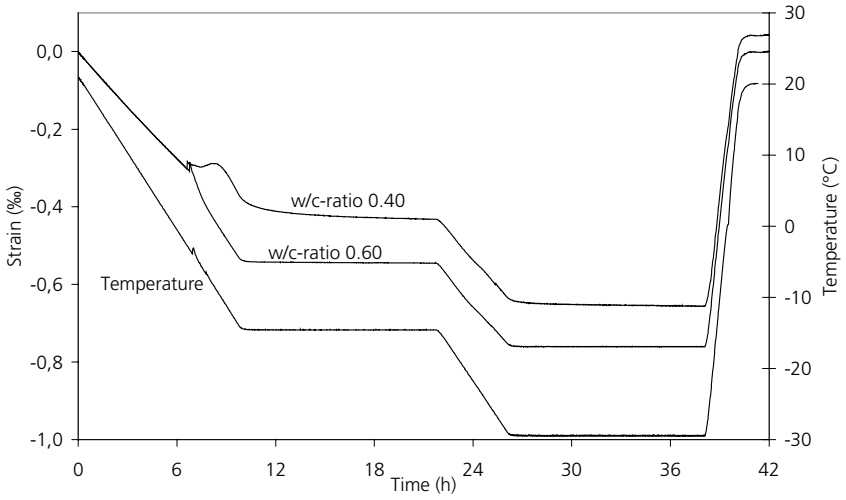

Figure 7.3.3. Length change and temperature curves for air-entrained concrete with w/c-ratio 0.60 and 0.40. Air content 6%.

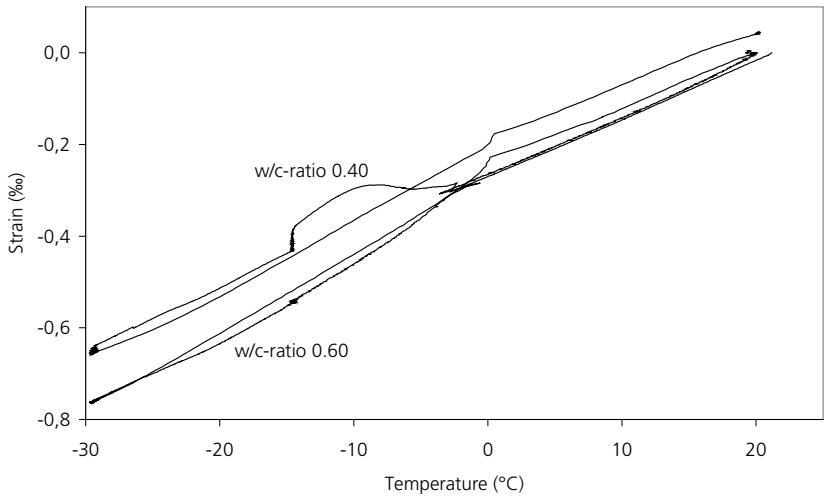

Figure 7.3.4. Length change versus temperature for air-entrained concrete with w/c-ratio 0.60 and 0.40. Air content 6%.

The following observations were made (concrete with w/c-ratio 0.45 behaves much the same, see APPENDIX to Chapter 7).

The results are consistent with results from the previous Test series 1 and 4 with air-entrained concrete.

- A small expansion is detectable when supercooling is overcome caused by hydraulic pressure, but it quickly reverses into contraction.
- The contraction after the initial formation of ice is larger than normal thermal contraction, partly due to the larger thermal expansion of ice compared with concrete, but primarily due to migration of water to the ice in the air voids, which causes drying and shrinkage. The higher the air content, the larger becomes the observed contraction. This is reasonable, since there is a competition between ice growth in capillaries and ice growth in air pores. The first causes expansion and the latter contraction. The smaller the spacing between air pores the bigger is migration to air pore ice. This observation is consistent with findings by Powers and Helmuth (1953).
- In the samples with w/c-ratio 0.40 there is a certain period of small expansion following the initial ice formation, which is not present at w/c-ratio 0.60. This has been seen in previous Test series, like Test series 1. This indicates that transport to capillary ice is somewhat bigger for the more dense concrete, which might depend on the higher amount of unfrozen water in such concrete. It might also depend on the smaller permeability. The distance between a capillary with ice and the nearest pore (gel pore or very small capillary) with unfrozen water is much smaller than the distance to the air-pore. Therefore, if the permeability is reduced, water transport to capillary ice will be increased despite the fact that the air-pore spacing is unchanged.
- During the isothermal period that follows at –15°C, the material with w/c-ratio 0.60 shows almost no change in length, while the material with w/c-ratio 0.40 shows a slight shrinkage. The background to the shrinkage is probably the same as described above for non-air-entrained concrete; i.e. migration of unfrozen water, e.g. supercooled water in isolated capillaries, to air pore ice.
- When the temperature is gradually lowered to -30°C, the specimen continues to contract, with only a slight deviation from the thermal contraction indicating some ice formation, which is too small to cause destruction. Figures and Table A7.1 in APPENDIX to Chapter 7 shows that this slight influence of ice formation on the dilation is larger the lower the air content and the higher the w/c-ratio.
- When temperature reduction makes a halt at -30°C, the material with w/c-ratio 0.60 shows no length changes, while a small shrinkage can be detected

for the material with the low w/c-ratio. This is in accordance with the results for non-air-entrained concrete

- None of the samples containing air-entrainment received a permanent damage of more than 0.10‰. They are therefore considered undamaged The reduction in residual resonance frequency was for some specimens higher than 10% indicating some negative effect of freezing.

7.3.4 Test series 6: Summary and discussion of results

All results from Test series 6 are presented in APPENDIX to Chapter 7. In Table A7.1 an overview of dilation at different stages during the freeze/thaw cycle is given. Furthermore, values of the change in residual resonance frequency caused by freeze/thaw, and the degree of saturation during freeze/thaw are listed.

Length change-temperature curves both versus temperature and versus time for all specimens are also shown in APPENDIX to Chapter 7, Figures A7.1-A7.6.

The objective of Test series 6, was to investigate how the duration of the lowest temperature affects the length changes, and from that draw conclusions on what mechanisms are acting. Therefore the discussion is concentrated to what happens when temperature is kept constant at –15°C and –30°C.

When temperature is kept constant at some low temperature level for some time, the theory of hydraulic pressure (Chapter 2) predicts contraction due to the fact that during isothermal conditions no ice forms, and no excess water are expelled. Contraction was not found in any concrete, with and without air-entrainment. If the material is in an expanded ('locked') state due to ice has formed at higher temperature, the contraction can be restricted to some extent, or entirely. The theory of microscopic ice lens growth, (Chapter 2) predicts expansion in non air-entrained material due to diffusion of gel-water to the capillary ice, or contraction in air-entrained material due to diffusion of gel-water to the air void ice. The first is unlikely when temperature is kept constant for long time since then local equilibrium between the phases (ice and water) ought to prevail. The latter can still occur.

In the discussion that follows on the length changes at constant temperature, -15°C and –30°C, it must be considered that these are very small, and calculated as the difference in length at the beginning and the end of the period. Measurement errors can therefore have some influence.

In Figure 7.3.5 the length changes during the isothermal period at –15°C are plotted versus the w/c-ratio. The figure indicates a slight tendency that a lower w/c-ratio gives bigger contraction, supporting the microscopic ice lens growth theory according to which a low w/c-ratio contains more unfreezable water than a material with a high w/c-ratio, see also Chapter 9. The relation between contraction and w/c-ratio is how-

ever in no ways distinctive, there are concrete with lower w/c-ratio that has smaller contraction than concrete with higher w/c-ratio.

Considering the hydraulic pressure theory, it might be reasonable to assume that a material with a high w/c-ratio has been exposed to a higher hydraulic pressure than a material of a lower w/c-ratio, since the bigger amount of capillary pores and a coarser pore system leads to more ice formation. On the other hand, the permeability is higher, which could balance this effect. If the rate of ice formation dominates, the relaxation in materials with high w/c-ratio should be larger than that in a material with low w/c-ratio, just the opposite of the (not very distinct) findings presented in Figure 7.3.5. However this will not contradict the existence of hydraulic pressure since ice may have blocked the possibility of contraction.

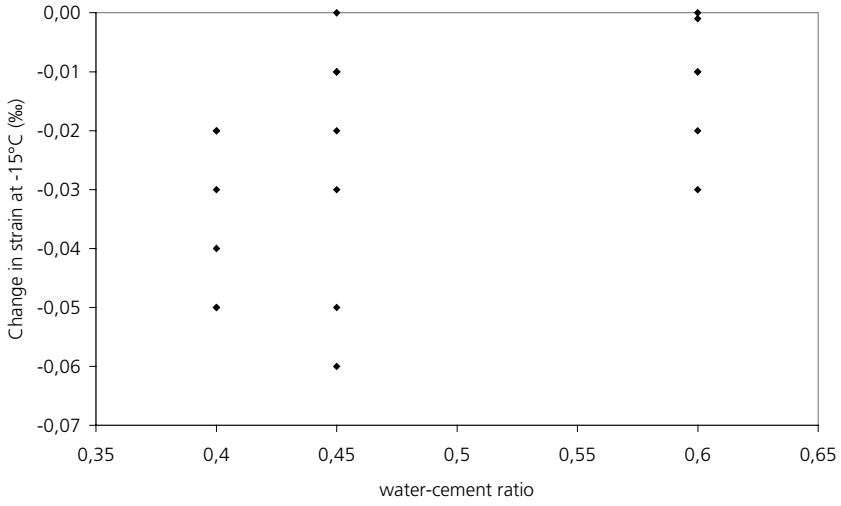

Figure 7.3.5. The influence of water-cement ratio on the length changes occurring during the isothermal period at -15°C. Different air contents.

In Figure 7.3.6 the length change during the constant period at –15°C is plotted versus the air content of the fresh concrete. The tendency, although very vague, is an increase in shrinkage with decreasing air content, which is opposite to what Powers and Helmuth (1953) found, and contrary to what should be expected by the microscopic ice lens growth theory. Release of hydraulic pressure could explain the observation since the pressure is higher in concrete with low air content. It must be considered that the spread in results is big.

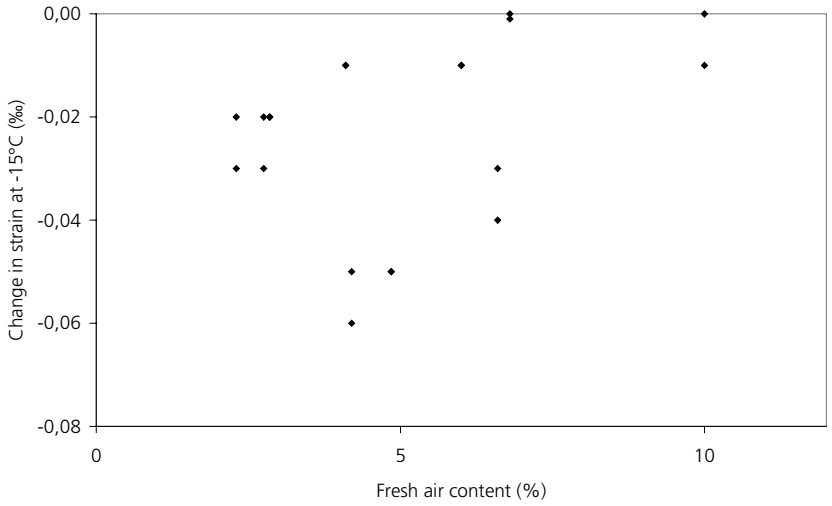

Figure 7.3.6. The influence of the fresh air content on the length change occurring during the isothermal period at -15°C. Different w/c-ratio.

In Figure 7.3.7 length changes at –15°C are plotted versus the degree of saturation, showing a tendency that contraction increases with increasing degree of saturation. This cannot be explained by the ice lens growth theory, but can be explained by the hydraulic pressure theory. A high degree of saturation means high hydraulic pressure. Consequently a bigger contraction must take place when temperature lowering comes to a halt.

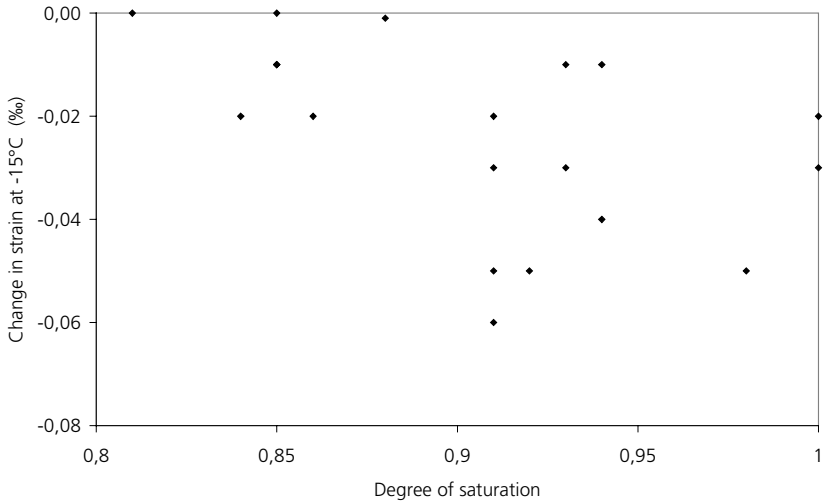

Figure 7.3.7. The influence of degree of saturation on the length changes occurring during the isothermal period at -15°C. Different air content and w/c-ratio.

Length changes at the second halt at –30°C are plotted in Figure 7.3.8 versus the w/c-ratio, and in Figure 7.3.9 versus the air content of the fresh concrete. No effect of the w/c-ratio could be found at this low temperature.

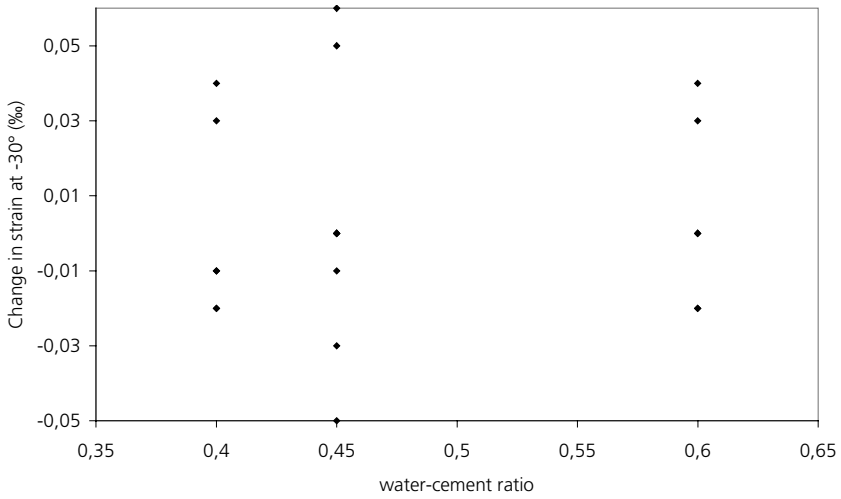

Figure 7.3.8. The influence of water-cement ratio on the length changes occurring during the isothermal period at -30°C. Different air content.

The importance of entrained air when temperature is –30°C for 12 hours is shown in Figure 7.3.9. All materials without air-entrainment show expansions during this isothermal period, while the materials with air-entrainment all contract or remain at constant length. Both the dilation of the material without air-entrainment and the contraction of concrete with entrained air are predicted by the theory of microscopic ice lens growth, as discussed above. The results cannot be explained by the hydraulic pressure theory, which predicts no change of strain or contraction when the temperature is held constant. The difference in behaviour between –15°C and -30°C might be a sign that the two mechanisms are active (or dominant) during different temperature ranges.

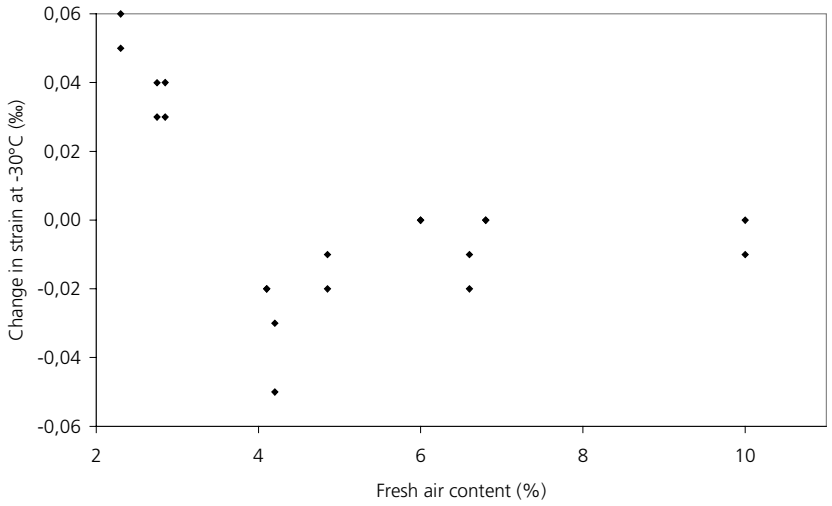

Figure 7.3.9. The influence of the fresh air content on the length changes occurring during the isothermal period at –30°C. Different w/c-ratio.

The damage parameters, permanent damage at +5°C, dilation at supercooling and the change in resonance frequency after the single moisture isolated freeze-thaw are presented in Figure 7.3.10 versus different material parameters, w/c-ratio, air content and degree of saturation.

No clear relationship between the degree of saturation in the materials and the damage parameters could be found. The reason is probably problems during drying and re-saturation of the samples for definition of pore volume, see paragraph 4.5.

The positive effect of air is very clear as in the previous Test series. The effect of w/c-ratio on damage is not clear and is obscured by the very positive effect of air for concrete of any w/c-ratio.

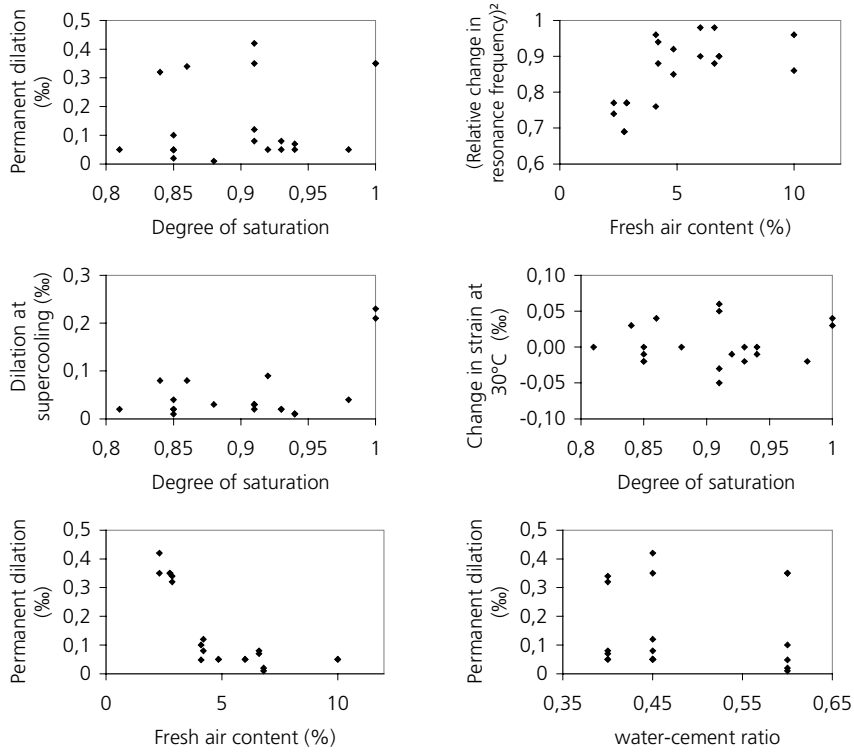

Figure 7.3.10 Effect of air content, w/c-ratio and degree of saturation on different damage parameters.

It is of interest to compare the results from this Test series with the results from Test series 4 in which the duration of constant temperature was only 3 hours. For *non-air-entrained* concrete Table 7.3.1 give the dilations observed at the end of the constant periods of –15°C and –30°C. Except for w/c-ratio 0.60 there is a certain tendency that a prolonged duration causes somewhat bigger expansion. This relative increase in expansion is about the same for both temperatures. It must be noted, however, that this difference between the two tests is *not related* to dilations occurring during the periods of constant temperature, but to different expansions occurring even before the first temperature halt at –15°C was made. This is seen if the dilations just when temperature lowering was stopped at –15°C are compared.

- w/c-ratio 0.60: Dil. Test series 6/Dil. Test series 4: 0.8
- w/c-ratio 0.45: -"- : 1.3
- w/c-ratio 0.40: -"- : 1.4

These relations are exactly the same as these in Table 7.3.1. Therefore the results indicate that the duration of lowest temperature has no real effect on damage occurring during freezing.

Table 7.3.1: Dilation at the end of periods with 12 hours versus 3 hours of constant temperature at –15°C and –30°C. Non-air-entrained concrete.

w/c-ratio	Dilation at –15°C 12 hours versus 3 hours	Dilation at –30°C 12 hours versus 3 hours
0.60	0.8	0.9
0.45	1.3	1.2
0.40	1.4	1.4

The effect of the lowest temperature was investigated in Test series 4 and found to be big for non-air-entrained concrete but virtually non-existing for air-entrained concrete. Test series 6 can also be used for such analyses. For non-air-entrained concrete the following relation between dilations at –30°C and –15°C were found:

w/c-ratio 0.60: $Dil_{-30°C}/Dil_{-15°C}=2.4$
w/c-ratio 0.45: 2.2
w/c-ratio 0.40: 2.1

These values are almost exactly as those found in Test series 4.

7.4 Test series 7: Pre-dried, re-saturated samples with adjusted degree of saturation

7.4.1 Introduction. Preparation of samples

To investigate whether the effect of a long duration of exposure to low temperature is affected by the degree of saturation, 14 new samples (2 of each concrete type that was considered undamaged after Test series 6), that had been water-stored for about 5 years, were dried for two months at room temperature over silica gel in presence of a carbon dioxide absorbent. Thereafter, they were placed in vacuum (2-3 mbar) for more than twelve hours before water was added. The samples were kept in water for 2-3 days before the adjustment of the moisture level was begun. They were dried at +50°C until their weight reached that corresponding to a degree of saturation of 0.8 or 0.9. These are values aimed at. The real degree of saturation could be somewhat different. The degree of saturation was calculated on the basis of the dry weight obtained at room temperature and the saturated weight after vacuum treatment. The specimens were then sealed.

The freeze/thaw test started no earlier than a week after the preparation. After the freeze/thaw test, all the samples were dried at +105°C, the degree of saturation again being calculated. The moisture-sealed specimen was subjected to the same freeze-thaw cycle as Test series 6, Figure 7.2.2. Two samples of each concrete type were tested.

7.4.2 Results

All results can be found in APPENDIX to Chapter 7, Table A7.2 and Figures A7.7-A7.12. Some representative results valid for concrete with w/c-ratio 0.45 are shown in Figure 7.4.1 and Figure 7.4.2.

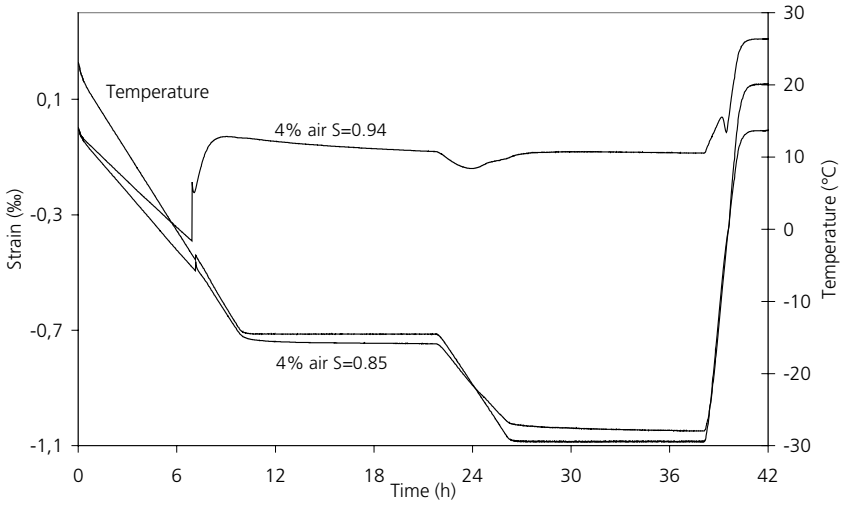

Figure 7.4.1. Length change and temperature versus time for pre-dried, re-saturated samples with w/c-ratio 0.45 and 4% air.

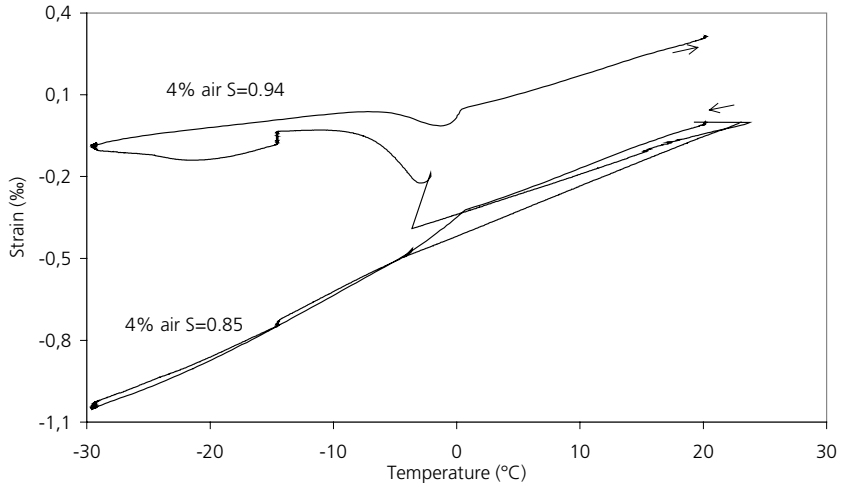

Figure 7.4.2. Length change versus temperature for pre-dried, re-saturated samples with w/c-ratio 0.45and 4% air.

The following observations are made (concrete with w/c-ratio 0.60 and 0.40 behaves much the same, see APPENDIX to Chapter 7)

- As expected and shown previously in Test series 3 low degree of saturation only gives contraction that is also somewhat bigger than normal thermal contraction when temperature is lowered to –15°C. At high degree of saturation the concrete expands, probably due to hydraulic pressure since water expelled at ice formation cannot find space to escape. Ice lens growth can however not be excluded. It cannot be distinguished from hydraulic pressure in this temperature range.
- During the isothermal period at -15°C the samples contract considerably when the degree of saturation is high. This can be explained, as described previously, with relaxation of the hydraulic pressure, which is high in such concrete as long as ice is formed, i.e. as long as temperature sinks. The specimen will not reach its original length though, since ice that has already formed will keep the material in an expanded state.
- Drying shrinkage caused by moisture migration is unlikely since the extra water contained in the specimen at high degree of saturation has been frozen already at lower temperature. Therefore it contains no more unfrozen water at -15°C than the specimen with the lower degree of saturation, and that does not contract. Its length is constant during the 12 hour when temperature is locked at –15°C.
- When temperature lowering starts once again, the drier specimen contracts by the same 'thermal contraction coefficient' as in the range 0°C to –15°C. The more moist specimen starts to contract as was also found in Test series 6. The reason is probably the same as described there, namely that a temperature change disturbs energy equilibrium between ice and water causing moisture movement to ice in air pores, causing a drying/shrinkage effect.
- When temperature continues to drop expansion occurs in the specimen with high moisture content, possibly due to pressure caused by ice lens growth, since the drier specimen, that has much more air-filled space contracts. Also the hydraulic pressure theory will however predict expansion in the moister specimen since the spacing between air-filled pores is very low in that specimen compared with the drier specimen.
- When temperature is kept constant at -30°C there is some indication of slight expansion in concrete with w/c-ratio 0.60 (see APPENDIX to Chapter 7). Concrete with w/c-ratio 0.40 show slight contraction in all specimens.

- As described in connection with Test series 6, expansion can only be explained by ice lens growth, or osmotic pressure, since no hydraulic pressure can be generated when the temperature is constant. Also the contraction occurring in the drier specimens can depend on ice lens growth in air pores accompanied by drying.
- During warming the concretes expand thermally and then contracts when most of the ice melts some degrees below zero.
- Concrete with high degrees of saturation suffered damage as judged by loss in residual resonance frequency and permanent expansion.

7.4.3 Test series 7: Summary of results and conclusions

All results from Test series 7 are presented in APPENDIX to Chapter 7. In Table A7.2 an overview of dilation at different stages during the freeze/thaw cycle is given. Furthermore, values of the change in residual resonance frequency caused by freeze/thaw, and the degree of saturation during freeze/thaw are listed.

Length change-temperature curves both versus temperature and versus time for all specimens are also shown in APPENDIX to Chapter 7, Figures A7.7-A7.12.

The question to be answered in Test series 7 was how concrete with varying degrees of saturation responds to long periods of constant temperature at –15°C or –30°C. At –15°C, concrete with high degree of saturation contracts markedly, which could depend on relaxation of internal pressure caused by the preceding ice formation. Concrete with low degree of saturation obtains no length change. At –30°C negligible length changes- positive or negative- occur in all specimens. Ice lens growth is the most likely cause in both cases.

A summary of the relation between w/c-ratio and degree of saturation on different damage parameters are shown in Figure 7.4.3.

As in Test series 3, damage increases with increasing degree of saturation. There is also a tendency that damage increases with increased w/c-ratio.

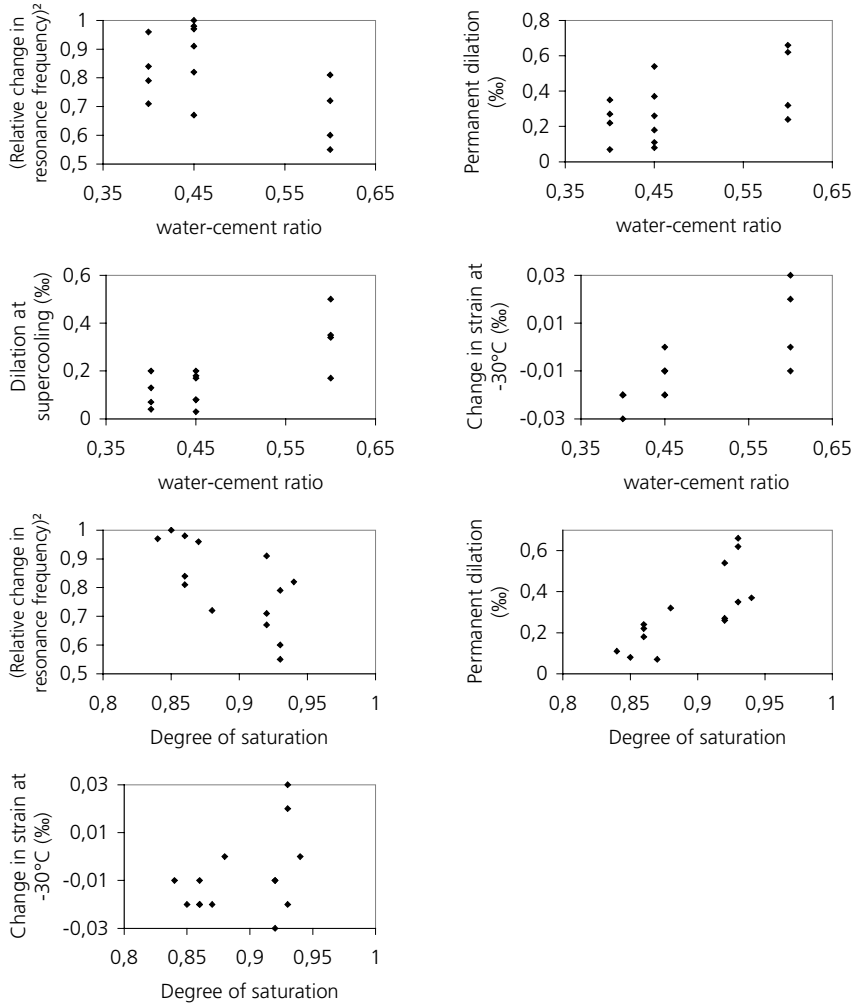

Figure 7.4.3. Effect of w/c-ratio and degree of saturation on different damage parameters.

8 Freezing and thawing experiments - Influence of long-term storage in NaCl-solution

8.1 Introduction

A large number of investigations have been performed regarding the influence of salt on deterioration by surface scaling. The influence of salt on internal frost deterioration, although believed to be less important than its effect on surface deterioration, has scarcely been investigated. In a traditional salt scaling test the surface is exposed to salt solution during the entire freeze/thaw cycle. Therefore, moisture and ions can move out from and into the specimen. This means that the moisture and salt levels in the concrete are undefined and varying depending on the design of the scaling test. In such tests it has often been found that damage (scaling) is most severe at a certain salt concentration of the solution to which the concrete is exposed. This worst concentration has been found to vary between about 1% and about 5% in different tests. The mechanism behind salt scaling is not fully clarified although some interesting hypothesis have been forwarded; e.g., Jacobsen (1995), Lindmark (1998), Kaufmann (1999), Rönning (2001), Tange Jepsen (2002) Utgenannt (2004). According to the mechanism by Lindmark (1998), surface scaling depends on moisture migration from the solution to capillary ice in the surface part of the specimen, a mechanism identical to the microscopic ice lens growth mechanism, and the frost heave mechanism in soil. This water makes the ice lenses grow and exert a pressure to the pore wall. This pressure makes the surface layer scale off.

In all tests described in this work the central idea has been to keep the *moisture level constant* during the test, and instead only vary the temperature conditions, like rate of freeze/thaw and duration of freeze/thaw. The same idea is used in Test series 8, but in this the salt concentration in the pore system was varied, whereby only one type of freeze/haw cycle was used. The same materials as were used in Test series 1-7 were also used in Test series 8, but the specimens had been stored in solutions of different sodium chloride content, instead of being stored in saturated lime-water, as in the other Test series. The storage time was almost 4.5 years so, because of the rather thin specimens (2 cm), one can assume that the pore solution was in equilibrium with the outer solution.

The moisture level was kept constant during the test by using moisture sealed specimens. The moisture level ('salt solution level') in all specimens was almost identical since they had been stored in the solution for the same length of time.

This test series can be seen as a purely 'exploratory study' with the aim to find, if possible, some general trends as regards the effect of a saline pore solution on the

behaviour during freeze/thaw of concrete of different qualities and air contents. The findings can hopefully be used as pieces in the building of a theory for the mechanism behind the salt scaling phenomenon.

8.2 Experimental technique and variables

Samples (2·2·17 cm) sawn from the same blocks as were used for test series 5-7 were stored in lime saturated sodium chloride solutions of differing concentrations 2, 4.5 and 11% by weight. Some specimens were also stored in salt-free lime-saturated water. For more details on the production and handling of the specimens prior to testing see Chapter 3 and 4.

The samples were tested using the 'normal' cycle also employed in Test series 1-3, see Figure 8.2.2. The freezing rate was 3.6°C/h, the isothermal period 3 hours, the lowest temperature -23°C, and the total duration of the cycle approximately 24 hours.

The test setup and the techniques are described in Chapter 4. The same damage parameters as were studied in Test series 5-7 were also studied here (change in residual resonance frequency, permanent dilation, dilation when supercooling was overcome, and dilation at -20°C). Concrete with all three water-cement ratios (0.40, 0,45, 0.60) were tested. Air contents used were, natural air content, and 6% air (10% for w/c-ratio 0.45). Two samples of each concrete type were tested, resulting in a total of 36 specimens being tested in Test series 8.

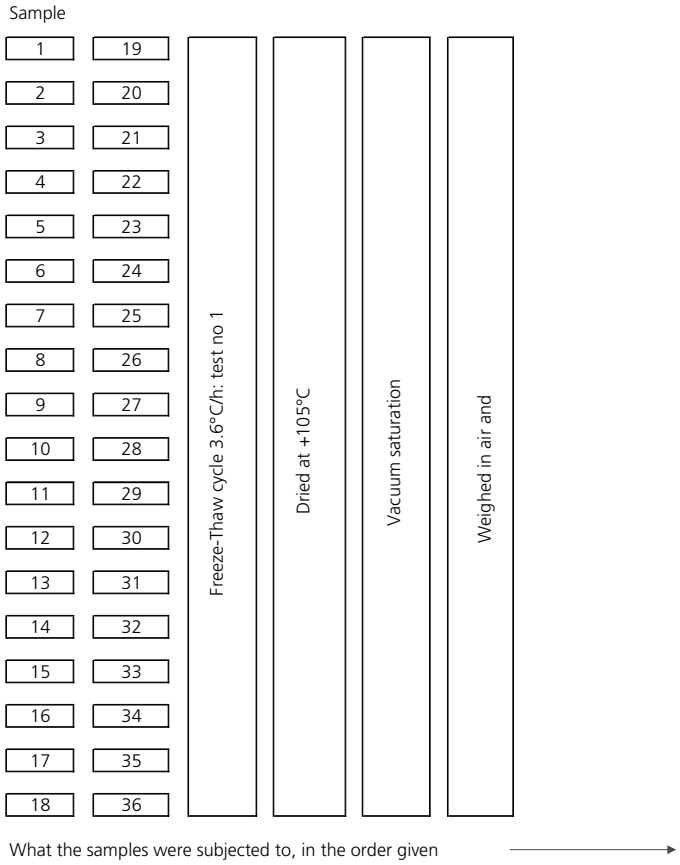

Figure 8.2.1. Test series 8; effect of storage in sodium chloride solutions. Specimens and test procedure.

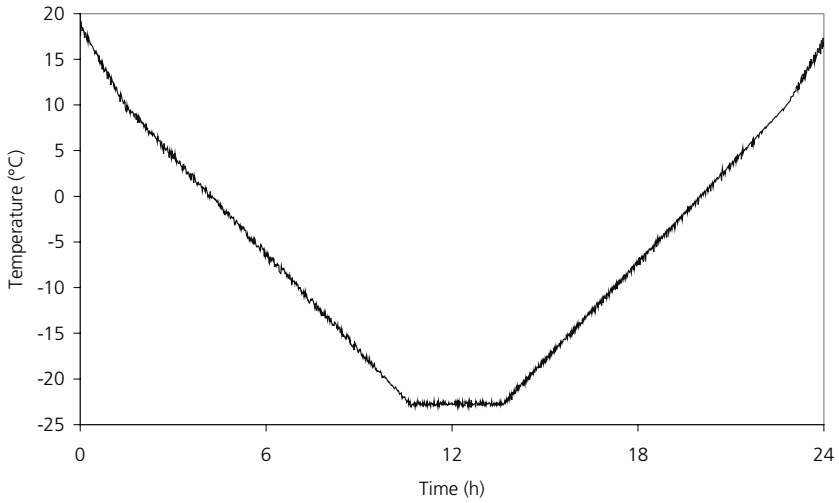

Figure 8.2.2. Temperature cycles of air in the climate chamber.

8.3 Test series 8: Results

8.3.1 Introduction

Damage parameters for all tests are shown in Table 8.3.1. All length change-time curves are shown below in this chapter. Specimens with the same w/c-ratio and air content stored in the different NaCl-solutions are presented in the same figure. One curve represents a single specimen.

8.3.2 Non-air-entrained concrete

Length change-time curves for all non-air-entrained concrete are shown in Figure 8.3.1-Figure 8.3.3. In all figures the temperature-time curve is valid for the specimen with pure water.

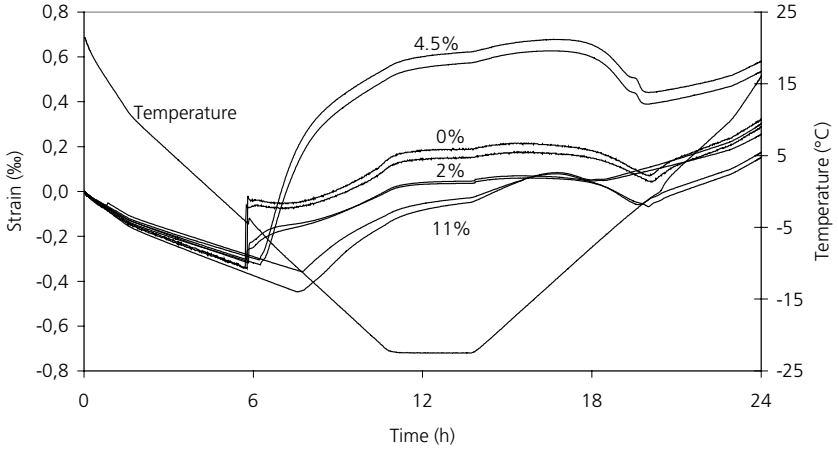

Figure 8.3.1. Length change versus temperature for samples with w/c-ratio 0.60 and natural air content stored in different NaCl-solution for more than four years.

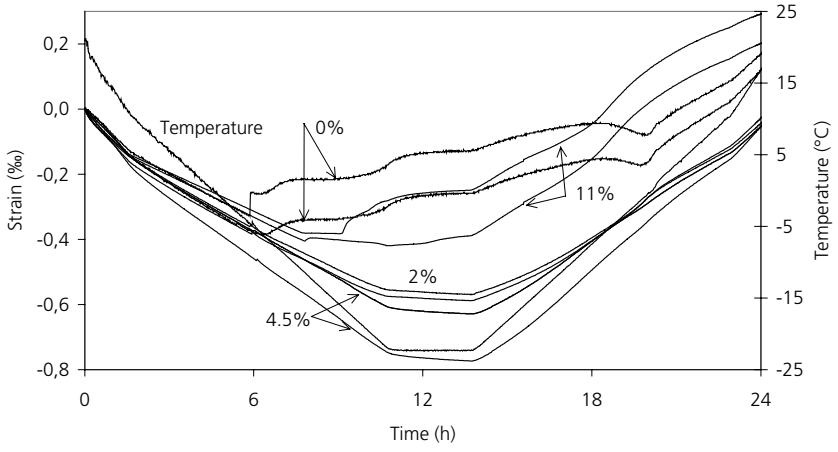

Figure 8.3.2. Length change versus temperature for samples with w/c-ratio 0.45 and natural air content stored in different NaCl-solution for more than four years.

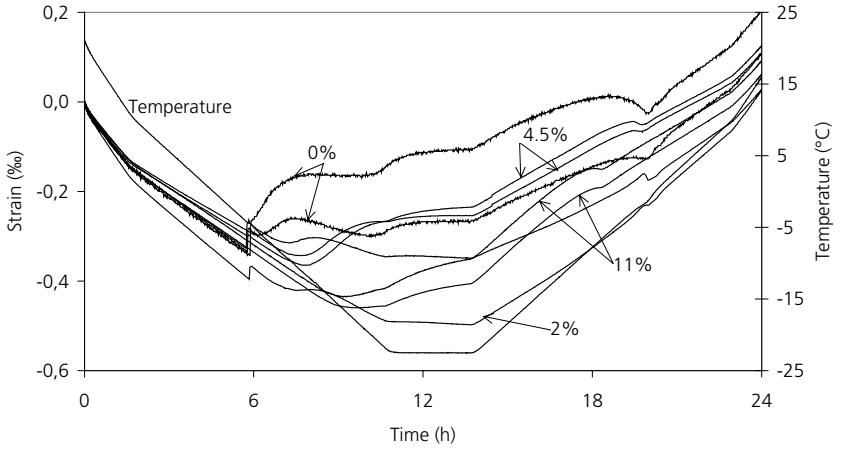

Figure 8.3.3. Length change versus temperature for samples with w/c-ratio 0.40 and natural air content stored in different NaCl-solution for more than four years.

Some comments to the results will be made.

Concrete with w/c-ratio 0.60:

- Supercooling occurs for pure water and 2% concentration.
- Onset of expansion, which is a sign of that major freezing starts, occurred at lower temperature the higher the salinity of the pore water; about –6°C for 4.5% and about –12°C for 11%. The theoretical freezing points for these concentrations are –3°C and –7°C. The fact that expansion did not start before these temperatures were reached is an indication that the salt concentration in the pores have been in equilibrium with the solution in which they were stored.
- The expansion during the temperature lowering part of the cycle is considerable for all salt concentrations and for pure water.
- Weak concentration (2%) and strong concentration (11%) give smaller expansion than pure water.
- The 'average' concentration 4.5% gives considerably bigger expansion than all other concentrations, including pure water. Thus, the test indicates the existence of a 'pessimum' salt concentration also for internal frost destruction. This statement is refuted, however, by tests with the other w/c-ratios.

- During the 3 hour period of constant temperature at –23°C, concrete with 11% salt solution, and to some extent also concrete with 4.5%, expand. Length is constant for pure water and 2% concentration.
- At warming the specimens with 4.5% and especially that with 11% salt concentration expands much more than the other specimens.
- The reduction in resonance frequency after thawing is:

  - 0% solution: 20% reduction in E
  - 2% : 20%
  - 4.5 % : 50%
  - 11% : 25%

Concrete with w/c-ratio 0.45

- Specimens with pure water and 2% showed supercooling, which is in accordance with w/c-ratio 0.60.
- Only specimens with the lowest (0%) and highest (11%) concentrations expanded during freezing. The specimen with pure water has the biggest expansion. Specimens with the intermediate concentrations showed really no expansion.
- One of the specimens with 11% solution expands more than the other. The reason could be somewhat different air pore structure in the two specimens. Very small differences can create big differences in behaviour when the degree of saturation is above the critical, which the case is for these specimens.
- During the 3 hour period of constant temperature at –23°C, there is a slight expansion of concrete with 11% solution. The concretes with 2% and 4.5% tend to contract slightly.
- At warming the specimens with 4.5% and 11% solution expands more than the other. This is in accordance with w/c-ratio 0.60. The warming curves for concentrations 4.5%, and to some extent for 2%, are remarkably straight. One can get the impression that they contained very small amount of frozen water which is also strengthen by the almost non-existing expansion during the freezing part of the curve.
- The reduction in resonance frequency after thawing is approximately:

  - 0% solution: 10%
  - 2% : 10%
  - 4.5 % : 10%
  - 11% : 25%

Concrete with w/c-ratio 0.40

- All specimens except one with 2% solution expanded during freezing. The biggest expansion occurred in the concrete with pure water.
- During the constant temperature period at –23°C specimens with 11% solution, and to some extent that with 4.5%, continued to expand, while concrete with 2% solution contracted slowly.
- During warming the specimens with 11% solution expanded more than the other.
- The reduction in resonance frequency after thawing is:

- 0% solution:		10%
- 2%	:	10%
- 4.5 %	:	20%
- 11%	:	15%

The results are not unambiguous and are not easy to interpret. Some comments and attempts in qualitative terms to explain the observations will be given.

1. Non-air-entrained concrete expands during freezing irrespectively of the salt concentration. This is reasonable, since there is lack of air-space for displaced water. It means that a proper air-entrainment should be required also when the pore water for some reason has become saline, e.g. after many years of exposure to seawater or de-icing salts. (However, the tests of air-entrained concrete presented in the next paragraph indicate that air is perhaps a negative factor.) There are some exceptions when no dilation was found, viz. w/c-ratio 0.45 with intermediate salt concentration (2 and 4.5%), which are difficult to explain. It seems as if no freezing, or very small freezing of pore water, has taken place in these specimens. This result was found in both the two repeated tests with the same concentration.

2. An increased salt concentration in the pore water will lead to a reduction in the amount of freezable water. Therefore, one might have expected lower expansion the higher the salt concentration. This is not the case however. For w/c-ratio 0.60, 4.5% salt gives higher expansion than all other concentrations, including pure water. For w/c-ratio 0.45, 11% salt gives bigger expansion than 2% or 4.5%. For w/c-ratio 0.40, 4.5% salt gives bigger expansion than 2%. This indicates that another phenomenon is causing damage than just volume expansion caused by ice formation.

3. When freezing takes place in a capillary containing salt water at temperature θ, only part of this freezes, which means that the concentration of the unfrozen solution in the pore increases. There will always be free energy equilibrium between the new concentration and the ice in the same pore. If there is local equilibrium in the specimen, also unfrozen solution in adjacent very narrow pores, in which the freezing point is lower than θ, will have the same free energy. No transport of water, and no ice formation would be possible. However, when temperature is suddenly lowered, and more ice is formed in the actual capillary, an energy difference will appear between the ice body and the unfrozen liquid, as described by the ice lens growth theory. This will cause migration of water from the 'unfrozen' pore, causing expansion by a growing ice lens.

   In the case with salt water, there will also be an immediately occurring salt concentration difference between the solution in the pore containing ice, and the unfrozen solution in the finer adjacent 'unfrozen' pore. Continued freezing will namely cause an increase in the concentration of the remaining solution in the 'frozen' pore. This concentration difference will increase the tendency of water flow to the 'frozen pore', unless salt ions move into the 'unfrozen' pore, and thereby increase the concentration in this to the same level as in the 'frozen' pore. There is a theoretical possibility that the salt concentration difference creates an osmotic pressure, provided the transport coefficient of ion diffusion into the 'unfrozen' pore, is lower than the transport coefficient of water into the 'frozen' pore. This explanation to the aggravating effect of salt has been forwarded by Powers (1955). The osmotic pressure might be more pronounced at low w/c-ratio since then the diffusivity of ions might be lower.

   Like normal ice lens growth, the possible osmotic effect should be active as long as temperature is lowered, since the concentration in "frozen" pores gradually increases as long as temperature is reduced and more of the solution in the pore is transformed into ice.

4. Increased salt concentration causes reduced amount of freezable water. Thus, the number of pores containing ice will be reduced. This will theoretically reduce the possibility of ice lens growth and osmotic pressure. Possibly, there exists a salt 'pessimum' concentration at which the negative effect of osmotic pressure is bigger than the positive effect of lowered amount of freezable water, and possibly that concentration is a function of the w/c-ratio. This could be an explanation to the observations made.

5. When freezing occurs, some salt solution is displaced towards the air pores where it immediately freezes. The concentration of the displaced solution could be lower than in the pore from which it was expelled, especially in dense concrete, since ions are 'filtered out' from the rapid flow. As described by the ice lens growth mechanism, the air-pore ice attracts unfrozen water from fine pores and from isolated pores containing supercooled water. The ice lens growth in air-pores occurs without causing pressure. However, in non-air-entrained concrete, the spacing between air-pore ice is too big for the protective mechanism to be effective.
6. When temperature is held constant at –23°C for three hours, specimens with 11% salt continues to expand markedly. There is also a slight tendency that 4.5% salt gives a slight expansion. This cannot be explained by the hydraulic pressure mechanism since no ice is formed when temperature is held constant, see Chapter 9. It is also difficult to explain by the *normal* ice lens growth mechanism, since local equilibrium between ice and unfrozen water ought to be established short time after temperature lowering has stopped. This is indicated by the specimens with pure water and 2% solution that stop to expand almost directly. The expansion might be explained by osmotic pressure, since this can act long after temperature drop has stopped.
7. The big expansion at warming of specimens with high salt concentration might possibly be explained by 'reversed' osmotic pressure. When ice melts in 'frozen pores' the salt concentration in these decreases, while it is still high in unfrozen pores due to the influx of ions during the freezing period. Thus, water from the 'frozen pore' with its weaker solution will tend to enter the unfrozen pores with their stronger solution, which might cause a pressure.

The reasoning above does not give full explanation to the somewhat contradicting results obtained.

8.3.3 Air-entrained concrete

Length change-time curves for all air-entrained concrete are shown in Figure 8.3.4-Figure 8.3.6. In all figures the temperature-time curve is valid for the specimen with pure water.

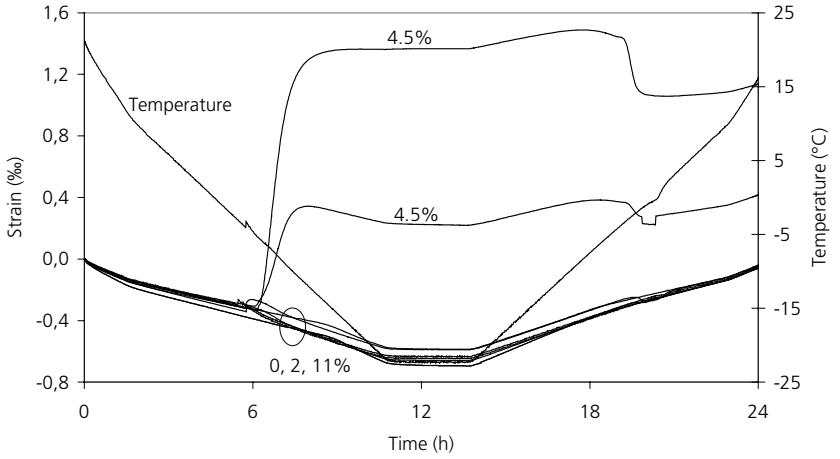

Figure 8.3.4. Length change versus temperature for samples with a w/c-ratio of 0.60 and a 6% air content stored in different NaCl-solution for more than four years. Mark the scale on the strain-axis.

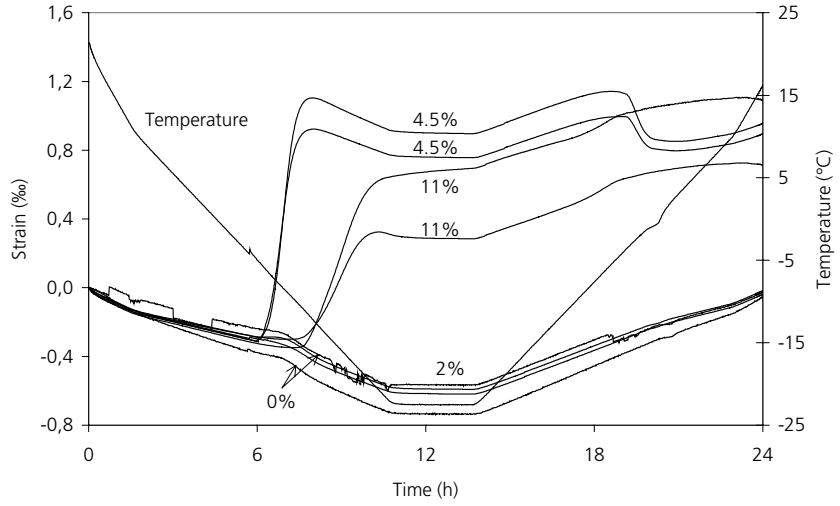

Figure 8.3.5. Length change versus temperature for samples with w/c-ratio 0.45 and 10% air content, stored in different NaCl-solution for more than four years.

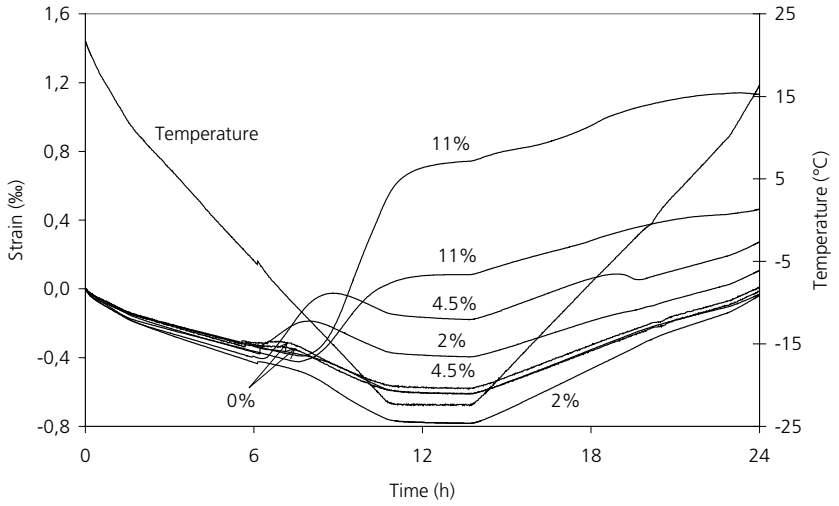

Figure 8.3.6. Length change versus temperature for samples with w/c-ratio 0.40 and 6% air content, stored in different NaCl-solution for more than four years.

Some comments to the results will be made.

Concrete with w/c-ratio 0.60:

- Normally, air-pores will protect the concrete from frost damage. This is also the case for specimens with pure water, and 2% or 11% salt solution. For the 4.5% solution extensive expansion occurs, as it did for the non-air-entrained concrete. The expansion is, however, even bigger in the air-entrained concrete; one specimen showing a dilation at -20°C of 1.8 ‰ compared to about 1 ‰ for the non air-entrained. This is very an unexpected behaviour. The expansion starts already at –5°C and continues to about -10°C.
- The concrete with 4.5% solution expands markedly when temperature is held constant at -23°C. For the other concentrations no expansion or contraction occurs.
- For the specimen with 4.5% concentration, considerable contraction occurs during warming in the range -5°C to 0°C. This indicates release of internal stresses caused by ice-bodies formed under pressure inside the capillary pore system.
- The reduction in resonance frequency after thawing is:

  - 0% solution: 5%
  - 2% : 5%
  - 4.5 % : 50%
  - 11% : 5%

Concrete with w/c-ratio 0.45

- As expected no expansion occurs for specimens with pure water or 2% concentration. On the other hand, big expansion occurs for concentration 11% and especially for concentration 4.5%. These expansions are much bigger than any of the expansions observed for the non-air-entrained concretes.
- When temperature is held constant at -23°C no length changes are observed for 0, 2 and 4.5%. Some slight expansion can be noticed for 11% solution.
- Considerable contraction during warming in the range -5°C to 0°C, similar to those observed for w/c-ratio 0.60 at 4.5%, was also seen here.
- The reduction in resonance frequency after thawing is:

  - 0% solution: 5%
  - 2% : 5%
  - 4.5 % : 40 à 65%
  - 11% : 40 à 45%

Concrete with w/c-ratio 0.40:

- The results are similar to those for w/c-ratio 0.45:
  - Big expansion during freezing for 11% salt concentration.
  - Considerable expansion for 4.5% concentration (one of the specimens).
  - No expansion for specimens with pure water.
- There is also some expansion for one of the specimens with 2% concentration, which differs from the other w/c-ratios.
- The reduction in resonance frequency after thawing is:

  - 0% solution: 5%
  - 2% : 5 à 15%%
  - 4.5 % : 20 à 35%
  - 11% : 40 à 45%

The interpretation of the results is difficult. An attempt will be made.

Air-entrainment is supposed to protect concrete from frost damage. In practice, and in a traditional open salt scaling test, this positive effect of air is obvious. In the actual test, air-entrainment turns out to be detrimental, at least for very high internal salt concentrations, 4.5% and 11%. For pure water in the pore system, air-entrainment is supposed to be protective for two reasons:

1. It furnishes space for expelled water from the freezing site.
2. It makes un-constrained, stress-free ice lens growth possible, thus hindering constrained ice lens growth in capillaries.

There is no reason to believe that the air-pores should not serve the first purpose, since the presence of salt does not make the air pores un-accessible to displaced water. Therefore, the reason must have something to do with ice lens growth, or with some additional mechanism, like osmotic pressure. Since all freezing in a capillary will cause an increase in the concentration of the remaining solution in this, the water movement from the adjacent pores with lower concentration into the capillary, causing ice lens growth, and possibly also osmotic pressure, described in paragraph 8.3.2, must appear also when there are air pores in the concrete. They cannot stop this local migration and pressure built-up. Migration will not stop until the pressure in the capillary is high enough to stop moisture migration. The consequence of the migration is that more ice might be formed in the capillaries when these contain salt solution, and that the specimen expands. Therefore, the mechanism might explain the observed expansion.

Initial freezing of water in capillaries, taking place when supercooling is overcome, forces a considerable amount of water out from the capillaries to the air pores, where it freezes. In concrete with high salt concentration no supercooling is observed, but salt solution ought to be expelled to the air-pores more gradually, as more and more ice is formed in the capillaries. The actual specimens had been stored for more than 4 years in salt solution. Therefore one can expect that some air pores contained some salt solution already when the test started. When the concrete contains pure water the ice in air-pores is also pure. Thus, in this case, when temperature is lowered unfrozen water will primarily move to the air-pore ice, which will protect the concrete. When the specimen contains salt solution also the air-pore ice is surrounded by salt solution. Theoretically the concentration of this should at each temperature be the same as in the capillaries containing ice-bodies. But this means that its concentration will be higher than that of unfrozen water in fine capillaries, since this corresponds to the initial concentration before freezing. Thus, there might be an osmotic pressure built-up also between air-pore solution and unfrozen water, which obstructs the stress-relieving effect of air-pore ice.

It must be noted that the reasoning above is purely qualitative.

The question remains why air saves concrete during freeze/thaw where the surface is exposed to salt solution, when it turns out to be negative in the tests presented here. In salt scaling tests it is found that high concentrations give less damage than low concentrations, when the opposite is valid here. It has even been found that specimens pre-stored for long time in salt solution, and therefore contains salt in the pore solution, scales less than specimens pre-stored in pure water, Lindmark (1995), Sellevold and Farsted (1992).

The differences between the two situations are:

1. In a scaling test, or in practice, the surface is exposed to salt solution during the entire cycle. Water and solution can flow into and out of the specimen during the test. Also small changes in the degree of saturation will cause big effects on the behaviour.
2. In a scaling test, or in practice, the concrete has big temperature gradients in the surface part where damage occurs.

Exactly how these differences can explain the different behaviour observed is a complicated question and cannot be analysed in this report.

8.3.4 Summary of results

A summary of all damage parameters observed during the test are shown in Table 8.3.1

Table 8.3.1 Data concerning damage parameters, where S_A or S_B= degree of saturation (for definition see 4.5), u= moisture ratio (for definition see 4.5), RF²= relative residual resonance frequency squared, Perm.dil.= permanent dilation (for definition see 4.4), dil.at sc.= dilation at supercooling (for definition see 4.4), dil at -20°C= dilation at -20°C (for definition see 4.4).

				dϕ/dt=3.6°C/h				
w/c-ratio	Air content (%)	S_A/S_B	u (%)	Conc. of NaCl (% of weight)	RF²	Permanent dilation (‰)	Dil at sc. (‰)	Dil. at -20°C (‰)
0.60	Natural	1/-	8.18	2	0.82	0.22	0.09	0.48
0.60	Natural	1/-	7.95	2	0.83	0.22	0.04	0.48
0.60	6	0.88/-	8.59	2	0.97	0.04	0.03	-0.04
0.60	6	0.88/-	8.42	2	0.98	0.01	0.06	-0.02
0.40	Natural	1/-	7.26	2	0.93	0.12	0.02	0.19
0.40	Natural	0.98/-	6.99	2	0.87	0.13	0.03	0.21
0.40	6	0.89/-	8.34	2	0.89	0.22	0.05	0.30
0.40	6	0.86/-	7.91	2	0.96	0.07	0.01	0.00
0.45	Natural	0.95/-	7.44	2	0.82	0.06	0.01	0.09
0.45	Natural	0.99/-	7.40	2	0.96	0.04	0.01	0.07
0.45	10	0.77/-	8.51	2	0.97	0.03	0.01	-0.07
0.45	10	0.79/-	9.01	2	0.92	0.05	0.03	-0.03
0.60	Natural	1/-	8.39	4.5	0.52	0.67	0	0.99
0.60	Natural	1/-	8.15	4.5	0.54	0.64	0	1.05

dϕ/dt=3.6°C/h								
w/c-ratio	Air content (%)	S_A/S_B	u (%)	Conc. of NaCl (% of weight)	RF²	Permanent dilation (‰)	Dil at sc. (‰)	Dil. at -20°C (‰)
0.60	6	1/-	10.04	4.5	0.22	1.28	0	1.80
0.60	6	0.98/-	9.31	4.5	0.56	0.51	0	0.76
0.40	Natural	1/-	7.43	4.5	0.84	0.26	0	0.19
0.40	Natural	1/-	7.56	4.5	0.82	0.21	0	0.20
0.40	6	0.86/-	7.89	4.5	0.95	0.05	0	0.15
0.40	6	0.93/-	8.54	4.5	0.84	0.40	0	0.41
0.45	Natural	0.97/-	6.89	4.5	0.91	0.07	0	0.02
0.45	Natural	0.97/-	7.02	4.5	0.92	0.04	0	0.03
0.45	10	0.88/-	10.18	4.5	0.35	1.06	0	1.44
0.45	10	0.87/-	10.01	4.5	0.59	0.99	0	1.23
0.60	Natural	1/-	7.75	11	0.74	0.32	0	0.34
0.60	Natural	1/-	7.80	11	0.77	0.40	0	0.42
0.60	6	0.89/-	8.05	11	0.96	0.06	0	-0.10
0.60	6	0.89/-	7.82	11	0.97	0.04	0	-0.01
0.40	Natural	1/-	7.08	11	0.85	0.17	0	0.08
0.40	Natural	1/-	6.99	11	0.87	0.14	0	0.07
0.40	6	1/-	9.68	11	0.64	1.33	0	0.82
0.40	6	0.97/-	8.48	11	0.80	0.67	0	0.76
0.45	Natural	1/-	7.90	11	0.84	0.40	0	0.17
0.45	Natural	1/-	7.72	11	0.85	0.31	0	0.08
0.45	10	1/-	11.94	11	0.41	1.30	0	1.04
0.45	10	1/-	11.75	11	0.54	0.91	0	0.73

In Figure 8.3.7 the residual resonance frequency for all experiments is plotted versus the w/c-ratio. In Figure 8.3.8 dilation is plotted versus the air content.

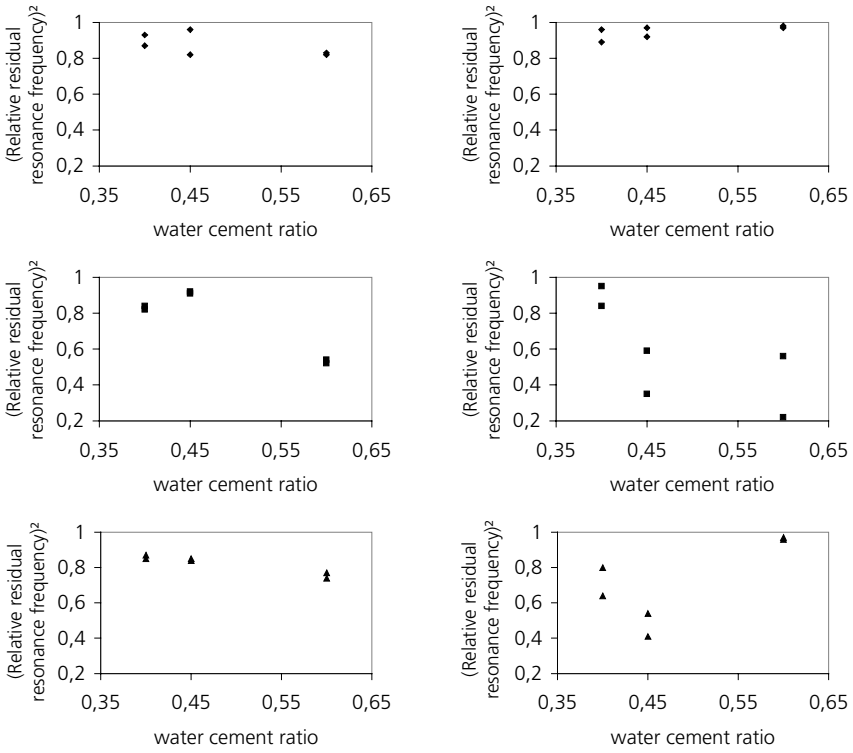

Figure 8.3.7. The residual resonance frequency squared (the dynamic E-modulus) plotted versus w/c-ratio for different air contents and salt concentrations. The column to the left shows results from samples without air entrainment and the column to the right show results of air-entrained specimen. The first row show results of samples stored in 2% NaCl-solution, the row in the middle from samples stored in 4.5% and the last row show results of samples stored in 11% NaCl-solution.

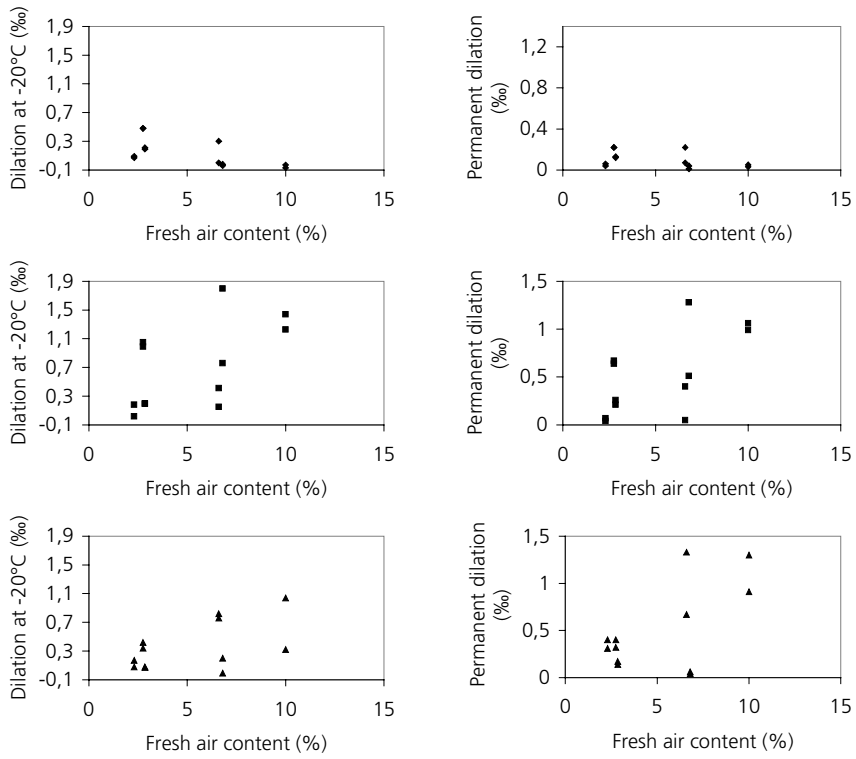

Figure 8.3.8. Dilation at –20°C and the permanent dilation plotted versus the air content of the fresh concrete. The first row show results for samples stored in 2% NaCl-solution, the row in the middle for samples stored in 4.5% and the last row show results for samples stored in 11% NaCl-solution.

Figure 8.3.7 shows a slight tendency that a decreased w/c-ratio is a positive factor. The effect of air and salt concentration however dominates over the effect of the w/c-ratio.

Figure 8.3.8 demonstrates the remarkable effect that high air content is not necessarily a positive factor when the specimens contain a strong salt solution (4.5% or 11%). For pure water and low concentration (2%) air is very positive as expected.

9 Investigations of freezing and thawing of water in concrete

9.1 Introduction

The micro-concrete types investigated in Chapter 5-8 responded differently to different types of freeze-thaw cycles and to different degrees of saturation. The aim of the present chapter is to supplement these observations of length change and damage during freeze-thaw by observations of ice formation and ice thawing, using the same materials, the same type of freeze-thaw cycles, the same pre-conditioning procedures, and the same degrees of saturation as were used for the 'dilation specimens' in Chapter 5-8.

In this chapter only the results of the calorimeter experiments are described. A combination of the dilation curves from Chapter 5-8 and the calorimeter results described here is made and discussed in Chapter 10.

In the present chapter also a short theoretical background to freezing of pore water is given.

9.2 Ice formation and melting in pore systems

9.2.1 Example of a calorimeter experiment

Figure 9.2.1 shows a typical result of a scanning calorimeter test of one of the micro-concretes. The sample had been stored in water ever since the time of casting.

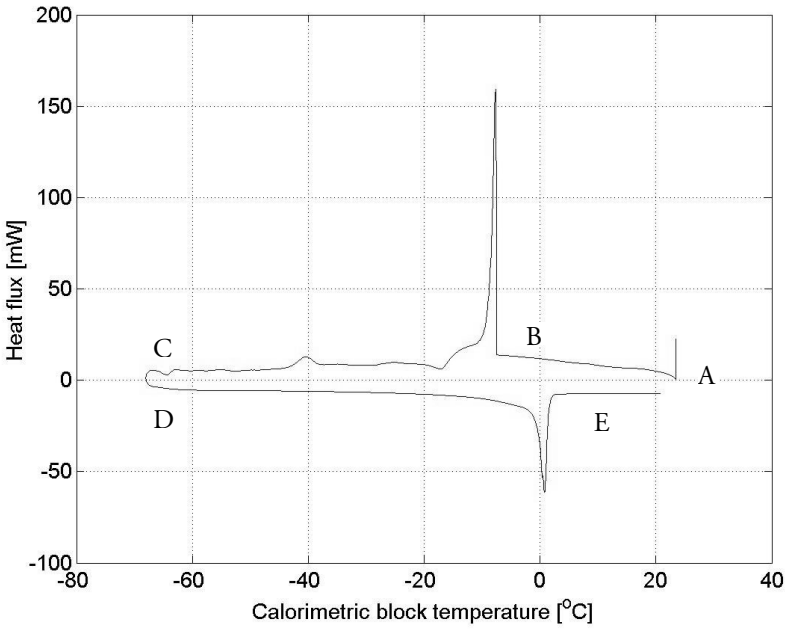

Figure 9.2.1. Heat flow from a water-stored micro-concrete sample (w/c-ratio 0.60) during freezing and thawing in the low temperature scanning calorimeter. Temperature is measured in the calorimeter block and not in the specimen.

When the temperature decreases at a constant rate, the material responds with a linear increase in heat flow (A-B). Since thermal capacity should be constant before freezing, the initial part of this gradual increase in heat flow probably depends on different temperature-time developments for the calorimeter block and the specimen, since the temperature was not the same in the specimen as in the block when the test started. The continued increase in heat flow is more difficult to explain. Possibly it is caused by adsorption phenomena when water from capillaries is forced into the fine gel pores when temperature is lowered, a mechanism described by Helmuth (1961). However, this part of the calorimeter curve has nothing to do with freezing and is therefore neglected.

At the lowering of temperature down to the temperature where the first ice formation occurs (B), the system consists of concrete and liquid pore-water. Ice formation begins at about -7°C, this depression in the freezing point being due to several factors, discussed below. When the temperature is lowered further (B-C) an exothermic peak can be discerned at about –40°C indicating some ice formation. No ice formation is observed at lower temperature. When temperature is gradually raised from –65°C (D-E) only minor ice melting is observed until about +1°C (E) where most of

the ice melts. As all temperatures in the diagram, this is the temperature of the calorimeter block and not of the specimen. The latter is some degrees lower during the warming phase.

The curves observed are determined by two main phenomena:

1: *Equilibrium:* freezing point depression of pore water, mainly caused by the actual pressure conditions in ice, unfrozen water, and water vapour. The smaller the pore size in which water is located, the bigger the freezing point depression.

2: *Non-equilibrium:* supercooling of water. The smaller the water volume, the bigger the supercooling.

The *freezing curve* involves both phenomena. The *melting curve* only involves freezing point depression. This difference between freezing and melting is the main cause why water freezes at lower temperature than it melts. The two phenomena are further discussed below. Relation between pore size and freezing point depression is also discussed.

9.2.2 Freezing point depression

There are numerous factors that influence the formation of ice, such as pressure in water, ice and vapour. These pressures depend on pore-size distribution, pore shape, and pore continuity, and on substances dissolved in the pore solution. Basic relations between pressure, concentration of pore solution, and freezing point are described by traditional thermodynamics. Formulas are given in textbooks like Laidler and Meiser (1995), Atkins (1998).

When ice is formed inside a closed pore from which water has no possibility to escape, the walls of the pores are able to exert pressure on the ice, increasing its chemical potential. With sufficient pressure, the ice comes into equilibrium with the water surrounding it, ice formation stopping. On the basis of thermodynamics, one can estimate what degree of pressure is needed to prevent ice formation in bulk water (the Clapeyrons equation).

$$\frac{dp}{dT} = \frac{\Delta H^{fus}}{T\Delta V^{l-s}} \qquad \text{Eq. 9.2.1}$$

where, dp is the pressure increase (Pa) for the temperature drop dT (K) if transformation to ice shall be hindered, ΔH^{fus} is the molar change in enthalpy at freezing (the latent heat of fusion), and $\Delta V^{l-s} = V^{l}-V^{s}$ is the change in volume of water at freezing. T is the freezing temperature (K). The following values are valid for water freezing at the normal temperature (273.15 K):

$\Delta H_m^{fus} = 6009$ J/mol
$V_m^l = 18.02\ 10^{-6}$ m³/mol
$V_m^s = 19.63\ 10^{-6}$ m³/mol
$T = 273.15$ K

Note, the values given are only valid for the normal freezing temperature (273.15 K). For freezing at lower temperature somewhat different values are valid. The biggest effect of temperature is on ΔH^{fus}. It is lowered to about 5300 J/mole at –20°C. The effect of temperature on the heat of fusion is discussed in Brun et al (1977).

Using these data one finds that the walls need to exert an added pressure of 13.7 MPa on the ice for each degree of decrease in temperature achieved in this way. For a material such as concrete, which has a tensile strength of approximately 3 MPa, such a pressure can never be built up before the material had ruptured before temperature has been lowered more than a fraction of a degree, see paragraph 2.3. One can thus conclude that the depression of the freezing point of micro-concrete shown by calorimetric measurement is not due to external pressure.

Water inside a pore system at low temperature forms a complicated network of ice, vapour and liquid water. Therefore, it is not possible to find any well-defined relation between pore size and freezing point. A thorough discussion of the effect of different meniscus systems existing inside a porous material, on the freezing point, is performed in Defay, Prigogine and Bellemans (1966). A short review of their work is now presented. The formulas are also presented in Tange Jepsen (2002).

As Defay et al. (1966) pointed out, there are three possibilities for what can happen to the meniscus system of a porous material when it freezes: (1) that both the ice (s=solid) and the pore liquid (l=liquid) are exposed to the water vapour (g=gas) but not to each other (case A); (2) that the pore liquid is in contact with both the ice and the vapour (case B); (3) that the ice is in contact with both the vapour and the pore liquid (case C), Figure 9.2.2.

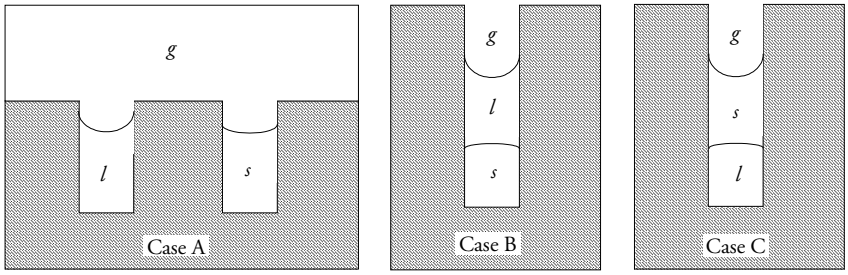

Figure 9.2.2. Possible menisci systems found in a porous material during freezing.

These three cases correspond to three different levels of depression of the freezing point (the triple point), and thus to three different pore sizes.

In derivation of all expressions the molar volume of water is neglected since it is very small in comparison to the molar volume of air, $V^l << V^g$, i.e. $(V^g - V^l) \approx V^g$. All expressions assume that the menisci are curved according to Figure 10.2.2; i.e. the menisci solid-gas and liquid gas are concave towards gas, the meniscus solid-liquid is convex towards liquid in Case B and concave towards liquid in Case C.

The following expression applies to case A:

$$\ln\frac{T}{T_0} = -\left(\frac{2}{\Delta H^{fus}}\right)\left(\frac{V^l\sigma^{g-l}}{r^{g-l}} - \frac{V^s\sigma^{g-s}}{r^{g-s}}\right) \qquad \text{Eq. 9.2.2}$$

If ice is considered to be under atmospheric pressure (the interface ice-gas is plane) the second term on the right hand side vanishes:

$$\ln\frac{T}{T_0} = -\left(\frac{2}{\Delta H^{fus}}\right)\frac{V^l\sigma^{g-l}}{r^{g-l}} \qquad \text{Eq. 9.2.3}$$

For case B, the following equation is valid:

$$\ln\frac{T}{T_0} = -\left(\frac{2}{\Delta H^{fus}}\right)\left(\frac{V^s\sigma^{l-s}}{r^{l-s}} + \frac{\left(V^l - V^s\right)\sigma^{g-l}}{r^{g-l}}\right) \qquad \text{Eq. 9.2.4}$$

The difference V^l-V^s is small compared to V^*. Therefore the second term on the right hand side is neglected. The equation changes to:

$$\ln\frac{T}{T_0} = -\left(\frac{2}{\Delta H^{fus}}\right)\frac{V^s\sigma^{l-s}}{r^{l-s}} \qquad \text{Eq. 9.2.5}$$

For case C the following equation is valid:

$$\ln\frac{T}{T_0} = -\left(\frac{2}{\Delta H^{fus}}\right)\left(\frac{V^l\sigma^{l-s}}{r^{l-s}} + \frac{\left(V^l - V^s\right)\sigma^{g-s}}{r^{g-s}}\right) \qquad \text{Eq. 9.2.6}$$

Neglecting the second term on the right hand side gives:

$$\ln\frac{T}{T_0} = -\left(\frac{2}{\Delta H^{fus}}\right)\frac{V^l\sigma^{l-s}}{r^{l-s}} \qquad \text{Eq. 9.2.7}$$

V^l and V^s are the molar volume of liquid and of solid [m^3/mol], σ^{g-l} and σ^{l-s} [J/m^2] are the surface energies between the gas-liquid and the liquid-solid phase, T is the freezing point [K], T_0 is the normal freezing point 273 [K], ΔH^{fus} is the heat of fusion [J/mol], and r^{g-l} and r^{l-s} [m] are the radii of the menisci between the gas and the liquid, and between the liquid and the solid.

The equations can be further reduced to relations between pore radius and freezing point (triple point) by assuming certain curvatures of ice and water menisci and considering the thickness of the adsorbed layer.

In the calculations that follow, the liquid water or the ice body are supposed to be in direct contact with the pore wall. The pore is assumed to be cylinder-shaped with radius r (neglecting the thickness of the adsorbed layer). Total wetting between the pore wall and the water meniscus is assumed. Thus, r^{l-s} and r^{g-l} are identical to the pore radius r.

The three equations will give different relations between the triple point and the pore radius. This is shown by the following example in which the pore radius corresponding to the triple point –30°C is calculated. The effect of temperature on molar volume and surface tension are neglected; $V^s \approx 2\cdot10^{-5}$ [m^3/mol], $V^l \approx 1.8\cdot10^{-5}$ [m^3/mol], $\sigma^{g-l} \approx 0.075$ [J/m^2], $\sigma^{s-l} \approx 0.035$ [J/m^2]. The heat of fusion at –30°C is supposed to be $4.9\cdot10^3$ [J/mol]. The three expressions give the following pore radii:

Eq. 9.2.3: r=4.7 nm
Eq. 9.2.4: r=2.5 nm
Eq. 9.2.7: r=2.2 nm

The difference is considerable. For a given pore size Eq. 9.2.3 gives the lowest freezing point and Eq. 9.2.7 the highest freezing point.

A real pore system is extremely much more complex than the idealised pores treated above. Therefore, it is not possible to exactly predict when water freezes or melts in each individual pore. It is quite clear however that the finer the pore system

the smaller fraction of pore water is frozen at each freezing temperature. Thus, the calorimeter experiments performed give a clear picture of the size distribution (fineness) of the pore system.

The presence of *salts* in pore water will decrease the freezing point. Provided no consideration is taken to capillary effects, and if the solution is weak, x_B<<1, and the depression of the freezing point is only slight, the depression of the freezing point (triple point) due to dissolved substances can be calculated approximately as

$$\Delta T \approx \frac{x_B R_m T^{*2}}{\Delta H_{A,m}^{fus}} \qquad \text{Eq. 9.2.8}$$

where x_B is the mole fraction of solvent B in the solution, R_m is the gas constant, 8.314 [J/mole,K], T* is the normal freezing point, 273.15 [K] for water and ΔH^{fus} is the molar heat of fusion [J/mole].

In Figure 9.2.1, the depression of the initial freezing point is 7°C. The concentration of dissolved substances needed for such a freezing point depression can be calculated as follows:

$$x_B = \frac{6009 \cdot 7}{8.315 \cdot 273.15^2} = 0.068$$

This means that if the depression of the initial freezing point were only due to dissolved substances, these would need to have a concentration of about 7% which is much higher than that in concrete as is shown by the following calculation.

The cement used had an alkali content expressed as equivalent Na_2O of 0.6%. In a concrete with 400 kg cement and 120 litres of pore water per m^3 the total amount of Na_2O is 2.4 kg, or 39 mole. When dissolved, each mole of Na_2O is dissociated in 2 mole Na and 2 mole OH; i.e. the total number of dissolved ions is 156. The mole fraction becomes 156/(156+120000/18)=0.023. The freezing point depression becomes 2.1 degree.

For concrete that were long-term stored in salt water the salt concentration in the pores is much higher. Provided the pore solution has the same concentration as the outer solution the following freezing points should be valid:

2% NaCl: ~-2°C
4.5% NaCl: ~-4.6°C
11% NaCl: ~-11.4°C

It can be seen in Figure 9.2.3 that the freezing point depression at onset of freezing is larger in all measurements of samples stored in 4.5% NaCl-solution. The lowest freezing point occurred when the freezing rate was the highest. In Figure 9.2.4 the difference in freezing point at onset of freezing between samples stored in lime-saturated water and in 4.5% NaCl-solution can be seen. The influence of supercooling is evident in both cases. The difference in freezing points is about 2 degrees. This difference is in fair accordance with the calculations above, since the freezing point should be about -2.1°C for specimens stored in pure water (provided dissolved ions in pore water were not leached out) and -4.6°C for specimens stored in salt solution. However, if some ions were leached from the specimens during the 4 years water storage (which seems reasonable) the difference increases indicating that supercooling of pure pore water is bigger than that of saline pore water. The freezing point is also in this case (Figure 9.2.4) seen to be lower when the freezing rate is higher.

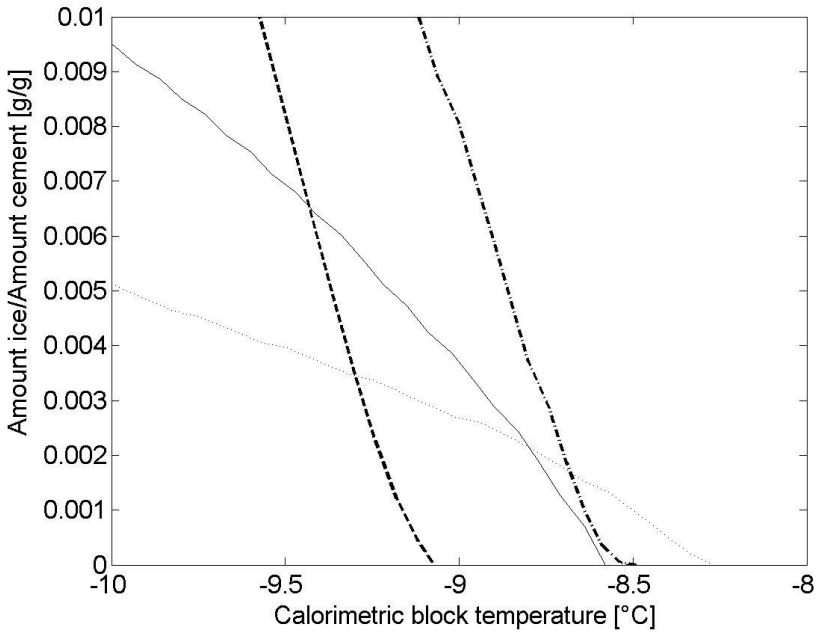

Figure 9.2.3. Freezing point determined at a calorimeter measurement for concrete with w/c-ratio 0.40 and 6% air long-term stored in 4.5% NaCl-solution. The three curves to the right was obtained during the 'normal' freeze-thaw cycle and the curve to the left during the 'rapid'.

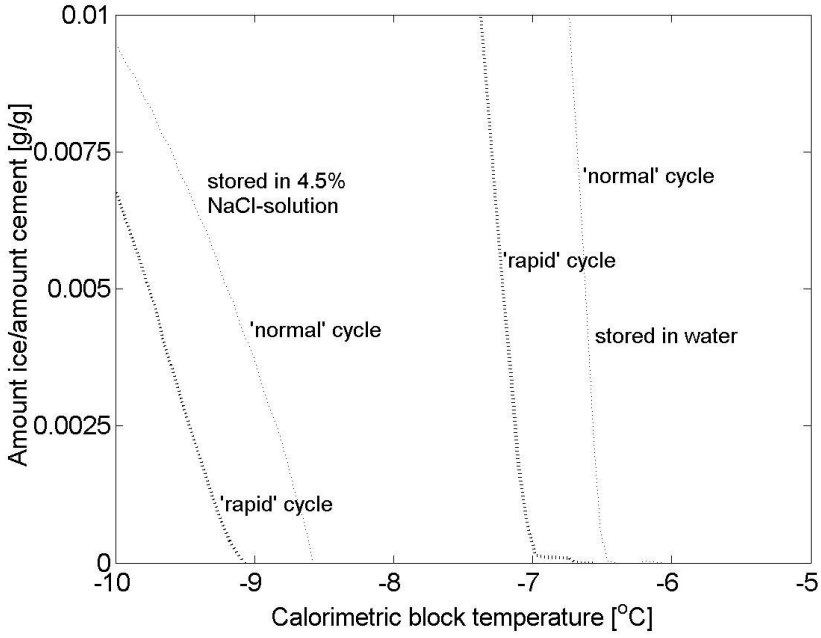

Figure 9.2.4. Difference in freezing point between samples long-term stored in lime-saturated water and in 4.5% NaCl-solution. w/c-ratio 0.40, 6% air.

9.2.3 Supercooling of water, hysteresis freezing-melting, spreading of ice

Bulk water has an equilibrium freezing point at normal pressure of 0°C (273.15 K). Normally, however, many degrees lower temperature is needed for freezing to occur. The phenomenon is called supercooling. Super-cooled water is unstable (non-equilibrium condition) and freezes if it is disturbed in some way; like by vibration, by addition of solid particles to the water, or by touching the water surface by a piece of ice. Then freezing of the super-cooled water is very rapid and the temperature rapidly rises to 0°C due to heat developed by the freezing water. Ice first forms at single nucleation spots and then rapidly spreads from these to the entire water volume by dendritic growth. The movement of the ice front has been investigated experimentally for supercooled water in glass capillaries and found to be about 10 mm/s, Helmuth (1960). Thus, for the actual specimen size in the calorimeter experiment the entire specimen should be 'nucleated' from the most distant nucleation spot within less than 5 seconds.

This type of nucleation of ice formation initiated by some sort of disturbance is called heterogeneous nucleation. The smaller the water volume, the bigger is the tendency of supercooling. Thus, small droplets have a lower average freezing point than

big droplets. The effect of droplet size on supercooling has been investigated by Langham and Mason (1958). They found that the average nucleation temperature of 1 mm droplets was as low as –24°C. Smaller drops were found to have even lower nucleation temperatures.

When temperature falls below about -40°C water cannot exist in liquid form. Then ice forms by homogeneous nucleation at which no outer nucleation agents are needed. This homogeneous nucleation is probably the reason why a certain ice formation is almost always found in concrete at about -40°C. Then, water that has been super-cooled in isolated pores unreachable by ice from adjacent coarser pores, freezes homogeneously.

In the calorimeter experiments like that shown in Figure 9.2.1 the first ice formation was not initiated until about –7°C. Then, a considerable amount of ice was formed 'momentarily' which is indicated by the peak in the heat flow diagram. At the same time some rapid expansion normally occurs, se figures in chapter 5-8. This rapid ice formation occurs in pores that are accessible to ice, i.e. pores with radii bigger than that corresponding to the nucleation temperature. There might exist pores of the same sizes in which ice formation does not occur because they are isolated from nucleated pores by narrow openings impossible for ice to penetrate at the actual temperature, Figure 9.2.5. Therefore, one cannot exclude that there, at each temperature during the temperature-lowering phase (freezing phase) in a calorimeter experiment, exists both water/ice at equilibrium in some pores and water that is supercooled in other pores. At temperature below about -40°C when homogeneous nucleation has occurred equilibrium conditions exist in all pores.

During the thawing phase in the calorimeter experiment, melting occurs in all pores at the temperature corresponding to the actual freezing/melting point. This difference between the freezing behaviour including local supercooling, and the melting behaviour occurring during equilibrium conditions is the most plausible reason for the big hysteresis almost always observed between freezing and melting in a calorimeter experiment.

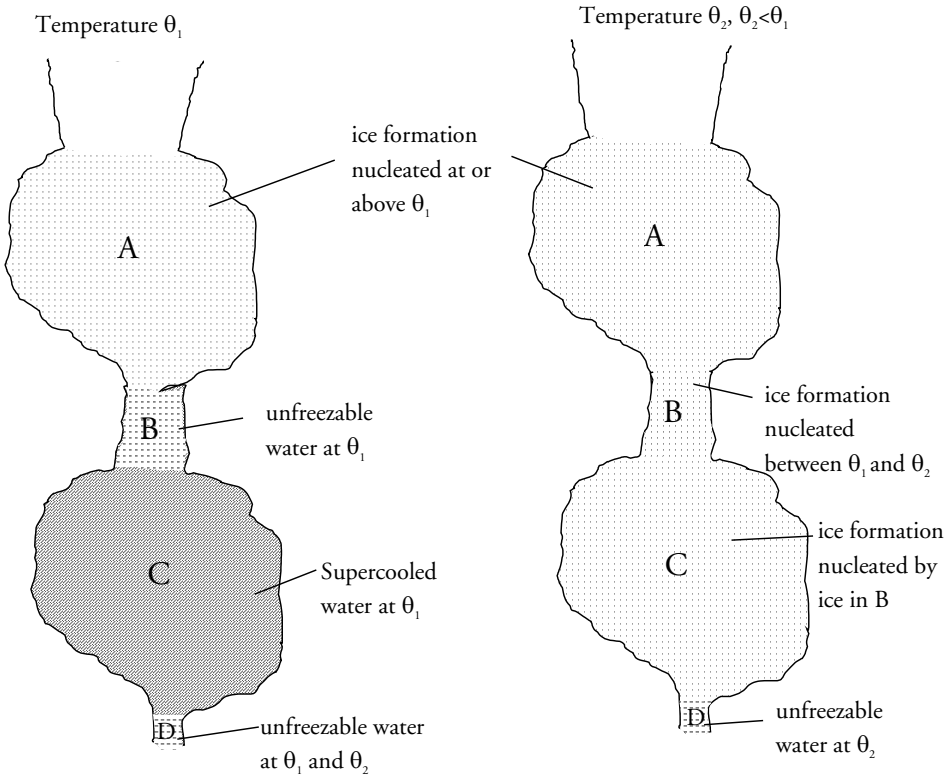

Figure 9.2.5. Fictions pore system containing ice, supercooled water and unfreezable water.

There are also other mechanisms suggested for appearance of hysteresis. It has been suggested that when water freezes the freezing temperature is governed by a spherical shape of the ice crystal, while at thawing melting is governed by a cylindrical shape Setzer (1997). This means that according to Eq. 9.2.2-Eq. 9.2.7 the freezing temperature is proportional to a factor

$$e^{(const.2/r)}$$

and melting by a factor

$$e^{(const.1/r)}$$

The 'constant' is somewhat temperature dependent (constant = surface tension divided by heat of fusion) but this is neglected here. Thus, the ratio freezing temperature/melting temperature (degree K) becomes:

$$\frac{T_{freeze}}{T_{melt}} = e^{\left(\frac{const.}{r}\right)} \qquad \text{Eq. 9.2.9}$$

Example:

For the pore with radius 4.7 nm and freezing temperature 243 K (-30°C) used in the example above (the calculation based on Eq. 9.2.3), the melting temperature is 257 K (-16°C).

The observed hysteresis is much bigger. Therefore, the example indicates that the different shape of ice bodies at freezing and melting cannot be the only cause of hysteresis.

Another explanation, that has been put forward, is that the pore structure is changed during freezing so that melting occurs in a pore system that is coarser than during freezing. If this is the case there should be no, or at least much smaller, hysteresis during a second freezing-thawing cycle. This has not been observed experimentally, however, see Figure 9.2.6.

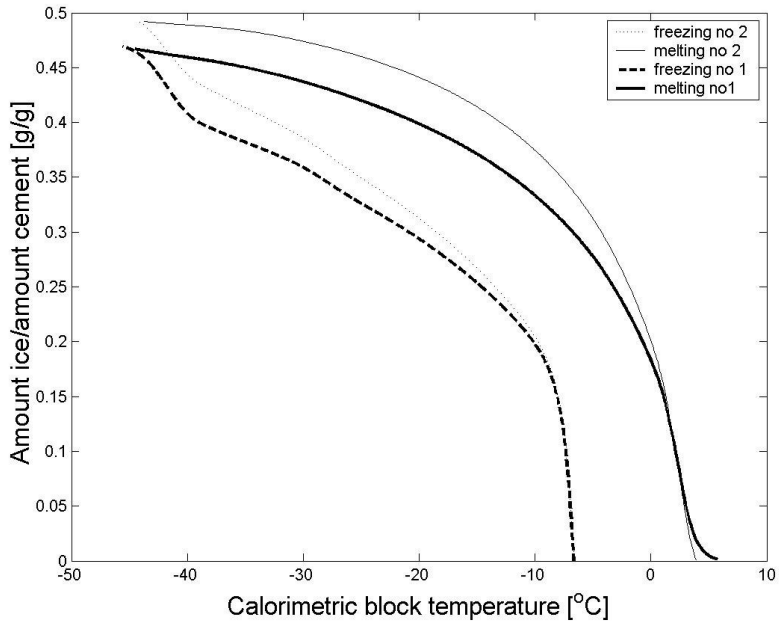

Figure 9.2.6. Result from a calorimetric experiment where the sample was subjected to two consecutive freeze-thaw cycles without leaving the calorimeter.

This means that no other explanation than local supercooling in isolated pores seems to explain the occurrence of the hysteresis between freezing and melting. The large freezing occurring at about -40°C strengthens this explanation.

There are two possibilities for how the formation of ice can continue after the nucleation of ice has occurred. In one of these cases, both ice, that is formed in the coarser pores, and the still unfrozen water being present in the smaller pores, have interfaces to the vapour phase, Case A in Figure 9.2.2. When the temperature decreases, equilibrium between the liquid and the gas phase is maintained by means of a decrease in the size of the liquid meniscus caused by evaporation of water, so that unfrozen water is contained in smaller and smaller pores the lower the temperature. This leads to a reduction of the vapour pressure of the residual pore water. Ice already formed in the larger pores grows because it attracts the unfrozen water held in smaller pores. By this mechanism drainage of the pore system occurs at the same time as the ice-filled part of the pore system increases causing pressure on the ice from the pore walls. Ice growth stops when equilibrium between the water and ice is established.

In the other case considered, an ice-liquid interface is existing, Cases B and C in Figure 9.2.2. Ice-formation continues by heterogeneous freezing of the liquid at the interface. This occurs when the temperature is sufficiently low to permit the formation of stabile ice crystals at the actual meniscus curvature, i.e. at the actual pore radius. This condition is given by Eq. 9.2.5 and Eq. 9.2.7. This type of ice formation can only occur when the water is not locally super-cooled according to the mechanism described above.

Lindmark (1998) performed calculations of changes in the interface energy for each of these two cases, finding that in the second case (presence of an ice-liquid interface) the increase of energy in the system is less. He therefore concluded that a spread of ice into the smaller pores without drainage taking place is probably what occurs. When the pore system also contains neck pores, i.e. pores too small to hold an ice crystal at the actual temperature, these parts of the pore system, may however, be drained. This is very similar to the mechanism described by Everett (1961).

There are three peaks in the ice formation process. The first occurs when the first water is nucleated a few degrees below 0°C. A second peak occurs at about -20°C. If the sample has not been pre-dried and re-saturated before the test, an increase in this second peak can be found. This is believed to be caused by nucleation of locally supercooled water in 'ink-bottle' pores, i.e. pores with too small entrances for seeding from ice in adjacent pores to take place. Transformation does not occur until the pore water at the entrance to these pores is nucleated, see Figure 9.2.5. The peak involved has been found to disappear when a sample has been pre-dried before re-saturation, and also when the w/c-ratio is very low (le Sage de Fontenay and Sellevold, 1980). The influence of pre-drying on the second peak has also been found in the experiments performed in paragraph 9.9.

The effect of drying might be explained by micro-cracking that opens the narrow entrances and because of that make nucleation possible and hinder local super-cooling. For materials with low w/c-ratio the lack of freezing of water at -20°C probably depends on the lack of pores in the actual size-range for freezing although this effect was not found in the studies presented in the paragraphs that follow.

A second increase in ice formation, which occurs at about -40°C, is believed to depend on homogeneous nucleation of all locally supercooled water since liquid water cannot exist below that temperature. This peak has been found to decrease in height with a decrease in the w/c-ratio see paragraphs 9.6- 9.9 and le Sage de Fontenay and Sellevold, (1980) which might depend on less freezable water in these types of concrete.

The melting at D-E (Figure 9.2.1) occurs continuously from about -55°C upwards, although most of it takes place at close to 0°C. Due to temperatures being measured in the calorimetric block rather than in the specimen itself, it may appear as though the melting occurred at temperatures somewhat above 0°C. Since it is a scanning calorimeter, the temperature of the calorimeter block increases with constant rate, while the specimen temperature slows down around 0°C because of heat required for melting the ice.

9.3 Low temperature scanning calorimeter

The calorimeter used in this study was a Setaram BT 2.15. This is a temperature-scanning twin calorimeter with a temperature range of -196°C-+200°C. Cylindrical specimens of maximum diameter 14 mm and maximum length 60 mm could be tested. The rate of temperature change could be varied between 0.6°C/h to 60°C/h and the detection limit of the calorimeter is 2-20 μW. A cross-section of the calorimeter is shown in Figure 9.3.1. The inner part consists of two identical chambers, one active for the sample and one passive for the reference, the signal the calorimeter provides being the difference between signals from the two. The two chambers are enclosed by heat-flow sensors, which are enclosed by the calorimetric block. The block is heated by peripheral resistor windings and the chamber surrounding the entire inner parts is gas-tight. Before a test starts is the air in the gas-tight tank replaced by dry nitrogen gas. The temperature of the calorimeter is controlled with a thermostat, which is located between the block and the resistor coils. To ensure a stabile climate and low temperatures, the calorimeter block is surrounded by liquid nitrogen, which during the measurements flows through a second gas-tight container situated outside the first. The outer part of the calorimeter is a heat insulator consisting of a mineral powder under vacuum.

'Flow mode' of nitrogen was used during the measurements. By flow mode is meant that liquid nitrogen is steadily flowing through the outer part of the calorimeter during the entire test, a nozzle located at the outlet being used to control the rate of flow. The liquid nitrogen was kept in a separate vessel that was connected to the calorimeter during the measurements.

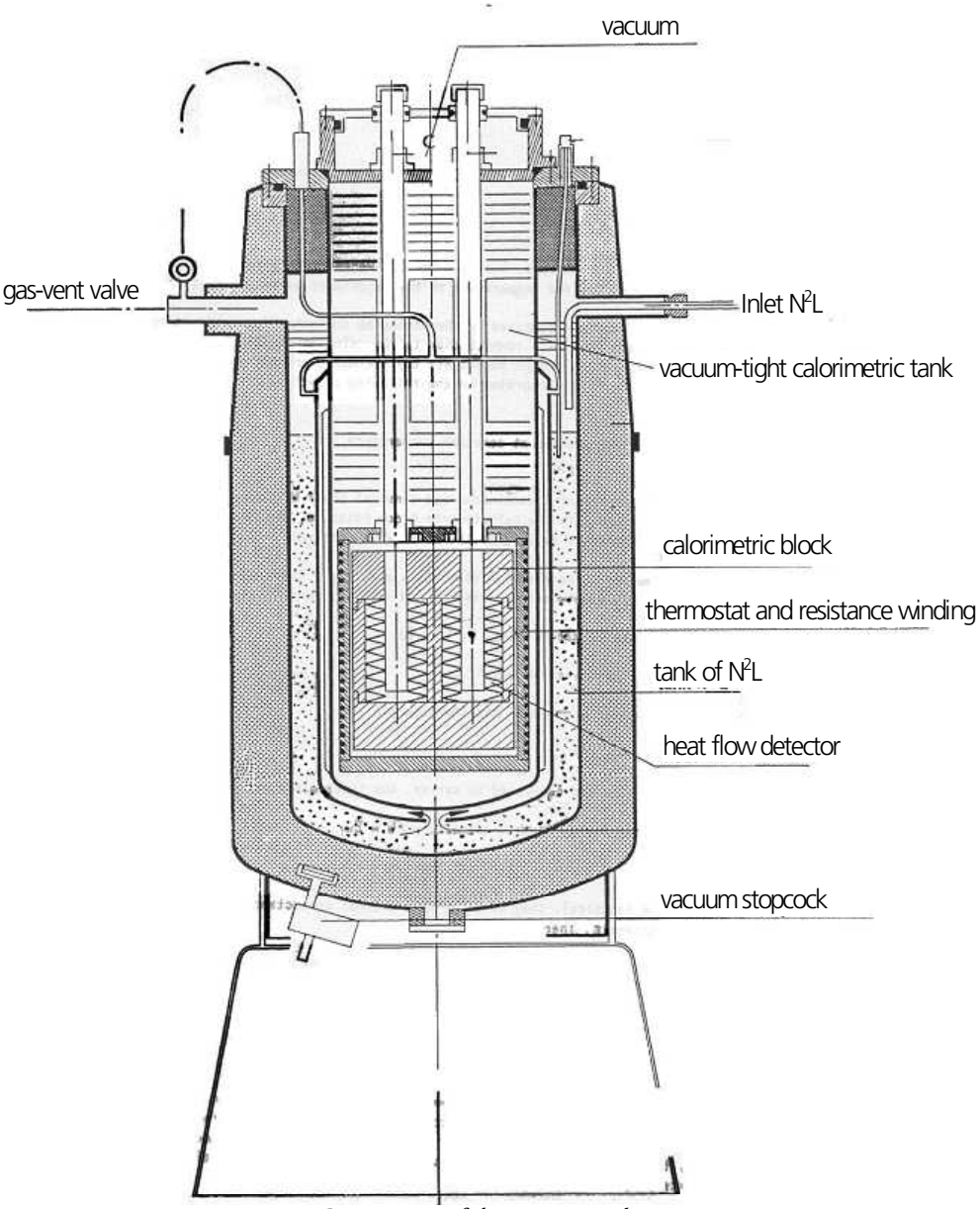

Figure 9.3.1. Cross section of the scanning calorimeter.

9.4 Calculation of ice formation and melting

In calculating the amount of ice formed during an experiment, it is important to determine a baseline (which includes the heat capacity of all the materials involved, such as the sample holder, matrix, water, super-cooled water and ice) where all the excess heat deviating from the baseline is that from ice formation. The most commonly used methods of achieving the baseline and the amount of frozen or melted water, were developed during the 1980s, and were designed for the computers of the time; le Sage de Fontenay and Sellevold, (1980). In that baseline calculation for the freezing curve a line was drawn from B to C (Figure 9.2.1) and the level at -10°C was adjusted (due to the change in heat capacity) according to how much ice that had formed then (calculated with the first line. For the melting curve was a line from D to E used (Figure 9.2.1). With the computers of today it is possible, and less time-consuming, to make more detailed calculations. The procedure described here was developed by the author in cooperation with Dr. Björn Johannesson at our department.

It was the intension to develop a calculation program that was entirely based on known temperature dependency of the heat capacities of all the involved materials (sample holder, matrix, water, supercooled water, ice etc.). This was however difficult so after a while the aim was lowered to result in a program based on graphic solutions, which produced reasonable results. This way of tackling the problem can of course be criticized but the results are reasonable, as is seen below.

The principles of the MATLAB program developed are described briefly in the next paragraphs. The entire computer program, and the data used for the calculations of all measurements discussed below in this chapter, can be found in Fridh and Johannesson (2005).

9.4.1 Calculation of the baseline

When the total heat of a measurement is calculated it should ideally be zero. However, as seen in Figure 9.4.1, this was not the case. This was seen in all measurements and is most probably an effect of an error (offset) in the baseline of the calorimeter of the calorimeter i.e. the heat developed or consumed had no freezing/melting taken place is not zero. The 'baseline-error' will add up to the seen difference in the end (marked by the arrows in the figure). In the measurement shown in Figure 9.4.1 the accumulated error in the total heat was about 10 J at the end of the 24 h measurement. If the accumulated error is independent of temperature, this corresponds to a 10/(24/3600)=115 μW error. This explanation is also consistent with that half of the final error is seen at the lowest temperature, which occurs after half the measurement.

Consideration to the base-line error is taken by the following procedures; see Figure 9.4.1-Figure 9.4.4.

1. In the calculation procedure the 'offset' (Figure 9.4.1) is adjusted so the start and the finish of the measurement coincides. The size of the offset found is portioned out linearly during the entire measurement

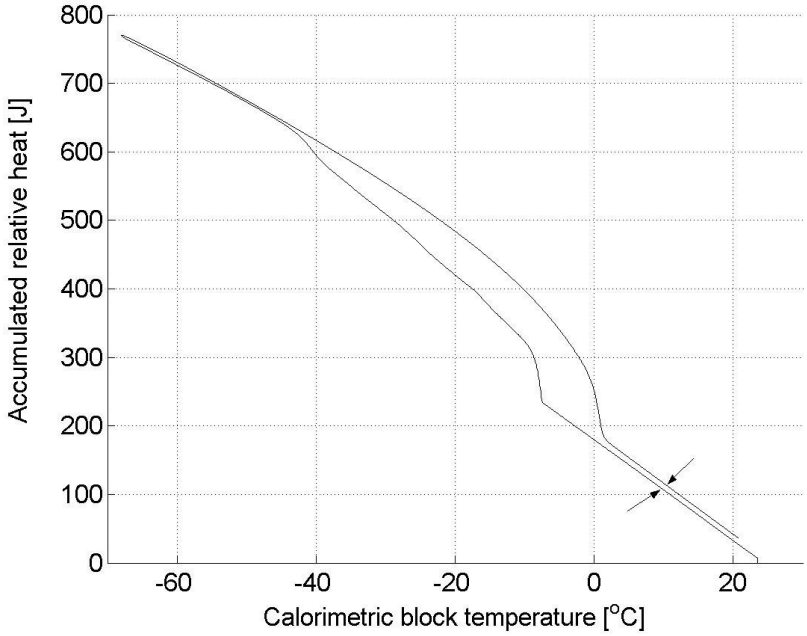

Figure 9.4.1. Total heat during a measurement. The gap between the curves is the accumulated error.

2. The parts of the curve representing a system containing only liquid and matrix (A-B) and only ice, matrix and unfreezable water (C-D), respectively are linearly extrapolated to points + in Figure 9.4.2. These two curves represent the 'extreme' baselines. The slope of the true baselines is somewhere between the slope of these two lines and the solid curves.

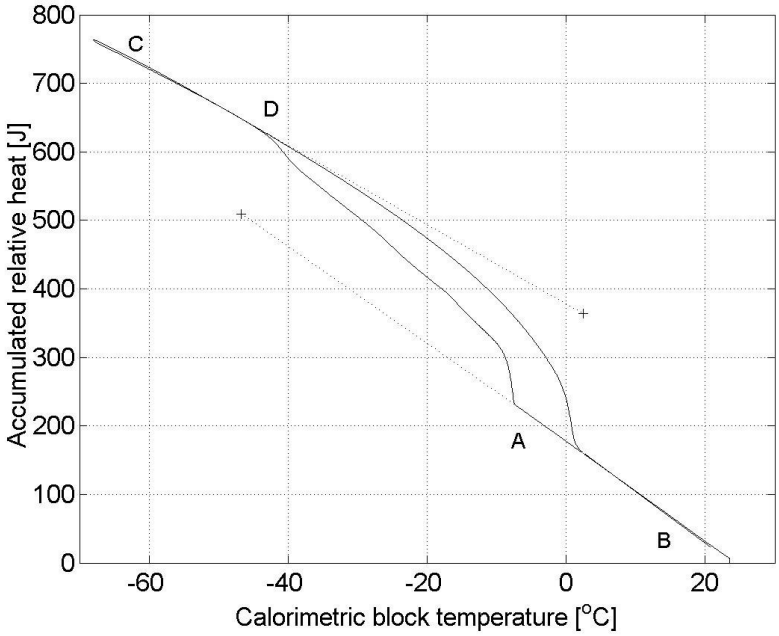

Figure 9.4.2. The two 'extreme' (limiting) baselines are found by extrapolation.

3. The baseline for freezing is the measured heat minus the heat of ice formation. The extrapolated baseline (A-+) is not correct as it assumes a constant heat capacity, which is not true as water and ice have different heat capacities and the heat capacity of the matrix and the instrument parts are not perfectly temperature independent. The same is true for the thawing curve. To generate realistic baselines to use in the evaluation, the mean value of heat production during freezing and heat consumption during melting was used to determine the final position of the baseline for the thawing curve (o) Figure 9.4.3. The final position of the baseline for the freezing curve (*) was determined through calculations using Eq. 9.4.1 until the same amount of ice was formed during freezing as was melted during thawing (Figure 9.4.3).

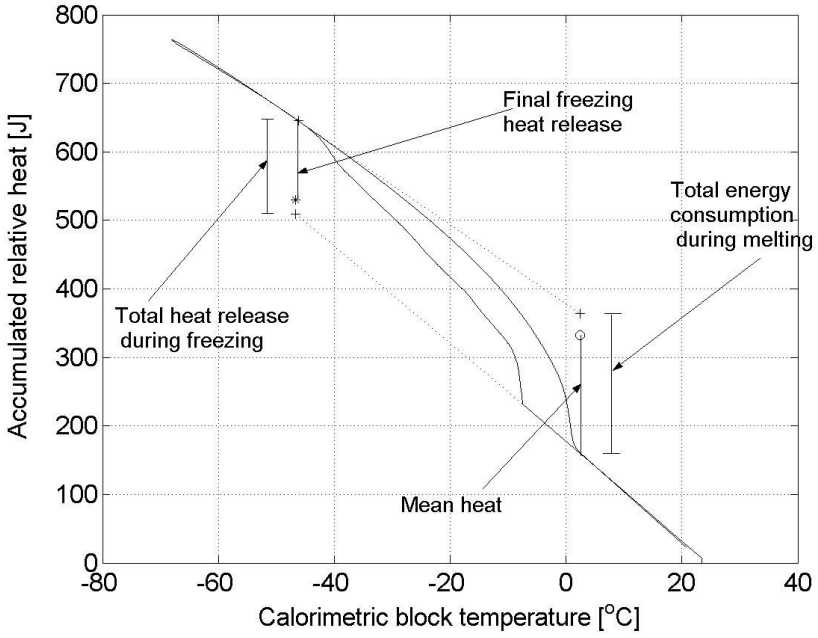

Figure 9.4.3. The final position of the baselines are determined.

4. The baseline is not a straight line as it is influenced by the amount of ice present. At the start of ice formation the baseline for the freezing part of the measurement is close to the extrapolated line for the liquid and matrix system (B-A-+ in Figure 9.4.2). At the end of the ice formation (freezing part) is the baseline close to the extrapolated line through the point *. How close the baseline is to the line B-A-+ at a certain temperature is determined by how much ice that has been formed at a given temperature. The distance between the line B-+ and the measured curve at a temperature in question represents this ice quantity. The final baseline is then calculated by moving the baseline towards the line B-* in relation to how large the distance is between the line B-+ and the measured curve. The same procedure but opposite (moving the baseline towards the line D-o) is done to the baseline for the thawing curve. The result is seen in Figure 9.4.4

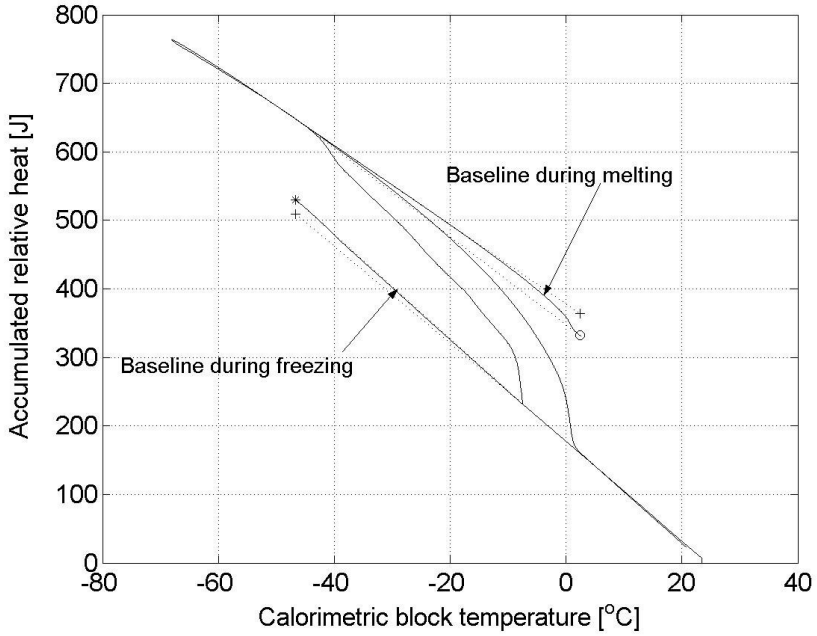

Figure 9.4.4. Calculated baselines (curved, solid) and linearly extrapolated baselines (dotted) for the same experiment as in Figure 9.4.1.

9.4.2 Calculation of the amount of ice formed and melted. Calibration

In calculating the amount of ice formed, the difference between the measured curve and the baseline is divided with the heat of fusion of water ΔH^{fus} [J/g]. le Sage de Fontenay, (1982):

$$\Delta H^{fus}(T) = 334 + 2.2T \qquad \text{Eq. 9.4.1}$$

where T is the temperature in °C. A more thorough analysis of the heat of fusion of water in porous systems is carried out in Brun et al (1977).

The computer programme for ice formation/melting was calibrated by testing a known amount of water (0.348 g) to a cycle with the rate 3.6°C/h, see Figure 9.5.1. The calorimeter curve is shown in Figure 9.4.5. The supercooling is very big.

The calculation of frozen water gave a result of 0.354 g, representing a discrepancy from the true value of less than 2%, see Figure 9.4.6. This was considered to be a degree of accuracy adequate for the investigations of micro-concrete presented below.

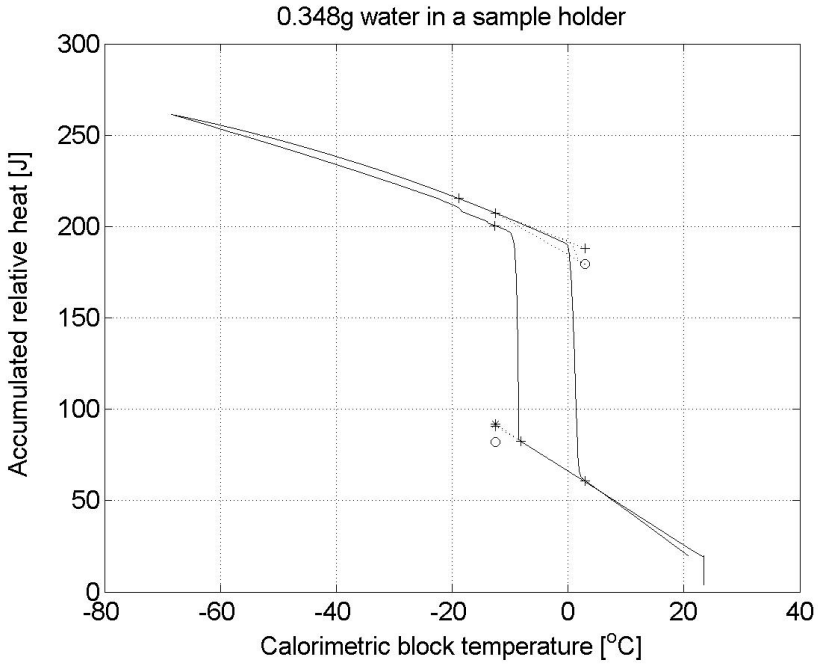

Figure 9.4.5. Calibration test for a sample of 0.348 g pure water.

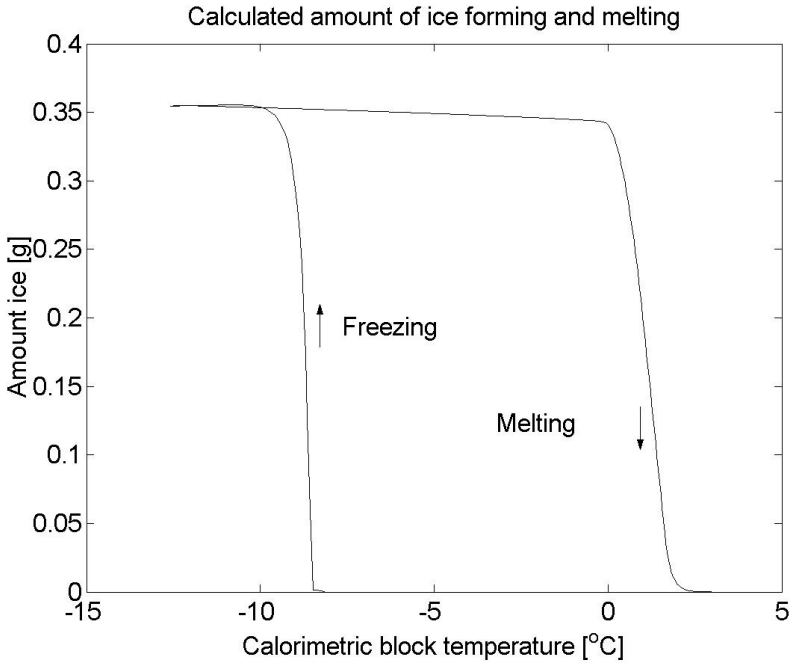

Figure 9.4.6. Calculated amount of ice forming and melting in the experiment shown in Figure 9.4.5.

9.5 Calorimeter experiments – Variables

9.5.1 Concrete types

The following micro-concrete types were tested. The recipes are given in APPENDIX to Chapter 3.

- water-cement ratio 0.60 and 0.40 with natural air content
- water-cement ratio 0.60 and 0.40 with nominal air content 6%

9.5.2 Specimens

The samples had a diameter of 11 mm and a length of 60 mm. They were drilled out of the same blocks as those from which the specimens used in the length change measurements (Chapter 5-8) were sawn; see Chapter 3 for details. They were drilled out perpendicular to the direction of casting so as to avoid any possible influence of any separation within the specimen, the outer 2 cm of the blocks being sawn off before drilling began.

One sample of each concrete type was used in all studies. An overview of all samples and how they were used is given in Table 9.5.1.

9.5.3 Storage between casting and testing

Before being investigated in the calorimeter the specimen had been stored in lime-saturated water or 4,5% NaCl-solution for more than four years. This pre-storage was the same as for the length change measurements in Test series 1, 4, 6 and 8 in Chapter 5-8 regarding length change measurements. Therefore, it is possible to directly compare results from these length change measurements with results of freezing and melting described in this chapter.

9.5.4 Pre-conditioning of the samples

How pre-drying influences the structure of the material and thereby how it influences the frost resistance has been subject to much discussion in previous research on frost resistance. The calorimeter technique is a valuable tool for studying the structure of a material. Therefore, in the study presented here, it was used for investigations of the influence of the same two drying techniques that were used during the length change measurements in Chapter 5-8; (1) drying in room temperature over silica gel, (2) drying at +105°C. In both cases the specimens were re-moistened by capillary absorption. Since it was only the influence of drying that was studied, no vacuum saturation of these samples was made. Thus, comparisons cannot be made with Test series 2 in Chapter 5.

As reference never-dried specimens in their natural moisture state after 4 years of capillary water uptake was investigated.

The pre-conditioning of the different samples were thus as follows:

Pre-conditioning Type 1, Samples Nr 1-4:
Natural moisture condition as it was when water storage was interrupted after 4 years. This pre-treatment corresponds to Test series 1, 4, 6 treated in Chapter 5-7. The different samples were tested with different temperature cycles as described in Figure 9.5.1.

Pre-conditioning Type 2, Sample Nr 1:
After the first calorimeter test, Sample 1 was pre-dried over silica gel at room temperature and re-saturated by capillary suction, aiming for the same weight as during the first test. The sample was tested again with the same temperature cycle as before.

Pre-conditioning Type 3, Sample Nr 1:
After the second calorimeter test, Sample 1 was pre-dried at +105°C and re-saturated by capillary suction, again aiming for the same weight as during the two earlier tests. The sample was tested again with the same temperature cycle as before.

The pre-conditioning procedures meant that one specimen (Sample 1) was investigated three times after different drying treatments but with as similar moisture contents as possible.

Despite the fact that large ice formation was seen in some of the samples, and that the length change measurement had shown large expansion in some of these materials pre-conditioned in the same way, re-use of Samples 1 was made. The aim was to study the change in ice-formation due to different drying techniques. The results obtained in the calorimeter are therefore the result of a combination of the influence of the drying method, and the effect of a repeated test with a specimen that might have obtained some damage during the preceding test.

The other three specimens (Nr. 2-4) were tested only once with their natural water content. After the final test all samples Nr. 1-4 were dried at +105°C and thereafter vacuum saturated. The weight in air and water was determined which made it possible to calculate the real moisture content during the test and the degree of saturation at the test. These values are given in Table 9.5.1.

Pre-conditioning of specimens stored in 4.5 % NaCl-solution:
The specimens were tested at the natural moisture condition they had when salt-water storage was interrupted after 4.5 years. This pre-treatment corresponds to Test series 8 in Chapter 8. Four samples were tested with different temperature cycles see Figure 9.5.1.

After the test all specimens were dried at +105°C, re-saturated by vacuum and weighed in water and in air in order to determine the degree of saturation during the test. The results of the salt water tests are shown in paragraph 9.13.

9.5.5 Temperature cycles

The aim was to investigate effects of the same type of variation as was used for the dilatometer test in Chapter 5-8.

Variations in the temperature cycles were:

Temperature cycle 1 and 2:

Different constant freezing-and-thawing rate down to 70°C.

- *cycle 1:* Rate 3.6°C/h.
- *cycle 2:* Rate 7.8°C/h.

Temperature cycles 3 and 4:

The temperature held constant during a certain time at –15°C and –30°C. Freezing-and-thawing rate between stops in temperature lowering is 3.6°C/h.

- *cycle 3:* 3 hours at -15°C and -30°C.
- *cycle 4:* 5 hours at -15°C and 12 hours at –30°C.

The different temperature regimes are shown in Figure 9.5.1.

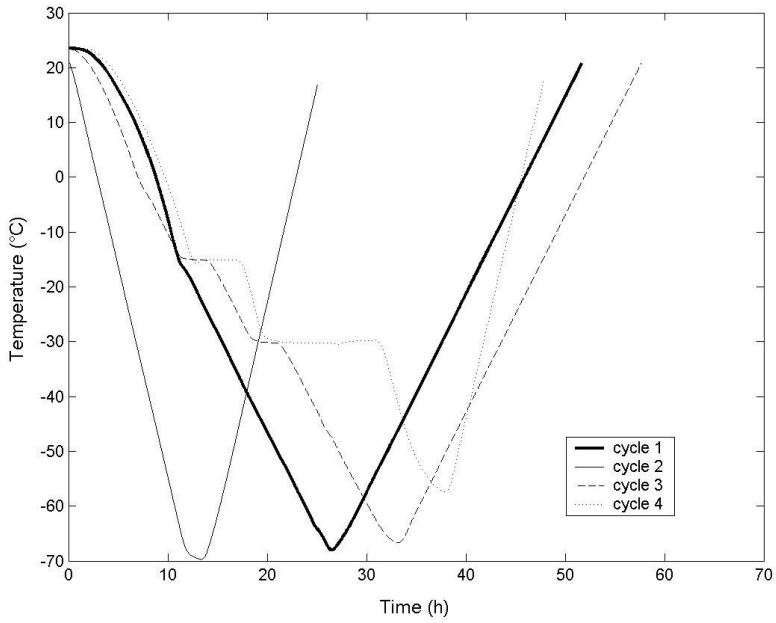

Figure 9.5.1. Temperature cycles used in the calorimetric studies.

9.5.6 Overview over the experiments

An overview of all calorimeter tests with specimens stored in water is given in Table 9.5.1. Properties of the specimens for each individual experiment are listed. This makes it possible to calculate the amount of non-freezable water, and to relate freezable water and non-freezable water to the cement content, or to a fraction of the total water content.

Table 9.5.1. Overview of all calorimeter experiments with specimens stored 4 years in water between casting and the first testing. Specimen No1 was tested three times. The other three specimens were tested one time each. The cement content, c, the total pore volume, V_p, the specimen volume, V, the total amount of evaporable water in the specimen, w_e, and the degree of saturation, S, at the test are given in the table.

Pre-conditioning	Cycle	Concrete type			
		0.60 natural air	0.60 6% air	0.40 natural air	0.40 6% air
		Sample No			
Type 1	Cycle 1	No 1	No 1	No 1	No 1
Natural water	3.6°C/h,	c= 2.02 g	c= 1.90 g	c= 2.98 g	c= 2.93 g
content after 4	-70°C	V_p= 1.15 cm^3	V_p= 1.20 cm^3	V_p= 1.19 cm^3	V_p= 1.12 cm^3
years of water		V= 5.77 cm^3	V= 5.44 cm^3	V= 5.68 cm^3	V= 5.59 cm^3
storage		w_e= 1.14 g	w_e= 1.11 g	w_e= 1.05 g	w_e= 1.12 g
		S= 0.956	S= 0.924	S= 0.882	S= 1
	Cycle 2	No 2	No 2	No 2	No 2
	7.8°C/h,	C= 1.92 g	c= 1.97 g	c= 2.88 g	c= 2.90 g
	-70°C	V_p= 0.96 cm^3	V_p= 1.16 cm^3	V_p= 0.88 cm^3	V_p= 1.07 cm^3
		V= 5.5 cm^3	V= 5.63 cm^3	V= 5.68 cm^3	V= 5.53 cm^3
		w_e= 0.98 g	w_e= 1.12 g	w_e= 0.88 g	w_e= 1.03 g
		S= 1	S= 0.962	S= 1	S= 0.963
	Cycle 3	No 3	No 3	No 3	No 3
	3.6°C/h,	C= 1.66 g	c= 1.92 g	c= 2.86 g	c= 3.00 g
	3h stop	V_p= 0.90 cm^3	V_p= 1.21 cm^3	V_p= 0.88 cm^3	V_p= 1.12 cm^3
		V= 4.7 cm^3	V= 5.48 cm^3	V= 5.74 cm^3	V= 5.71 cm^3
		w_e= 0.90 g	w_e= 1.21 g	w_e= 0.88 g	w_e= 1.12 g
		S= 1	S= 1	S= 1	S= 1

Pre-conditioning	Cycle	Concrete type			
		0.60 natural air	0.60 6% air	0.40 natural air	0.40 6% air
		Sample No			
	Cycle 4	No 4	No 4	No 4	No 4
	3.6°C/h,	C= 2.00 g	w_e= 1.14 g	c= 2.91 g	c= 2.97 g
	12h stop	V_p= 0.97 cm^3		V_p= 0.90 cm^3	V_p= 1.10 cm^3
		V= 5.7 cm^3		V= 5.54 cm^3	V= 5.65 cm^3
		w_e= 0.94 g		w_e= 0.90 g	w_e= 1.09 g
		S= 0.97		S= 1	S= 0.992
Type 2	Cycle 1	No 1	No 1	No 1	No 1
Silica gel + capil-	3.6°C/h,	c= 2.02 g	c= 1.90 g	c= 2.98 g	c= 2.93 g
lary suction	-70°C	V_p= 1.19 cm^3	V_p= 1.20 cm^3	V_p= 1.19 cm^3	V_p= 1.12 cm^3
		V= 5.77 cm^3	V= 5.44 cm^3	V= 5.68 cm^3	V= 5.59 cm^3
		w_e= 1.06 g	w_e= 1.02 g	w= 0.97 g	w_e= 0.98 g
		S= 0.89	S= 0.845	S= 0.809	S= 0.880
Type 3	Cycle 1	No 1	No 1	No 1	No 1
+105°C + capil-	3.6°C/h,	c= 2.02 g	c= 1.90 g	c= 2.98 g	c= 2.93 g
lary suction	-70°C	V_p= 1.19 cm^3	V_p= 1.20 cm^3	V_p= 1.19 cm^3	V_p= 1.12 cm^3
		V= 5.77 cm^3	V= 5.44 cm^3	V= 5.68 cm^3	V= 5.59 cm^3
		w_e= 1.08 g	w_e= 1.03 g	w_e= 1.07 g	w_e= 1.07 g
		S= 0.908	S= 0.856	S= 0.898	S= 0.956

9.6 Influence of the cooling/warming rate on ice formation and melting

9.6.1 Introduction

The aim of this investigation was to see if the rate of temperature change influences the amount of ice present at different temperatures. It is known that the amount of supercooling of bulk water tends to increase with increasing freezing rate. Thus, if this is the case also for pore water, one might expect more ice to be formed at a given temperature the lower the rate of temperature lowering. On the other hand the amount of ice present at heating ought to be uninfluenced by the heating rate.

Two different rates of temperature change were investigated; 3.6°C/h and 7.8°C/h (Temperature cycle 1 and 2). The real temperature obtained in the calorimeter block is shown in Figure 9.5.1. The samples used had the natural water content reached after 4 years of water storage. One sample of each concrete type was used for each temperature cycle.

9.6.2 Results for w/c-ratio 0.60

Frozen water as function of temperature is shown in the Figure 9.6.1 and Figure 9.6.2, each curve representing a single specimen. In these figures, the amount of frozen water is related to the cement content. By use of data from Table 9.5.1 the amount of frozen water as fraction of total water content can be calculated. These data can also be used for calculating the amount of non-freezable water.

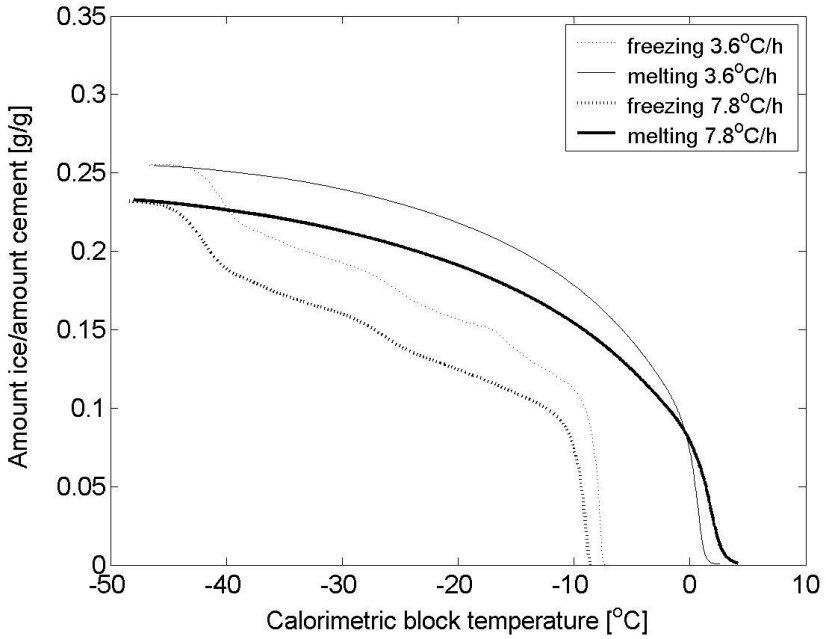

Figure 9.6.1. Effect of the cooling/heating rate on the amount of frozen and melted water for a w/c-ratio of 0.60 and a natural air content.

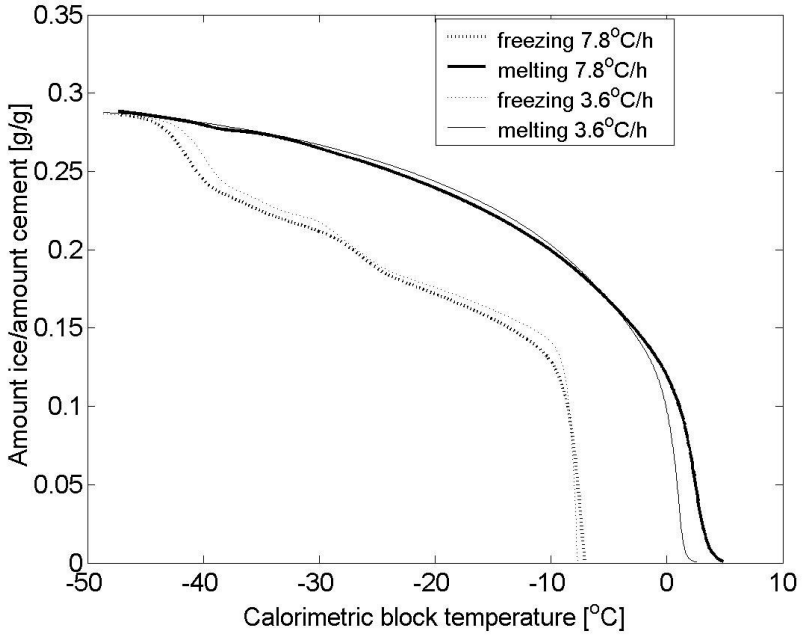

Figure 9.6.2. Effect of the cooling/heating rate on the amount of frozen and melted water for a w/c-ratio 0.60 and a 6% air content.

Non-air-entrained samples

Ice formation was nucleated at about -8 à –9°C. The supercooling was about 1 degree bigger for the more rapid cooling. Very big amount of water is frozen directly when supercooled water is nucleated; almost 45% of the total amount of water frozen at -45°C. For the samples without air-entrainment, the largest amount of ice was formed in the sample exposed to the 'normal' cycle, which was expected since the actual sample contained almost 9% more evaporable water. This corresponds almost exactly to the 'extra' ice formation. Almost all of the difference in ice formation between the two samples is found when supercooling is overcome. The formation of ice thereafter is very similar, the two 'peaks' at approximately -25°C and -40°C included. A third weak peak (at about -16°C) can be seen in the 3.6°C/h specimen. Figure 9.5.1 shows that there was a certain increase in the rate of cooling at that temperature which could be the reason for the small increase in freezing.

The melting curve is continuous without 'jumps'. Most of the melting takes place close to 0°C. The delayed melting in the sample exposed to the rapid cycle is presumably caused by the greater temperature lag between the sample and the calorimetric block.

Air-entrained samples

In the samples containing entrained air, ice starts to form at approximately the same temperature as for the non-air-entrained samples (-8°C), and the largest supercooling were found for the 'rapid' cycle. As for the non-air-entrained concrete, about 50% of all freezable water froze in conjunction with nucleation of supercooled water. The shapes of the two freezing curves are very similar, which can be explained by the fact that the amount of evaporable water was the same (1.11 g and 1.12 g, respectively). The shape of the ice formation curve is almost the same as for the non-air-entrained concrete, with increased ice formation at about -25°C and -40°C. Melting is gradual at both warming rates, a delay occurring in the sample subjected to the 'rapid' cycle. More ice is formed in the sample containing air entrainment than in samples without air, this being due to the higher water content of the former. Since the length change measurements (Chapter 5-8) indicate contraction to have occurred in samples with air entrainment, it appears likely that the ice is largely formed in the air pores, although it cannot be totally ruled out that some ice was formed on the surface of the specimen or in the sample holder.

9.6.3 Results for w/c-ratio 0.40

The results are shown in the Figure 9.6.3-Figure 9.6.4, each curve representing a single specimen. In these figures, the amount of frozen water is related to the cement content. By use of data from Table 9.5.1 the amount of frozen water as fraction of total water content can be calculated. These data can also be used for calculating the amount of non-freezable water.

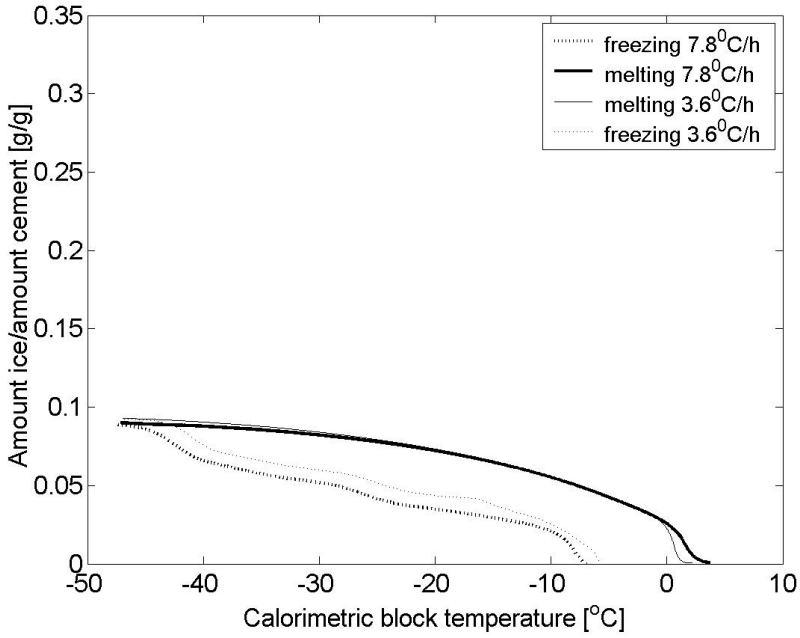

Figure 9.6.3. Effect of the cooling/heating rate on the amount of frozen and melted water for a w/c-ratio of 0.40 and a natural air content.

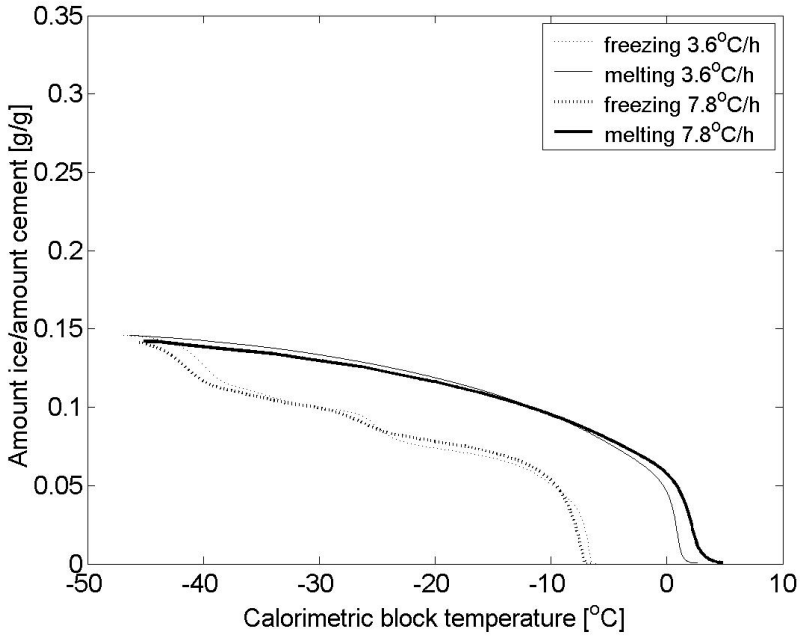

Figure 9.6.4. Effect of the cooling/heating rate on the amount of frozen and melted water for a w/c-ratio 0.40 and a 6% air content.

Non-air-entrained concrete

Water is supercooled to about -6 à –8°C, most for the rapid cooling. The fraction of water freezing at nucleation of super-cooled water is about 20%, which is considerably smaller than for w/c-ratio 0.60. The shape of the freezing curves are virtually the same, with two weak peaks at -25°C and -40°C. The sample subjected to the 'normal' cycle forms somewhat greater amount of ice at higher temperature and less at -40°C. The total amount of ice formed being almost identical. The content of evaporable water was 1.05 g and 0.88 g, respectively. The similarity of the freezing curves is difficult o explain when difference in evaporable water is so big. Possibly, there is an error made at the determination of evaporable water.

The melting curves are identical for the two warming rates.

Air-entrained concrete

Supercooling was the same for both specimens, and so was the amount of ice formed at nucleation of supercooled water. The freezing and the melting curves are almost identical for both temperature rates. The evaporable water content was 1.12 g for the sample subjected to the 'normal' cycle and 1.03 g in the sample subjected to the 'rapid'. More ice was found to form in the material with air entrainment (40% more) which depends on the bigger water content in these specimens. The amount of non-freezable water was about the same for air-entrained and non-air-entrained concrete, see Figure 9.11.4.

9.6.4 Comparison between w/c-ratio 0.60 and 0.40

- The amount (g/gcem) of freezable water was 2-2.5 times as great for w/c-ratio 0.60 as for w/c-ratio 0.40.
- For both w/c-ratios a considerable amount of ice was formed at about –40°C, which is the temperature at which homogeneous nucleation of water occurs.
- For both w/c-ratios, ice formed over the entire interval from nucleation of supercooled water to -40°C.
- For both w/c-ratios a big fraction of all freezable water froze when supercooled water was nucleated at between -6C and -9°C. This means that the same big fraction of freezable water has freezing points between these temperatures.
- For both w/c-ratios there is big hysteresis between freezing and melting.
- For both w/c-ratios ice starts to melt already at low temperature, but most melting occurs in the interval -5°C to 0°C.
- For both w/c-ratios the effect of freezing rate on freezing and melting is none, or very small. However, supercooling tends to increase with increasing freezing rate.

9.6.5 Conclusions concerning the influence of freezing rate

The influence of the freezing rate on ice formation and melting at any given temperature was found to be very small if any.

More ice was generally found to be formed in material with air-entrainment than in non-air-entrained concrete, which depends on that these concretes contained more water. This additional water was held in the air pores, and it has a freezing point of about 0°C.

The fact that ice-melting starts already at very low temperature can explain why internal stresses formed by expansion that has occurred during freezing to low temperature, relaxes directly as soon as warming starts; e.g. see Test series 1 or 4 in paragraphs 5.3.3 and 6.3.2.

The fact that the freezing rate has no effect on the ice formation process could be one reason why no effect of freezing rate on length changes could be found in the tests in Chapter 5.

9.7 Investigations of the effect of 3 hour halts at temperature -15°C and -30°C

9.7.1 Introduction

The aim of this investigation was to determine whether any sign of ice formation could be detected when the temperature was held constant, and also if any differences in ice formation between various temperature levels at which temperature was kept constant could be seen. The temperature cycle was therefore altered so as to include two isothermal periods, each three hours long, at -15°C and -30°C (cycle 3). The temperature cycle employed is shown in Figure 9.5.1.

The samples used are described in Table 9.5.1. They had the natural water content reached after 4 years of water storage. One sample of each concrete type was used.

9.7.2 Results

The results are shown in Figure 9.7.1-Figure 9.7.4. Only the cooling part of the test is shown since the aim of the test was to show how freezing proceeds. The melting part showed the same big hysteresis as shown in the diagrams in paragraph 9.6.

As before, the amount ice is related to the cement content in the specimen. Data in Table 9.5.1can be used for re-calculating the data to amount of ice as fraction of total evaporable water or for calculating non-freezable water.

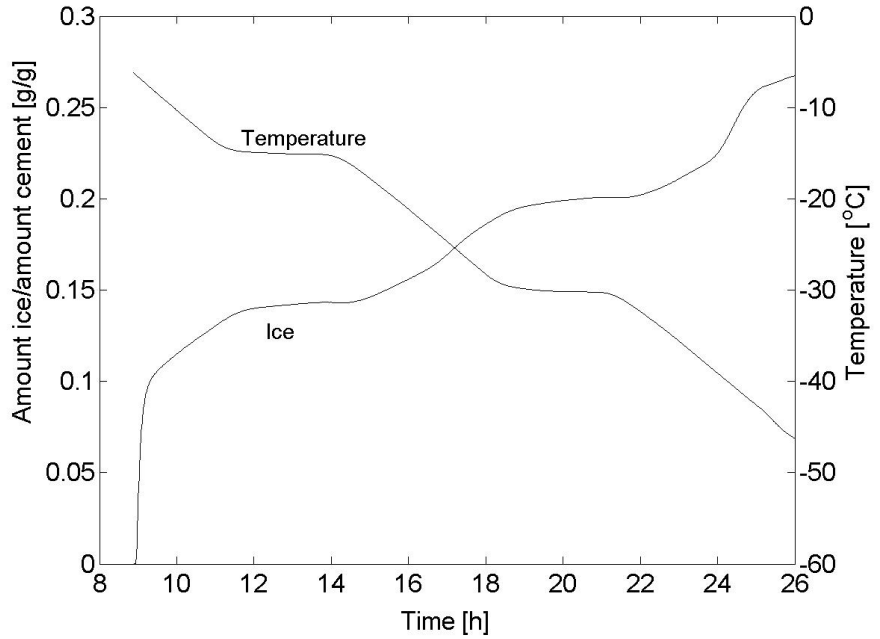

Figure 9.7.1. Amount of frozen water as function of time and temperature. Temperature held constant for 3 hours at –15°C and –30°C. Concrete with w/c-ratio 0.60 and natural air content.

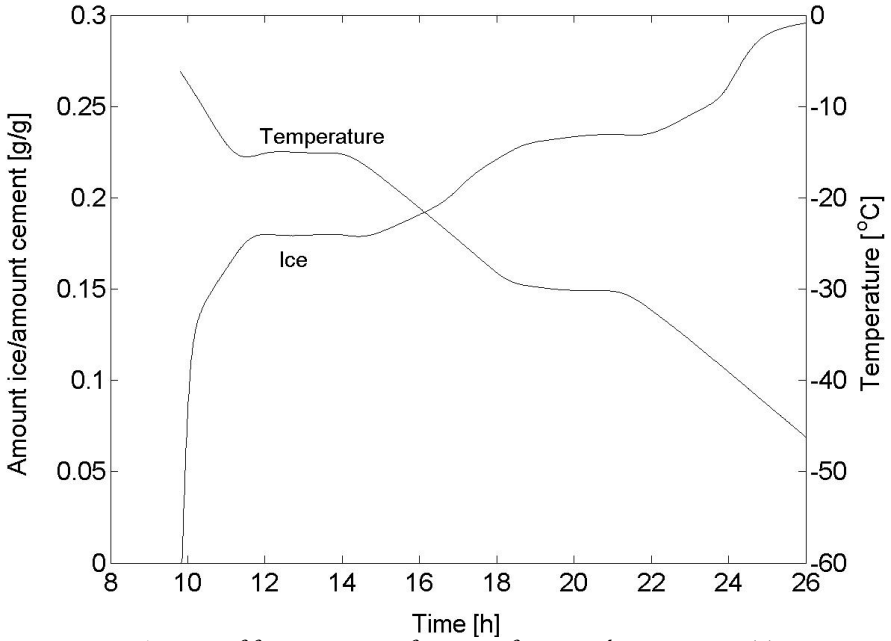

Figure 9.7.2. Amount of frozen water as function of time and temperature. Temperature held constant for 3 hours at –15°C and –30°C. Concrete with w/c-ratio 0.60 and 6% air.

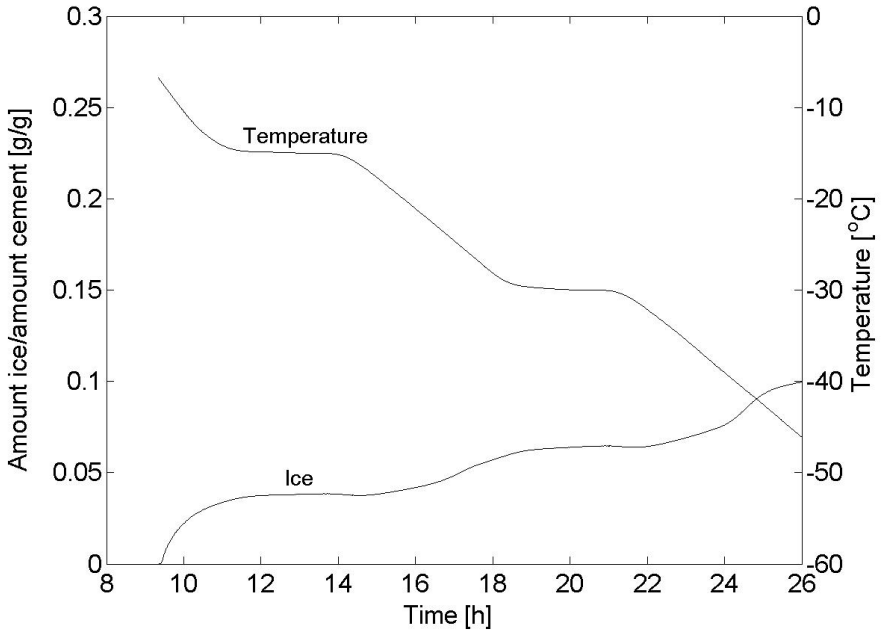

Figure 9.7.3. Amount of frozen water as function of time and temperature. Temperature held constant for 3 hours at –15°C and –30°C. Concrete with w/c-ratio 0.40 and natural air content.

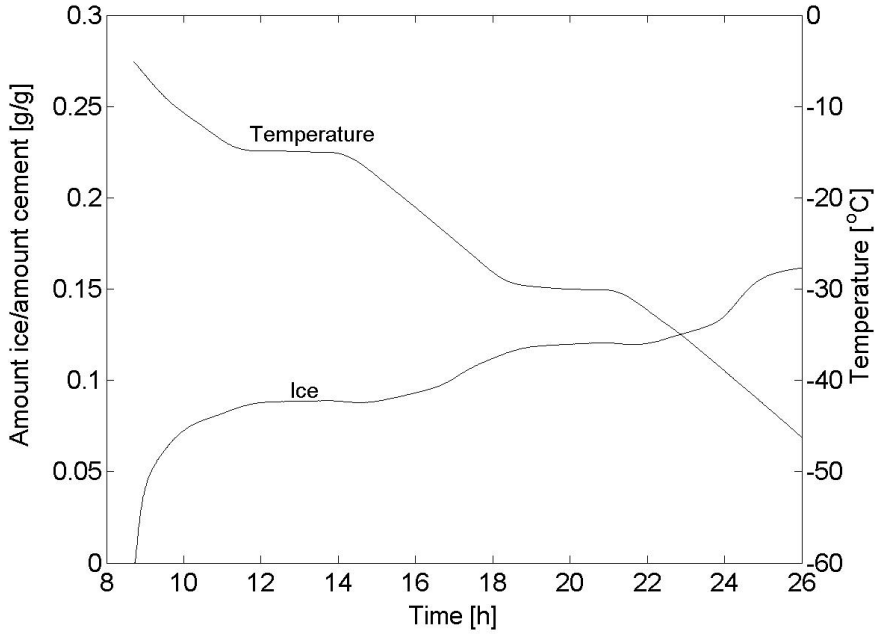

Figure 9.7.4. Amount of frozen water as function of time and temperature. Temperature held constant for 3 hours at –15°C and –30°C. Concrete with w/c-ratio 0.40 and 6% air.

As soon as cooling makes a halt at -15°C or -15°C no appreciable sign of ice formation could be observed in any of the specimens. The very small formation of ice that did occur was apparently due to the temperature not being completely constant. As soon as cooling resumes after the halts new ice starts to form.

The tendencies found in the previous study that more ice is forming, the higher the w/c-ratio and the higher the air content, were also found in this study. Again it can be explained by higher water content in such samples; see Table 9.5.1.

In all specimens a substantial amount of ice is formed at about -40°C.

9.7.3 Effect of 3 hours halts in cooling. Conclusions

There are no indications of ice forming during the period of constant temperature, regardless of the temperature level. This can explain why almost no length changes were observed during the constant temperature periods in Test series 4, see paragraph 6.3.

Since no ice formation is found during constant temperature, ice lens growth cannot have taken place. Therefore, the observations of continuous expansion during isothermal conditions found by Powers and Helmuth (1953), see Figure 2.4.3b, and their explanation for that, microscopic ice lens growth, has not been confirmed. The way Powers and Helmuth made their experiments are not clear from their report. Evidently they were not performed in the same manner as the tests in this work, namely using moisture sealed samples.

9.8 Investigations of the effect of 12h long halts at temperature –15°C and –30°C

9.8.1 Introduction

It has been claimed that the process of micro-ice lens-growth is slow but that if it is allowed to continue for a sufficient period of time it might produce a significant ice formation and strain in the material. This effect could however not be verified in the length change tests performed in Chapter 7.

To further investigate the effect of long duration of constant temperature, but in this case directly on ice formation, calorimeter tests involving an increased duration of a halt in the temperature lowering process were performed. The halts were made at the same temperature levels as were used in the test described in paragraph 9.7; i.e.-15°C and –30°C.

The results from this study could be directly compared with the results from the study in paragraph 9.7.

The maximum possible duration of a calorimeter measurement is determined by the amount of liquid nitrogen available. In the actual experiments a vessel of 100 litres was used. This meant that it was only possible to have one single twelve-hour halt for which the temperature of -30°C was chosen. For the halt at -15°C, a period of approximately five hours was selected. The temperature cycle is shown in Figure 9.5.1 (cycle 4).

The samples used are described in Table 9.5.1. They had the natural water content reached after 4 years of water storage. One sample of each concrete type was used.

9.8.2 Results

The results are shown in Figure 9.8.1-Figure 9.8.4. The amount ice is related to the cement content in the specimen. Data in Table 9.5.1 can be used for re-calculating the data to amount of ice as fraction of total evaporable water or for calculating non-freezable water.

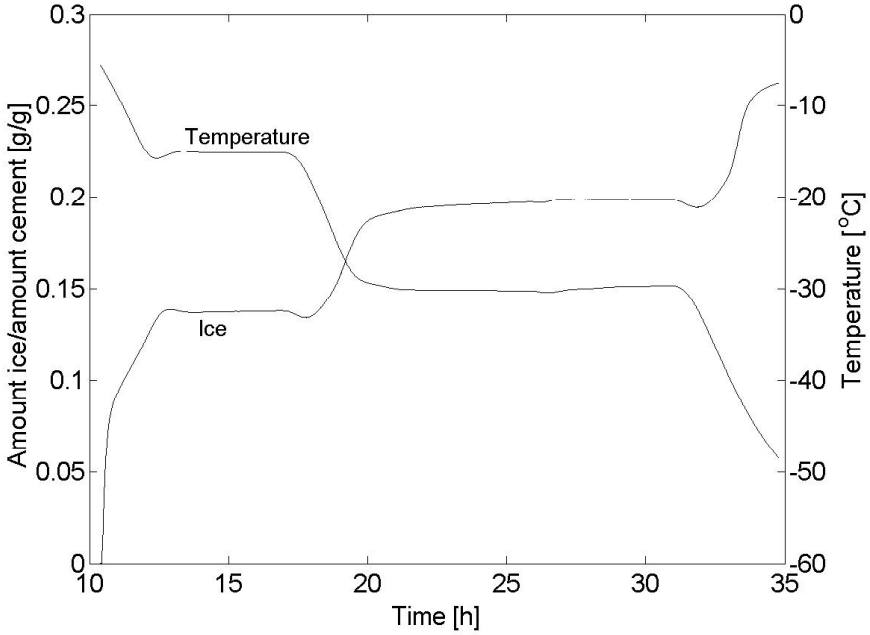

Figure 9.8.1. Amount of frozen water as function of time and temperature. Temperature held constant for 5 hours at –15°C and 12 hours at –30°C. Concrete with w/c-ratio 0.60 and natural air.

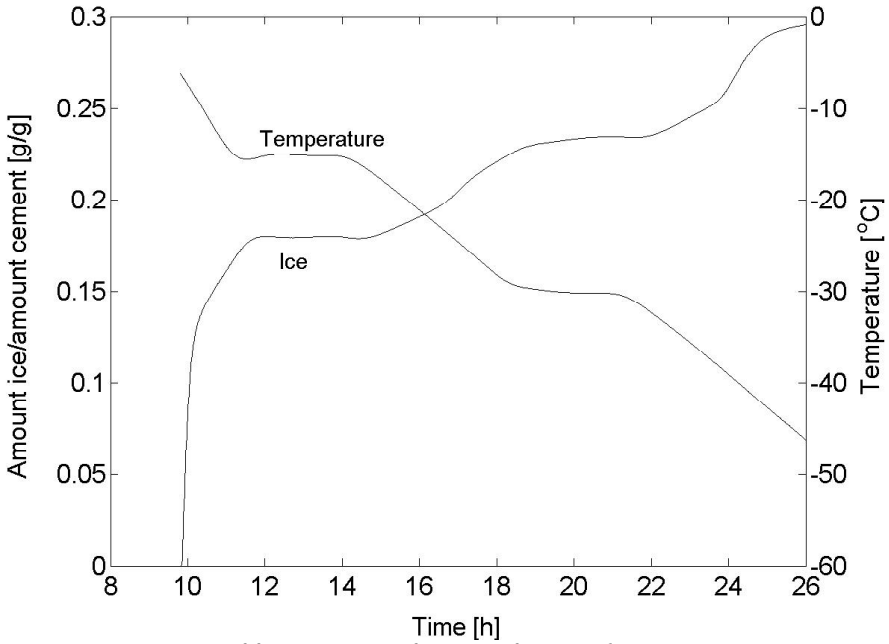

Figure 9.8.2. Amount of frozen water as function of time and temperature. Temperature held constant for 5 hours at –15°C and 12 hours at –30°C. Concrete with w/c-ratio 0.60 and 6% air.

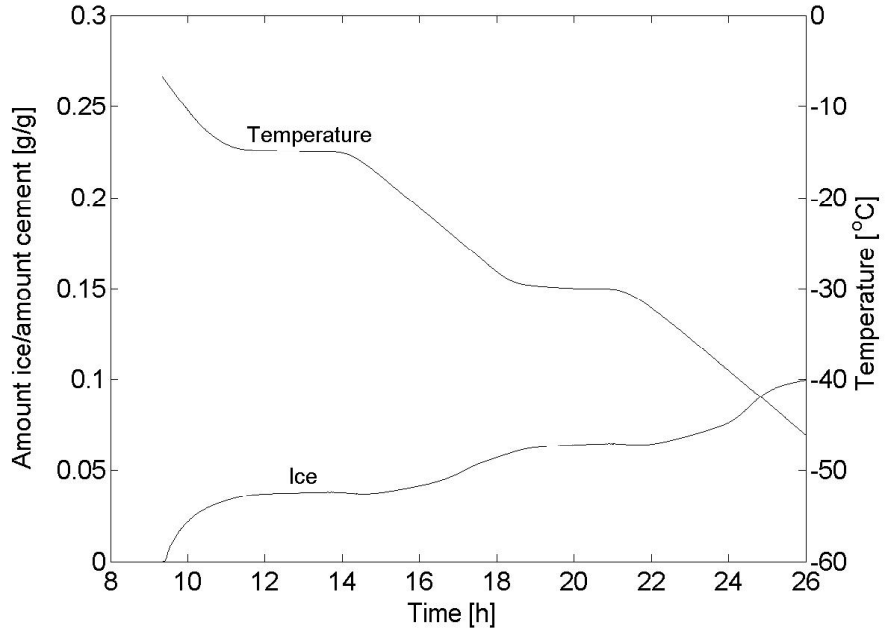

Figure 9.8.3. Amount of frozen water as function of time and temperature. Temperature held constant for 5 hours at –15°C and 12 hours at –30°C. Concrete with w/c-ratio 0.40 and natural air.

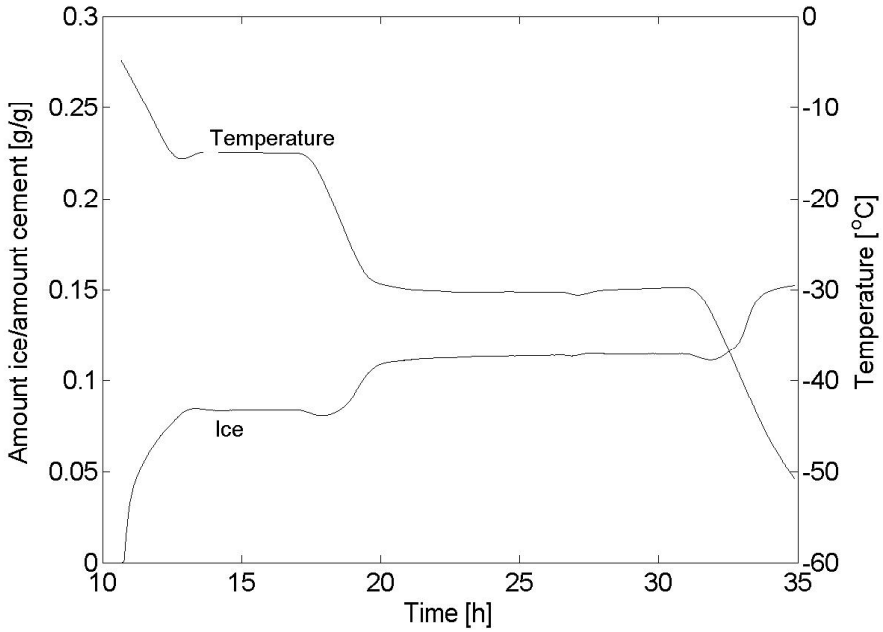

Figure 9.8.4. Amount of frozen water as function of time and temperature. Temperature held constant for 5 hours at –15°C and 12 hours at –30°C. Concrete with w/c-ratio 0.40 and 6% air.

Even when the duration of constant temperature was increased to as much as twelve hours, there were still no signs of ice formation, which would have been the case if transfer of water to ice in capillaries predicted by the ice lens growth mechanism had taken place. When cooling was resumed new ice formation started. Very big ice formation occurred at about -40°C. More ice was found to form in material with entrained air and in material with higher w/c-ratio, which is consistent with the other measurements.

Note: There is a short period directly after termination of the period of constant temperature, during which some ice seems so melt. This occurs for all specimens, but could not be seen in the tests in paragraph 9.7. The observation is difficult to explain. It must depend on heat flow from the calorimeter block to the specimen, while heat flow in the other direction is to be expected during cooling. The reason is possibly heat inertia of the calorimeter cells leading to a bigger than normal temperature difference between the block and the specimen for some time. If this is the reason, the effect is fictitious and an effect of a temporary change of the base line. Such a change is not considered at the calculation of ice.

9.8.3 Effect of long temperature halts. Conclusions

Extending the duration of constant temperature from 3 hours to 5 or 12 hours did not affect the observations made in the test in paragraph 9.7, namely that all ice formation stops when temperature is held constant.

9.9 Investigations of the effect of drying

9.9.1 Introduction

It has been found by many researchers that a pre-drying of concrete, before re-saturation is made, significantly increases the amount of water that is freezable at 'normal' freezing temperatures; e.g. Vuorinen (1973), Sellevold et al. (1982), Bager and Sellevold (1986b). Some tests of the drying effect were also performed in the present study. The primary aim was to compare how the two drying techniques employed during Test series 2, 3, 5 and 7 (length change measurements) affected the freezing and melting of pore water. The drying and re-saturation were as follows:

- Drying at +20°C in a closed box containing silica gel and carbon dioxide for a month followed by immersion in water for a period of 7-20 days until they either regained the water content they had lost during drying or until the absorption rate had become negligible.
- Drying at +105°C for 7 days followed by followed by immersion in water for a period of a month until they either regained the water content they had lost during drying or until the absorption rate had become negligible.

The water contents obtained in the specimens are given in Table 9.5.1.

9.9.2 Results

The results are shown in Figure 9.9.1-Figure 9.9.4. The amount of ice is related to the cement content in the specimen. Data in Table 9.5.1 can be used for re-calculating the data to amount of ice as fraction of total evaporable water or for calculating non-freezable water.

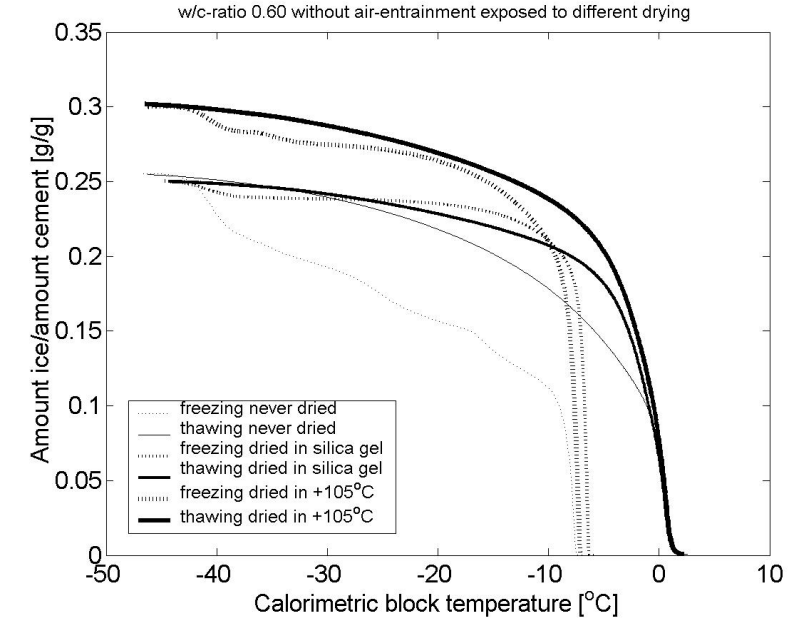

Figure 9.9.1. Amount of frozen water as function of temperature. Different drying procedures prior to re-saturation and testing. Concrete with w/c-ratio 0.60 and natural air.

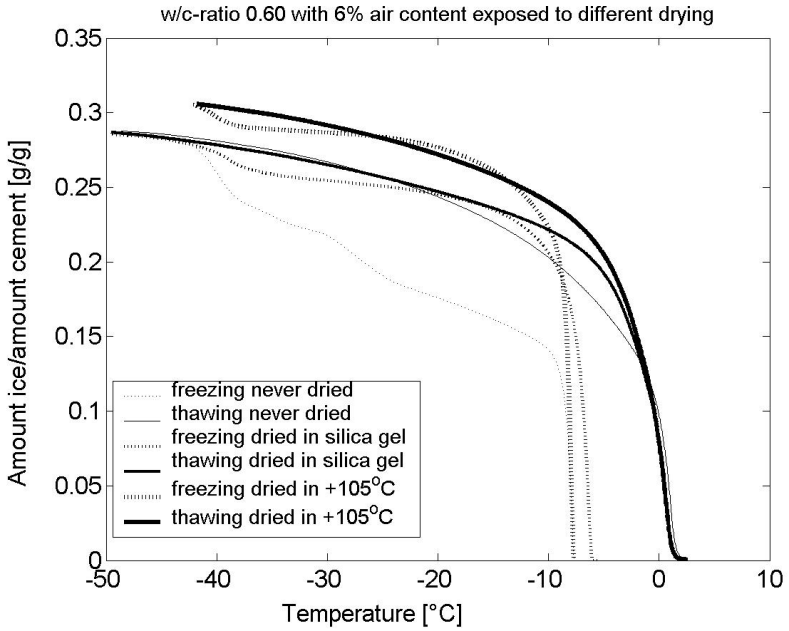

Figure 9.9.2. Amount of frozen water as function of temperature. Different drying procedures prior to re-saturation and testing. Concrete with w/c-ratio 0.60 and 6% air.

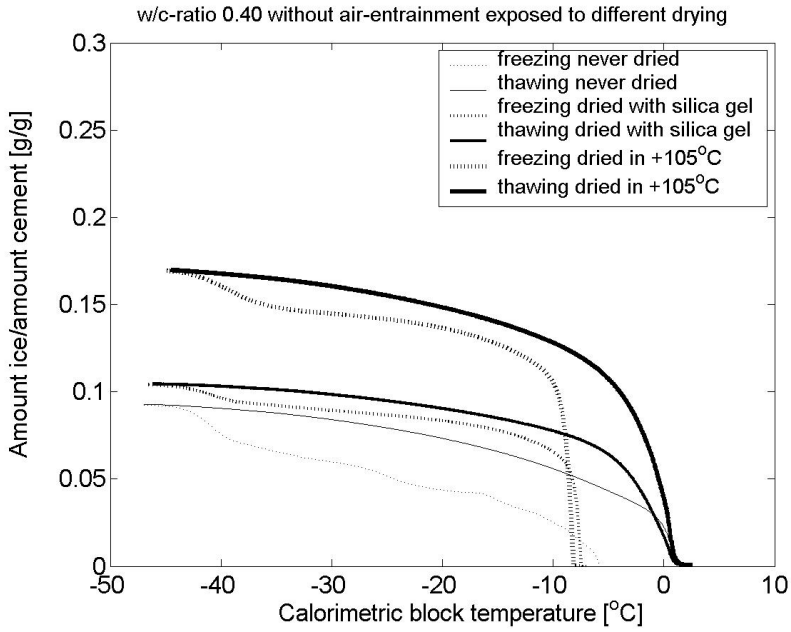

Figure 9.9.3. Amount of frozen water as function of temperature. Different drying procedures prior to re-saturation and testing. Concrete with w/c-ratio 0.40 and natural air.

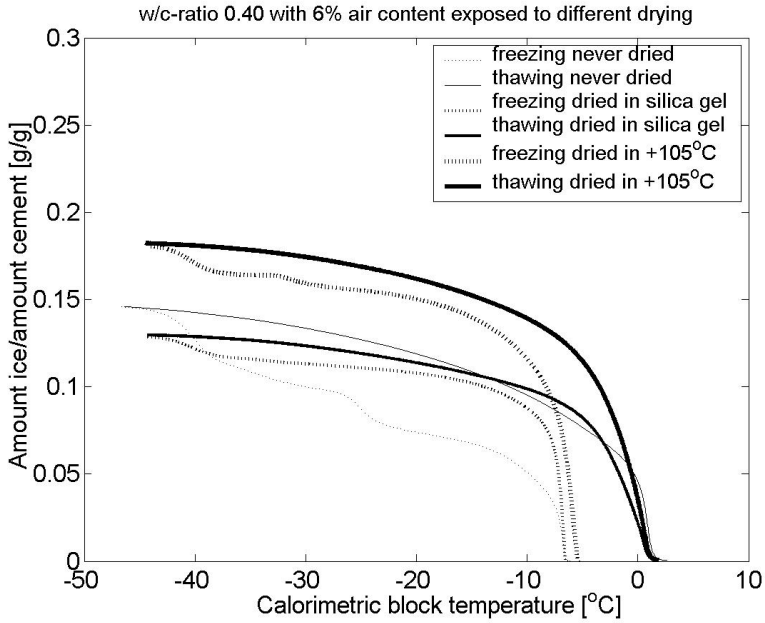

Figure 9.9.4. Amount of frozen water as function of temperature. Different drying procedures prior to re-saturation and testing. Concrete with w/c-ratio 0.40 and 6% air.

The first nucleation of ice formation occurs at about -5 à –8°C. There is no effect of the drying procedure.

Drying causes a drastic change in the ice formation curve, as has previously been shown by Bager and Sellevold (1986b). In pre-dried specimens most ice formation takes place before -10°C and only small ice formation at -40°C. In never-dried specimens ice formation takes place gradually from nucleation at about -7°C to -40°C where an additional big ice formation occurs.

The most plausible explanation to this change is that the never-dried specimens contain a substantial amount of locally supercooled water down to very low temperature. There are some 'peaks' in the curves at about -15°C and -25°C indicating that some of this water is nucleated, probably by ice that has been able to penetrate the entrances to the pore with supercooled water. Drying probably causes micro-cracking or other 'coarsening effects' that opens the entrances to these pores which makes it possible for water to be nucleated at the 'correct' temperature for the actual pore size, Eq. 9.2.2-Eq. 9.2.7. It is sometimes claimed that drying causes a general coarsening of the pore structure, and that this should be the reason for its effect on freezing. This is unlikely, however, since drying at +20°C is a rather mild procedure, that could possibly not cause the very drastic effect on the pore size distribution required for the observed effect on freezing.

Drying at +20°C over silica gel does not increase the total amount of ice formed at -45°C, only the temperature at which is formed. Drying at +105°C cause a certain increase in the amount of ice formed at -45°C, the amount of non-freezable water decreases.

For pre-dried specimens, the freezing curve and the melting curves show almost no hysteresis down to the initial nucleation temperature, except for the small hysteresis caused by a small amount of ice formed by homogeneous nucleation of locally super-cooled water at -40°C. This agreement is an additional strong indication that the hysteresis in never-dried specimens depends on local supercooling.

The difference in amount of evaporable water between dried and never-dried specimens should be considered. In all tests, except one, it was impossible to regain the same amount of evaporable water as before drying. For drying at +20°C drying caused a decrease in evaporable water of about 11%. For drying at +105°C the reduction was about 4%. The most plausible reason is that the water absorption time was 4 years before drying but only about one month after drying.

9.9.3 Conclusions regarding the influence of drying

The same type of drying effects was observed for both w/c-ratios and both air contents. Pre-drying over silica-gel at room temperature caused almost no difference in the total amount of ice formed down to -45°C. On the other hand, the ice formation process was drastically changed. Pre-drying made ice form at much higher temperature than in never-dried concrete. Furthermore, the hysteresis between ice formation and ice melting vanished almost completely (except for hysteresis caused by delayed initial nucleation due to supercooling. The reason for this effect of pre-drying is believed to be the destruction of narrow entrances to larger pores, making nucleation of water in these possible.

Pre-drying at 105°C caused exactly the same type of change in the ice formation process. Besides, an increase in total amount of ice formed down to -45°C was found.

The fact that drying makes more ice form at lower temperature should reasonably have an effect on the frost resistance of concrete. At normal freezing the lowest temperature in a real structure, or in a freeze/thaw test is about -20°C. At that temperature, a concrete with w/c-ratio 0.60 can have 50% more frozen water if it has been pre-dried at +20°C than if it has never been dried, Figure 9.9.1. This should be considered when the length change measurements in Test series 1 are compared with Test series 3, or Test series 4 with 5, or Test series 6 with 7.

9.10 Rate of ice formation

In Figure 9.10.1 and 9.10.2 the rate of ice formation is plotted versus temperature for air-entrained concrete with w/c-ratio 0.60 and 0.40. Both virgin and pre-dried and re-saturated specimens are shown. Three peaks in the freezing rate are clearly visible; (i) the very rapid ice formation rate when super-cooled water is nucleated at some degrees below zero, (ii) the increased rate within the range -23°C to -30°C with the highest rate at about -26°C, (iii) the high rate at about -40°C. Drying causes a reduction in the middle peak, and in the peak at -40°C. This indicates that drying causes an 'opening' of the pore structure reducing hysteresis between freezing and melting, by making nucleation of pore water at higher temperature possible.

The y-scale in the figure makes it difficult to read the real ice formation rate, e.g. the exact effect of cooling rate on ice formation rate. An increased cooling rate causes an increased ice formation rate since the same amount of ice has to be formed in shorter time. The fact that the same amount of ice is formed at each temperature is seen in Figure 9.6.2 and Figure 9.6.4.

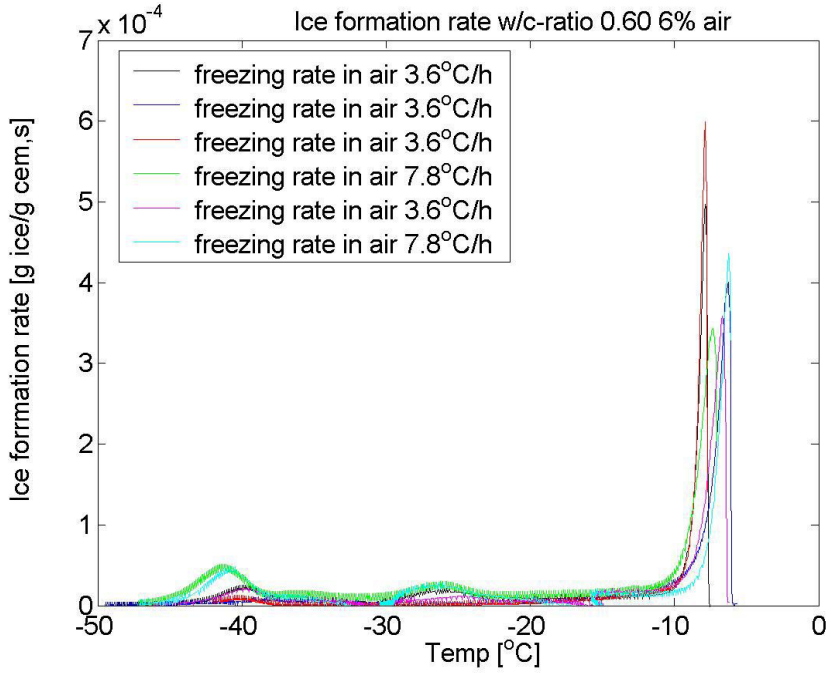

Figure 9.10.1. Ice formation rate in material with a w/c-ratio of 0.60 and 6% air.

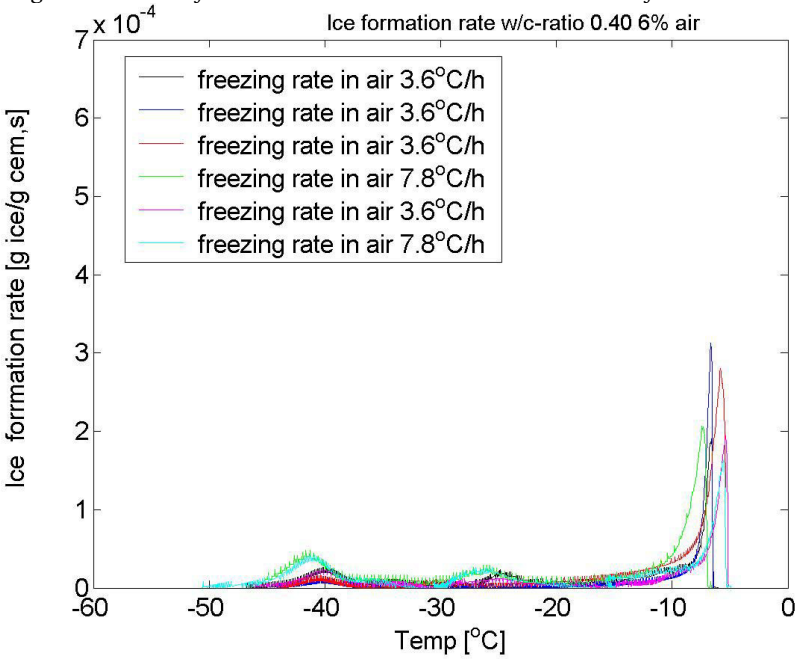

Figure 9.10.2. Ice formation rate in material with a w/c-ratio of 0.40 containing 6% air.

9.11 Non-freezable water

9.11.1 Introduction

Powers and Brownyard (1948) found that the non-freezable water of materials of equal w/c-ratio and degree of hydration was independent of the amount of evaporable water and only dependent on temperature; the lower the temperature the lower the amount of non-freezable water. In a work by Fagerlund (1974) this was also found to be valid for other porous materials like autoclaved cellular concrete, sand-lime brick, clay brick and others. The prerequisite for this to be valid is of course that the total water content is higher than the non-freezable water content. In both studies mentioned the determination of freezable water was determined by thawing of specimens pre-frozen to different temperatures. Thus, supercooling effects were not present. The result is expected since the amount of non-freezable water ($w_{nf}(\theta)$) at a given temperature should be a function of the pore structure while the freezable water at the same temperature ($w_f(\theta)$) is also a function of the total amount of pore water (w_e).

$$w_f(\theta) = w_e - w_{nf}(\theta) \qquad \text{Eq. 9.11.1}$$

where $w_{nf}(\theta)$ is independent of the amount of pore water and only a function of temperature.

To examine this matter further, the non-freezable water content for Samples 1 and 2 subjected to cycle 1 and 2 (continuous temperature curves) is calculated by Eq. 9.11.1. The freezable water content is calculated from the curves in Figure 9.6.1-Figure 9.6.4 and Figure 9.9.1-Figure 9.9.4. The data are obtained from the freezing curve.

9.11.2 Results

Non-freezable water expressed as fraction of total pore volume (porosity) is shown in Figure 9.11.1 and Figure 9.11.2. In Figure 9.11.3 and Figure 9.11.4 the same data are expressed in relation to the cement content. In this way the effect of different air contents, and different water contents can be eliminated and a more direct comparison between samples with the same w/c-ratio and the same pre-conditioning be made.

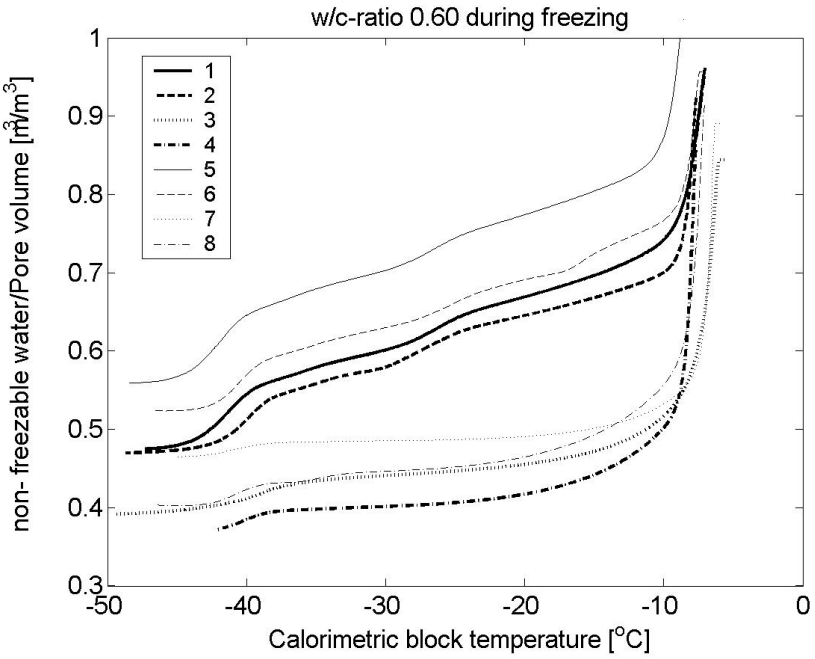

Figure 9.11.1. The amount of unfrozen water during freezing in relation to the total pore volume (total porosity) of all samples with a w/c-ratio of 0.60 subjected to cycles 1 and 2 (continuous freeze-thaw cycle).

Curve 1: 6% air, cycle 2, never dried. w_e=1.12 g
Curve 2: 6% air, cycle 1, never dried. w_e=1.11 g
Curve 3: 6% air, cycle 1, dried over silica gel. w_e=1.02 g
Curve 4: 6% air, cycle 1, dried at +105°C. w_e=1.03 g
Curve 5: no air entrainment, cycle 2, never dried. w_e=0.98 g
Curve 6: no air entrainment, cycle 1, never dried. w_e=1.14 g
Curve 7: no air entrainment, cycle 1, dried silica gel. w_e=1.06 g
Curve 8: no air entrainment, cycle 1, dried +105°C. w_e=1.08 g

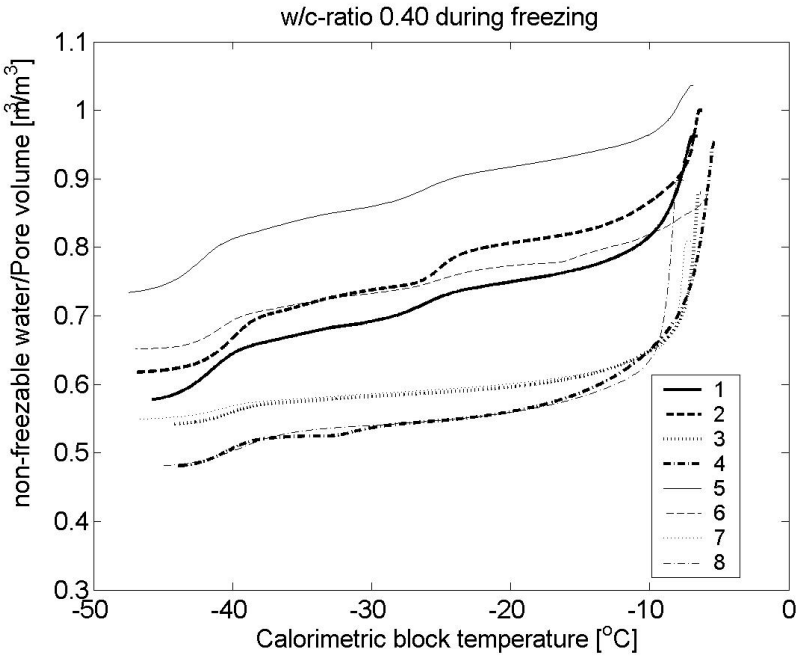

Figure 9.11.2. The amount of unfrozen water during freezing in relation to the total pore volume (total porosity) of all samples with a w/c-ratio of 0.40 subjected to cycles 1 and 2 (continuous freeze-thaw cycle).

Curve 1: 6% air, cycle 2, never dried. w_e=1.03 g
Curve 2: 6% air, cycle 1, never dried. w_e=1.12 g
Curve 3: 6% air, cycle 1, dried over silica gel. w_e=0.98 g
Curve 4: 6% air, cycle 1, dried at +105°C. w_e=1.07 g
Curve 5: no air entrainment, cycle 2, never dried. w_e=0.88 g
Curve 6: no air entrainment, cycle 1, never dried. w_e=1.05 g
Curve 7: no air entrainment, cycle 1, dried over silica gel. w_e=0.97
Curve 8: no air entrainment, cycle 1, dried at +105°C. w_e=1.07 g

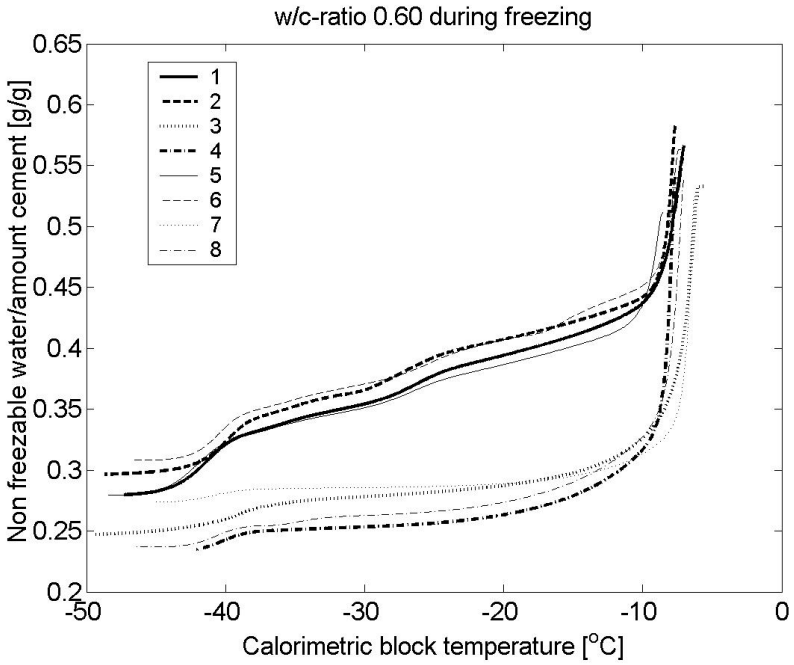

Figure 9.11.3. The amount of unfrozen water during freezing in relation to the cement content of all samples with a w/c-ratio of 0.60 subjected to cycles 1 and 2 (continuous freeze-thaw cycle).

Curve 1: 6% air, cycle 2, never dried. w_e=1.12 g
Curve 2: 6% air, cycle 1, never dried. w_e=1.11 g
Curve 3: 6% air, cycle 1, dried over silica gel. w_e=1.02 g
Curve 4: 6% air, cycle 1, dried at +105°C. w_e=1.03 g
Curve 5: no air entrainment, cycle 2, never dried. w_e=0.98 g
Curve 6: no air entrainment, cycle 1, never dried. w_e=1.14 g
Curve 7: no air entrainment, cycle 1, dried over silica gel. w_e=1.06 g
Curve 8: no air entrainment, cycle 1, dried at +105°C. w_e=1.08 g

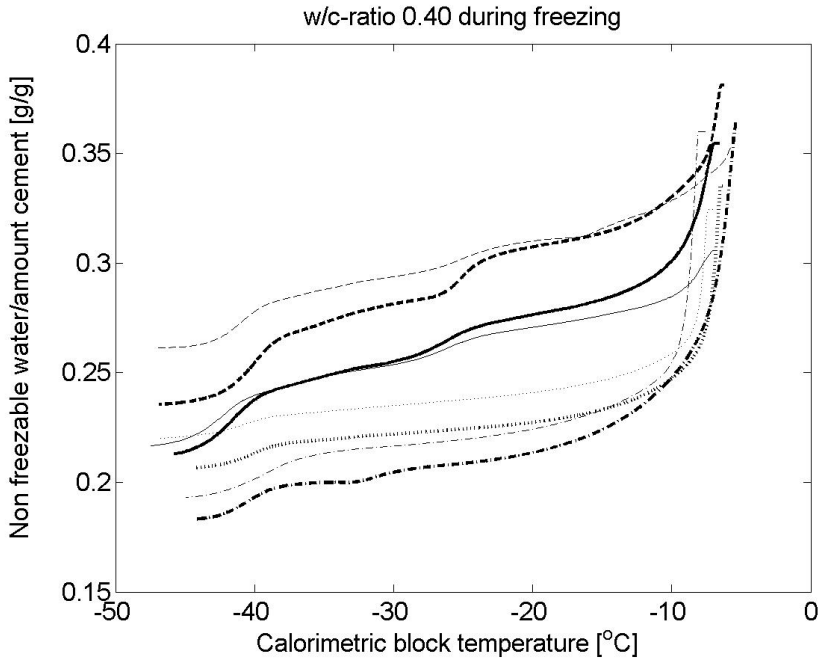

Figure 9.11.4. The amount of unfrozen water during freezing in relation to the cement content of all samples with a w/c-ratio of 0.40 subjected to cycles 1 and 2 (continuous freeze-thaw cycle).

Curve 1: 6% air, cycle 2, never dried. w_e=1.03 g
Curve 2: 6% air, cycle 1, never dried. w_e=1.12 g
Curve 3: 6% air, cycle 1, dried over silica gel. w_e=0.98 g
Curve 4: 6% air, cycle 1, dried at +105°C. w_e=1.07 g
Curve 5: no air entrainment, cycle 2, never dried. w_e=0.88 g
Curve 6: no air entrainment, cycle 1, never dried. w_e=1.05 g
Curve 7: no air entrainment, cycle 1, dried over silica gel. w_e=0.97
Curve 8: no air entrainment, cycle 1, dried at +105°C. w_e=1.07 g

9.11.3 Discussions and conclusions

The non-freezable water content can be regarded as a material property describing the pore structure of the material, whereas the outer environment decides the evaporable water content. The aim was to see if that statement could be confirmed. Figure 9.11.1 and Figure 9.11.2 could not be directly used for that purpose since the non-evaporable water is plotted versus the total porosity including air, and the amount of air pores were different in different specimens. Therefore the discussion below is based on Figure 9.11.3 and Figure 9.11.4.

w/c-ratio 0.60, Figure 9.11.3:
Curves 1, 2, 5, 6 are valid for *never-dried* concrete and can therefore be compared. It is very interesting to note that all these curves assembles in one group indicating that the non-freezable water is fairly constant, as expected. Deviations between the curves exist, but are not very big. It is also interesting to note that 'jumps' in the curves occur at about the same temperatures (-25°C and –40°C).

Curves 3, 4, 7, 8 are valid for *pre-dried* concrete. They assemble in another group, lower than the previous, and therefore showing that pre-drying has caused a substantial reduction in the non-freezable water, especially at high temperature. The curves have a smooth shape until -40°C, which indicates that water freezes in a more 'continuous' fashion than in the never-dried specimens. Curves 4 and 8 are valid for specimens pre-dried at +105°C. They deviate from those pre dried at +20°C (curves 3 and 7) which shows that drying at +105°C, causes more drastic structural changes.

w/c-ratio 0.40, Figure 9.11.4:
The results are similar to those for w/c-ratio 0.60; never-dried specimens assemble in one group, although with wider spread than for w/c-ratio 0.60, and pre-dried in another. Hard drying at +105°C causes bigger reduction in non-freezable water than isothermal drying at +20°C.

Comparison of w/c-ratio 0.60 and 0.40:
The non-freezable water contents for never-dried concrete during freezing are listed in Table 9.11.1 for the three temperature levels, -15°C, -25°C, -35°C.

Table 9.11.1: Non-freezable water for never-dried specimens. (Based on average values at freezing. The spread for w/c-ratio 0.40 is quite big, see Figure 9.11.4).

w/c-ratio	w_{nf}/c (g/g)			w_{nf}/w_n (g/g)		
	-15°C	-25°C	-35°C	-15°C	-25°C	-35°C
0.60	0.42	0.38	0.35	2.6	2.4	2.2
0.40	0.29	0.28	0.26	2.2	2.2	2.0

The values are a bit lower for w/c-ratio 0.40, which can be explained by a somewhat lower degree of hydration. According to the measurements by Powers & Brownyard (1948) the non-freezable water, as determined by thawing experiments, is a multiple of the amount of non-evaporable water, w_n ($w_n/c=0.20\alpha$ where α is the degree of hydration). Assuming the degree of hydration to be 0.8 for w/c-ratio 0.60 and 0.65 for w/c-ratio 0.40, the relation between measured w_{nf} and calculated w_n obtains the values given in Table 9.11.1. The difference between the two w/c-ratios is fairly small, as should be expected. For thawing, Powers & Brownyard (1948) found a

value $w_n/w_{nf} \approx 1$. Thus, at freezing the relation is about twice as high, which can possibly be explained by the hysteresis between freezing and melting.

9.12 Calculations of sorption isotherms from freezing and thawing experiments

9.12.1 Theory

Powers and Brownyard (1948) pointed out that there should be a relation between the non-freezable water content as function of temperature and the sorption isotherm, i.e. absorbed water as function of the relative humidity (RH), determined at some constant temperature. This analogy has later been discussed by other researchers.

If a good correlation could be found between the sorption isotherms and the freezing-melting curves, the latter could be used for a rapid determination of sorption isotherms. Vice versa, the sorption isotherms, which can be determined by very easy means, could be used for estimation of freezing and melting, which normally requires costly and complicated equipment.

In a sorption isotherm, the volume of absorbed water at a particular relative humidity corresponds to the total volume of pores smaller than a given pore size given by the Kelvin equation. In the same way, a depression of the freezing point to a given temperature corresponds to a particular pore size, the volume of non-freezable water being the total volume of pores that are smaller than that.

This also means that a pore size distribution can be determined from the non-freezable water curve in analogy with a calculation of pore sizes from the sorption isotherm; this possibility has been discussed in Fagerlund (1973a), Brun et al. (1977), Bager and Sellevold (1980b) and others.

In all these calculations the radius of curvature of the water-air meniscus (Case A in Figure 9.2.2) or the ice-water meniscus (Cases B and C) have been set to be equal to the pore radius (or the 'Kelvin radius', which is the pore radius excluding adsorbed layer). This assumption is not necessarily correct, but the calculation made below is merely 'exploratory' to see if there is some sort of reasonable relation between the two curves.

Combination of the Kelvin equation for the normal temperature +20°C used at determination of a sorption isotherm, and the equation for freezing point depression, one of equations Eq. 9.2.2-Eq. 9.2.7, gives a relation between the relative humidity (Φ_m) at which water condensates in a pore of given size and the temperature at which this water freezes.

The Kelvin equation is:

$$\ln(\phi_m) = -\frac{\sigma^{g-l} V^l}{RT_{sorp} r_h} \qquad \text{Eq. 9.12.1}$$

where T_{sorp} is the temperature at determination of the sorption isotherm. Solving this equation for r, and inserting that value in one of Eq. 9.2.2-Eq. 9.2.7 gives the following relation between relative humidity Φ_m and freezing temperature T (K). The equilibrium water content at a certain relative humidity corresponds to the non-freezable water content at the corresponding temperature.

$$\ln(\phi_m) = \sigma V \left(\frac{\Delta H^{fus}}{RT_{sorp}} \right) \ln\left(\frac{T}{T_0} \right) \qquad \text{Eq. 9.12.2}$$

ΔH^{fus} is the heat of fusion valid fort he actual freezing temperature, see Eq. 9.4.1. T_0 is the normal freezing point, 273K. The coefficient σ is a ratio between the surface tensions of different phases (ice, water, vapour) and V is a ratio between molar volume of water and ice.

The following values are valid for the three different cases in Figure 9.2.2

Case A: $\sigma=\sigma^{g-l}/\sigma^{g-l}=1$	$V=V^l/V^l=1$
Case B: $\sigma=\sigma^{g-l}/\sigma^{l-s}=0.075/0.035=2.14$	$V=V^l/V^s=0.9$
Case C: $\sigma=\sigma^{g-l}/\sigma^{l-s}=2.14$	$V=V^l/V^l=1$

Example: A freezing point depression of 20°C corresponds to the following relative humidity at +20°C (Note: ΔH^{fus} at -20°C (253 K) is $5.3 \cdot 10^3$ J/mole):

Case A: $\Phi_m=0.85$
Case B: $\Phi_m=0.73$
Case C: $\Phi_m=0.70$

This means that the calculated sorption isotherm will depend on which of the expressions for freezing point depression is selected. This will be shown in the next paragraph.

The sorption isotherm is different at absorption than at desorption. This hysteresis is possibly caused by a similar (but not the same) mechanism as hysteresis between ice formation and ice melting; i.e. phenomenon depending on the existence of 'neck pores'. At sorption these neck-pores isolate the coarser pores, making it impossible for them to be drained at desorption until the neck pore has been emptied. Principally, freezing corresponds to desorption and melting to absorption. Therefore, the desorp-

tion curve should be calculated from the non-freezable water at freezing and the absorption isotherm from the non-freezable water at melting.

9.12.2 Measurement of sorption isotherms and pore size distribution

I: The experimental method

Sorption isotherms were determined for two of the materials, w/c-ratio 0.60 and 0.40 both without air entrainment. The sorption measurement method used is described in Wadsö, Svennberg and Dueck, (2003). Eight crushed samples (7.2 cm^3 each) were placed over saturated salt solutions contained in jars. The relative humidities (RH) were 11% (LiCL), 33% ($MgCl_2$), 59% (NaBr), 75% (NaCl), 85% (KCl), 91% ($BaCl_2$), 94% (KNO_2) and 97% (K_2SO_4). The samples were placed in aluminum pans hung on hooks that went through the lid of the jar. The weight of the hook and and the sample pan was determined by reference weights. The balance had a range of measurement of 220 ± 0.0005 g with a readability of 0.0001 g. The balance and the jars were stored in a climate conditioned room held at +20°C and 54% RH. One sample for each climate and material was investigated.

When moisture equilibrium with RH in the jar had been established, the jar with pan and sample was dried at +105°C. In order not to disturb the determination of dry weight the lid with its pan and specimen was after drying rapidly moved to another jar containing drying agent (0.4 molecular sieve) where it cooled. The weight was determined after cooling to room temperature.

The sorption method described was chosen because it could be used for studying samples without exposing them to the surrounding air during weighing.

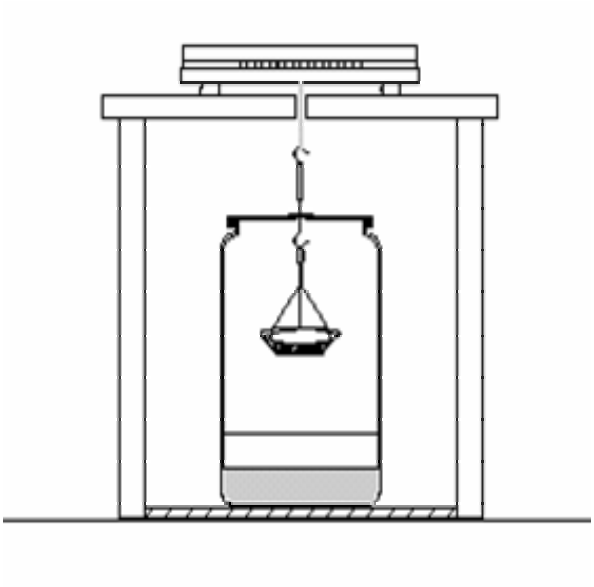

Figure 9.12.1. Sorption measurement arrangement.

II: Tested materials

Since the influence of drying was investigated for samples that were tested in the differential scanning calorimeter, see paragraph 9.9, sorption isotherms were determined for samples treated in the same way. All material had been continuously stored in lime-saturated water for five years before determination.

For determination of a complete isotherm, one single 'mother-prism' (20x20x170 mm) was divided in 8 pieces (~18x20x20 mm). Each piece was weighed in water and air to obtain its volume. Each piece was then crushed separately in a plastic bag. The crushed pieces were placed at the 8 different RH.

After terminated all samples were dried at +105°C according to the method described above.

III: Types of isotherms

Five different isotherms were determined. They are denoted A-E.

Desorption isotherm A; never-dried (virgin) concrete:

The 8 pieces were placed in the different RH-jars without any pre-drying. Isotherm A is therefore the 'virgin' desorption isotherm.

Absorption isotherm B; +105°C-dried concrete:

The 8 pieces were pre-dried at +105°C for 6 days. Before they were placed in the different RH-jars they were cooled over silica gel.

Absorption isotherm C; room temperature dried concrete:
Before they were placed in the RH-jars, the 8 pieces were pre-dried for a month at room-temperature over silica gel and CO_2 absorbent.

Desorption isotherm D; room temperature dried and re-saturated concrete:
The 8 pieces were pre-dried at room temperature over silica gel. Then they were placed in a box containing deionised water for a month, before they were placed in the RH-jars.

Desorption isotherm E; +105°C-dried and re-saturated concrete:
The procedure is the same as for desorption isotherm D, but pre-drying was made at +105°C.

IV: Measured sorption isotherms
The different isotherms are shown in Figure 9.12.2 and Figure 9.12.3.

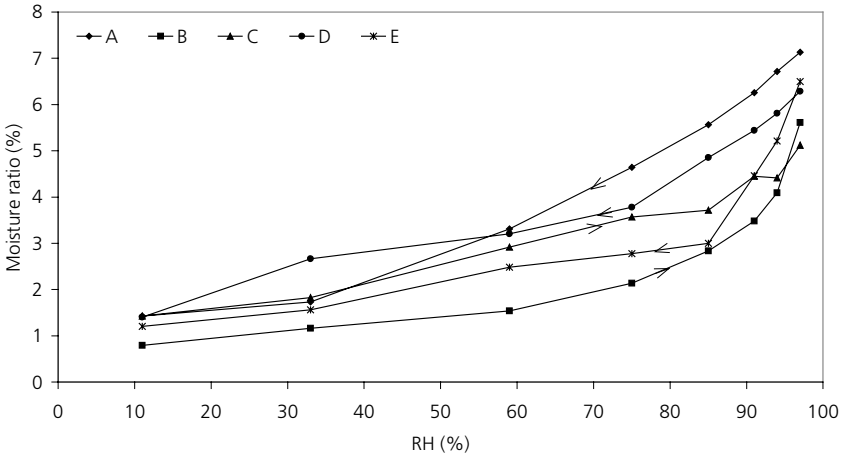

Figure 9.12.2. Sorption isotherms for w/c-ratio of 0.60 with natural air content.

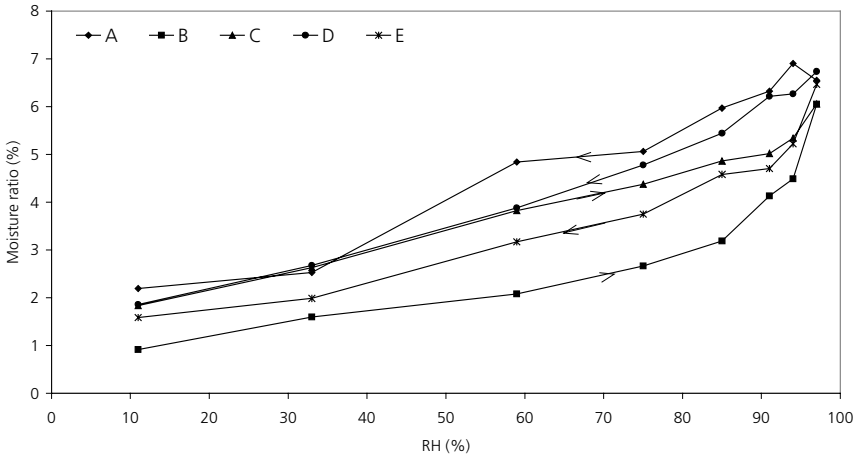

Figure 9.12.3. Sorption isotherm for w/c-ratio of 0.40 with natural air content.

The isotherms differ. The 'virgin' (A) desorption isotherm is the highest of all, and is above the desorption isotherm for pre-dried and re-saturated concrete (E). Pre-drying has very big effect on the sorption isotherms. The absorption isotherm for room temperature dried concrete (C) is higher than that of +105°C dried concrete (B), which was expected, since so hard drying is known to destroy the fine structure of the cement gel. After such drying, water cannot re-enter the cement gel.

V: Pore size distribution

Absorption isotherms B and C were used for calculation of the pore size distribution. The method used is described in Gregg and Sing (1967). The Halsey equation is used for calculation of the thickness of the adsorbed layer over the entire RH-range. The Kelvin equation (Eq. 9.12.1) is used for calculation of the radius of the water meniscus within the capillary condensation range, which is assumed to be at RH>45%. The calculations assume T=293 K, a surface tension of 0.073 N/m and the pores being circular cylindrical. The result is shown in Figure 9.12.4 and Figure 9.12.5.

The drying procedure was found to strongly influence the pore size distribution at a w/c-ratio of 0.60, whereas the influence was much less for a w/c-ratio of 0.40. Whether the measured influence is really a change in pore size distribution or an effect of reduced amount of 'neck-pores', caused by drying is unclear. Neck-pores cause hysteresis between absorption and desorption, and are thus influencing the sorption isotherm.

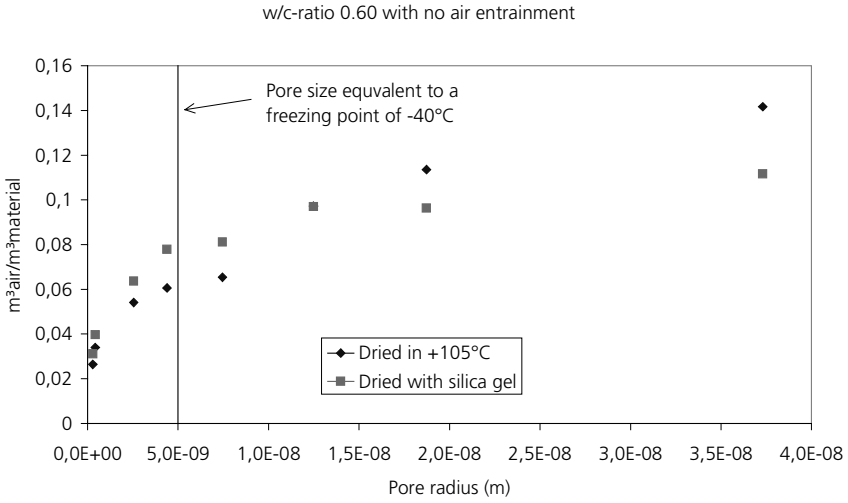

Figure 9.12.4. Pore size distribution for a w/c-ratio of 0.60 without air-entrainment.

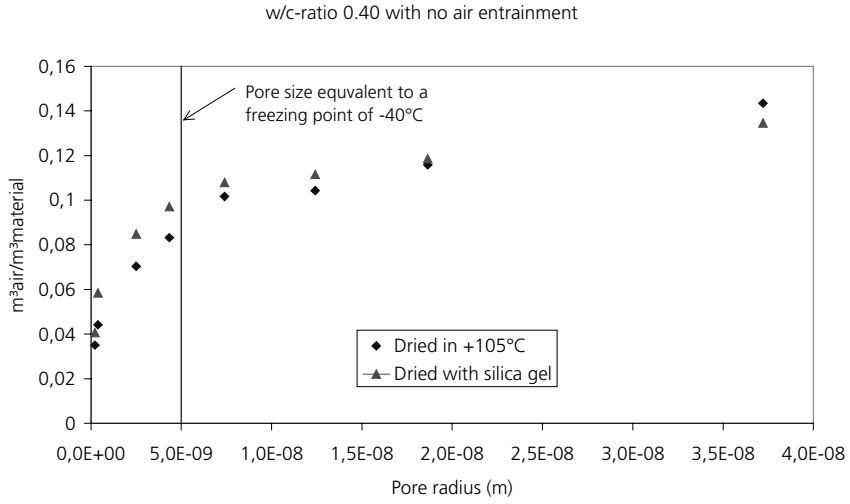

Figure 9.12.5. Pore size distribution for a w/c-ratio of 0.40 without air-entrainment.

VI: Specific surface

The specific surface was calculated on the basis of the results at RH 11% and 33%, using BET-plots for the absorption both after drying at +105°C and after a month over silica gel in a closed container. (B and C)

Table 9.12.1. Specific surface of investigated materials.

	Specific surface (m²/g)	
Material	Dried over silica gel	Dried at +105°C
w/c-ratio of 0.60 without air entrainment	42.21	27.36
w/c-ratio of 0.40 without air entrainment	63.48	37.76

As can be seen, the specific surface is strongly affected by the drying procedure. When the samples were dried at +105°C, the pore system became 35-40% coarser than when they were dried over silica gel. This confirms the observations made by other researchers, that severe drying causes irreversible collapse of the fine pore structure.

9.12.3 Calculated absorption isotherms

In the calculated absorption isotherms below, the non-freezable water from the melting curves in paragraph 9.9 have been used. The reason why these curves were used is that a determination of absorption isotherms always starts with pre-dried samples. Thus, for a fair comparison it was important to also use pre-dried (but resaturated) specimens for the calculated isotherms.

Absorption isotherms of specimens pre-dried at +105°C:

In Figure 9.12.6 and Figure 9.12.7, the measured absorption isotherms in samples dried at +105°C (isotherm B) are compared with the calculated curves based on measurements of melting of ice for samples that were first dried at +105°C and then resaturated before the calorimeter test (see paragraph 9.9)

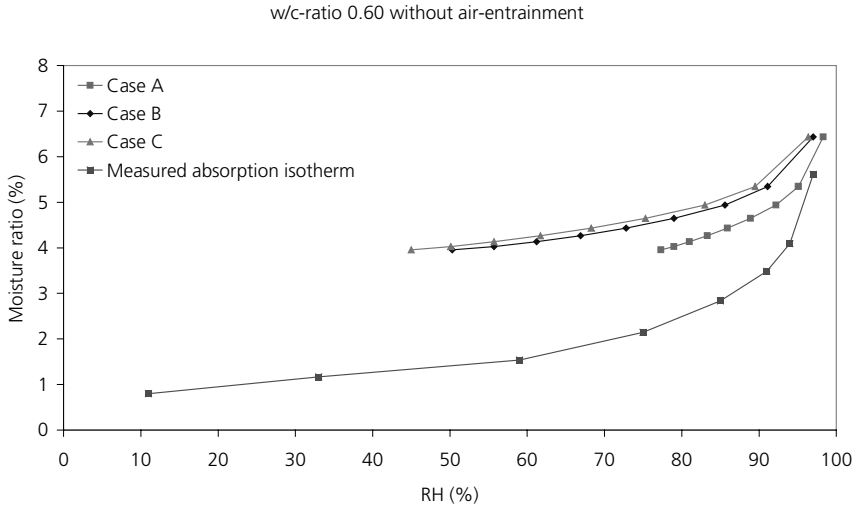

Figure 9.12.6. Calculated and measured absorption isotherms for materials with a w/c-ratio of 0.60 without air-entrainment dried at +105°C.

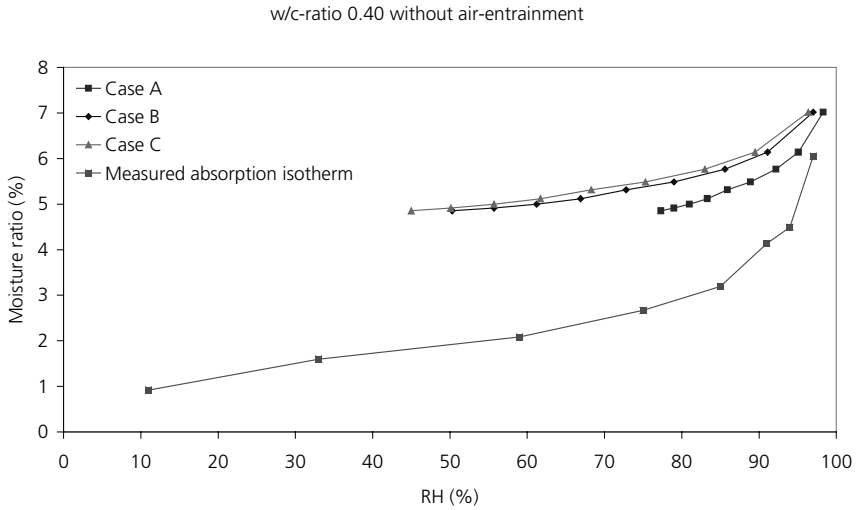

Figure 9.12.7. Calculated and measured absorption isotherms for material with a w/c-ratio of 0.40 without air-entrainment dried at +105°C.

The highest correlation was found for case A, based on concave liquid-gas interphases towards air and plane gas-solid interphases. The calculations resulted in an overestimation of the absorption in all three cases and in both the materials studied. In paragraph 9.9 where ice formation in dried and resaturated samples were studied, it was found that the melting curve also changed when a sample had been dried, especially at +105°C. There was a much more concentrated melting at around 0°C than in the never-dried specimen. Therefore, it might be that the pre-drying might have caused other effects with regard to freezing/melting than regard to absorption.

Absorption isotherms of specimens pre-dried over silica gel

In Figure 9.12.8 and Figure 9.12.9 tests of specimens exposed to milder pre-drying are shown. Both vapour absorption isotherms (isotherm C) and melting curves were obtained for the materials after drying in a closed box containing silica gel and carbon dioxide absorbents. Non-freezable water used for calculation of the isotherms was taken from the melting curves shown in paragraph 9.9.

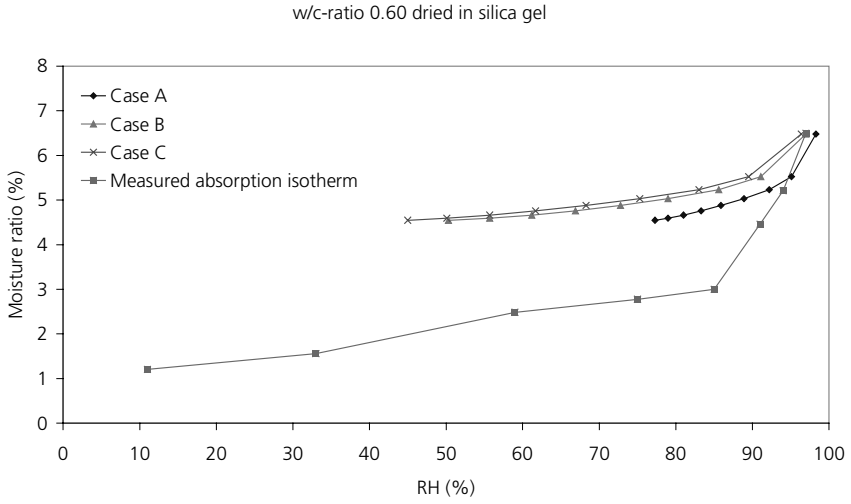

Figure 9.12.8. Calculated and measured absorption isotherms for material with a w/c-ratio of 0.60 without air-entrainment dried over silica gel.

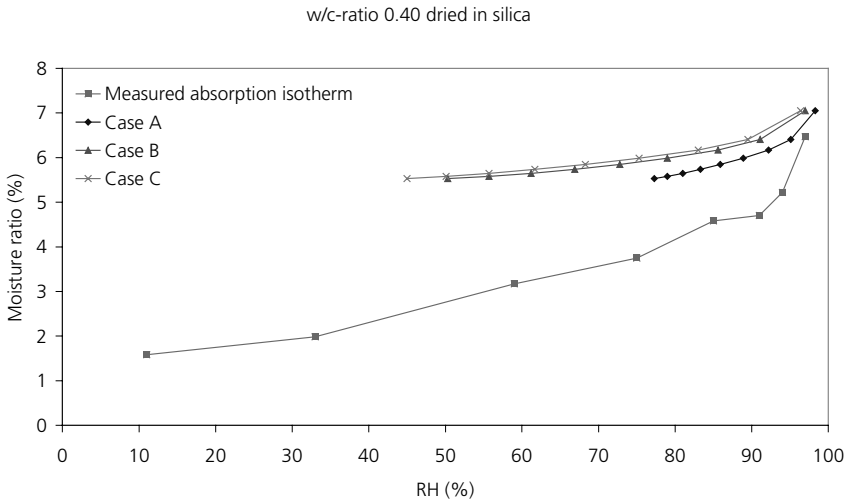

Figure 9.12.9. Calculated and measured absorption isotherms for material with a w/c-ratio of 0.40 without air-entrainment dried over silica gel.

The results obtained for these, not as harshly dried samples are very similar to those for samples dried at +105°C, although the level is slightly higher, which depends on a smaller amount of freezable water. The difference between the calculated and the measured absorption was of the same order for both drying procedures.

9.12.4 Calculated desorption isotherms

The amount of desorbed water is always greater at any given relative humidity than the amount of absorbed water, and the freezing curve is always lower at any given temperature than the thawing curve. For this reason, the amount of desorbed water found at any given moment ought to correspond to the freezing curve, since this contains a greater amount of non-freezable water than the thawing curve.

Therefore, in the calculated desorption isotherms below, the non-freezable water from the freezing curves in paragraph 9.6 have been used. For a fair comparison with the measured desorption isotherm (A) it was important to also use virgin specimens for the calculated isotherms.

In Figure 9.12.10 and Figure 9.12.11 the measured and calculated desorption isotherms are shown.

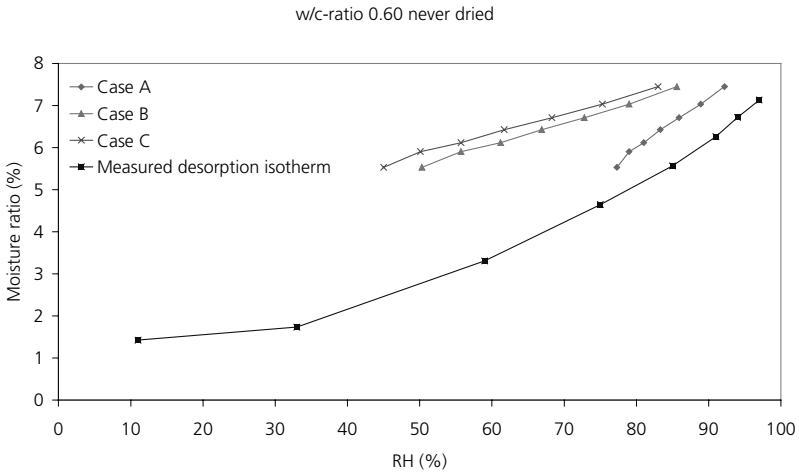

Figure 9.12.10. Calculated and measured desorption isotherms for material with a w/c-ratio of 0.60 without air-entrainment. Never-dried specimens.

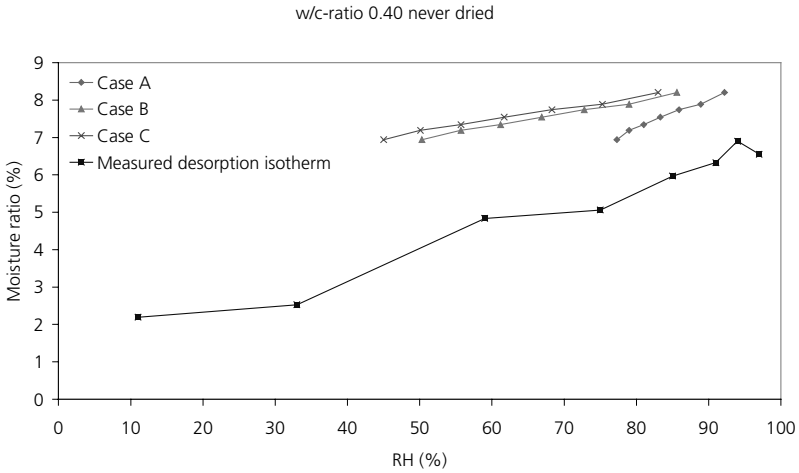

Figure 9.12.11. Calculated and measured desorption isotherms for material with a w/c-ratio of 0.40 without air-entrainment. Never-dried specimens.

As was the case for the absorption isotherms, the difference between the measured and the calculated desorption isotherms are big. The meniscus system Case A in Figure 9.2.2 gives the closest agreement, but even this predicts too high values of desorbed water.

9.12.5 Conclusions

Powers and Brownyard, (1948) obtained a much higher level of concordance between measured isotherms and calculated than found here. They calculated the non-freezable water content from measurements of the dilation at warming of pre-frozen specimens of saturated pastes. The specimens were immersed in toluene during the measurement, which made it necessary to correct Eq. 9.12.2 for surface tension between toluene and water. A discussion of the reliability of the method was carried out.

The main reason why the Powers & Brownyard results are much better correlated with measured sorption isotherms, than results of the present study, is the much lower non-freezable water obtained in their study. According to Table 9.11.1 the relation w_{nf}/w_n was around 2 or 2.5 in the present study, but only about 1 in the Powers & Brownyard study. The reason for this discrepancy is not known.

Fagerlund, (1974) carried out the same calculations as above for other porous materials and found them to agree fairly well with sorption isotherms published in Ahlgren (1972). The calorimeter used was, however, quite primitive with an error in measured freezable water that could be rather big. Thus the agreement found could be somewhat fortuitous.

The calibration of the ice formation made in the present study for a sample of pure water yielded a 2% error level, which compared to the other measurements, mentioned above, is a high level of precision. It thus appears likely that the relation between relative humidity and freezing point given by Eq. 9.12.2 is not correct, which should mean, that one can not safely use sorption isotherms for predicting ice formation.

The determination of freezable water relies on a correct determination of the base line. If that is not correct, a certain error in the calculated ice formation will arise. Furthermore, the temperature dependence of the heat of fusion of water in very fine pores, is not well-known. An error in the assumed value will also cause an error in the calculated amount of ice. These possible errors might be one cause for the deviance between calculated and measured sorption isotherms. The most likely reason is, however, the big simplifications made as regards the geometry of different phases inside a freezing material, and in the Kelvin equation.

9.13 Investigation of the effect of saline pore water

9.13.1 Introduction

In Chapter 8, results of dilatometer tests of freeze-thaw of specimens that had been long-term stored in NaCl-solution of different strength are shown. As a complement to these studies, some calorimeter tests were also made in order to see the effect of salt solution on freezing and melting of pore water. Only one concrete type was studied (w/c-ratio 0.40, 6% air) and only one salt concentration (4.5%). All four freeze-thaw cycles shown in Figure 9.5.1 were employed. The test variables and the specimen data are shown in Table 9.13.1.

9.13.2 Results

The results are shown in Figure 9.13.1-Figure 9.13.3. The amount of frozen water is expressed in relation to the cement content in the specimen. Non-freezable water content can be evaluated from the specimen data given in Table 9.13.1.

Table 9.13.1. Overview of all calorimeter experiments with specimens stored in 4.5% NaCl-solution between casting and testing. Each specimen was tested once. The cement content, the total pore volume, the specimen volume, the total amount of evaporable water in the specimen and the degree of saturation at the test are given in the table.

Pre-conditioning	Cycle	0.40 6% air
Type 1	Cycle 1	No 1
Natural salt-water	3.6°C/h, -70°C	c= 2.99 g
content after 5 years of		V_p= 1.07 cm^3
storage in 4.5% NaCl-		V= 5.69 cm^3
solution		w= 1.01 g
		S= 0.937
	Cycle 2	No 2
	7.8°C/h, -70°C	C= 2.93 g
		V_p= 1.23 cm^3
		V= 5.53 cm^3
		w= 1.01 g
		S= 0.82
	Cycle 3	No 3
	3.6°C/h, 3h	C= 2.90 g
	stop	V_p= 1.08 cm^3
		V= 5.52 cm^3
		w= 0.94 g
		S= 0.88
	Cycle 4	No 4
	3.6°C/h, 12h	C= 2.94 g
	stop	V_p= 1.03 cm^3
		V= 5.60 cm^3
		w= 0.91 g
		S= 0.89

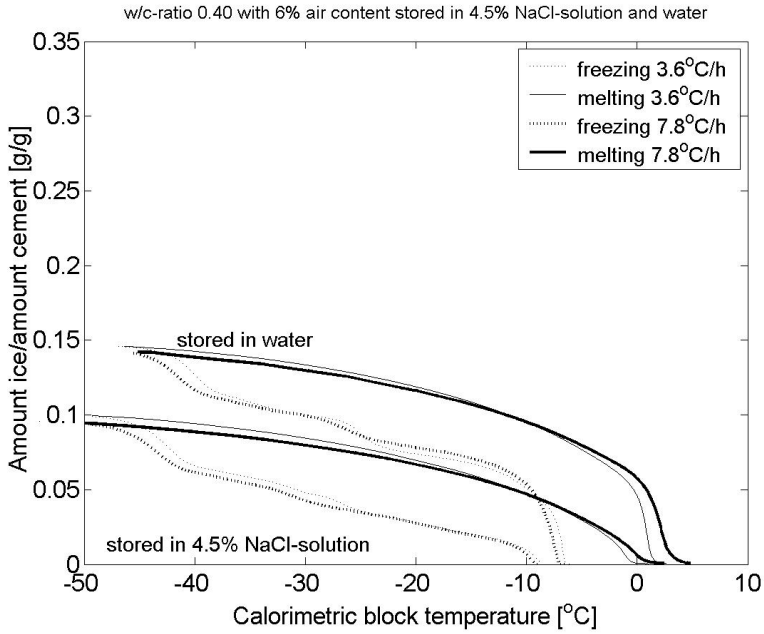

Figure 9.13.1. The amount of frozen water as function of temperature for samples pre-stored in 4.5% NaCl-solution. w/c-ratio 0.40 and 6% air. Different temperature changing rate (cycle 1 and 2).

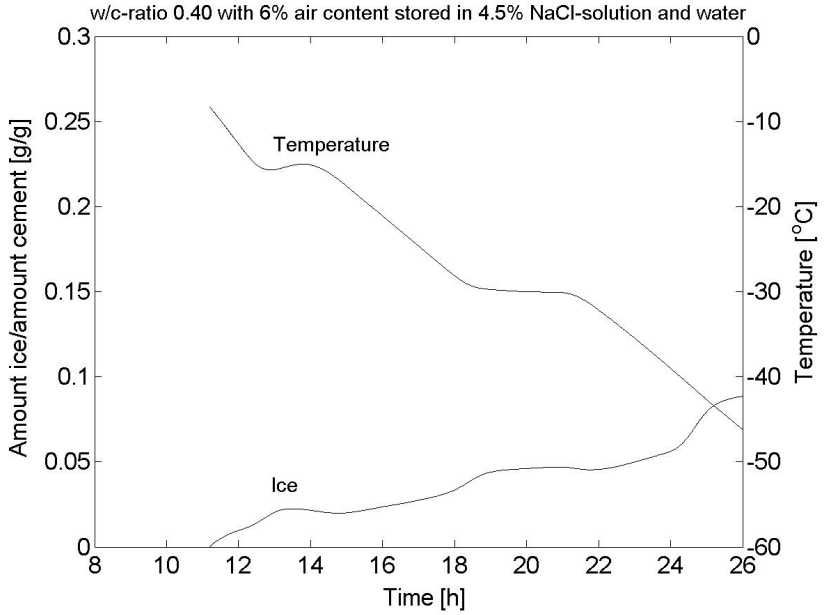

Figure 9.13.2 The amount of frozen water as function of time and temperature for samples pre-stored in 4.5% NaCl-solution. w/c-ratio 0.40 and 6% air. Cycle 3 (3 hour halts at –15°C and –30°C).

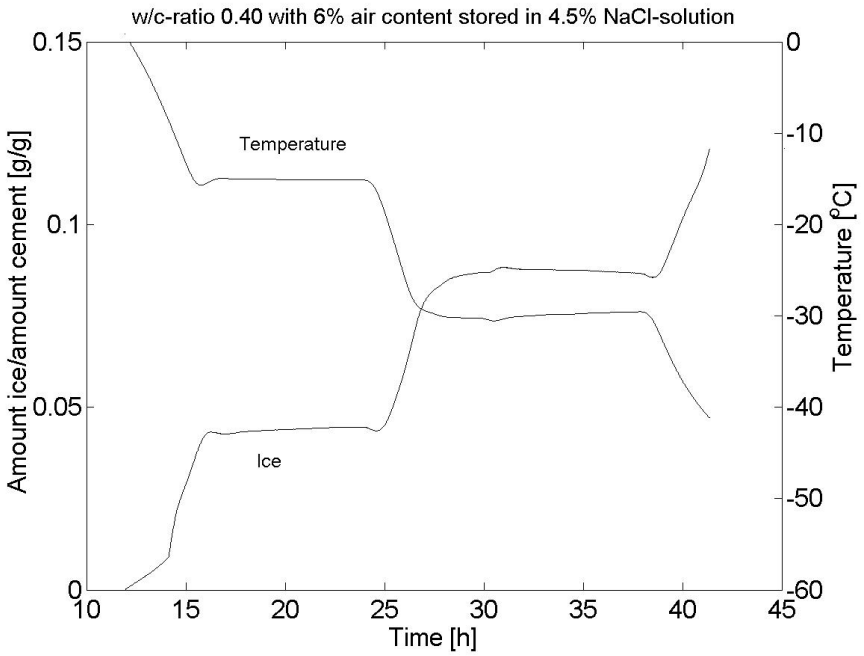

Figure 9.13.3. The amount of frozen water as function of time and temperature for samples pre-stored in 4.5% NaCl-solution. w/c-ratio 0.40 and 6% air. Cycle 4 (5 hour halt at –15°C and 12 hour halt at -30°C).

Effect of rate of temperature change (Figure 9.13.1)

As expected, less ice was formed in the samples stored in NaCl-solution than in samples stored in lime-saturated water. Freezing started at lower temperature in samples containing salt; -9°C versus -7°C. The amount of ice formed when supercooling was overcome was considerably smaller for samples containing salt. The expected freezing temperature for these samples was -4.6°C. The low amount of ice formed at nucleation of freezing indicates that a small amount of water is freezable between -4.6 and -9°C. For samples with saline pore water, the same big ice formation occurred at about -40°C as for samples with pure pore water.

Hysteresis between ice formation and ice melting is big also for samples with salt which indicates that supercooled solution exist in isolated pores enclosed by narrow 'neck-pores'.

There is no effect of the cooling rate for any of the samples.

Effect of short halts at –15°C and –30°C (Figure 9.13.2)
An increase in temperature during the first period of isothermal temperature could be noted. Why this occurred is unknown, but ought to depend on some error in the temperature regulation of the calorimeter. It resulted in melting of some ice. During the second isothermal period (at -30°C), the temperature was more stable, but a slight decrease in temperature occurred, resulting in a certain increase in the amount calculated of ice formation during this period. Despite these problems in the equipment, there were no indications that ice formed when the temperature was held constant. This is in accordance with results with pure water, see Figure 9.7.4

Effect of long halts at –15°C and –30°C (Figure 9.13.3)
No ice was formed during the long temperature halts, which is in accordance with the results with pure water, see Figure 9.8.4.

9.13.3 Conclusions concerning the influence of saline pore water

Saline pore water reduces the amount of freezable water considerably. For the actual concrete the freezable water at -30°C was only 50% of that obtained for a sample with normal pore water. All characteristics of freezing and melting of a normal concrete was also observed for samples with saline pore water:

1. Big supercooling before onset of freezing.
2. Big hysteresis between ice formation and ice melting.
3. Big amount of ice formation at about -40°C.

10 Freezing and thawing experiments - Summary

10.1 Introduction

The most important observations from Chapter 5-8 are described below. Reference to Chapter 9 is made.

Long-term water storage (never-dried with natural water content). Test series 1, 4, and 6.

1. As expected, all *non-air-entrained concretes* obtained big expansion during freezing. The expansion was always above the fracture tensile strain, which is about 0.15‰. Consequently, they also showed big permanent expansion after complete thawing, and considerable loss in dynamic E-modulus, as determined by fundamental frequency of transverse vibration. This behaviour deviates from traditional salt-scaling tests, where it is often found that non-air-entrained concrete is fairly resistant when the water-cement ratio is 0.40, especially if the concrete has had some carbonation, Utgenannt (2004). The fact that very dense, high performance concrete with w/c-ratio as low as 0.25, can be vulnerable to internal frost damage has previously been found by some researchers, e.g. Malhotra et al. (1987). This was also shown to be the case when the concrete contained air.

   These results indicate that internal frost could be a more serious damage cause for dense concrete than surface scaling caused by frost in combination with salt. The specimens had certainly been stored for 4 years in water before the test, but that is not an unrealistic exposure for hydraulic structures, bridge piers in water and similar structures. In a laboratory test of frost resistance water storage time before the test is considerably shorter, why internal damage might no be obtained, or revealed .

2. Almost in all cases *air-entrained concrete* obtained contraction during freezing. The contraction was bigger than the normal contraction calculated from the extrapolated contraction of the unfrozen concrete. There are indications, however, of a certain expansion in concrete with w/c-ratio 0.40, and also with 0.45. All concretes with w/c-ratio 0.60 only had contraction. This behaviour also indicates that dense concrete might be more vulnerable to internal frost than more open concrete. In the actual test no air-entrained concrete obtained permanent dilation bigger than the estimated fracture value 0.15‰ or loss in E-modulus bigger than 10%.

3. In most specimens substantial *supercooling* (3 to 5 degrees) was observed. Nucleation probably started somewhere on the specimen surface and rapidly

spread through the entire specimen. Within less than 5 seconds all available supercooled water in the entire specimen ought to have been nucleated. A calculation based on the temperature rise occurring at nucleation showed that 20% or more of all freezable water is formed momentarily at this nucleation. Nucleation therefore caused big momentary expansion in all *non-air-entrained* specimens. In most cases for non-air-entrained concrete, this ice formation was big enough to cause damage in the specimen. In air-entrained concrete the expansion was small, and could not lead to damage.

The most plausible cause of expansion of non-air-entrained concrete is hydraulic pressure created when excess water caused by the 9% increase in volume when water freezes has to be expelled to air-filled spaces (air-pores). These are not readily available (reachable) in non-air-entrained concrete.

In a real structure, supercooling could be much smaller, if any. Kaufmann (1999) who studied freezing of bridge decks found no supercooling, which was believed to depend on presence of ice crystals in surrounding air ('white frost'). In a hydraulic structure, however, and similar structures, supercooling of the same order as in the experiments probably can exist.

4. During warming *non-air-entrained* expanded somewhat at the beginning, but contracted when most ice melted within the range –10°C to 0°C. Thus, melting of ice in non-air-entrained concrete caused substantial relieve of stresses, indicating that most ice had been formed in-situ in the pores as if these were 'closed containers' from which water could not escape during freezing.

   Air-entrained concrete expanded along almost the same path as they contracted during freezing. Thus melting did not cause any marked effect on length for these specimens, indicating that much water had been transferred to air-pores where it froze without causing stresses. As said in point 2 there are indications that such transfer had been more limited in the dense concrete with w/c-ratio 0.40 and 0.45.

5. When cooling was stopped for 3 or 12 hours at –15°C or –30°C all length changes immediately ceased almost totally, indicating that also ice formation stopped immediately. This was also confirmed by the calorimeter studies, Chapter 9, paragraph 9.7 and 9.8. The hypothesis put forward by Powers and Helmuth (1953), that expansion at constant temperature will occur, and that it depends on microscopic ice lens growth, could therefore not be verified.

   At the halt at –15°C there is a certain contraction in all specimens probably caused by release of internal tension caused by the previous ice formation.

At the halt at –30°C there is a small expansion in some of the specimens. It cannot be explained by ice formation since no ice is formed according to the calorimeter experiments, paragraph 9.7 and 9.8. The movements are small and have no importance for frost damage.

6. The duration of a halt in temperature change had no effect. 3 hours or 12 hours halt gave exactly the same result, namely almost complete halt in length changes .
7. No effect whatsoever on expansions or contractions could be seen of an increase of the rate of cooling and warming from 3.6°C/h to 7.8°C/h. Neither the expansion or contraction during freezing, nor the expansion or contraction during thawing was affected by the change of freezing/warming rate.
8. For *non-air-entrained* specimens, expansion during freezing was found to be directly proportional to the lowest temperature when this was within the temperature range –15°C to –30°C. This means that the expansion was twice as big at –30°C as at –15°C. For *air-entrained* concrete, no effect of the lowest temperature could be seen, since all specimens contracted.

Vacuum-saturated (pre-dried and re-saturated). Test series 2.

1. The results were trivial; as expected, all specimens had big expansion and big permanent damage.
2. When temperature lowering was stopped at –23°C expansion immediately stopped indicating that all formation of ice also stopped.
3. The volume expansions observed were often considerably smaller than the expected 9% of the volume of frozen water. The most plausible reason is that the saturation was not complete.

Adjusted degrees of saturation (pre-dried and re-saturated). Test series 3, 5 and 7.

1. As expected, also air-entrained concrete expanded during freezing when the degree of saturation was high; above the critical. Thus, air-entrained concrete with high degree of saturation behaves exactly as non-air-entrained concrete. This depends on that air-pores have been inactivated by being water-filled before the test started.
2. The higher the degree of saturation, the bigger the damage. The effect of degree of saturation overshadows the effects of w/c-ratio and air content.

3. No effect whatsoever on an increase in the rate of freezing from 3.6°C/h to 7.8°C/h could be observed.
4. When temperature lowering was stopped at –15°C and –30°C (Test series 5 and 7) expansion immediately stopped. The duration of the temperature halts had no influence at any degree of saturation.

Effect of pre-drying. Test series 1 versus 3, 4 versus 5 and 6 versus 7.
Non-air-entrained samples, which were given a degree of saturation in an artificial way showed somewhat larger dilations than never-dried samples in which the same degree of saturation was obtained by long-term 'natural' capillary absorption. This is exemplified by comparison of Test series 4 with Test series 5, see Figure 10.1.1. The most probable reason is that much more ice was formed in pre-dried re-saturated, see paragraph 9.9. The reason for the increased ice formation is discussed there.

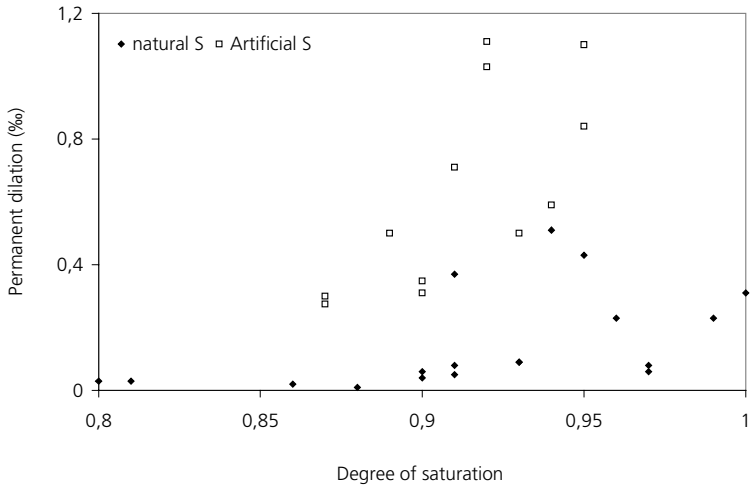

Figure 10.1.1. Difference in permanent dilations between never-dried and dried-resaturated samples.

Relation between different damage parameters
There is a fairly linear relation between dilation at lowest freezing temperature and permanent dilation. Examples for Test series 1 are shown in Figure 10.1.2 and for Test series 4 and 6 in Figure 10.1.3.

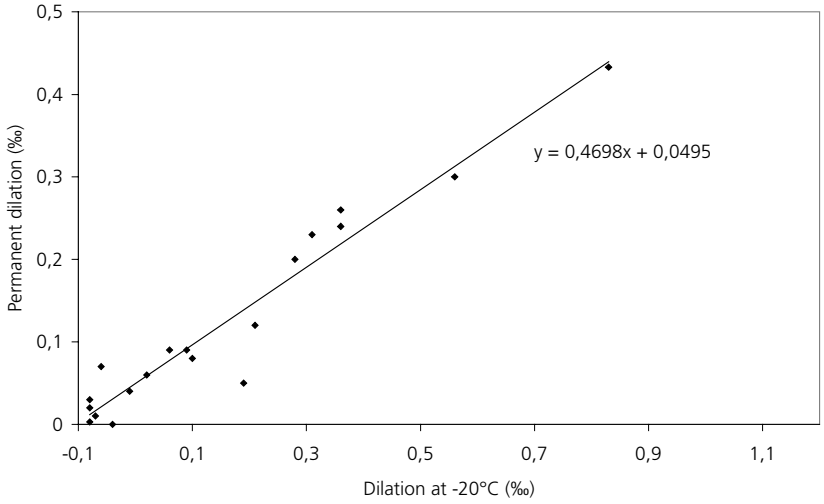

Figure 10.1.2. Relation between dilation at –20°C and permanent dilation in Test series 1.

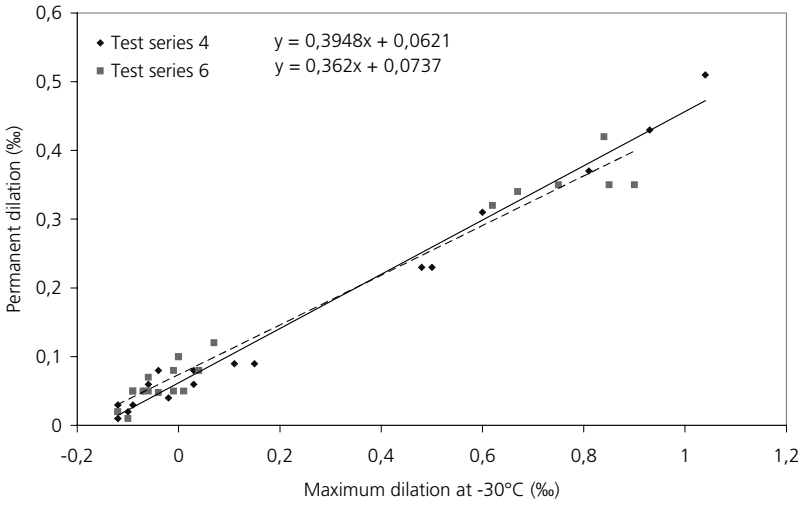

Figure 10.1.3. Relation between dilation at -30°C (3 hours or 12 hours duration) and permanent dilation for Test series 4 and 6.

A comparison of Test series 1 or 4 with test series 6 shows that a long duration of constant temperature at low temperature has no big effect on damage.

Saline pore water

1. The presence of salt in pore water was found to have big effects on expansion and damage.

2. At some salt concentration, that was different for each w/c-ratio and air content, the dilation and damage was bigger than for pure pore water, or for other salt concentrations. Measurements of ice formation (paragraph 9.13) show that the amount of freezable water is very much reduced when the specimen contains salt. Therefore, the increased expansion must depend on some other mechanism than increased ice volume.
3. Air-entrained concrete containing saline pore water of high concentration was found to be more vulnerable to internal frost damage than non-air-entrained concrete.
4. The length changes stopped immediately when temperature lowering was stopped at -23°C.

10.2 Destruction mechanisms

On the basis of observed length changes and ice formation/melting curves, some qualitative conclusions concerning destruction mechanisms might be made. Concerning a description of destruction mechanisms, see Chapter 2.

1. The positive effect of air is obvious, but this is explained by both major mechanisms, hydraulic pressure and ice lens growth. Possibly different mechanisms are active at different stages of the freeze/thaw process.
2. *Nucleation of supercooled water* causes very rapid ice formation and rapid and big expansion in non-air-entrained concrete. Expansion and damage is probably caused by *hydraulic pressure*. Possibly only part of the excess water caused by ice formation can be forced away to the few air-pores in such concrete. Thus, ice formation occurs more or less as in a 'closed container', which is a special case of the hydraulic pressure theory, valid for zero permeability.
3. The gradual volume increase, which takes place in *non-air-entrained concrete*, when temperature is lowered from nucleation temperature to the lowest temperature, can depend both on hydraulic pressure and on ice lens growth. Measurements of ice formation showed that this is steadily increasing with reduced temperature (e.g. compare Figure 9.6.1 with Figure 5.3.3) indicating that both mechanisms can be active.

   According to the *hydraulic pressure theory*, pressure should be directly proportional to the rate of ice formation. Whether this is the case can be tested by comparing length change curves and ice formation curves for specimens that expand during freezing. Such a concrete is that with w/c-ratio 0.60 and

no air-entrainment. The length change curves for two cooling rates are shown in Figure 5.3.3. The ice formation curves for the same cooling rates are shown in Figure 9.6.1. Temperature before nucleation cannot be used at the test of hydraulic pressure, since nucleation takes place at considerably lower temperature in the calorimeter experiment. Therefore, the test is restricted to the temperature range -10°C to -20°C. The test is made for the following temperature intervals:

-10°C to -15°C
-15°C to -20°C

The expansion rate dε/dt (‰/h) and the rate of ice formation dw_f/dt (g/g_{cem}·h) are taken from Figure 5.3.3 and Figure 9.6.1, and are plotted in Table 10.2.1.

The hydraulic pressure mechanism might be valid if the ratio between expansion rate and rate of ice formation is constant for different ice formation rates. This ratio is calculated in Table 10.2.1.

Table 10.2.1: Expansion rate and rate of ice formation. Concrete with w/c-ratio 0.60 and no air-entrainment. Data from Figure 5.3.3 and Figure 9.6.1.

Temp. int.	normal freezing rate, 3.6 °C/h			rapid freezing rate, 7.8 °C/h		
(°C)	dε/dt (‰/h)	dw_f/dt (g/g_{cem}·h)	$\frac{d\varepsilon/dt}{dw_f/dt}$	dε/dt (‰/h)	dw_f/dt (g/g_{cem}·h)	$\frac{d\varepsilon/dt}{dw_f/dt}$
-10 -(-15)	0.08	0.17	0.5	0.23	0.53	0.4
-15 -(-20)	0.11	0.12	0.9	0.24	0.27	0.9

It is interesting to note that the ratio between expansion and freezing rate is fairly the same within the same temperature interval independently of the cooling rate. The ratio is, however, increasing with decreasing temperature. This does not necessarily contradict the hydraulic pressure theory, since permeability could be expected to be reduced with reduced temperature. Only the effect of temperature on the viscosity of water will cause an increase in the ratio with a factor of at least 1.5 from –10°C to –20°C. This cannot explain the entire increase observed. The rest might be explained by reduced permeability caused by ice blocking the path for expelled water.

It is also interesting to note that both the expansion rate and the rate of ice formation are increased with increased cooling rate. The relation between cooling rates, expansion rates and ice formation rates are shown in Table 10.2.2.

Table 10.2.2. Relation between cooling rate, expansion rate and ice formation rate. Data from Table 10.2.1.

Temperature interval	Ratio of cooling rates	Ratio of expansion rates	Ratio of ice formation rates
-10°C to –15°C	2.2	2.9	3.1
-15°C to –20°C	2.2	2.2	2.2

For the temperature range –15°C to –20°C, the ice formation rate is increased exactly as much as the cooling rate. This is a rather trivial result, since the same amount of ice has to be formed at half the time when the cooling rate is doubled. The deviation at higher temperature probably depends on the big supercooling at the calorimeter experiments.

A very interesting result is that the rate of expansion is directly proportional to the rate of ice formation. When this is doubled, the expansion rate is also doubled. The expansion rate is directly proportional to the hydraulic pressure. The results therefore support the hydraulic pressure mechanism. Anyhow, they do not contradict that mechanism.

Also the *ice lens growth* mechanism might be promoted by an increased rate of temperature lowering, since that should cause bigger disturbance of free energy between water and ice, driving the process. On the other hand, increased freezing rate means that available time for ice lens growth is shorter. It might be that these effects counterbalance, which can explain why no effect of freezing rate was found.

There is also the possibility that a worsening effect of hydraulic pressure when freezing rate is increased is counterbalanced by a lessening effect of pressure from ice lens growth. It is not possible from the experiments to tell which mechanism is dominant.

4. The contraction of *air-entrained* concrete at temperature lowering is often taken as a proof of the ice lens growth theory. Ice in air-pores should attract water from the cement gel causing drying shrinkage. Therefore, these tests should in fact verify that ice lens growth is the dominant destruction mechanism. However, there are tests made for material containing practically no unfreezable water, and these do also contract much more than the normal thermal contraction. One example for hard-burnt brick is shown in Figure 10.2.1; Fagerlund (1972). Another example for sandstone is shown in Figure 10.2.2; Wessman (1997).

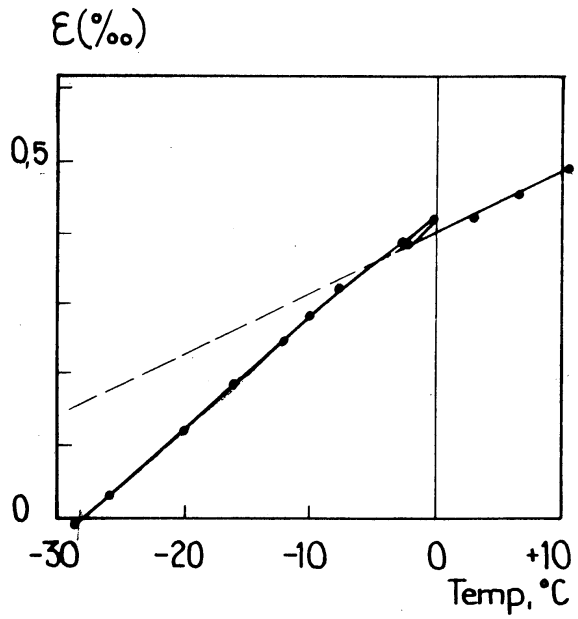

Figure 10.2.1. Length change versus temperature during freezing. Hard burnt brick with porosity 32%. Degree of saturation 0.68. Fagerlund (1972).

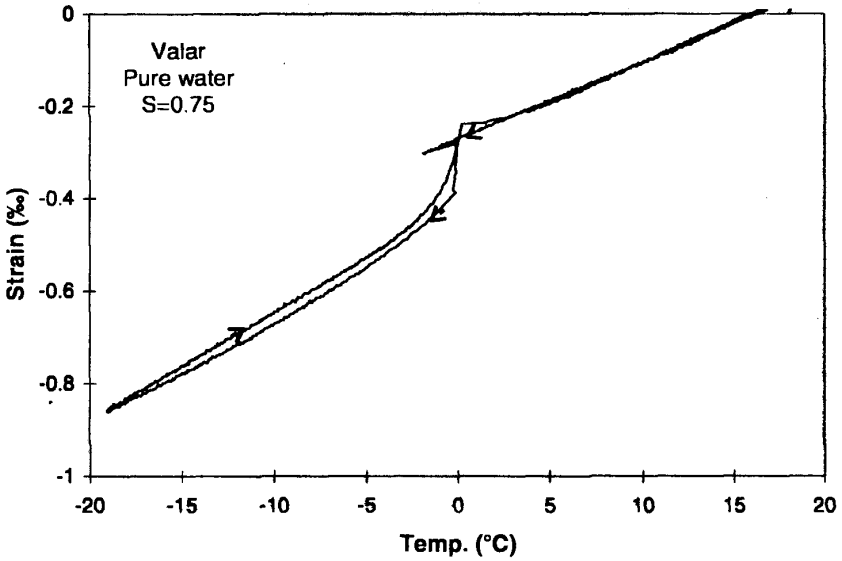

Figure 10.2.2. Length change versus temperature during freeze-thaw. Natural sandstone with porosity 17.4%. Degree of saturation 0.75; Wessman (1997).

For the *brick* ice lens growth is impossible, since it contains practically no unfrozen water, which was confirmed by tests. The most plausible mechanism is the big thermal contraction/expansion coefficient of ice compared to the stone itself. This can be shown by the following approximate calculation valid for the brick in Figure 10.2.1.

The thermal contraction coefficient of a composite material, α, might be approximately described by Eq. 2.5.1. The following data for ice are given in paragraph 2.5; Bulk modulus $1.5 \cdot 10^{10}$(Pa), Thermal expansivity $5 \cdot 10^{-5}$ m/mK

For stone material the bulk modulus depends on the porosity. For the brick in Figure 10.2.1 a plausible value is about $2 \cdot 10^{10}$ Pa. The thermal expansivity is about $0.8 \cdot 10^{-5}$m/mK for the unfrozen brick in Figure 10.2.1. The latter is calculated from the contraction before freezing.

According to calorimeter measurements, the amount of ice in the brick was $V_i = 0.22$. Almost all of this was formed at a few degrees below zero, which explains the linear contraction later on.

The calculated thermal contraction of the frozen brick becomes $\alpha = 1.5 \cdot 10^{-5}$ m/mK.

The observed thermal contraction is also $\alpha = 1.5 \cdot 10^{-5}$ m/mK.

The calculation indicates that *all* contraction of the frozen brick could be explained by this composite action of contraction of ice and solid material. Therefore, at least some of the contraction observed for *air-entrained concrete* can depend on the same mechanism. This is shown by a calculation for the concrete with w/c-ratio 0.60, Figure 5.3.7. The amount of frozen water in concrete with w/c-ratio 0.60 at –15°C is about $V_i = 0.07$, see paragraph 9.6. The contraction coefficient for concrete is about 10^{-5} and the bulk modulus about $2 \cdot 10^{10}$ Pa. The measured contraction coefficient of unfrozen concrete according to the test is $\alpha_s = 10^{-5}$ m/mK.

The calculated contraction coefficient becomes: $\alpha = 1.25 \cdot 10^{-5}$ m/mK.

The measured contraction coefficient of the frozen concrete is about $\alpha = 1.85 \cdot 10^{-5}$ m/mK. All contraction can therefore not be explained by the effect of ice contraction.

Concrete with w/c-ratio 0.40 has smaller contraction than w/c-ratio 0.60, which could depend on that the amount of frozen water is smaller. It is only about $V_i = 0.04$.

The behaviour of the sandstone in Figure 10.2.2 is more complex. Freezing of all pore water occurs within the range 0°C to –2°C. This is accompanied by considerable contraction, a phenomenon found for all sandstones

when the water content was low. The same behaviour has been observed for light-weight concrete at low moisture contents; Fagerlund (1972). The only plausible mechanism is that much of the ice formation takes place by rapid ice lens growth causing drying out the non-saturated material. When all pore water has turned into ice, there can only be thermal contraction that explains the continued contraction. The amount of ice is V_i= 0.13. The measured thermal expansivity of unfrozen sandstone is $1.6 \cdot 10^{-5}$ m/mK. The bulk modulus of sandstone is about $1.3 \cdot 10^{10}$ Pa. Thus, the calculated thermal expansivity of frozen sandstone is $2 \cdot 10^{-5}$ m/mK. The observed thermal coefficient is $2.1 \cdot 10^{-5}$ m/mK. The agreement is satisfactory.

5. The fact that almost no length changes took place when temperature was held constant, irrespectively of the duration of constant temperature, can be explained by the ice lens growth mechanism, since this predicts that ice can only grow when there is unbalance in free energy between ice and water, and that requires that temperature is changed. According to the hydraulic pressure mechanism the concrete should contract as soon as temperature is held constant and no ice is formed. The fact that no important contraction takes place does however not contradict the hydraulic pressure mechanism. Ice in non-air-entrained concrete might have caused considerable hydraulic pressure when it was formed leading to fracture (non-elastic deformation). When no more ice is formed the cracks and the ice hinders the concrete from contracting.

6. The direct proportionality between lowest temperature and expansion, which was found for non-air-entrained concrete (Figure 6.3.5) can be explained by the ice lens growth theory. A reduction in the lowest temperature by a factor 2 automatically leads to an increase by a factor 2 of the time when moisture migration to ice lenses can occur. Measurements of ice formation (paragraph 9.8) show that the amount of ice is not proportional to the lowest temperature, however, much less ice is formed between –15°C and –30°C than between 0°C and –15°C. This does not contradict the ice lens growth mechanism since there is not necessarily a direct proportionality between ice formed and expansion; viz. water flow does also cause shrinkage, and that is not necessarily directly proportional to the amount of ice or to the water flow.

   The proportionality can only be explained by the hydraulic pressure theory provided the permeability is supposed to be gradually reduced with reduced temperature because of ice blocking the water flow, and because of the con-

siderable higher viscosity of water at low temperature[1]. Then the lower rate of ice formation at lower temperature can be compensated for by a reduced permeability. According to the theory, the hydraulic pressure is namely directly proportional to the rate of ice formation and inversely proportional to permeability.

7. It has been claimed by some researchers that the main forces and damage occurs during the thawing phase. This could not be verified, since thawing always produced contraction compared to the expected expansion caused by pure thermal movement. Thus for all materials thawing must have caused relieve of stresses built up during the freezing phase.

8. The moisture isolated tests performed with specimens containing saline pore water gave some unexpected results, particularly for the salt concentrations 4.5% and 11%. The most confusing result was that air-entrainment did not protect the concrete. It even turned out to be detrimental, since the expansion and damage became even bigger than it was for non-air-entrained concrete.

   The reason behind these findings was not clarified. Some qualitative explanations are forwarded, but are not confirmed. More experimental and quantitative studies ought to be performed.

[1]) Based on measured viscosity of supercooled water in the range 0°C to –10°C one can estimate that the relation between viscosities are: $\eta_{-20}/\eta_0 = 2.2$ and $\eta_{-40}/\eta_0 = 5$. Handbook of Chemistry and Physics (1989).

11 Simultaneous measurements of ice formation/melting and length changes

11.1 Introduction

The length change measuring technique applied in Chapter 5-8 and the calorimeter measuring technique applied in Chapter 9 both proved to be useful in studying the effect of various moisture and temperature conditions on the behaviour of concrete during freezing and thawing. A combination of the two techniques would give still more detailed information on frost destruction mechanisms. Therefore, in Chapter 10, an attempt was made to link the results obtained by the two techniques. However, different samples were used for dilation and calorimeter tests. The specimen size was different, and although it was attempted to use exactly the same temperature cycles in the two types of experiments, for natural reasons there were some differences, like differences in supercooling. Therefore, although results of the analysis of the two types of tests performed in Chapter 10 are promising there could be questions on its relevance.

When the research project started attempts were made to make the measurements simultaneously by supplying the Setaram Calorimeter used in Chapter 9 with a device for measuring length change. Although much time and effort were devoted to this in earlier stages of the project, the results achieved were rather disappointing. It turned out to be very difficult to separate the movement of the calorimeter itself from movement of the specimen. Therefore, this technique had to be abandoned.

Later in the project, a combined calorimeter-dilatometer developed by Dr. Sture Lindmark, who was previously working at our Division, was used. This apparatus makes use of bigger specimens than those used in the Setaram calorimeter but this turned out not to be a drawback. The precision both in measurement of freezing/melting and in measurement of length changes was satisfactory. The apparatus was calibrated and tested by the author in cooperation with Dr. Lars Wadsö who is a researcher at our Division. A brief description of the apparatus is presented here. For further details regarding the apparatus and its calibration, see APPENDIX to Chapter 11, which is a reproduction of the article Fridh, Lindmark, Wadsö, (2003).

The idea of using a combined calorimeter-dilatometer for studies of frost destruction mechanisms emanates from a paper by Verbeck, Klieger (1958). An apparatus of this type was built and used in the 1970:ies for studies of freezing of cement paste and ceramic materials; some results are published in Fagerlund (1973b). The precision was not as high however as the one used in the present work. Combined calo-

rimetry and dilatometry using a Setram calorimeter has later been utilized by Penttala (1998).

11.2 Aim

The aim of the studies presented in this chapter was to examine the possibilities the combined calorimeter-dilatometer might provide in studies of frost destruction mechanisms. The aim was also to try to validate the studies presented in Chapters 5-9, but not to make a complete investigation of the same parameters as dealt with there.

11.3 The combined calorimeter-dilatometer

The apparatus and its function is described in more detail in APPENDIX to Chapter 11.

This instrument represents a combination of a scanning calorimeter of the heat-conduction type and an LVDT (Linear Variable Differential Transducer) dilatometer. It simultaneously measures heat production and heat consumption during freezing or thawing and the associated changes in length. Figure 11.3.1 and Figure 11.3.2 show cross-sections of the instrument.

The heat-flow is measured by eight thermocouple heat flow meters, which surround an aluminium vessel-holder. The sample (150 mm in height, 40 mm in diameter), is placed in a cylindrical Invar vessel located in the vessel holder (Figure 11.3.2). Invar, which is a metal alloy containing 36% Ni and 64% Fe, has a low coefficient of thermal expansivity ($2 \cdot 10^{-6}$ 1/K). The sample is situated between a cylindrical stud (diameter 2 mm) at the bottom and the LVDT dilatometer (Figure 11.3.2) at the top.

The calorimeter part of the instrument is of twin type consisting of two identical calorimeters, the sample in question being placed in the one, and a reference sample in the other (Figure 11.3.1). The reference should have approximately the same thermal properties as the sample and not show any phase transitions in the temperature region in which the measurements are made. In all of the measurements presented here, a reference sample of polyoxymethylene (POM) polymer with a heat capacity of 1.47 J/(g,K) (concrete C≈ 0.95 J/(g,K)) was employed The sample calorimeter and the reference calorimeter are connected differentially so that disturbances that affect either or both calorimeters are compensated for.

Surrounding the two calorimeter vessels are two aluminium heat sinks, the entire instrument being housed in a box made of 2 mm aluminium plate. Most of the

empty volume the instrument contains is filled with an insulating material consisting of extruded polystyrene.

The instrument is placed in a programmable low-temperature freezer with air as cooling and heating medium and an internal fan. The temperature of the calorimeter is controlled by the temperature of the surrounding air. The temperature is scanned rather slowly, normally. at 3 K/h.

The two LVDT dilatometers are fastened to the lids of the two Invar vessels (Figure 11.3.2). The temperature is measured at five separate points inside the calorimeter by means of type K thermocouples. The five points are; (i) the sample, (ii) the vessel holder, (iii) the heat sink of the sample, (iv) the reference vessel-holder, and (v) of the heat sink of the reference sample (these locations are shown in Figure 11.3.2).

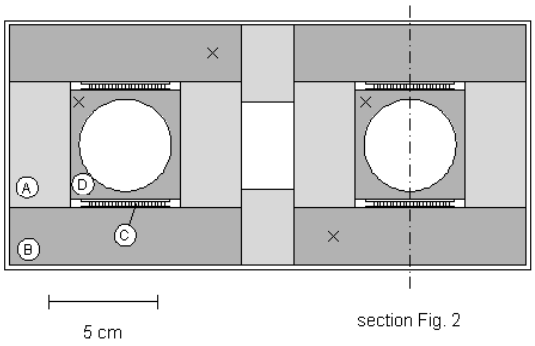

Figure 11.3.1. Schematic drawing of instrument (horizontal cross section). (A) Insulation, (B) Heat sink, (C) Heat flow sensor, (D) Vessel holder. The sample is placed in the vessel holder at the left and a reference sample is placed in the vessel holder at the right. The position of each of the thermocouples for temperature measurement is indicated by an x. The empty space in the center of the calorimeter houses the electrical wiring. The thermocouple of the sample is placed in a drilled hole situated as close to its center as possible.

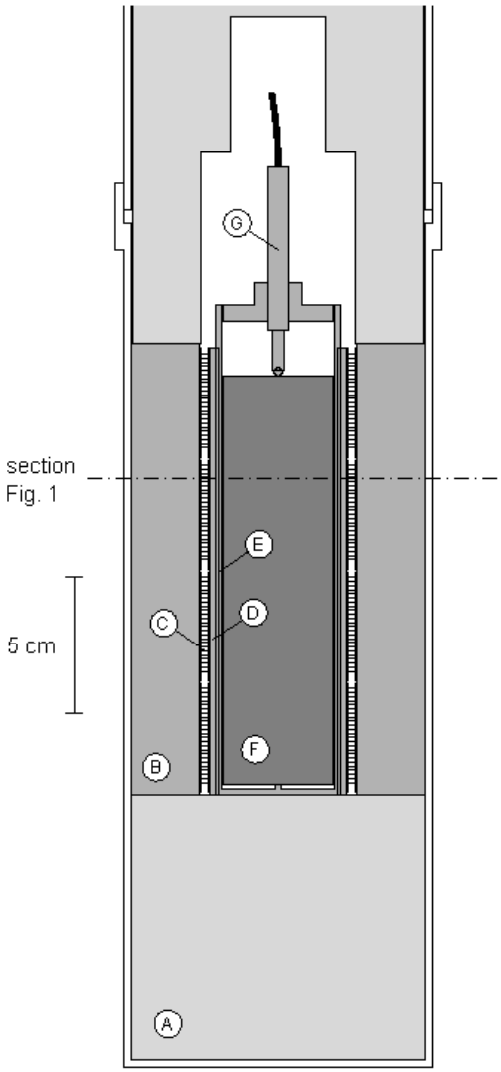

Figure 11.3.2. Schematic drawing of the instrument (vertical cross section). (A) Insulation, (B) Heat sink, (C) Heat flow sensor, (D) Vessel holder, (E) Vessel, (F) Sample, (G) LVDT Dilatometer. The top section of the calorimeter (containing insulation) is not shown.

Methods for evaluating the dilatometer and calorimeter results are described in APPENDIX to Chapter 11.

One very important difference between these measurements and the ones reported in Chapter 9 was that the temperature was measured in the middle of the sample instead of in the calorimetric block. In the latter case it sometimes looks as if ice in the specimen is present at temperatures above 0°C. In order to avoid this problem in the new equipment, a hole was drilled to the centre of the sample, and a thermocouple was placed in the hole. Thus the specimen temperature, and not the calorimeter block temperature, can be used in the evaluation.

A measurement with the combined calorimeter-dilatometer gives three outputs; (i) specimen temperature, (ii) heat flow rate, (iii) sample length change.

The temperature is only measured in one point in the sample. This is not representative for the whole specimen, due to temperature gradients within this. As an example, the sample thaws from the outside. This means that the measured temperature in the specimen is lower than at the surface or in the calorimeter vessel since ice still is being thawed inside the sample. However, the temperature gradients within the sample are low, and the temperature in all parts of the sample seldom differs more from the measured temperature than about 1 K.

Heat flow sensors measure the heat flow rate. As the thermal inertia of the parts inside these heat flow sensors is rather high (sample with water and ice, phase transformation of water/ice, vessel, vessel holder), and there is an air gap between the vessel and the vessel holder, the time constant of the calorimeter is rather high. The time constant is essentially the heat capacity of the parts inside the heat flow sensors divided by the thermal conductance between the sample and the heat sink outside the heat flow sensors. From electrical calibrations using a polymer sample with the same size as the mortar samples the time constant was found to be 1400 s. This is probably in the correct order also for the mortar samples as the polymer has similar heat capacity and thermal conductivity as the mortar. A high time constant results in a sizeable delay between when heat is produced in the sample and when the heat flow sensors measure this heat.

It is possible to correct for the time lag of the heat flow rate measurements of the scanning calorimeter by a procedure, which is similar to the so called Tian correction for isothermal calorimetry. Assume that we have a calorimeter with a sample with a heat capacity C (J/K) and a thermal conductance from the scanning heat sink to the sample of k (W/K). Let P (W) be the true heat production rate in the sample and F (W) the measured heat flow rate (heat leaving the sample through the heat flow sensors). If the temperature of the sample and scanning heat sink are $T_s(t)$ and $T_0(t)$, respectively we can write the following two equations describing heat flow (Fouriers law of heat conduction) and heat balance:

$$F = k(T_s(t) - T_0(t)) \qquad \text{Eq. 11.3.1}$$

$$\frac{dT_s}{dt} = \frac{P - F}{C} \qquad \text{Eq. 11.3.2}$$

By solving for T_s in Eq. 11.3.1, introducing this into Eq. 11.3.2, and solving for the true heat production rate we get:

$$P = F + \frac{C}{k}\frac{dF}{dt} + C\frac{dT_0}{dt} \qquad \text{Eq. 11.3.3}$$

This shows that the output signal is corrupted both by the thermal inertia and by the scanning rate. As noted above, C/k is the time constant (τ in units of s) and by introducing the (constant) scanning rate σ (K/s) we can write:

$$P = F + \tau\frac{dF}{dt} + C\sigma \qquad \text{Eq. 11.3.4}$$

With this equation we can calculate the heat production (or consumption) rate in the sample from the measured heat flow rate (through the heat flow sensors). It should be noted that the above equations involve some simplifying assumptions so the model should be considered as an approximate model. One such assumption is that the heat capacity C is inside the heat flow sensors having the thermal conductance k. In the real calorimeter this is not quite true as part of the resistance to heat flow is in the air gap situated between the sample holder and the sample ampoule holder (with about half the heat capacity on each side).

The third parameter, the sample length change, is measured for the whole sample and without any time delay. It is a sum of the length changes of all parts of the sample.

11.4 Test variables

11.4.1 Tested materials

Six materials (micro-concretes) were investigated; 2 w/c-ratios (0.60 and 0.40), and 3 air contents (natural, nominal 4%, nominal 6%). The goal was to obtain materials with properties as close as possible to those of the materials used before (see APPENDIX to Chapter 3) in the tests described in Chapters 5-9, the previous recipes thus being used with minor adjustments. The basic material variables are shown in Chapter 3. The detailed recipes and air contents are presented in APPENDIX to

Chapter 11. A separate 400x400x150 mm mould was produced for casting one block for each of the six materials. During the first 24 hours, the newly cast micro-concrete in the mould was covered with wet cloths, covered by a plastic foil. After the blocks had been demoulded, they were stored submerged in lime-saturated water for two years before specimens (diameter 36 mm, length 150 mm) were drilled out perpendicular to the direction of casting. The two outer centimetres had been sawed off prior to drilling so as to avoid any influence of the surface of the mould. When a sample was tested it had either just been drilled out of the block, or had been vacuum-saturated. Prior to vacuum saturation, samples were dried at +105°C.

The degree of saturation in the specimen during the test (denoted S_A) defined in Eq. 4.5.3 was determined according to method described in paragraph 4.5. The values are given in the figures below showing the results. Data for the specimens used in the tests are given in Table 11.4.1.

11.4.2 Temperature cycles

The freeze/thaw cycles used were as follows. The cycles are shown in Figure 11.4.1.

- Cycle I: The majority of the specimens were subjected to a temperature cycle aimed at resembling as closely as possible the 'normal' freezing and thawing cycle used in the studies presented in Chapter 5 and 9. Both vacuum-saturated samples and samples with natural water content reached after 2 years in water were tested. Results for specimens with natural water content are presented in this paragraph. Figure 11.5.1-Figure 11.5.8.
- Cycle II: Two samples that were vacuum-saturated were tested with a freeze-thaw cycle resembling the one that was used in Chapter 7 and 9 for studies of the influence of duration of lowest temperature.

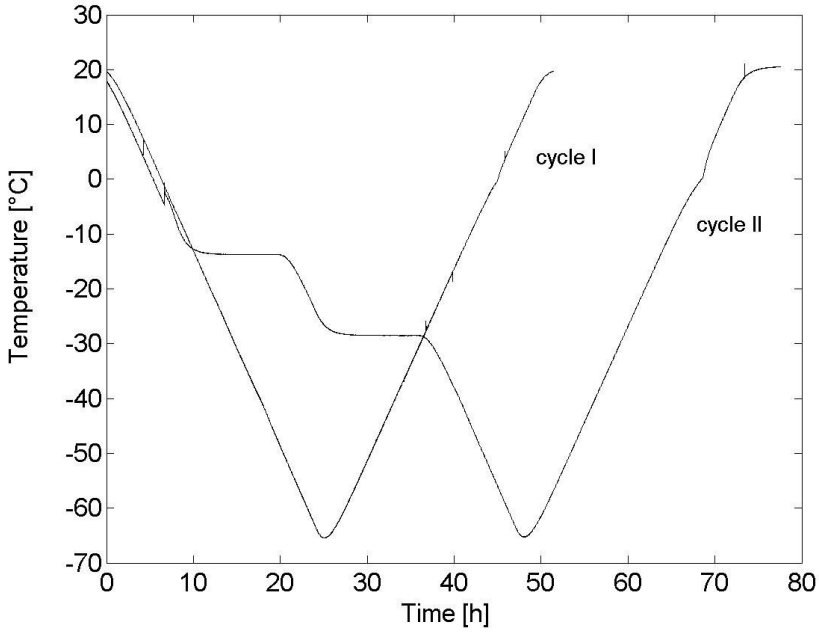

Figure 11.4.1. Typical temperature cycles in specimens.

11.4.3 Damage parameters

Damage caused by the one-cycle freeze/thaw was determined in the same way as for the length change measurements in Chapter 5-8:

1. Maximum dilation during the cooling phase
2. Permanent dilation after thawing
3. Dynamic E-modulus

Dilation is defined by Figure 4.4.4. Dynamic E-modulus is determined from the resonance frequency at transverse vibration of the specimen. This was determined before and after the freeze/thaw cycle by use of the apparatus Grindosonic, see paragraph 4.4.

11.4.4 Overview over the experiments

An overview over the experiments and properties for each specimen are given in Table 11.4.1. Not all experiments were presented as diagrams but as damage data in Table 11.4.1. Results for saturated specimens are shown in paragraph 11.7.

Table 11.4.1. Overview over experiments presented in paragraphs 11.5 and 11.6. C-cement content, w_e=amount evaporable water, S_A degree of saturation (for definition see paragraph 4.5)

w/c-ratio	Fresh air content (%)	Cycle I			Cycle II		
		C (g)	w_e (g)	S_A	C (g)	w_e (g)	S_A
0.60	1.9	49.25	21.60	0.987	48.32	22.79	1
	1.9	48.61	23.762	1			
	5.0	48.23	20.31	0.814			
	5.0	49.33	24.18	1			
	6.7	48.20	21.47	0.719			
	6.7	50.89	29.59	1			
0.40	2.5	72.58	20.02	0.905			
	2.5	73.10	20.24	1	73.10	21.27	1
	4.9	72.48	19.62	0.783			
	4.9	74.75	24.68	1			
	6.4	71.82	21.29	0.756			
	6.4	75.77	27.09	1			

11.5 Temperature cycle I (continuous)

11.5.1 Introduction

The results of length change and ice formation and melting for two non-air-entrained and two air-entrained samples exposed to freeze-thaw cycle I are shown in Figure 11.5.1-Figure 11.5.8. To be able to display the results graphically it was necessary to use different scales in different figures.

11.5.2 Non-air entrained materials

Examples of results for non-air-entrained samples are shown in Figure 11.5.1-Figure 11.5.4. For each concrete two types of diagrams are shown; the first shows individual curves for ice formation/melting and length change. The second shows length change versus ice formation/melting.

w/c-ratio 0.60

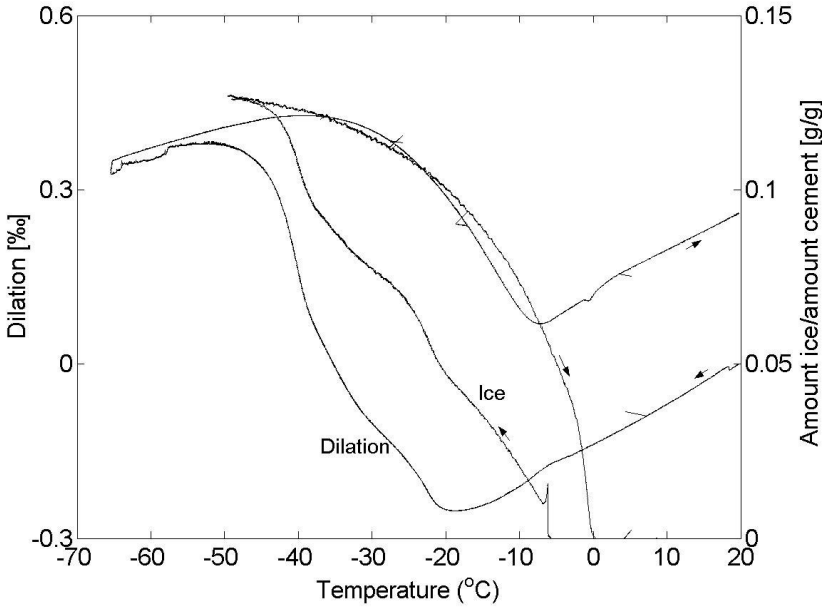

Figure 11.5.1. Ice formation and melting, and length change in a sample with a w/c-ratio of 0.60 without air-entrainment, S_A=0.987.

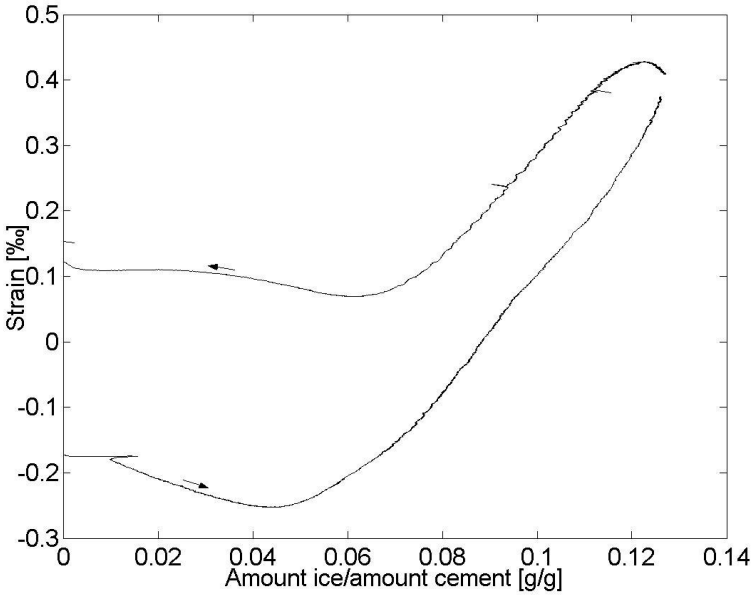

Figure 11.5.2. Strain versus ice formation and melting in a sample with w/c-ratio 0.60 with no air-entrainment. S_A=0.987.

At the beginning there is no ice formation and consequently linear contraction. Nucleation of the first ice causes no length change. Thereafter, as more ice is gradually formed, the contraction increases and is somewhat bigger than contraction extrapolated from the unfrozen specimen. At about -20°C, when a sufficient amount of ice has formed, there is no room left for the additional ice formation and the specimen starts to expand. It can be clearly seen that within the temperature range -20°C to -45°C a change in ice formation affects the dilation in almost the same proportion. Since the rate of temperature lowering is constant this observation means that the rate of expansion is directly proportional to the rate of ice formation. Such behaviour is predicted both by the hydraulic pressure mechanism and the closed container mechanism.

The total volume expansion between -20°C and -45°C is about 3·0.08‰=2.4‰ or 0.34 cm^3 (expansion calculated from the extrapolated thermal contraction). The corresponding ice formation is about 0.075 g/g cement, which gives about 4.0 cm^3 of frozen water in the specimen. Its expansion at freezing is 0.36 cm^3. Thus, all ice formation within this temperature range causes expansion indicating that ice formation occurs as in a closed container.

A simple *test of the hydraulic pressure mechanism* can be made by comparing the ice formation rate and the expansion rate in two temperature intervals with different rates; -20°C to -25°C and -38°C to -42°C.

According to the hydraulic pressure mechanism the following relation is valid, assuming all parameters (including permeability) being constant.

$$P_h = Const \frac{dw_f}{dt} \qquad \text{Eq. 11.5.1}$$

where P_h is the hydraulic pressure and dw_f/dt is the rate of ice formation.
The expansion rate of the specimen ought to be proportional to the hydraulic pressure: i.e.:

$$\frac{dL}{dt} = Const \frac{dw_f}{dt} \qquad \text{Eq. 11.5.2}$$

where dL/dt is the rate of expansion.

Range -20°C to -25°C: dwf/dt=0.014 g per g cement per hour
dL/dT= 0.059 ‰ per hour
Range -38°C to -42°C: dwf/dt=0.022 g per g cement per hour
dL/dT= 0.165 ‰ per hour

The ratio of ice formation rates is: 0.022/0.014=1.6
The ratio of expansion rates is: 0.165/0.059=2.8

Thus, the expansion rate is higher at the lower temperature, which contradicts the hydraulic pressure theory. However, complete agreement should exist if the permeability is supposed to be about halved at the lower temperature. This is not unrealistic considering the big amount of ice formed and the lower viscosity at lower temperature.

During heating there is at first a period of expansion, probably caused by combined relaxation of ice pressure due to some melting, and ordinary thermal expansion. At temperature above about -30°C, the specimen contracts almost linearly with the amount of ice melted. The last ice melting taking place between -5°C and 0°C seems to cause expansion, which is equal to the expansion of the unfrozen specimen. One should have expected that this expansion should not have started until all ice was melted. The reason for this discrepancy is the time lag between the actual temperature in the specimen determining expansion and the observed melting calculated from the calorimeter response. This defect has minor importance, however, since damage takes place during freezing and not during thawing.

The completely thawed specimen has big permanent expansion indicating severe frost damage.

w/c-ratio 0.40

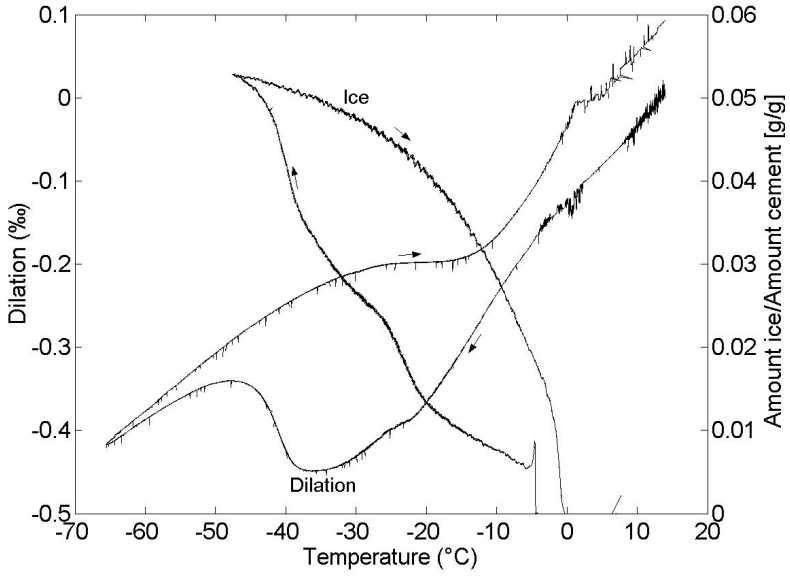

Figure 11.5.3. Ice formation and melting, and length change in a sample with a w/c-ratio of 0.40 without air-entrainment, S_A=0.905.

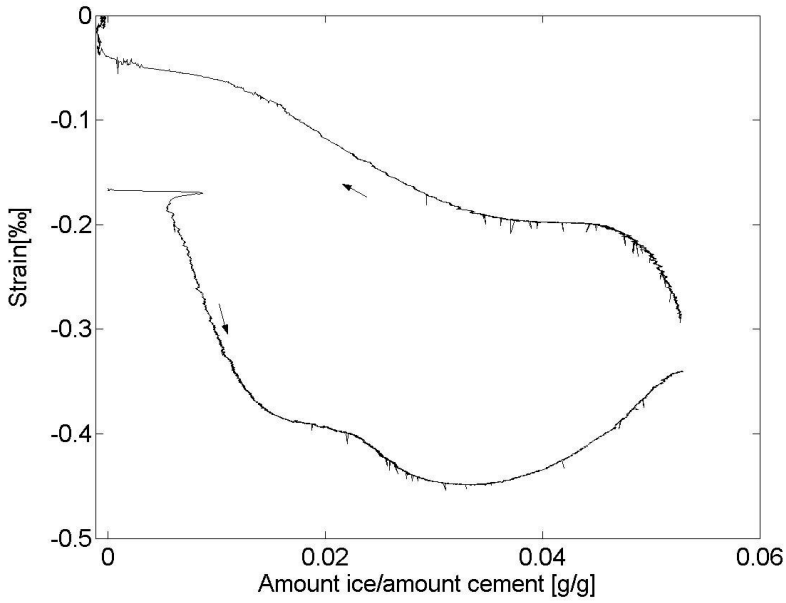

Figure 11.5.4. Strain versus ice formation and melting in a sample with w/c-ratio 0.40 with no air-entrainment. S_A=0.905.

The amount of ice formed, and the dilation are smaller than for w/c-ratio 0.60, as expected. A big difference from the specimen with w/c-ratio 0.60 is that the specimen continues to contract to as far as -35°C. This contraction, being bigger than the normal thermal contraction, indicates that microscopic ice lens growth, accompanied by drying, takes place. The volume contraction between -5°C and -35°C is about 3·0.27‰=0.8‰ or 0.12 cm^3. The amount of ice formed within the same temperature range is about 0.03 g/g cement or 2.2 g in the specimen. This corresponds to an expansion of 0.09·2.2= 0.2 cm^3. Thus, the contraction is of the same order as the volume expansion of water at freezing.

There is a slight decrease in contraction (a 'bump' in the contraction curve) within the range -20°C to -30°C. In this range the rate of ice formation is increased. Thus, the 'bump' might be explained by hydraulic pressure occurring as a consequence of increased rate in ice formation due to local supercooling is overcome.

When temperature is reduced further, from about -38°C to -45°C very much ice is formed. The specimen expands, probably because this rapidly formed new ice formation cannot be totally taken care of within the pores. The volume expansion between -38°C and -45°C is about 0.3‰ or 0.04 cm^3. The corresponding ice formation in this range is about 0.017 g/g cement or 1.3 cm^3 of frozen water. The volume

expansion of ice is 0.12 cm^3. Thus, within this temperature range the specimen expansion is about 40% of the volume expansion of ice.

At warming, the specimen expands until -30°C as a consequence of thermal expansion somewhat reduced due to relaxation of internal stress caused by melting. Within the range -30°C to -15°C the specimen length is almost constant despite big ice melting, which shows that relaxation of internal stresses due to melting almost exactly compensates thermal expansion due to warming. Thereafter the specimen contracts in direct proportion to the amount of melted ice.

At complete thawing, the specimen does not regain its initial length. The permanent expansion indicates that some damage has occurred, probably due to the ice formation around -40°C.

11.5.3 Air entrained materials

Examples of results for air-entrained samples are shown in Figure 11.5.5-Figure 11.5.8. For each concrete two types of diagrams are shown; the first shows individual curves for ice formation/melting and length change. The second shows length change versus ice formation/melting

w/c-ratio 0.60

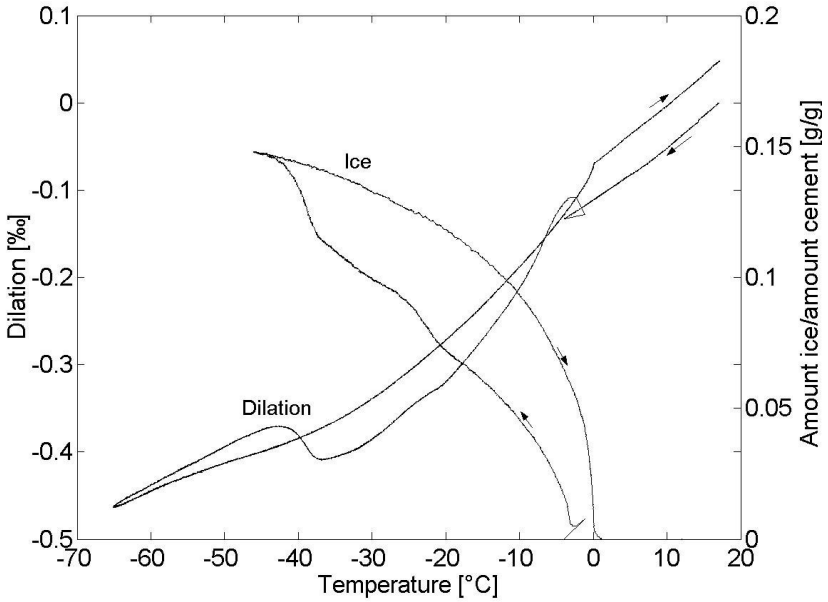

Figure 11.5.5. Ice formation and melting, and length change in a sample with a w/c-ratio of 0.60 and 6% air content, S_A=0.719.

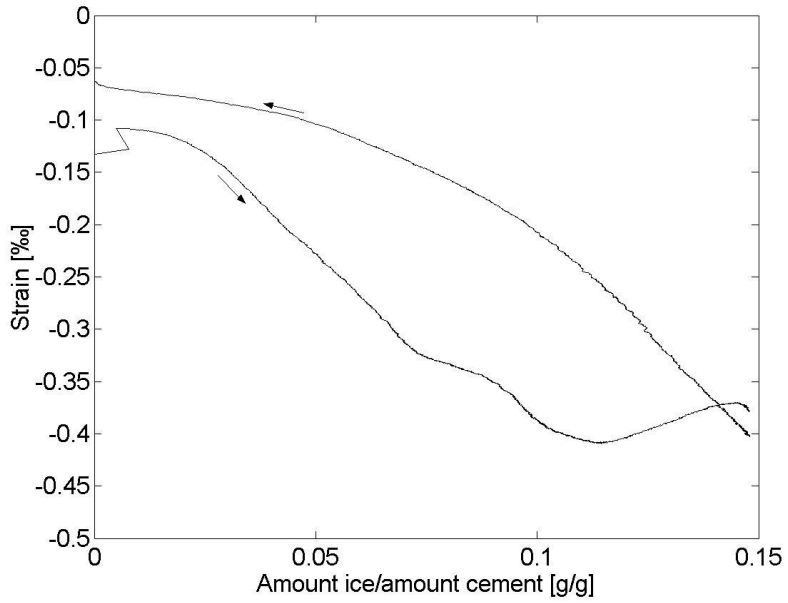

Figure 11.5.6. Strain versus ice formation and melting in a sample with w/c-ratio 0.60 and 6% air content, S_A=0.719.

A difference from the non-air-entrained concretes is that supercooling produces some expansion. This is small, however, and cannot cause damage.

The result is similar to that for non-air-entrained concrete with w/c-ratio 0.40, see Figure 11.5.3 and Figure 11.5.4. There is considerable contraction down to about -35°C, probably caused by a combination of normal thermal contraction and shrinkage caused by ice lens growth. Also for this specimen there is a slight decrease in contraction (a 'bump' in the contraction curve) within the range -20°C to -28°C. The 'bump' is accompanied by an increase in ice formation rate.

Within the range -38°C to -42°C there is considerable expansion probably as a consequence of the rapid and quite big ice formation. The volume expansion is about 0.24‰ or 0.035 cm^3. The corresponding ice formation is 0.034 g/g cement or 1.7 cm^3 frozen water. The volume expansion at freezing is 0.15 cm^3. Thus, most of the ice expansion in this range does not cause expansion of the specimen.

Warming causes a gradual expansion. The curve, expansion versus amount of melted ice, becomes more levelled the higher the temperature. Thus, a given amount of melted ice creates smaller expansion the closer to 0°C the temperature is. This indicates that internal stress exists also in air-entrained concrete and that this stress is

more relaxed at higher temperature. The completely thawed specimen has some permanent expansion indication that damage has occurred.

w/c-ratio 0.40

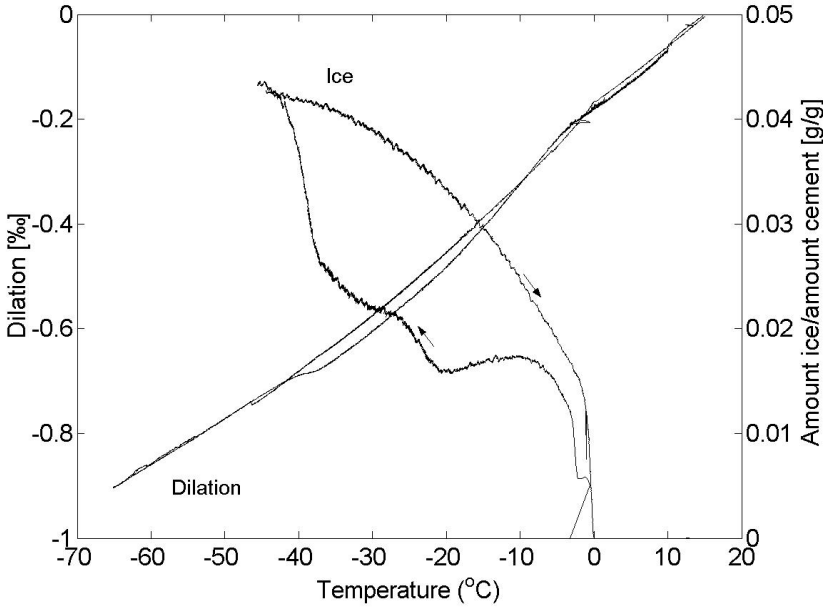

Figure 11.5.7. Ice formation and melting, and length change in a sample with a w/c-ratio of 0.40 and 4% air content, S_A=0.783.

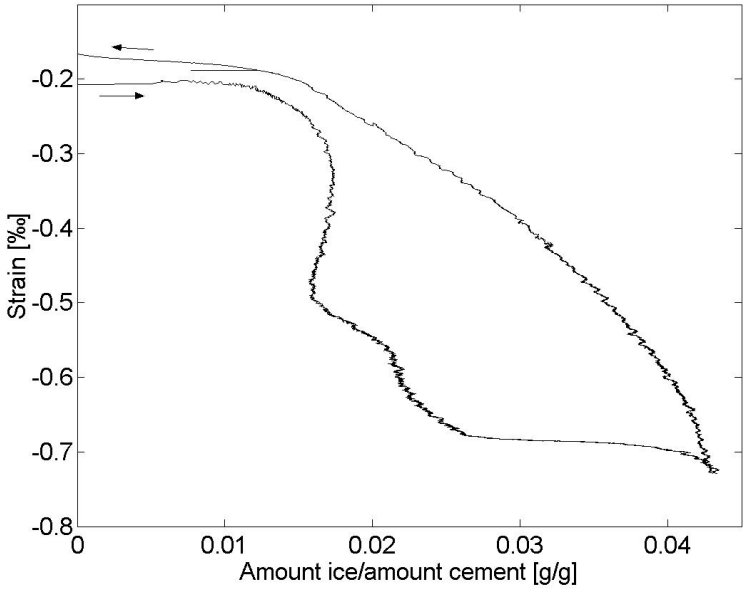

Figure 11.5.8. Strain versus ice formation and melting in a sample with w/c-ratio 0.40 and 4% air content, S=0.783.

The behaviour is very similar to that for w/c-ratio 0.60. Contraction bigger than normal thermal contraction down to about -35°C à -38°C and thereafter small expansion accompanied by considerable ice formation down to about -42°C.

11.5.4 Temperature cycle I. Summary

In this summary all the 12 tests performed with the combined calorimeter-dilatometer are considered, not only the 4 tests presented by figures above.

A: Summary, dilation-calorimeter curves

The behaviour is similar for all concrete types:

1. No, or slight, expansion when the first ice is nucleated at a few degrees below 0°C. The expansion is not big enough to cause damage.
2. Contraction that is bigger than normal thermal contraction from about -5°C down to about -20°C for non-air-entrained concrete with w/c-ratio 0.60 and to about -35°C for air-entrained concrete and non-air-entrained concrete with w/c-ratio 0.40. The contraction occurs despite considerable continuous ice formation within this temperature range. The reason for the extra contraction is probably drying caused by ice lens growth. The volume contraction of ice is bigger than that of concrete and will therefore also contribute to the extra contraction.
3. Within the range -20°C to -30°C there is a decrease of the normal contraction rate accompanied by an increase in the rate of ice formation. This 'bump' in the contraction curve might be caused by hydraulic pressure appearing as a result of the more rapid ice formation.
4. Considerable expansion within the temperature range -20°C to -45°C for non-air-entrained concrete with w/c-ratio 0.60. The volume expansion is equal to the volume expansion of frozen water indication 'closed container freezing'. For non-air-entrained concrete with w/c-ratio 0.40 expansions in this temperature range does not take place.
5. Considerable expansion and ice formation for all concrete types within the range -38°C to -42°C.
6. Warming of non-air-entrained concrete causes continuous expansion. The expansion rate is largest at low temperature but is gradually reduced as more and more ice melts and internal stresses thereby are relieved. For non-air-entrained concrete with w/c-ratio 0.60 considerable contractions takes place at temperature above about -30°C. This is caused by melting of 'constrained' ice.

B: Summary, damage parameters

After terminated freeze/thaw the fundamental frequency of transverse vibration was determined. The square of this is a measure of the 'dynamic E-modulus'. The results are shown in Figure 11.5.9.

Table 11.5.1. Data concerning the damage parameters, where S_A is the degree of saturation (for its definition see 4.5), RF^2 is the relative residual resonance frequency squared, Perm.dil. is the permanent dilation (see 4.4 for definition), Max dil is the maximum dilation when thermal contraction is accounted for.

w/c-ratio	Nom. air content (fresh) %	S_A	RF^2	Perm.dil (‰)	Max.dil (‰)
0.4	Natural (2.45)	0.905	0.96	0.08	0.35
0.4	Natural (2.45)	1	0.84	0.47	1.06
0.6	Natural (1.9)	0.987	0.78	0.27	0.73
0.6	Natural (1.9)	1	0.60	0.86	2.14
0.4	4 (4.9)	0.783	1	0	0
0.4	4 (4.9)	1	0.80	0.52	1.18
0.6	4 (5)	0.814	0.98	0	0
0.6	4 (5)	1	0.76	0.45	1.36
0.4	6 (6.4)	0.756	0.99	0.47	0.71
0.4	6 (6.4)	1	0.89	0.23	0.61
0.6	6 (6.7)	0.719	0.96	0.05	0.06
0.6	6 (6.7)	1	0.12	0.51	1.4

In Figure 11.5.9 different damage parameters are plotted against each other and against the concrete parameters, degree of saturation, w/c-ratio and air content. As was found in the length change tests in Chapter 5-7 the degree of saturation is the parameter that has the biggest effect on damage. The relation between permanent dilation and maximum dilation is fairly constant, as was found in the previous length change tests.

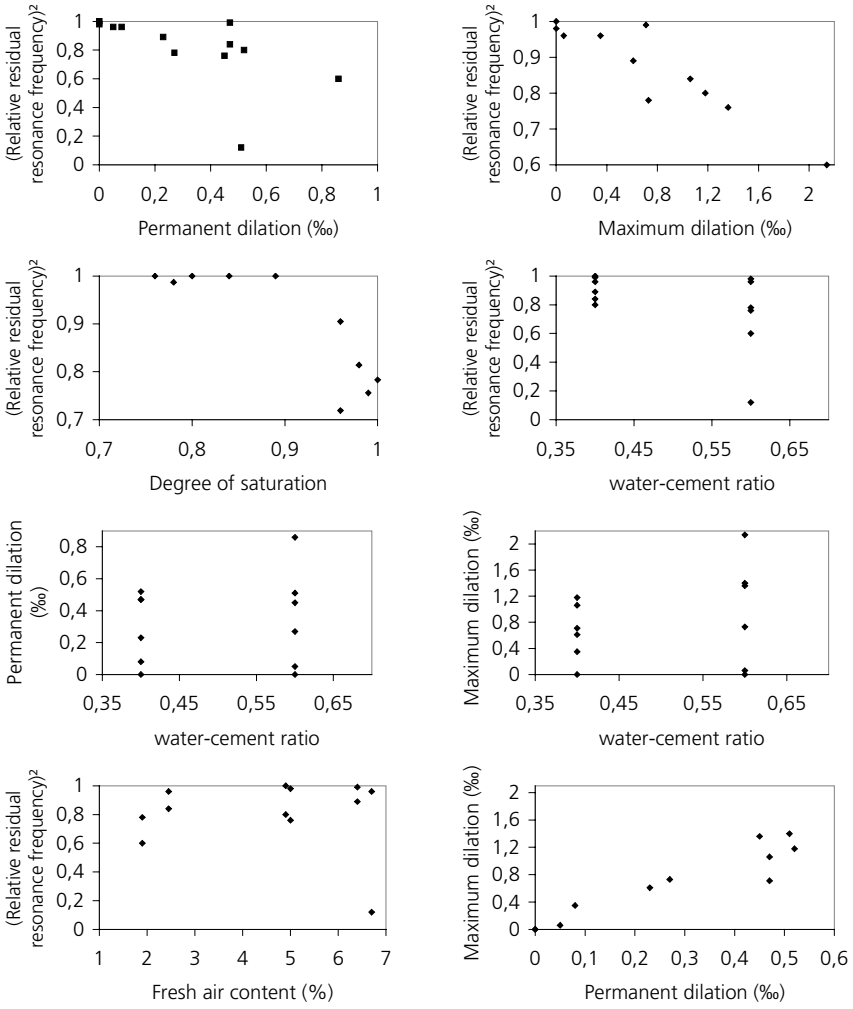

Figure 11.5.9. Damage parameters, data from Table 11.5.1.

11.6 Temperature cycle II (two isothermal periods)

Two specimens were investigated with Temperature cycle II. Both specimens were vacuum saturated. The results are shown in Figure 11.6.1 to Figure 11.6.4.

w/c-ratio 0.60

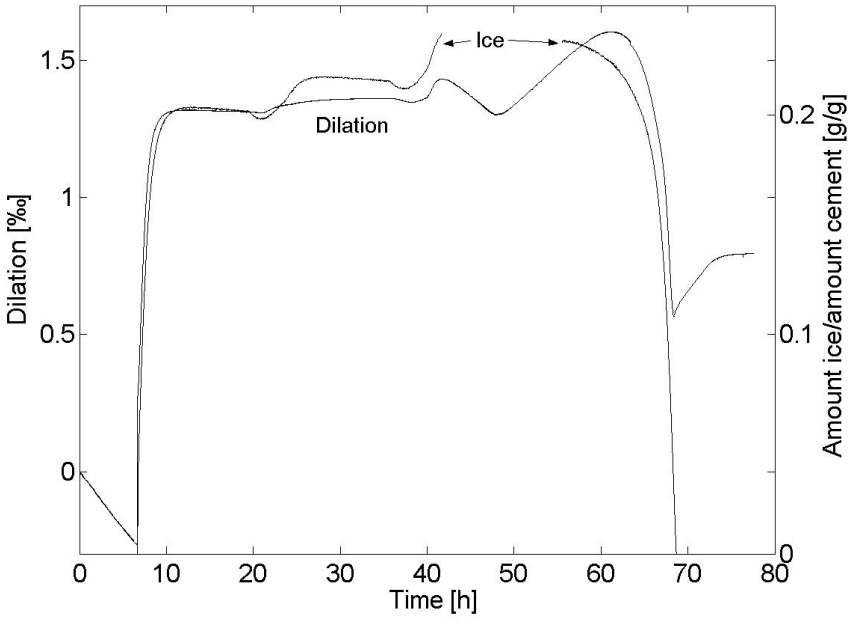

Figure 11.6.1. Dilation and ice formation or melting in a non-air-entrained vacuum saturated sample with w/c-ratio 0.60.

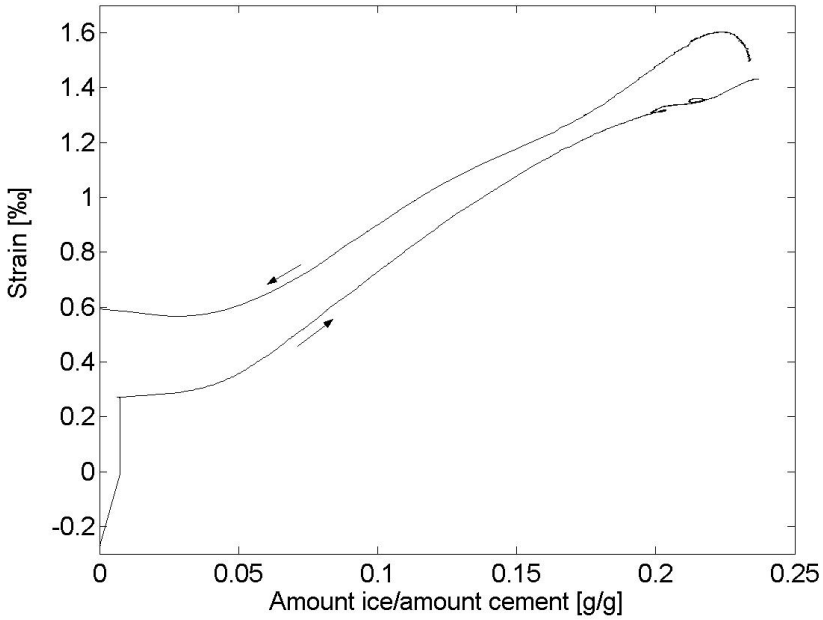

Figure 11.6.2. Strain versus ice formation or melting in a non-air-entrained vacuum saturated sample with w/c-ratio 0.60.

The dilation curve is almost affine with the ice formation curve. When temperature is lowered to -15°C big ice formation and big expansion occurs. The volume expansion in this temperature range is about 4.8‰ or 0.67 cm^3. The amount of ice formed is about 0.2 g/g cement or about 10 cm^3. This gives an ice expansion of about 0.9 cm^3. Thus, almost all expansion that is caused by ice formation gives volume expansion of the specimen, indicating that ice is formed as in a closed container. This is logical since there is no pore space empty if saturation has been complete. The only possibility to relieve some stresses is that excess water is forced out through the specimen surface.

When temperature is held constant at -15°C and -30°C for 12 hours no ice formation and no volume change takes place.

At melting the contraction curve is fairly affine with the ice melting curve showing that internal stresses are relieved when ice melts. The contraction curve lies above the expansion curve showing that damage has occurred.

w/c-ratio 0.40

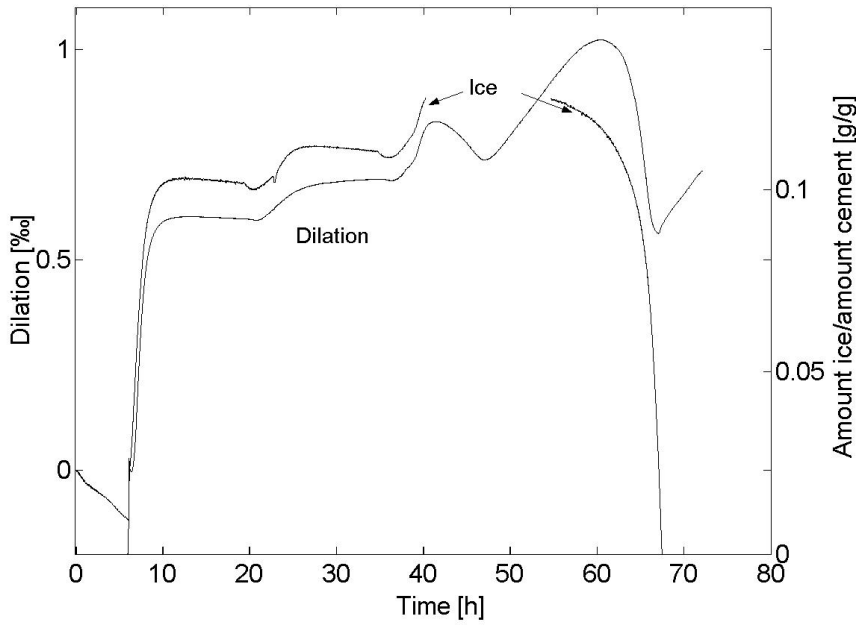

Figure 11.6.3. Dilation and ice formation or melting in a non-air-entrained vacuum saturated sample with w/c-ratio 0.40.

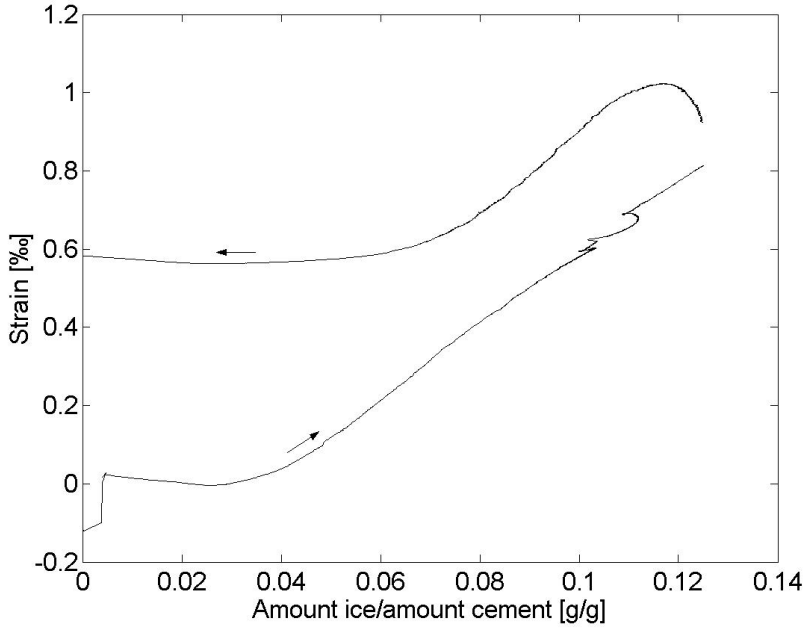

Figure 11.6.4. Strain versus ice formation or melting in a non-air-entrained vacuum saturated sample with w/c-ratio 0.40

Also for w/c-ratio 0.40 the dilation curve is rather affine with the ice formation curve. The dilation between when the first ice is formed and -15°C is about 2.1‰ or 0.32 cm^3. The ice formation is about 0.1 g/g cement or 7.5 cm^3 frozen water giving an ice expansion of 0.68 cm^3. Thus, some of the ice expansion has been taken care of within the pore system. This means that all air-pore space in this dense concrete could not be water filled at the vacuum treatment.

No ice formation and almost no length changes were observed when temperature was held constant.

When most of the ice melts around 0°C, there is a time lag between the registration of melted ice and the contraction. This is caused by the large amount of ice in saturated specimens.

11.7 The influence of the degree of saturation

In paragraphs 11.5 and 11.6 results for specimens with natural water contents reached after two years in water are presented. Some specimens were completely saturated after pre-drying and vacuum treatment. Results from tests of these specimens are presented below in Figure 11.7.1- Figure 11.7.4. Data from specimens with natural water content are plotted in the same figures for comparison.

w/c-ratio 0.60

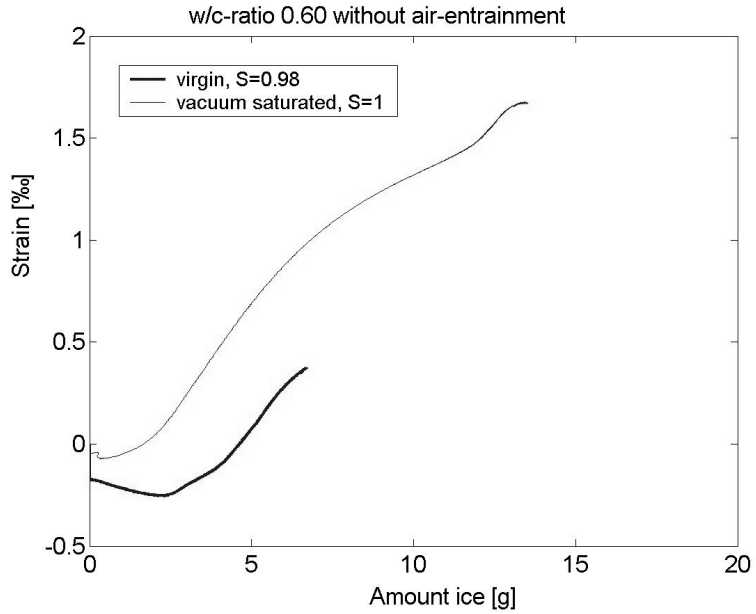

Figure 11.7.1. Strain due to the amount of ice formed in a material with a w/c-ratio of 0.60 without air-entrainment.

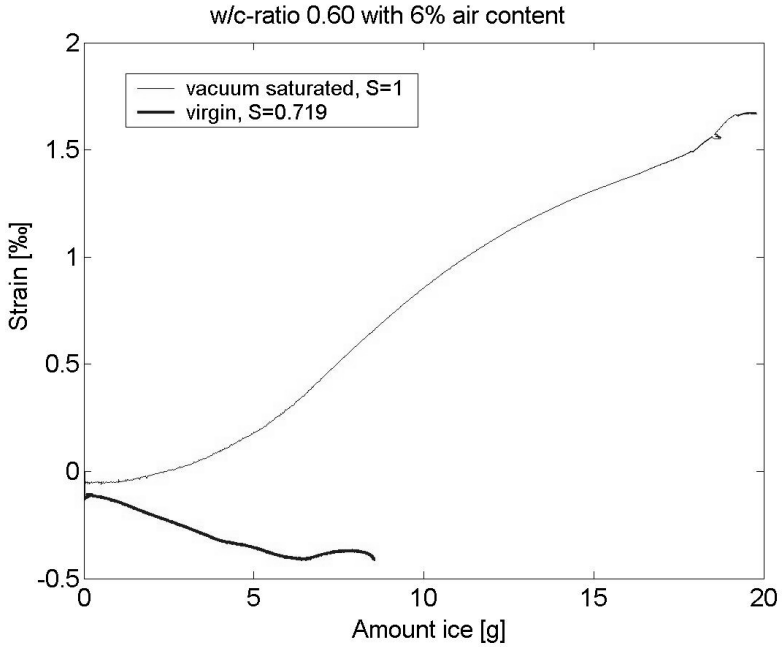

Figure 11.7.2. Strain due to the amount of ice formed in a material with a w/c-ratio of 0.60 and 6% air content.

For *saturated non-air-entrained concrete* there is almost a direct proportionality between ice formed and expansion (except for the very first ice formation where a certain contraction occurs). This is expected since there is no space left for ice formation. When the amount of ice formed is 10 g corresponding to an expansion of 0.9 cm^3, the volume expansion is 4‰ corresponding to 0.6 cm^3. This indicates that some ice has found room inside the specimen in pores that were not completely saturated. Some water might also have been expelled thorough the specimen surface.

The *non-saturated concrete without air-entrainment* (S=0.98) has considerably lower expansion showing that the first ice is accommodated in air-filled spaces. First when some ice is formed the volume expansion follows ice formation in the same way as for saturated concrete

For *saturated air-entrained concrete* expansion does not follow the ice formation curve which clearly shows that the specimen was not completely saturated. At an ice formation of 20 g corresponding to 1.8 cm^3 expansion, the volume expansion of the specimen is only 5.1 ‰ corresponding to a specimen expansion of 0.75 cm^3.

The non-saturated specimen contracts as more ice is formed.

w/c-ratio 0.40

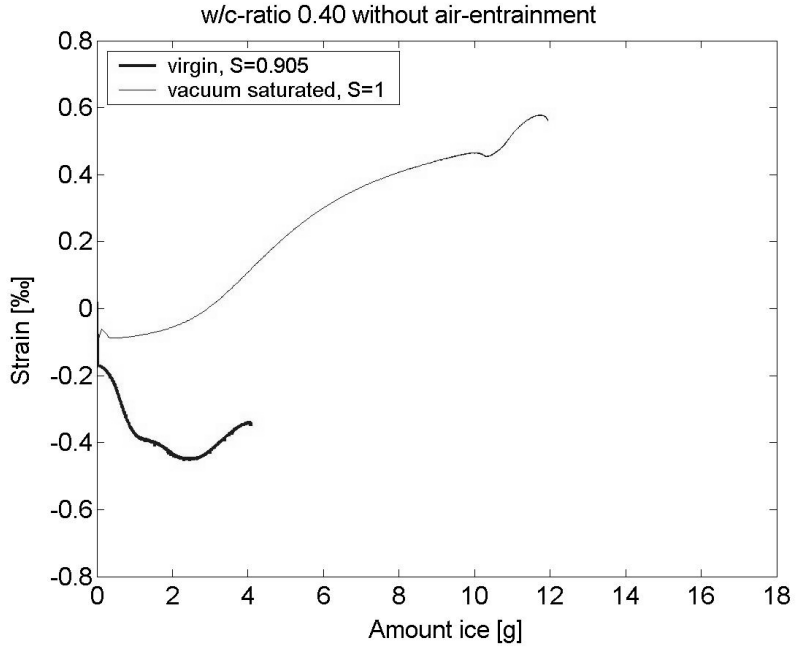

Figure 11.7.3. Strain due to the amount of ice formed in a material with a w/c-ratio of 0.40 without air-entrainment.

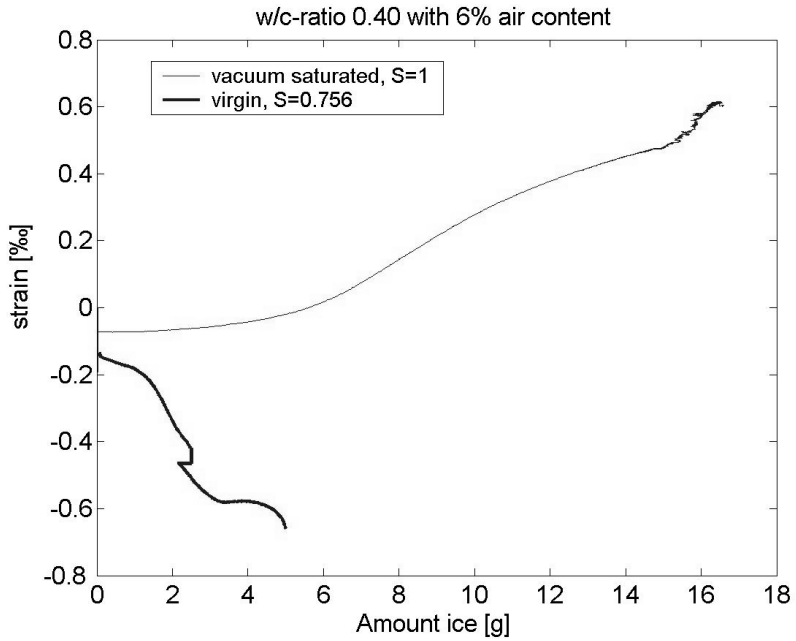

Figure 11.7.4. Strain due to the amount of ice formed in a material with a w/c-ratio of 0.40 and 6% air content.

The *saturated non-air-entrained* concrete expands all the time as more ice is formed. The expansion is however lower for the initial ice formation. As for w/c-ratio 0.60 the expansion is too small indicating that the specimen was not saturated; 10 g ice only caused 0.2 cm^3 expansion of the specimen, when 0.9 cm^3 is expected in a saturated specimen.

The *saturated air-entrained* concrete had even lower expansion showing the difficulty in saturating concrete with low w/c-ratio and high air content.

12 Conclusions and future work

12.1 Conclusions

The *general* aim of this work was to try to identify the destruction mechanism behind internal frost damage, by performing studies of the effect of important internal and external variables, varied independently of each other. By observations of the effect of each variable on the freeze/thaw behaviour, information on the acting mechanism should be obtained. The general aim could not be fully reached, since the two main mechanisms, the hydraulic pressure mechanism and the ice lens growth mechanism, can cause similar effects on concrete that is more than critically saturated. Furthermore, it seems as if different mechanisms are active at different stages of the freezing process, and at different concrete types. The studies, however, produced a large amount of data from which the following conclusions can be drawn, and also speculations about the destruction process be made:

1. Initial ice formation when super-cooled water is nucleated was often big. It caused big and rapid destructive expansion of *non-air-entrained concrete*. The cause of expansion is probably *hydraulic pressure* appearing as a result of water being forced away from the freezing site due to the 9% increase in volume at ice formation. Thus, each capillary, in which ice formation took place, behaved like a sort of *"closed container"* expanding as ice was formed in it. Expansion was not recovered when the first freezing was terminated which indicates that capillary ice blocks specimen contraction.

   In *air-entrained concrete*, initial expansion was observed, but it was not big enough to cause permanent damage. This strengthens the hypothesis that the hydraulic pressure mechanism is active at early nucleation. In air-entrained concrete the spacing between air pores is so small that water can be expelled without causing big internal stress.

   In a real structure surrounded by air supercooling is probably much smaller, and can therefore not cause damage.

2. The rate of ice formation, after the early ice formation when super-cooled water was nucleated, was almost directly proportional to the rate of cooling. Also the rate of expansion of *non-air-entrained concrete* was almost directly proportional to the rate of cooling and ice formation. This seems to confirm the *hydraulic pressure mechanism* according to which expansion is directly proportional to internal pressure. It does not fully confirm the closed container

mechanism, however, since expansion was smaller than the 9% increase in volume at freezing.

3. The cooling rate had no effect on the expansion-temperature curve of *non-air-entrained concrete*. At first sight this might contradict the conclusion above, that expansion rate was proportional to the cooling rate. However, it does not, since an increased cooling rate also means a shorter exposure time. Thus, increasing the cooling rate will cause the same total expansion at each given temperature. Total expansion is proportional to the amount of ice formed, and not to the rate by which this is formed.
4. The ratio between expansion rate and ice formation rate was found to increase with decreased temperature. This does not contradict the hydraulic pressure mechanism since viscosity of water is very much reduced with reduced temperature; using viscosity data for super-cooled water, one can estimate that the permeability of concrete at -40°C is only about 20% of the value at 0°C. Ice blocking the flow path of expelled water will further reduce permeability.
5. For most *air-entrained concrete,* cooling caused contraction that was bigger than the normal thermal contraction of the unfrozen concrete. This shows that no destructive pressure appears inside the concrete. This behaviour is predicted both by the hydraulic pressure mechanism and the ice lens growth mechanism. The fact that the contraction was bigger than the thermal indicates that growth of ice in air-pores takes place. It does however not contradict a simultaneously occurring hydraulic pressure, which in this case is not big enough to cause expansion. Some of the "extra" contraction could be explained by the bigger thermal contraction coefficient of ice than of concrete.
6. In *air-entrained concrete* with low water-cement ratio (0.40) some expansion was observed during freezing, indicating internal pressure. This was however not big enough to cause damage. The expansion could possibly be explained by the hydraulic pressure mechanism, since concrete with low w/c-ratio has considerably smaller permeability. On the other hand, also the rate of ice formation is smaller, reducing hydraulic pressure. The expansion could also be explained by the ice lens growth mechanism since more unfrozen water driving the process is available at lower w/c-ratio. It is not possible from the results to tell which mechanism is dominant.
7. When cooling is momentarily stopped, expansion of *non-air entrained concrete* and contraction of *air-entrained concrete* immediately stopped. Also ice

formation was found to stop immediately. These observations contradict the *hydraulic pressure* mechanism since according to that, the concrete ought to contract momentarily when ice formation stops. Ice formed by "closed *container* freezing" might however hinder contraction when hydraulic pressure vanishes. According to the *ice lens growth* mechanism, continued expansion is expected, unless local equilibrium between unfrozen water and ice is established immediately when temperature change is stopped. The halt in length changes does therefore not contradict or confirm any of the destruction theories.

8. The duration of a constant low temperature had no effect on length changes, which is reasonable sine all ice formation was stopped as long as temperature was held constant.

9. For *non-air-entrained concrete* a reduction of the lowest temperature from -15°C to –30°C caused a doubling of expansion. This can be explained both by the combined hydraulic pressure/closed container theory, and by the ice lens growth theory. Lowered temperature causes increased hydraulic pressure, also when the ice formation rate is reduced at lower temperature, depending on the lower permeability. Furthermore, even if hydraulic pressure should be reduced, ice formed in expanded capillaries will block contraction. Lowered temperature means longer freezing time. This makes ice lens growth continue for longer time. In the actual freezing cycle time is namely directly proportional to temperature.

10. In *air-entrained concrete* lowered temperature had no big effect on contraction. There are some uncertain indications that contraction increases with decreased temperature. Such a behaviour is predicted by the ice lens growth theory, since lower temperature gives longer available time for moisture transfer and drying.

11. Rapid ice formation was always observed at about -40°C. The few measurements of length changes, that were performed at that low temperature in the combined calorimeter-dilatometer showed rapid and big expansion at about -40°C. This is a clear indication of hydraulic pressure. The reason for the big ice formation is probably that locally super-cooled water freezes by homogeneous nucleation.
12. Warming from the lowest temperature caused expansion in almost all samples. The expansion was, however always smaller than the expected thermal expansion of a stress-free specimen, which indicates that internal stresses are

relieved when temperature is increased. Calculations and observations confirm that warming does not cause any destructive forces.

13. Thawing of ice always occurs at higher temperature than freezing of ice. This hysteresis phenomenon probably depends on local supercooling in isolated capillaries during the freezing phase. The hysteresis is much less pronounced in pre-dried and re-saturated concrete.

14. Increased w/c-ratio had the following effects; (i) increased amount of freezable water and decreased fraction of non-freezable water, (ii) increased expansion and damage in non-air-entrained concrete, both at nucleation of supercooled water and at continued freezing after that, (iii) bigger positive effect of air-entrainment. These effects, except the last, were anticipated already before the work.

15. Increased air content had very favourable effect, since expansion during freezing changed to contraction, or to very much reduced expansion (for w/c-ratio 0.40).

16. The moisture content during the test was the material parameter that had dominating effect, overshadowing effects of w/c-ratio and air content. The higher the degree of saturation, the bigger the amount of frozen water, since water absorbed in air pores is freezable, the bigger the expansion, and the bigger the damage. Increased degree of saturation has the same very negative effect as a combination of reduced air content and increased amount of freezable water.

17. Saline pore water was found to cause some highly unexpected results, such as bigger expansion despite lower amount of freezable water, and also negative effects of air pores. The observations cannot be explained by the usual theories. Possibly, the expansion is caused by osmotic pressure occurring as a result of salt concentration differences between water in pores containing ice and unfrozen water.

There were some additional conclusions to be drawn:

1. The results were reproducible. The same typical behaviour was found in repeated tests performed in different test series using different specimens, but the same pre-treatment.

2. The tests clearly demonstrated that one single freeze-thaw cycle is enough to distinguish a frost resistant concrete from a non-resistant. Thus, the multi-freeze/thaw cycles used in traditional tests are not required. They probably

lead to a water absorption that is unnatural, and not representative for the real structure.

3. The attempt to determine freezing and thawing of pore water by using the sorption isotherms turned out not to work. The non-freezable water was under-estimated. This shows that low temperature calorimetry has to be used.
4. The combined calorimeter-dilatometer instrument seems to be a valuable tool for further studies of freeze-thaw of porous materials. It must also be a good instrument for evaluation of the frost resistance of new untried materials.

12.2 Future research

Only some of the most essential research fields are taken up:

1. *Service life and water absorption in air pores*
   The ultimate aim of all durability studies should be to make it possible to develop reliable methods for *service life prediction*. This should also be the aim of studies of internal frost action. The present work, like many others, clearly indicates that frost damage will depend on the moisture condition in the concrete structure. Therefore, much effort should be spent on trying to find relations between the moisture level in the concrete and internal damage. The moisture condition in the structure varies with time, and these variations determine service life. They must therefore be known.

   Frost damage almost always requires that some air pores are water-filled. Methods should therefore be developed for calculation of the water absorption process in air-pore systems of different shape, and to find methods for translating external moisture conditions into internal moisture-time field in the concrete structure.

2. *The critical distance*
   It seems to be verified, both theoretically and experimentally, that frost damage will only occur when the spacing between air-filled pores transgresses a critical distance. The value of this is unclear. It is also unclear how the critical distance should be calculated. Its value also has to depend on how water is distributed in the air pore system, and that is a function of the moisture history. A service life model cannot be established until the true critical distance and how this depends on moisture conditions have been determined by combined theoretical and experimental work.

3. *The destruction process*
   The present work provides much information that has been used for qualitative reasoning of destruction mechanisms. The information is based on observations of the concrete response in terms of length changes and ice formation. The exact destruction mechanism could however not be established due to lack of some information. Suggested research is:

   - For assessment of hydraulic pressure and closed container freezing more information is needed on the permeability as function of temperature. Permeability measurements could possibly be made on frozen specimens of simple shape.

- A mechanical model for relations between internal hydraulic pressure and expansion/contraction ought to be developed. A serious complication is that fracture, and therefore non-linear (plastic) deformation occurs.
- For assessment of ice lens growth direct measurements of internal water flow ought to be made. This is hardly possible. Experimental observations of changes in relative humidity in the concrete might be used as a substitute. The idea has previously been exploited by Penttala (1998) and (1999). The combined calorimeter-dilatometer described in Chapter 11 could be a suitable base-instrument for such studies.

4. *The closed container mechanism*
   The closed container mechanism might be active in concrete with water-filled defects (cracks, saturated coarse aggregate, separation pockets, etc.) Such defects are very important since they might cause extensive destruction. The significance of the closed container mechanism for understanding destruction caused by defects ought to be investigated.

References

Ahlgren, L. (1972), 'Moisture fixation in porous building materials', Division of Building Technology, Report 36, In Swedish.

Arnfelt, H. (1943), 'Damage on concrete pavements by wintertime salt treatment', Statens Väginstitut, Meddelande 66, (In Swedish).

Atkins, P.W. (1998), 'Physical chemistry, 6th ed.' Oxford University Press.

Bager, D.H. and Sellevold, E.J. (1980a), 'Ice Formation in Hardened Cement Paste – II. Steam cured Pastes with Variable Moisture Contents', *Durability of Building Materials and Components, ASTM STP 691*. P.J. Sereda and G.G. Litvan, Eds., American Society for Testing and Materials, pp. 439-454.

Bager, D.H. and Sellevold, E.J. (1980b), 'Low temperature calorimetry as a pore structure probe', proceedings of the 7th International congress on the chemistry of cement, vol IV, Paris, pp 394-399.

Bager, D.H. and Sellevold, E.J. (1986a), 'Ice Formation in Hardened Cement Paste, Part I – Room Temperature Cured Pastes With Variable Moisture Contents', *Cement and Concrete Research,* vol 16, pp. 709-720.

Bager, D.H. and Sellevold, E.J. (1986b), 'Ice Formation in Hardened Cement Paste, Part II – Drying and Resaturation on Room Temperature Cured Pastes', *Cement and Concrete Research,* vol 16, pp. 835-844.

Bager, D.H. and Sellevold, E.J. (1987), 'Ice Formation in Hardened Cement Paste, Part III – Slow Resaturation of Room Temperature Cured Pastes', *Cement and Concrete Research,* vol 17, pp. 1-11.

Bergström, S-G. (1955), 'Salt damage on concrete pavements wintertime', Swedish Cement and Concrete Research Institute, Investigations No. 3, (In Swedish).

Beskow, G. (1935), 'Frost formation and frost heave with special consideration to roads and railways', Sv Geol underökn Årsbok 26 (1932), No 3. (In Swedish).

Brun, M., Lallemand, A., Quinson, J-F. and Eyraud, C. (1977), 'A new method for the simultaneous determination of the size and shape of pores: The thermoporometry', *Themochimica Acta*, 21, pp 59-88.

Cady, P.D. (1969), 'Mechanisms of frost action in concrete aggregates', Journal of materials, vol 4, No 2.

Cahn, R.W. (1966), 'Metal Systems', Composite Materials, Edited by Hollidy, L. Elsevier Publishing Company.

Collins, A.R. (1944), 'The destruction of concrete by frost', *Journal of the Institute of civil engineering*, 23, London.

CONTECVET (2001). EC Innovation project IN30902I. 'A validated Users Manual for assessing the residual service life of concrete structures. Manual for assessing concrete structures affected by frost', Division of Building Materials, Lund Institute of Technology.

Defay, R., Prigogine, I. and Bellemans, A. (1966), 'Surface tension and adsorption', Trans. by Everett, D.H., Longmans, Green & Co Ltd.

Everett, D.H. (1961), 'The thermodynamics of frost damage to porous solids', Trans. Faraday Soc, 57.

Fagerlund, G. (1972), 'Critical degrees of saturation at freezing of porous and brittle materials', Division of Building Materials, Lund Institute of Technology, Report 34, in Swedish.

Fagerlund, G. (1973a), 'Determination of pore-size distribution from freezing-point depression', Matériaux et constructions, vol 6, No 33.

Fagerlund, G. (1973b), 'Significance of critical degree of saturation at freezing of porous and brittle materials', ACI Symposium "Durability of concrete", Ottawa 1973, ACI Special publications, Detroit 1975.

Fagerlund, G. (1974), 'Non-freezable water contents of porous building materials', Division of Building Materials, Lund Institute of Technology, Report 42.

Fagerlund, G. (1977), 'The international cooperative test of the critical degree of saturation method of assessing the freeze/thaw resistance of concrete', *Materials and Structures*, vol. 10, no. 56.

Fagerlund, G. (1980), 'Testing of frost resistance', *International Colloquim on Frost-Resistance of Concrete*, Vienna, Mitteilungen aus den Forschungsinstitut des Vereins der Österreichischen Zement-Fabrikanten, Heft 33.

Fagerlund, G. (1992), 'Effects of the freezing rate on the frost resistance of concrete', *Nordic Concrete Research*, Publication no. 11, pp 20-36.

Fagerlund, G. (1997), 'Internal frost attack – State of the art', Proc. Rilem Workshop 'Resistance of concrete to freezing and thawing with or without de-icing chemicals, eds. Setzer M.J. and Auberg R., Essen.

Fagerlund, G. (2004), 'A service life model for internal frost damage in concrete', Division of Building Materials, Lund Institute of Technology, Report TVBM-3119.

Fagerlund, G. and Johannesson, B. (2005), 'Concrete for low temperature storage of natural gas. Ice formation and frost resistance.', Division of Building Materials, Lund Institute of Technology, Report TVBM-7185.

Fridh, K. and Johannesson, B. (2005), 'Calculating ice amounts from calorimetric measurements', Division of Building Materials, Lund Institute of Technology, Report TVBM-7186.

Fletcher, N.H. (1970), 'The chemical physics of ice', Cambridge University Press.

Fridh, K., Lindmark, S. and Wadsö, L. (2003), 'A combined temperature scanning calorimeter and dilatometer for studies of freeze/thaw effects in porous materials', *Nordic Concrete Research*, Publication no. 29, pp 37-51.

Gregg, S.J. and Sing, K.S.W. (1967), 'Adsorption, surface area and porosity', Academic Press, London and New York.

Handbook of Chemistry and Physics (1989), 70th Edition, CRC Press.

Helmuth, R.A. (1960), 'Capillary size restrictions on ice formation in hardened Portland cement pastes', 4th *International symposium on the chemistry of cement*, Washington D.C.

Helmuth, R.A. (1961) 'Dimensional Changes of Hardened Portland Cement Pastes Caused by Temperature Changes', Highway Research Board, Proceedings Vol 60, p315-335.

Jacobsen, S. (1995), 'Scaling and cracking in unsealed freeze/thaw testing of Portland cement and silica fume concretes', Doctoral thesis, Division of Structural Engineering, Concrete section, The Norwegian Institute of Technology.

Kaufmann, Josef. (1999), 'Experimental Identification of Damage Mechanisms in Cementitious Porous Materials on Phase Transition of Pore Solution under Frost De-Icing Salt Attack', École Polytechnique Fédéral de Lausanne, Thése No 2037.

Klamrowski, G. and Neustupny, P. (1984), 'Untersuchungen zur Prüfung von Beton auf Frostwiderstand', Bundesanstalt für Materialprüfung (BAM), Forschungsbericht 100.

Klieger, P. (1956), 'Effect of entrained air on strength and durability of concrete with various sizes of aggregates', Highway Research Board, Bulletin 128.

Klieger, P. (1980), 'Something for nothing – Almost', Concrete International.

Kukko, H. (1995), 'Frost effects on high strength concrete without air-entrainment', Concrete under severe conditions, Eds Sakai, K., Banthia, N., Gjørv, O.E., E & FN Spon.

Laidler, K.J. and Meiser, J.H. (1995), 'Physical Chemistry', 2nd ed. Houghton Mifflin Company, Boston.

Langham, E.J. and Mason, B.J. (1958), 'The heterogeneous and homogeneous nucleation of supercooled water', Proc. Royal Society, London, A247.

le Sage de Fontenay, C. (1982), 'Ice formation in cement paste' (Danish), Technical University of Denmark, Department of civil engineering, Building Materials Laboratory, Technical report 101/82.

le Sage de Fontenay, C. and Sellevold, E.J. (1980), 'Ice Formation in Hardened Cement paste – I. Mature Water Saturated Pastes', *Durability of Building Materials and Components, ASTM STP 691*. P.J. Sereda and G.G. Litvan, Eds., American Society for Testing and Materials, pp. 425-438.

Lindmark, S. (1995), 'Influence of testing conditions on salt scaling resistance of concrete', Division of Building Materials, Lund Institute of Technology, Project High Performance Concrete, Rapport M2:05.

Lindmark, S. (1998), 'Mechanisms of salt frost scaling of Portland cement-bound materials: Studies and hypothesis', Doctoral thesis, Division of Building Materials, Lund Institute of Technology, TVBM-1017.

Lindmark, S. (2000), 'Studies of relationships between the air void system and the salt frost resistance of concrete', In Swedish, Division of Building Materials, Lund Institute of Technology, SBUF-project 9010, TVBM-3089.

Malhotra, M.V., Painter, K.A. and Bilodeau, A. (1987), 'Mechanical properties and freezing thawing resistance of high strength concrete incorporating silica fume'. ASTM, Cement Concrete and Aggregate. Vol 9, No 2.

Marchand, J., Pleau, R. and Gagné, R. (1995), 'Deterioration of concrete due to freezing and thawing', *Materials Science of Concrete IV*, Jan Skalny, Sidney Mindess Eds.

Mather, B. (1982), Discussion of 'Critical air void spacing factors for concretes submitted to slow freeze-thaw cycles' by Pigeon, M. and Lachance, M, *Journal of the American Concrete Institute*, pp. 239-240.

Penttala, V. (1998), 'Freezing-Induced Strains and Pressures in Wet Porous Materials and Especially in Concrete Mortars', *Advanced Cement based Materials,* Vol 7, Nr 1, pp 8-19.

Penttala, V. (1999), 'Strains and Pressures Induced by Freezing Mortars Exposed in Sodium Chloride Solution', *Concrete Science and Engineering,* Vol 1, pp 2-14

Petersson, P-E. (1975), 'Salt-frost resistance of concrete. Field tests', Swedish National Testing and Research Institute, SP Report 1995:73, (In Swedish).

Pigeon, M. and Lachance, M. (1981), 'Critical air void spacing factors for concretes submitted to slow freeze-thaw cycles', *Journal of the American Concrete Institute*, 78, pp. 282-291.

Pigeon, M. and Pleau, R. (1995), 'Durability of concrete in cold climates', Modern Concrete Technology series, Vol. 4, E & FN Spon.

Pigeon, M., Prévost, J. and Simard, J-M. (1985), 'Freeze-thaw durability versus freezing rate', *Journal of the American Concrete Institute,* 82, pp. 684- 692.

Powers, T.C and Brownyard, T.L. (1948), 'Studies of the physical properties of hardened Portland cement paste. Part 8. The freezing of water in hardened Portland cement paste', Research Laboratories of the Portland Cement Association, Bull. 22.

Powers, T.C and Helmuth, R.A. (1953), 'Theory of volume changes in hardened Portland-cement paste during freezing', Proceedings, *Highway Research Board* 32, Bull. 46.

Powers, T.C. (1945), 'A working hypothesis for further studies of frost resistance' *Journal of the American Concrete Institute*, 16, pp. 245-272.

Powers, T.C. (1949), 'The air requirements of frost-resistant concrete', Proceedings, *Highway Research Board* 29, PCA Bull. 33.

Powers, T.C. (1955), 'Basic considerations pertaining to freezing and thawing tests', Proceedings, ASTM, V.55,PP. 1132-1155.

Powers, T.C. (1956), 'Resistance of concrete to frost at early ages', Proceedings, Rilem Symposium on winter concreting.

Powers, T.C. (1965), 'The mechanism of frost action in concrete', Stanton Walker Lecture No 3, Silver Springs, Md. National Sand and Gravel Association/National Ready Mixed Concrete Association.

REHABCON (2004). Strategy for Maintenance and Rehabilitation in Concrete Structures. EC Innovation Project No. IPS-2000-0063. Work Package 2.3 Evaluation of alternative repair and upgrading options. Div. Building Materials, Lund Institute of Technology. Report TVBM-7177.

Rønning, T. (2001), 'Freeze-thaw resistance of concrete, effect of: curing conditions moisture exchange and materials', Doctoral thesis, Department of Structural Engineering, Faculty of Civil and Environmental Engineering, Norwegian University of Science and Technology, Trondheim.

Schulson, E.M. (1998), 'Ice damage to concrete', Cold Regions Research & Engineering Laboratory, Special report 98-6.

Sellevold, E.J., Bager, D.H., Klitgaard-Jensen, E. and Knudsen,T. (1982), 'Silica fume cement pastes hydration and pore structure', In Condensed Silica Fume in Concrete, Technical Institute of Norway. Institute of Building Materials, Report BML 82.610.

Sellevold, E.J. and Farsted, T. (1992), 'Frost/salt-testing of concrete. Effects of test parameters and concrete moisture history in freeze-thaw and de-icing resistance of concrete', Research Seminar, Lund June 1991. Lund Institute of Technology, Division of Building Materials, Report TVBM-3048.

Setzer, M.J. (1997), 'Basis of testing the freeze-thaw resistance: surface and internal deterioration', Proc. Rilem workshop 'Resistance of concrete to freezing and thawing with or without de-icing chemicals, Eds. Setzer M.J. and Auberg R, E & FN Spon.

Setzer, M.J. and Auberg, R. (1997), Rilem workshop: Resistance of concrete to freezing and thawing with or without de-icing chemicals, E & FN Spon.

Setzer, M.J. (2002), 'Development of the micro-ice-lens model', Frost Resistance of Concrete, Proceedings, Editors, Setzer, M.J., Auberg, R., Keck, H-J., Rilem Publications S.A.R.L, Canchan.

Setzer, M.J., Auberg, R. and Keck, H_J. (2002), Frost Resistance of Concrete, Proceedings, Rilem Publications S.A.R.L, Canchan.

Taber, S. (1930), 'Mechanics of frost heaving', Journal of Geology, 38, pp. 303-317.

Tange Jepsen, M. (2002), 'Salt frost scaling – interaction of transport mechanisms and ice formation in concrete', Doctoral thesis, Building Technology, Danish Technological Institute and Aalborg University.

Utgenannt, P. (2004), 'The influence of aging on the salt-frost resistance of concrete', Doctoral thesis, Division of Building Materials, Lund Institute of Technology, TVBM-1021.

Valore, R.C. (1950), 'Volume changes in small concrete cylinders during freezing and thawing' *Journal of American Concrete Institute*, vol 21, no 6.

Verbeck, G., Klieger, P. (1957), 'Studies of salt scaling of concrete', *Highway Research Board,* Bulletin 150.

Verbeck, G., Klieger, P. (1958), 'Calorimeter – Strain Apparatus for Study of Freezing and Thawing Concrete", *Highway Research Board,* Bulletin 176.

Vesikari, E. (1985), 'Image analysis in determining pore size distributions of concrete' Technical Research centre of Finland, Research notes 437.

Vesikari, E. (1988), 'The effects of ageing on durability of concrete including by-products', VTT Symposium 89, Durable concrete with industrial by-products.

Vuorinen, J, (1969), 'On the behaviour of hardened concrete during freezing', The State Institute for Technical Research, Finland, publication 145.

Vuorinen, J. (1973), 'On determination of effective degree of saturation of concrete', Imatran Voima OY, Concrete and Soils Laboratory, Internal Report.

Wadsö, L., Svennberg, K. and Dueck, A. (2003), 'An experimentally simple method for measuring sorption isotherms', Drying Technol. 22(10) 2427-2440.

Warris, B. (1964), 'The influence of air entrainment on the frost resistance of concrete', Swedish Cement and Concrete Research Institute, Proceedings No 36.

Wessman, L. (1997), 'Studies on the frost resistance of natural stone', Division of Building Materials, Lund Institute of Technology, TVBM-3077.

Wong, A.Y.C., Anderson,V.L. and Hilsdorf,H.K. (1973), 'The effect of drying on the freeze-thaw durability of concrete', Univ.of Illinois, Bulletin 60, No 66.

APPENDIX to Chapter 3

Contents

A3.1 Overview of experiments

A single experiment with a specimen pre-stored in lime-saturated water is marked with an 'x'.

A single experiment with a specimen pre-stored in sodium chloride of 2%, 4.5% or 11% concentration is marked with an '+', 'o' or '#' respectively.

Concerning different moisture conditions ('natural', 'vacuum saturation' and 'adjusted saturation'), see paragraph 4.5.

Concerning different freezing conditions ('temperature change rate', 'minimum temperature level' and 'minimum temperature duration'), see Chapters 5-8.

Table A3.1: Studies involving w/c-ratio 0.40.

		Natural moisture			Vacuum saturation			Adjusted saturation		
		no AEA	4% air	6% air	no AEA	4% air	6% air	no AEA	4% air	6% air
Freeze-thaw Test Series 1-8 (Study 1, Chapter 4-8)										
Temp. change rate[1)]	1	xx	xx	xx			xx		xx	xx
Test series 1-3	2	xx	xx	xx					xx	xx
Min. temp. level Test series 4-5		xx	xx	xx					xx	xx
Min. temp. duration Test series 6-7	1	xx	xx	xx					xx	xx
Salt water storage. Test series 8		++ oo ##		++ oo ##						
Calorimetry (Study 2, Chapter 9)										
Temp. change rate[1)]	1	x		x o						
	2	x		x o						
Min. temp. level		x		x o						
Min. temp. duration		x		x o						
Combined dilatometry and calorimetry (Study 3, Chapter 11)										
Temp. change rate[1)]	1	x	x	x	x	x	x			
	2									
Min. temp. level										
Min. temp. duration					x					
Determination of sorption isotherm (Study 2, Chapter 9)										
Adsorption		x								
Desorption		x								
Scanning		x								

[1)] 1= 'normal' freeze-thaw cycle. 2= 'rapid' freeze-thaw cycle

A single experiment with a specimen pre-stored in lime-saturated water is marked with an 'x'.

A single experiment with a specimen pre-stored in sodium chloride of 2%, 4.5% or 11% concentration is marked with an '+', 'o' or '#' respectively.

Concerning different moisture conditions ('natural', 'vacuum saturation' and 'adjusted saturation'), see paragraph 4.5.

Concerning different freezing conditions ('temperature change rate', 'minimum temperature level' and 'minimum temperature duration'), see Chapters 5-8.

Table A3.2. Studies involving w/c- ratio 0.45.

		Natural moisture			Vacuum saturation			Adjusted saturation		
		no AEA	4% air	6% air *10% air*	no AEA	4% air	6% air *10% air*	no AEA	4% air	6% air *10% air*
Freeze-thaw Test series 1-8 (Study 1, Chapter 4-8)										
Temp.change rate[1)] Test series 1-3	1	xx	xx	xx *xx (10%)*		xx	xx *xx (10%)*		xx	xx *xx (10%)*
	2	xx	xx	xx *xx (10%)*					xx	xx *xx (10%)*
Min.temp. level. Test series 4-5		xx		xx *xx (10%)*						xx *xx (10%)*
Min.temp. duration.Test series 6-7		xx	xx	xx *xx (10%)*					xx	xx *xx (10%)*
Salt water storage.Test series 8		++ oo ##		++ *(10%)* oo *(10%)* ## *(10%)*						
Calorimetry (Study 2, Chapter 9)										
Temp. change rate	1									
	2									
Min. temp level										
Min.temp. duration										
Combined dilatometry and calorimetry (Study 3, Chapter 11)										
Temp. change rate[1)]	1									
	2									
Min.temp. level										
Min.temp. duration										
Determination of sorption isotherm (Study 2, Chapter 9)										
Adsorption										
Desorption										
Scanning										

[1)] 1= 'normal' freeze-thaw cycle. 2= 'rapid' freeze-thaw cycle

A single experiment with a specimen pre-stored in lime-saturated water is marked with an 'x'.

A single experiment with a specimen pre-stored in sodium chloride of 2%, 4.5% or 11% concentration is marked with an '+', 'o' or '#' respectively.

Concerning different moisture conditions ('natural', 'vacuum saturation' and 'adjusted saturation'), see paragraph 4.5.

Concerning different freezing conditions ('temperature change rate', 'minimum temperature level' and 'minimum temperature duration'), see Chapters 5-8.

Table A3.3. Studies involving w/c-ratio 0.60.

		Natural moisture			Vacuum saturation			Adjusted saturation		
		no AEA	4% air	6% air	no AEA	4% air	6% air	no AEA	4% air	6% air
Freeze-thaw Test series 1-8 (Study 1, Chapter 4-8)										
Temp. change rate[1)] Test series 1-3	1	xx	xx	xx		xx	xx		xx	xx
	2	xx	xx	xx					xx	xx
Min. temp. level Test series 4-5		xx	xx	xx					xx	xx
Min. temp duration Test series 6-7		xx	xx	xx					xx	xx
Salt water storage.Test series 8		++ oo ##		++ oo ##						
Calorimetry (Study 2, Chapter 9)										
Temp.change rate[1)]	1	x		x						
	2	x		x						
Min. temp. level		x		x						
Min.temp. duration		x		x						
Combined dilatometry and calorimetry (Study 3, Chapter 11)										
Temp. change rate[1)]	1	x	x	x	x	x	x			
	2									
Min. temp. level										
Min.temp. duration					x					
Determination of sorption isotherm (Study 2, Chapter 9)										
Adsorption		x								
Desorption		x								
Scanning		x								

[1)]1= 'normal' freeze-thaw cycle. [2)]= 'rapid' freeze-thaw cycle

A3.2 Mix proportions. Properties of the fresh concrete (except for samples used in Chapter 11)

Casting period: October-November 1997

Specimens of each mix: 3 blocks, 400x400x150 mm, 3 cubes, 150 mm

The mix proportions, the density of the fresh concrete, the air content of the fresh concrete, and the 28-day cube strength are listed in Table A3.1.

Table A3.4: Mix composition. Properties of the fresh concrete. 28-days compressive strength

w/c	Nominal air content (%)	Cement (kg/m^3)	Water (kg/m^3)	Sand 0-3 mm (kg/m^3)	Gravel 4-8 mm (kg/m^3)	AEA [1)] (kg/m^3)	Fresh air content (%)	Density of fresh concrete (kg/m^3)	Cube strength (MPa)	Slump (mm)
0.40	non-AE	525	215	816	816	0	2.9	2354	73.7	10
	4	525	215	763	763	1.2	4.9	2228	61.9	40
	6	525	215	736	763	1.7	6.6	2256	59.5	60
0.45	non-AE	478	215	810	810	0	2.3	2364	58.5	29
	4	478	215	783	783	0.75	4.2	2315	63.3	42
	6	478	215	756	756	1.35	6.0	2268	53.5	70
	10	478	215	756	756	1.88	10.0	2147	44.1	70
0.6	non-AE	350	210	897	897	0	2.8	2331	39.2	15
	4	350	210	844	844	0.4	4.1	2298	37.6	34
	6	350	210	817	817	1.5	6.8	2220	35.7	40

[1]) Neutralized Vinsol Resin 10% strength. Water in the admixture is not included in the w/c-ratio

A3.3 Air-pore structure of the hardened concrete

The size distribution of the air voids was determined for all ten materials. The technique employed was image analysis. Careful preparation of the surfaces, including grinding in several steps, dying of the surface with a felt-tip pen and filling of the air voids with white zink paste, is crucial if the results are to be accurate. Different sections of the surface of the samples (the total surface of each sample being 100x100 mm) were photographed a total of 250 times, each picture generating about 10-15 parameters that related to the white areas of each picture.

The parameters obtained from these pictures were used as input in a calculation program developed by Dr. Sture Lindmark, (Lindmark, 2000) based on a theory presented in (Vesikari, 1985). The program calculates the probability that a given 2-dimensional surface appearing as a white area in the photograph represents an air void of a particular size class, this being done for all of the white areas in each of the photographs, the final result being the probable number of spheres found in each size class. The air void distributions of all ten materials are shown in the figures that follow.

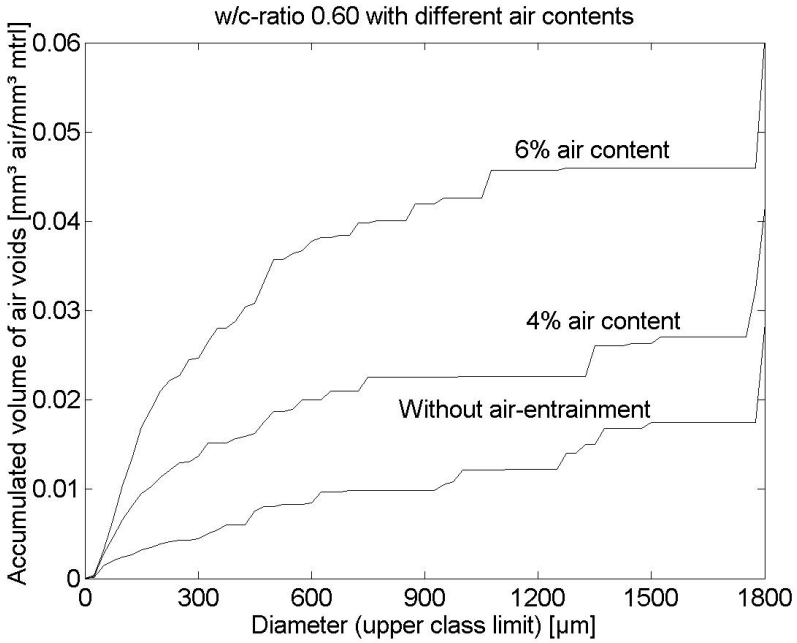

Figure A3.1. Size distribution of air voids in a material with w/c-ratio of 0.60 and differing amounts of air-entrainment.

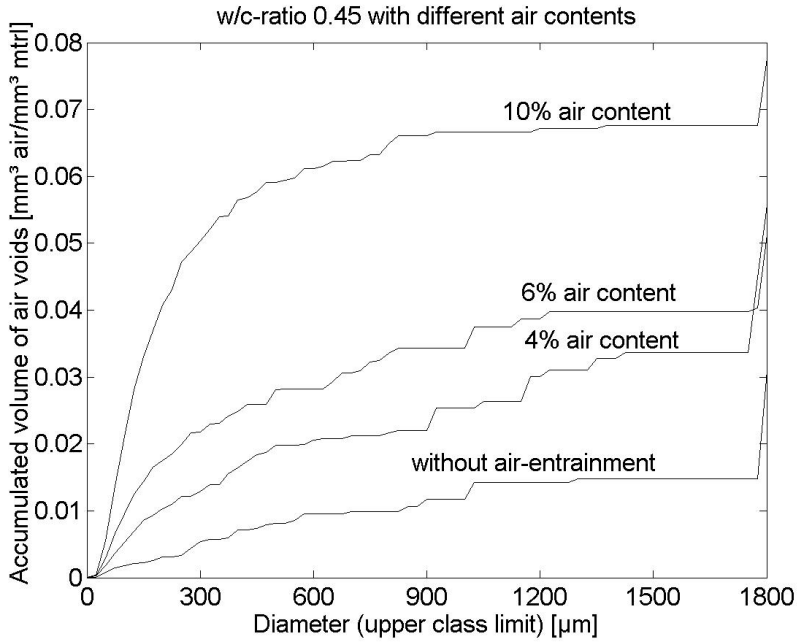

Figure A3.2. Size distribution of air voids in a material with w/c-ratio of 0.45 and differing amounts of air-entrainment.

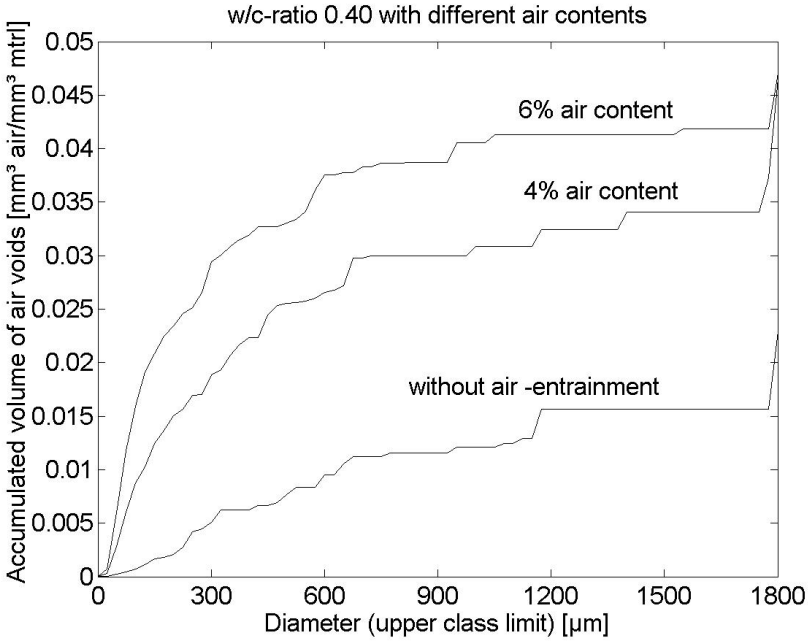

Figure A3.3. Size distribution of air voids in a material with w/c-ratio of 0.40 and differing amounts of air-entrainment.

The air contents of the materials as measured at casting corresponds fairly well with that measured by image analysis. The largest deviation was found for materials containing the greatest amount of air.

The Powers spacing factor, L (mm) is calculated by:

$$L = \left(\frac{3}{\alpha}\right)\left(1.4\left(\frac{V_p}{a}+1\right)^{1/3}-1\right)$$

where, α is the specific surface of the air pore system (mm^{-1}), V_p is the volume of cement paste excluding the air-pores (% of the total concrete volume), a is the hardened air content (% of the concrete volume). V_p=C(0.32+w/c)10 where C is the cement content (kg/m^3) and 0.32 is the specific volume of cement (litre/kg).

The results are presented in Table A3.2.

Table A3.5 Air pore structural parameters of the hardened concrete.

w/c	Nominal air content (%)	Fresh air content (%)	Hardened air Content, (%)	Specific surface α (mm^{-1})	Powers spacing factor, L (mm)
0.40	natural	2.9	2.3	13.9	0.57
	4	4.9	4.7	28.5	0.2
	6	6.6	4.7	44.7	0.13
0.45	natural	2.3	3.1	13.3	0.51
	4	4.2	5.1	28.9	0.19
	6	6.0	5.6	18.1	0.29
	10	10.0	7.8	39.4	0.11
0.60	natural	2.8	2.9	16.5	0.4
	4	4.1	4.2	24.9	0.22
	6	6.8	6.0	28.5	0.16

*) In the calculation program created by Lindmark (2000) the measured white area is controlled and sorted out regarding to shape and roundness, leaving out those objects, which are believed not to actually contribute to the protection of the material.

W/c-ratio 0.45 with a nominal air content of 6% had a remarkable low specific surface and high Powers spacing factor. A reason for this has not been found.

A3.4 Sieve curves

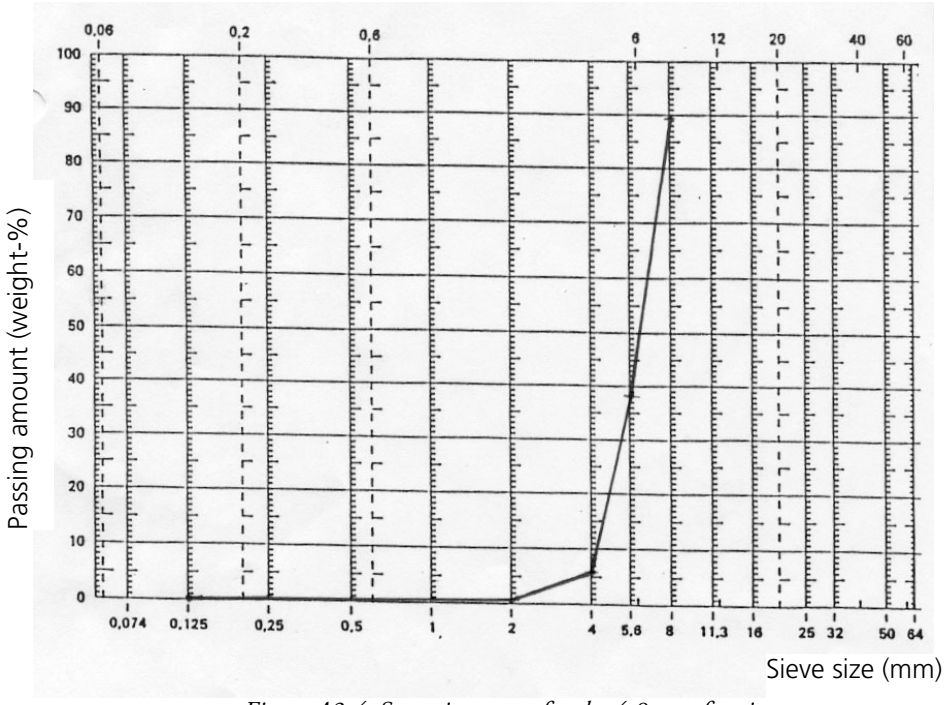

Figure A3.4. Screening curve for the 4-8 mm fraction.

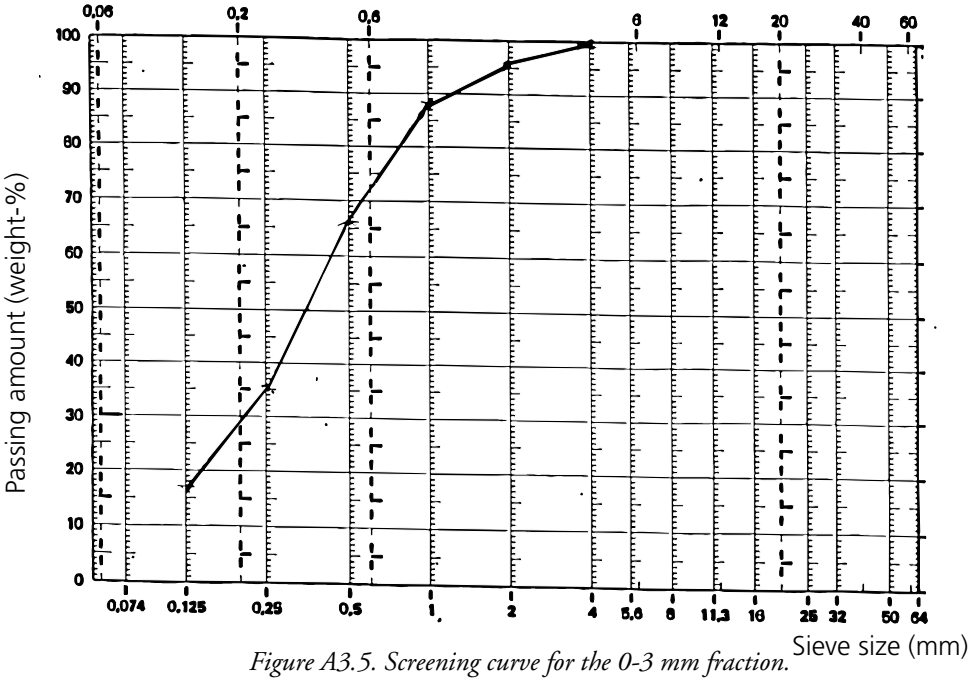

Figure A3.5. Screening curve for the 0-3 mm fraction.

APPENDIX to Chapter 5

A5.1 Test series 1 - Never-dried specimens with 'natural' water content

Contents

Table A5.1: Damage parameters for all experiments in Test series 1

w/c-ratio	nom.air cont. (%)	S_A/S_B	u (%)	$d\theta/dt$=3.6°C/h RF²	Perm.dil. (‰)	dil. at sc/ dil at -20°C (‰)	$d\theta/dt$=7.8°C/h RF²	Perm.dil. (‰)	dil. at sc/ dil. at -20°C (‰)
0.60	Nat.	-/-		0.79	0.40	0.32/0.62			
0.60	Nat.	-/-		0.77	0.36	0.22/0.58			
0.60	Nat.	-/-	8.12				0.81	0.30	0.2/0.56
0.60	Nat.	-/-	8.27				0.83	0.433	0.2/0.83
0.60	4	0.93/-	8.97	0.86	0.02	0.07/-0.01			
0.60	4	0.96/-	8.81	0.96	0.02	0.05/-0.08			
0.60	4	-/0.92	8.81				0.92	-0.04	0.01/-0.01
0.60	4	-/0.94	9.00				0.94	-0.07	0.09/-0.06
0.60	6	0.89/-	9.24	0.94	0.02	0.03/-0.09			
0.60	6	0.91/-	9.17	0.96	0.02	0.03/-0.09			
0.60	6	-/0.89	9.11				0.94	0.02	0.04/-0.08
0.60	6	-/0.87	9.02				0.96	0.03	0.04/-0.08
0.40	Nat.	-/-		0.88	0.29	0.08/0.39			
0.40	Nat.	-/-		0.92	0.18	0.05/0.24			
0.40	Nat.	-/-	7.98				0.88	0.23	0.07/0.31
0.40	Nat.	-/-	7.71				0.88	0.2	0.04/0.28
0.40	4	-/-		0.92	0.42	0.75/0.87			
0.40	4	-/-		0.96	0.12	0.04/0.19			
0.40	4	-/-	8.81				0.92	0.12	0.01/0.21
0.40	4	-/-	8.70				0.94	0.05	0.02/0.19
0.40	6	0.95/-	9.44	0.96	0.06	0.03/-0.005			
0.40	6	-/0.97	9.20	0.96	0.09	0.02/-0.02			
0.40	6	-/0.90	9.05				0.96	0.06	0.03/0.02
0.40	6	-/0.91	9.09				0.94	0.09	0.03/0.06
0.45	Nat.	-/-		0.88	0.19	0.01/0.32			
0.45	Nat.	-/-		0.90	0.23	0.07/0.35			
0.45	Nat.	-/-	7.94				0.88	0.24	0.006/0.36
0.45	Nat.	-/-	7.87				0.88	0.26	0.003/0.36
0.45	4	-/0.91	10.87	0.96	0.04	0.01/-0.09			
0.45	4	-/0.92	10.79	0.98	0.04	0.006/-0.07			
0.45	4	-/0.91	9.29				0.98	0	0/-0.04
0.45	4	-/0.90	8.84				0.96	0.08	*
0.45	10	0.84/-	9.88	0.96	0.03	*			
0.45	10	0.80/-	9.99	0.98	0.02	0.01/-0.06			
0.45	10	-/0.84	9.83				0.96	0,003	0/-0.08
0.45	10	-/0.84	9.93				0.96	0.01	0/-0.07
0.45	6	-/0.93	8.93	0.96	0.07	0.01/-0.01			
0.45	6	-/0.92	8.54	0.96	0.05	0.01/0.02			
0.45	6	-/0.96	8.61				0.94	0.09	0.02/0.09
0.45	6	-/0.96	8.88				0.94	0.08	0.02/0.10

** The Lvdt-sensor malfunctioned*

RF² is the relative resonance frequency before and after freeze/thaw, squared. Perm. dil. is the permanent dilation. dil. at sc. is the dilation at supercooling. dil at -20°C is the dilation at -20°C. Dilation is defined in Figure 4.4.4. S_A and S_B are the degrees of saturation, see Equations (4.5.3) and (4.5.5), u is the moisture content, see Equation (4.5.2)

Figures A5.1-A5.16: Length change diagrams. Test series 1

Each curve represents a single specimen. All samples of the same concrete type, have the same starting point in the figures (not necessarily at zero ‰ strain). The starting points of the various curves have been so placed as to allow all specimen of the same w/c-ratio to be shown in the same figure. Specimens with the lowest air content have the highest starting point, and specimens with the highest air content the lowest starting point. The surface temperature versus time for of one of the samples is also shown in the figures showing length-change versus time. The curves represent the total response of the specimens, including the measuring frame and the sensor. The thermal movements of the frame and sensor are small compared to the specimen and are completely linear. Therefore they have only a minor influence on the results and can be neglected.

w/c-ratio 0.60: Normal freezing rate

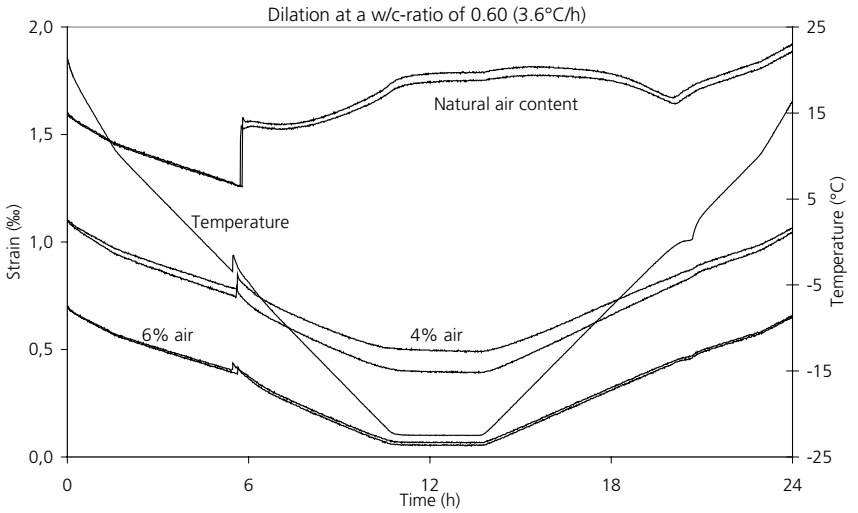

Figure A5.1. Length change and temperature versus time for samples with natural water content and w/c-ratio 0.60 containing either natural air (starting point 1.6 ‰ strain), 4% air (starting point 1.1 ‰ strain) or 6% air (starting point 0.7 ‰ strain), when exposed to a 'normal' cycle.

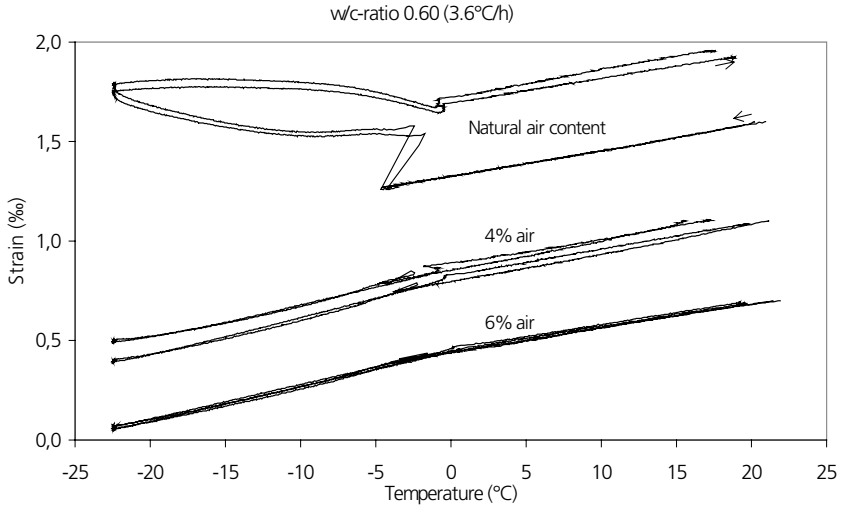

Figure A5.2. Length change versus temperature for samples with natural water content and w/c-ratio 0.60 containing either natural air (starting point 1.6 ‰ strain), 4% air (starting point 1.1 ‰ strain) or 6% air (starting point 0.7 ‰ strain), when exposed to a 'normal' cycle.

w/c-ratio 0.60: Rapid freezing

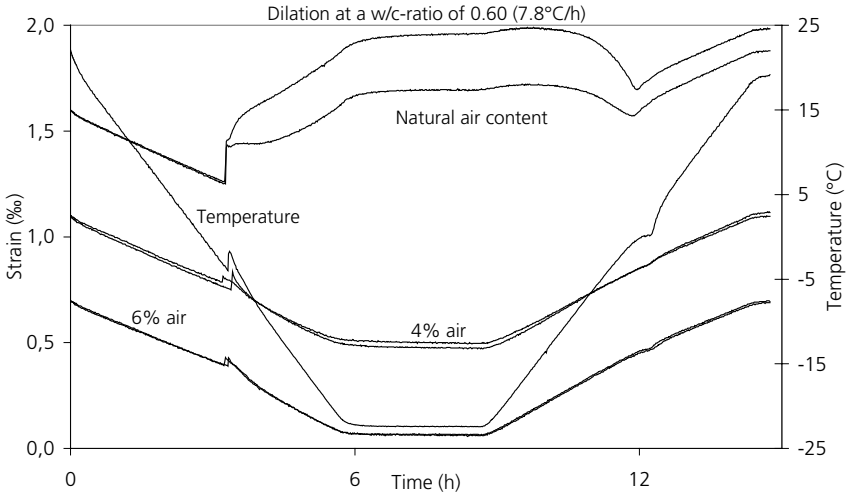

Figure A5.3. Length change and temperature versus time for samples with natural water content and w/c-ratio 0.60 containing either natural air (starting point 1.6 ‰ strain), 4% air (starting point 1.1 ‰ strain) or 6% air (starting point 0.7 ‰ strain), when exposed to a 'rapid' cycle.

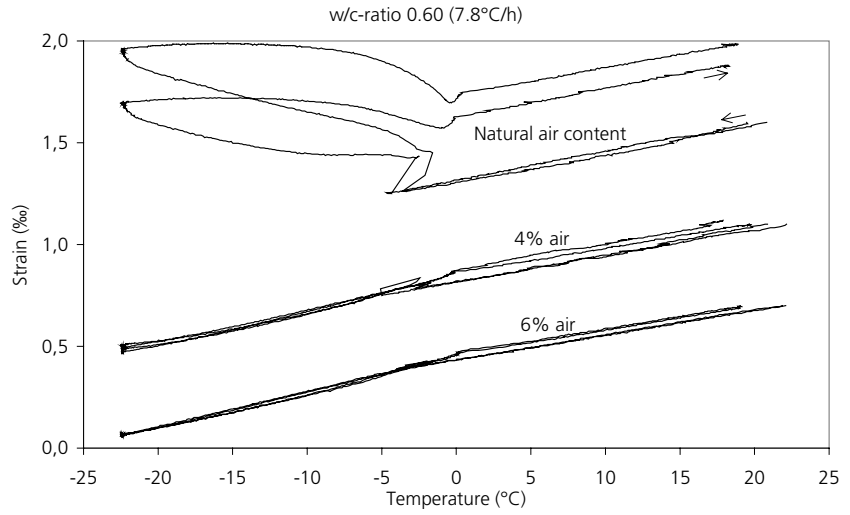

Figure A5.4. Length change versus temperature for samples with natural water content and w/c-ratio 0.60 containing either natural air (starting point 1.6 ‰ strain), 4% air (starting point 1.1 ‰ strain) or 6% air (starting point 0.7 ‰ strain), when exposed to a 'rapid' cycle.

w/c-ratio 0.45: Normal freezing rate

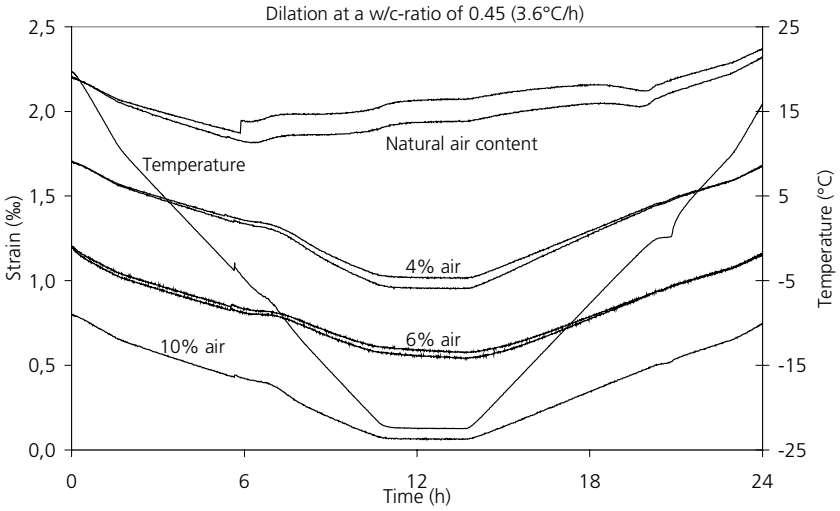

Figure A5.5. Length change and temperature versus time for samples with natural water content and w/c-ratio 0.45 containing either natural air (starting point 2.2 ‰ strain), 4% air (starting point 1.7 ‰ strain) or 6% air (starting point 1.2 ‰ strain) or 10% air (starting point 0.8 ‰ strain), when exposed to a 'normal' cycle.

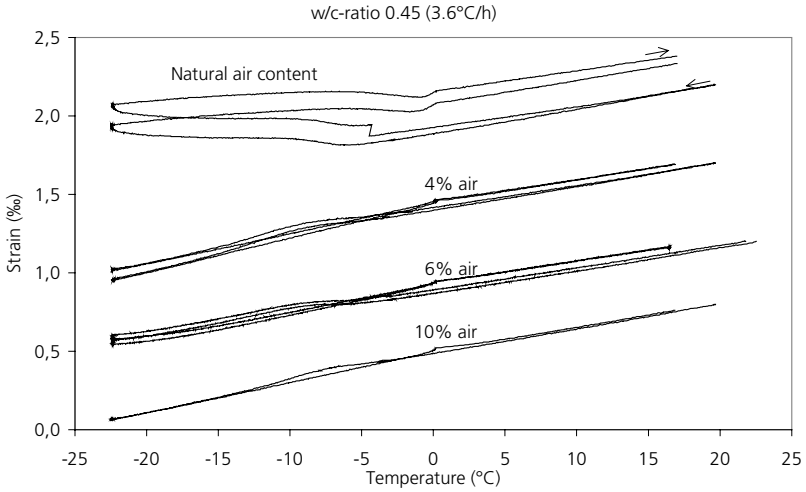

Figure A5.6. Length change versus temperature for samples with natural water content and w/c-ratio 0.45 containing either natural air (starting point 2.2 ‰ strain), 4% air (starting point 1.7 ‰ strain) or 6% air (starting point 1.2 ‰ strain) or 10% air (starting point 0.8 ‰ strain), when exposed to a 'normal' cycle.

w/c-ratio 0.45: Rapid freezing

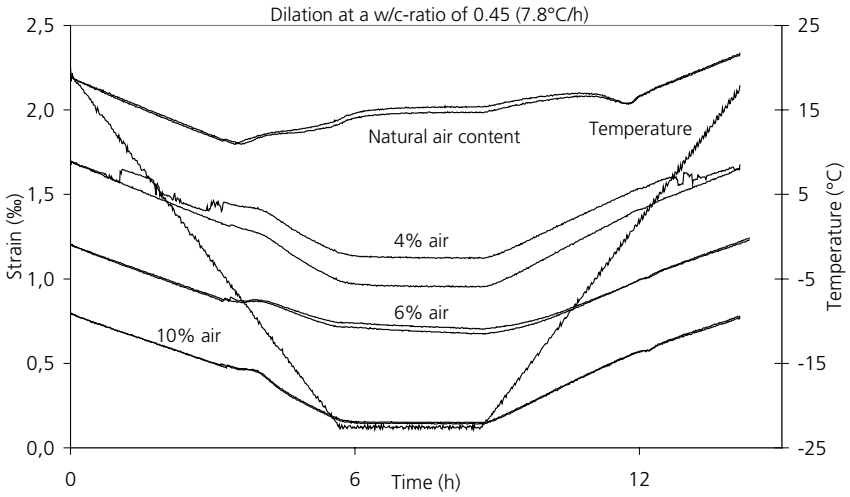

Figure A5.7. Length change and temperature versus time for samples with natural water content and w/c-ratio 0.45 containing either natural air (starting point 2.2 ‰ strain), 4% air (starting point 1.7 ‰ strain) or 6% air (starting point 1.2 ‰ strain) or 10% air (starting point 0.8 ‰ strain), when exposed to a 'rapid' cycle.

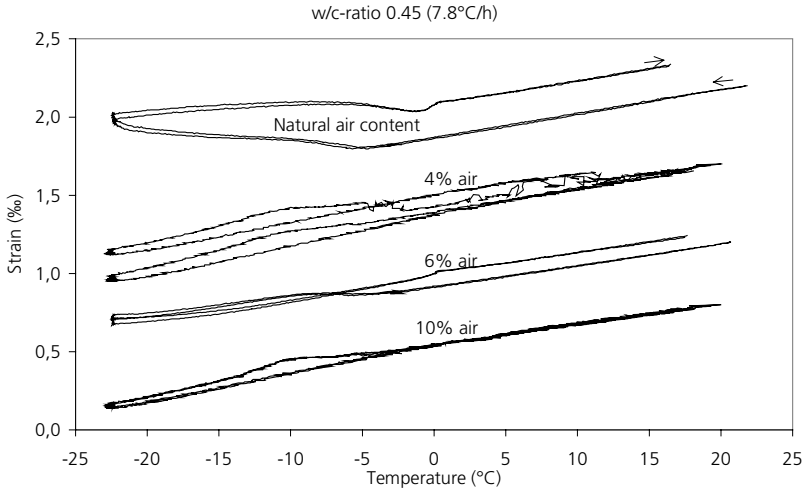

Figure A5.8. Length change versus temperature for samples with natural water content and w/c-ratio 0.45 containing either natural air (starting point 2.2 ‰ strain), 4% air (starting point 1.7 ‰ strain) or 6% air (starting point 1.2 ‰ strain) or 10% air (starting point 0.8 ‰ strain), when exposed to a 'rapid' cycle.

w/c-ratio 0.40: Normal freezing rate

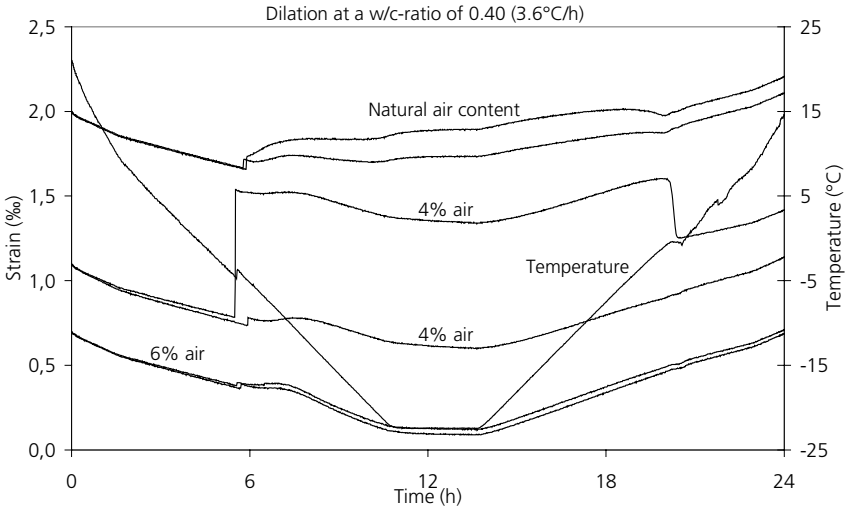

Figure A5.9. Length change and temperature versus time for samples with natural water content and w/c-ratio 0.40 containing either natural air (starting point 2.0 ‰ strain), 4% air (starting point 1.1 ‰ strain) or 6% air (starting point 0.7 ‰ strain), when exposed to a 'normal' cycle.

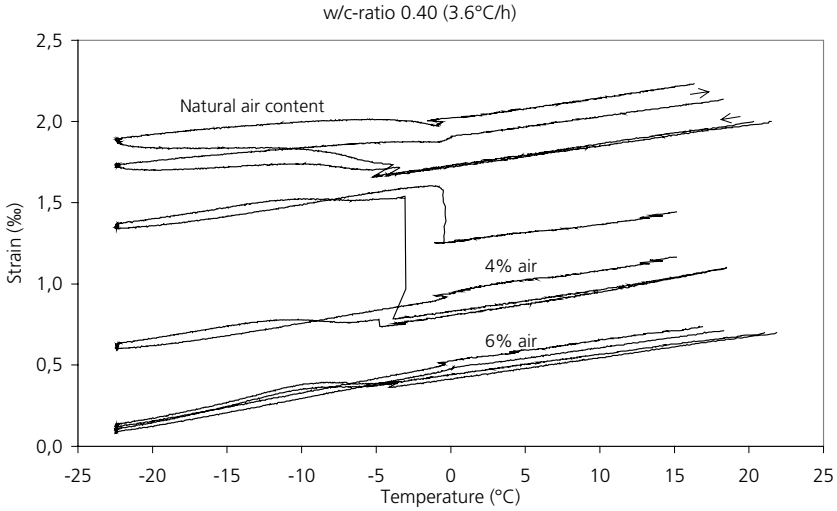

Figure A.5.10. Length change versus temperature for samples with natural water content and w/c-ratio 0.40 containing either natural air (starting point 2.0 ‰ strain), 4% air (starting point 1.1 ‰ strain) or 6% air (starting point 0.7 ‰ strain), when exposed to a 'normal' cycle.

w/c-ratio 0.40: Rapid freezing

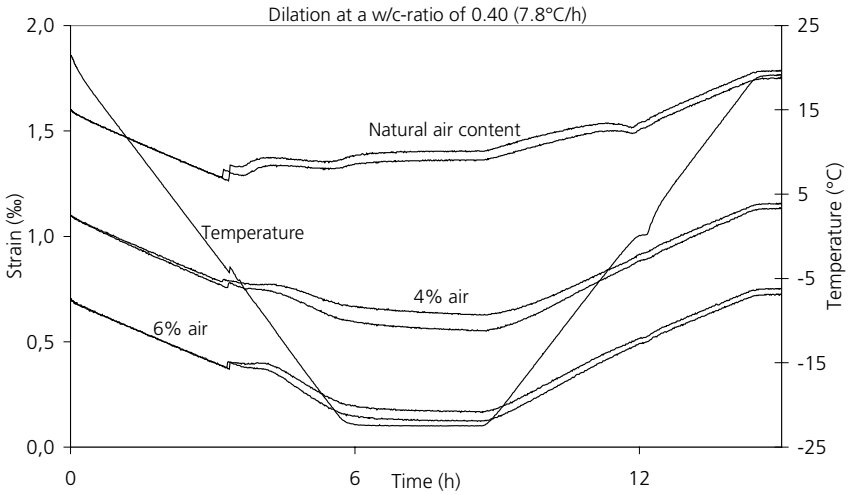

Figure A5.11. Length change and temperature versus time for samples with natural water content and w/c-ratio 0.40 containing either natural air (starting point 1.6 ‰ strain), 4% air (starting point 1.1 ‰ strain) or 6% air (starting point 0.7 ‰ strain), when exposed to a 'rapid' cycle.

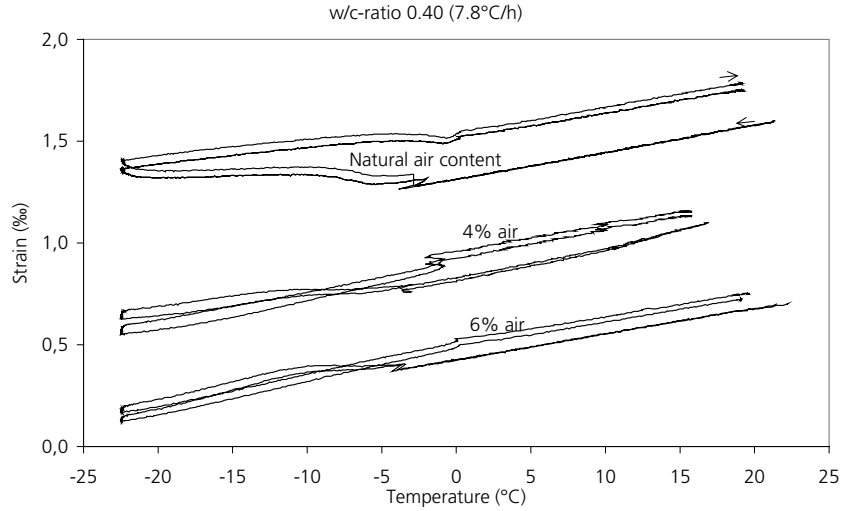

Figure A5.12. Length change versus temperature for samples with natural water content and w/c-ratio 0.40 containing either natural air (starting point 1.6 ‰ strain), 4% air (starting point 1.1 ‰ strain) or 6% air (starting point 0.7 ‰ strain), when exposed to a 'rapid' cycle.

Figures A5.13-A5.16: Damage parameters versus degree of saturation. Test series 1

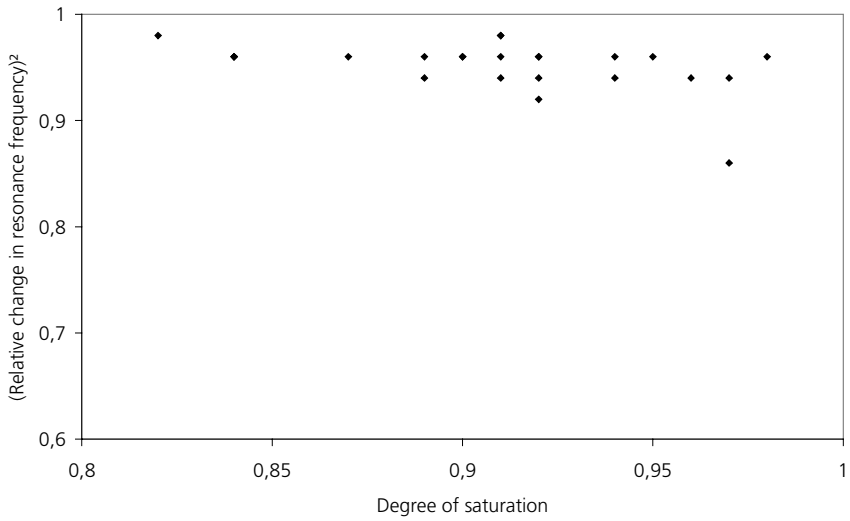

Figure A5.13. The relative residual resonance frequency squared (dynamic E-modulus) versus the degree of saturation for most samples in Test series 1.

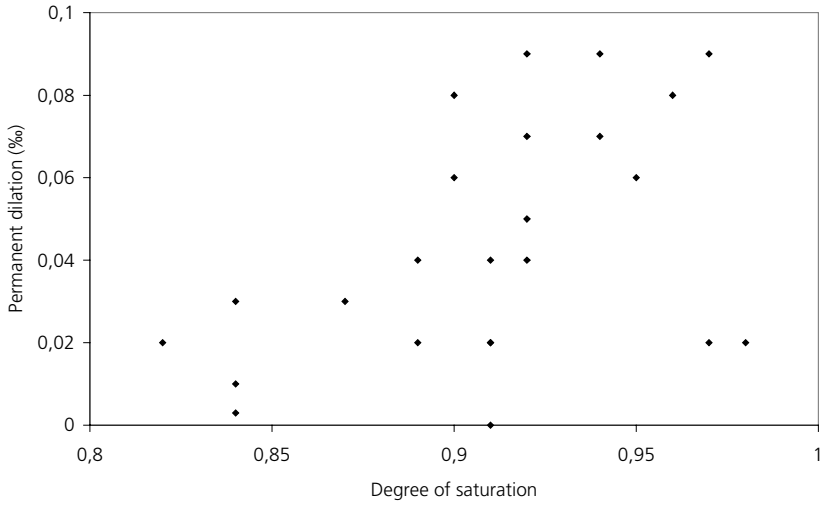

Figure A5.14. Permanent dilation versus the degree of saturation for most samples in Test series 1.

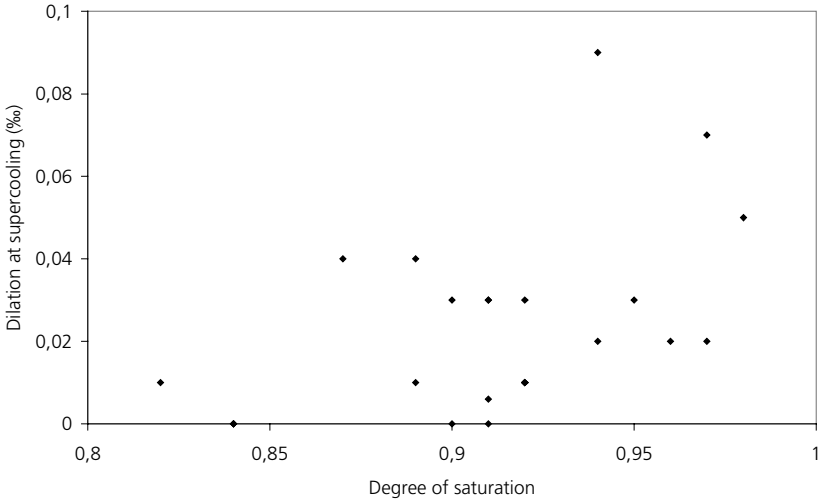

Figure A5.15. Dilation at supercooling versus the degree of saturation for most samples in Test series 1.

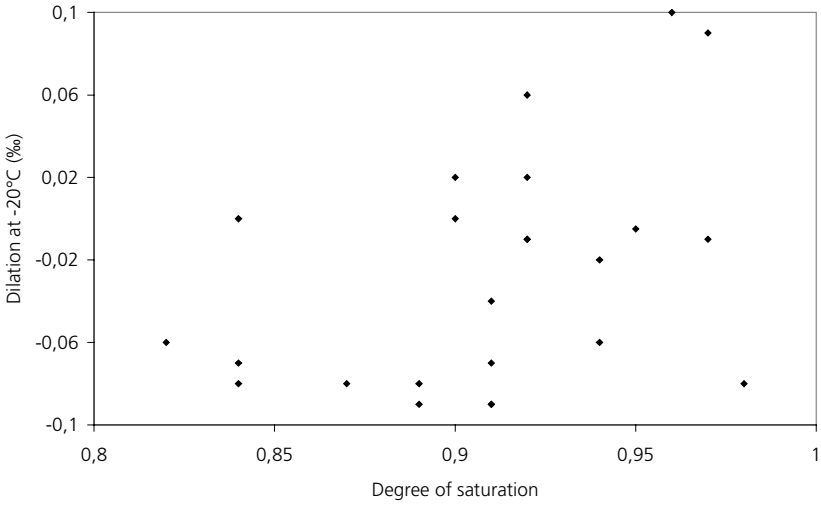

Figure A5.16. Dilation at –20°C versus the degree of saturation for most samples in Test series 1.

Table A5.2: Weights and volumes of the specimens in Test series 1

w/c	air %	Freezing Rate (°C/h)	Q_{test} (g)		$Q_{+105°C}$ (g)		Vol (cm^3)		V_{P_3} (cm^3)	
0.60	no	3.6	157.76	163.12						
	4	3.6	166.97	166.78	153.23	153.27	72.3	71.6	14.7	14.1
	6	3.6	185.05	167.36	169.38	153.31	81.5	73.3	17.6	15.5
0.60	no	7.8	169.02	192.24	156.33	177.56				
	4	7.8	166.91	164.28	153.39	150.71	72.2	70.8	14.6	14.4
	6	7.8	186.94	195.29	171.33	179.13	82.0	85.9	17.6	18.6
0.45	no	3.6	185.69	189.78						
	4	3.6	174.31	176.23	159.39	161.19	76.1	76.6	16.4	16.4
	6	3.6	193.15	193.24	177.31	178.03	83.4	83.0	17.1	16.6
	10	3.6	175.69	172.78	159.90	157.09	78.5	78.5	18.9	19.5
0.45	no	7.8	187.46	176.22	173.67	163.35				
	4	7.8	175.07	177.51	160.19	163.09	75.7	76.3	16.3	16.0
	6	7.8	195.93	194.86	180.40	178.97	82.5	82.6	16.1	16.5
	10	7.8	178.69	179.76	162.69	163.52	79.8	80.3	19.0	19.3
0.40	no	3.6	179.69	194.81						
	4	3.6	157.18	168.69						
	6	3.6	178.89	177.77	163.46	162.80	77.4	76.7	16.3	15.4
0.40	no	7.8	182.41	180.83	168.93	167.88				
	4	7.8	156.02	143.94	143.39	132.42				
	6	7.8	180.69	173.49	165.70	159.04	78.0	74.4	16.7	15.7

A5.2 Test series 2 - Pre-dried, Vacuum-saturated specimens

Contents

Table A5.3: Damage parameters for all experiments in Test series 2

dθ/dt=3.6°C/h						
w/c-ratio	Nom.air content (%)	S_A/S_B	u (%)	RF²	Perm.dilation (‰)	dil. at sc/ dil at -20°C (‰)
0.60	4	-/1	9.15	0.58	0.54	0.10/0.90
0.60	4	-/1	8.99	0.58	0.45	0.18/0.76
0.60	6	-/1	10.14	0.59	0.23	0.07/0.38
0.60	6	-/1	10.00	0.90	0.09	0.06/0.12
0.40	6	-/1	9.94	0.72	0.31	0.03/0.45
0.40	6	-/1	9.80	0.79	0.33	0.14/0.52
0.45	4	-/1	10.32	0.44	0.84	0.25/1.45
0.45	4	-/1	10.20	0.32	0.78	0.10/1.37
0.45	10	-/1	11.73	0.36	0.97	0.06/1.57
0.45	10	-/1	12.10	0.40	0.69	0.06/1.11
0.45	6	-/1	9.65	0.36	1.36	0.29/2.20
0.45	6	-/1	9.31	0.30	1.42	0.38/2.19

RF² is the relative resonance frequency before and after freeze/thaw, squared. Perm. dil. is the permanent dilation. dil at -20°C is the dilation at -20°C. Dilation is defined in Figure 4.4.4. S_B is the degree of saturation, see equation. (4.5.5). u is the moisture content, see equation (4.5.2). Note the value S_B=1 is not necessarily correct. In reality the value might be a bit lower as indicated by the dilation at -20°C, which is lower than expected. As mentioned in paragraph 4.5 it was not possible to obtain correct values for the dry weight and thus for the amount of water during the experiment, which leads to uncertainties in the degree of saturation.

Figures A5.17-A5.22: Length change diagrams. Test series 2

Each curve represents a single specimen. All samples of the same concrete type, have the same starting point in the figures (not necessarily at zero ‰ strain). The starting points of the various curves have been so placed as to allow all specimen of the same w/c-ratio to be shown in the same figure. Specimens with the lowest air content have the highest starting point, and specimens with the highest air content the lowest starting point. The surface temperature versus time for of one of the samples is also shown. The curves represent the total response of the specimens, including the measuring frame and the sensor. The thermal movements of the frame and sensor are small compared to the specimen and are completely linear. Therefore they have only a minor influence on the results and can be neglected.

w/c-ratio 0.60: 4% and 6% air

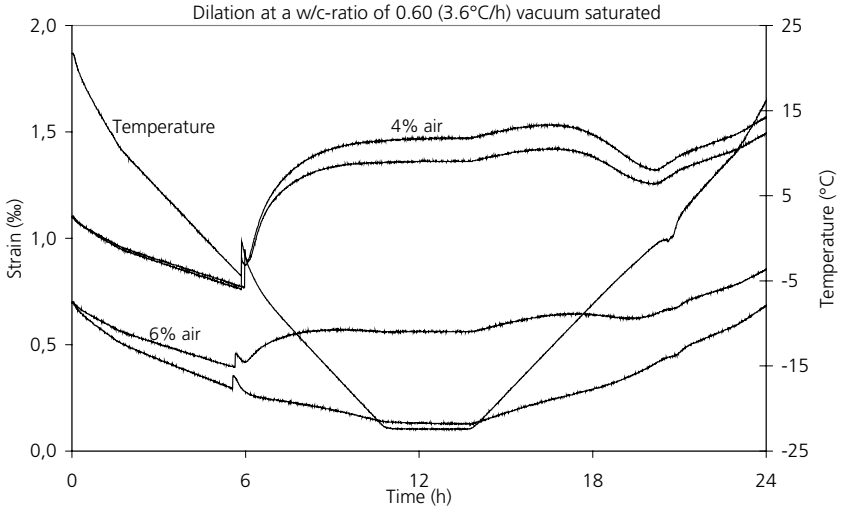

Figure A5.17. Length change and temperature versus time for vacuum-saturated specimens with a w/c-ratio of 0.60 containing 4% air (starting point 1.1 ‰ strain) or 6% air (starting point 0.7 ‰ strain) and exposed to a 'normal' cycle.

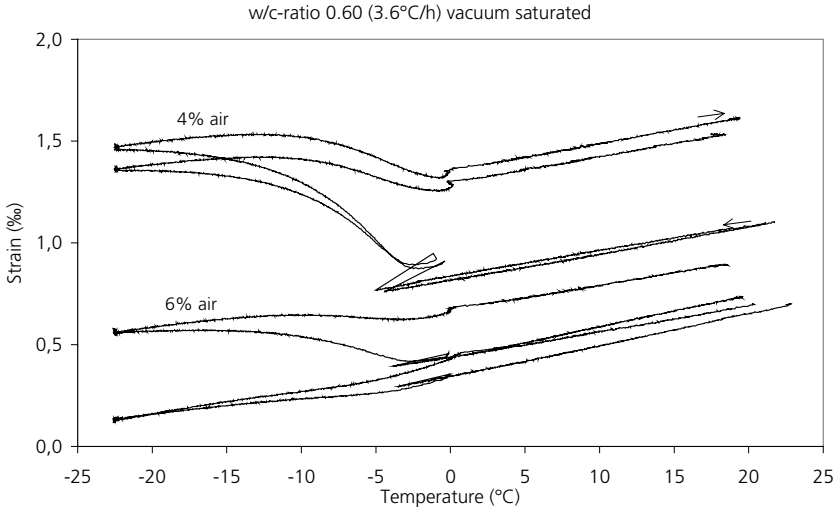

Figure A5.18. Length change versus temperature of vacuum-saturated samples with a 0.60 w/c-ratio and 4% air (starting point 1.1 ‰ strain) or 6% air (starting point 0.7 ‰ strain) when exposed to a 'normal' cycle.

w/c-ratio 0.45: 4%, 6% and 10% air

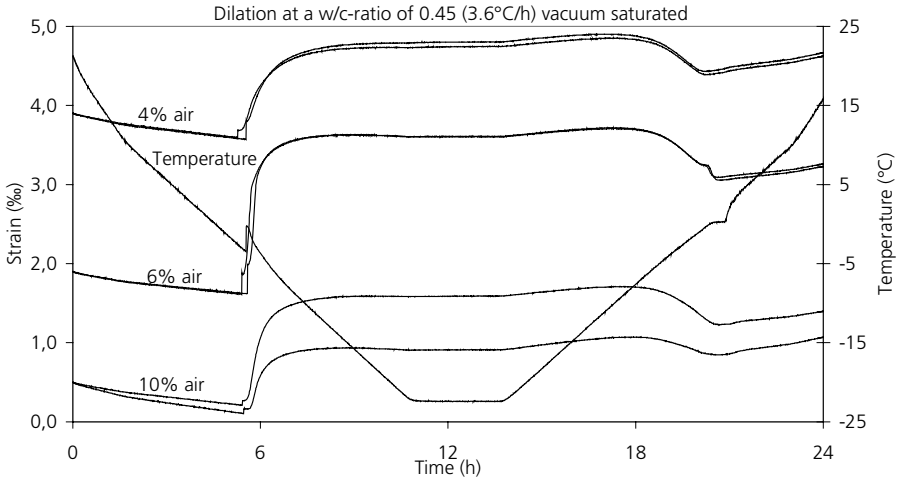

Figure A5.19. Length change and temperature versus time for vacuum-saturated specimens with a w/c-ratio of 0.45 containing 4% air (starting point 3.9 ‰ strain) or 6% air (starting point 1.9 ‰ strain) or 10% air (starting point 0.5 ‰ strain) and exposed to a 'normal' cycle.

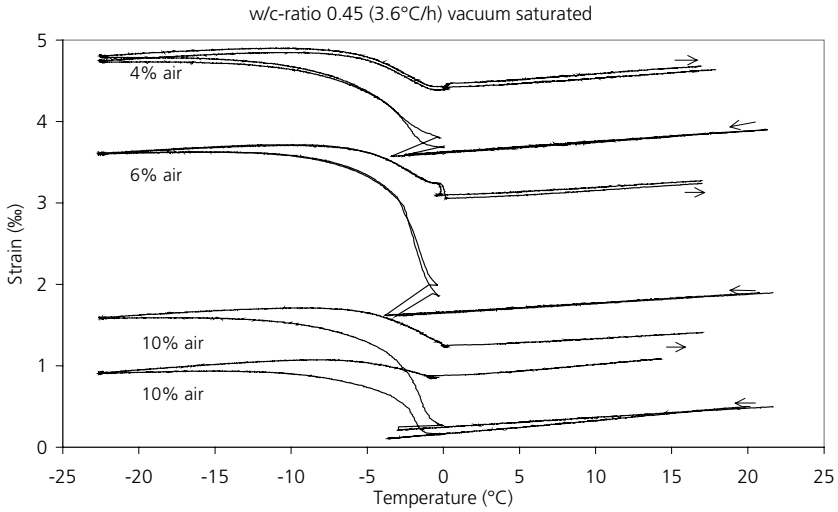

Figure A5.20. Length change versus temperature of vacuum-saturated samples with a 0.45 w/c-ratio and 4% air (starting point 3.9 ‰ strain) or 6% air (starting point 1.9 ‰ strain) or 10% air (starting point 0.5 ‰ strain) when exposed to a 'normal' cycle. Note the scale used on the y-axis.

w/c-ratio 0.40: 6% air

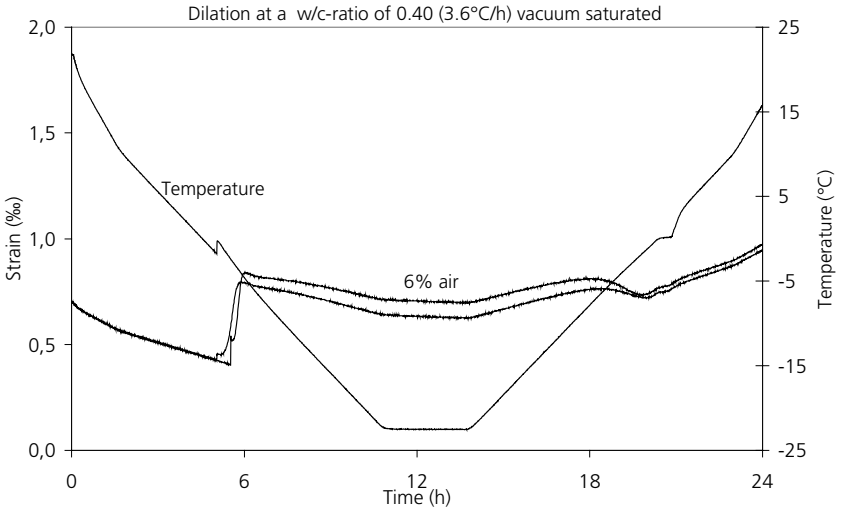

Figure A5.21. Length change and temperature versus time for vacuum-saturated samples with a w/c-ratio of 0.40 containing 6% air (starting point 0.7 ‰ strain) and exposed to a 'normal' cycle.

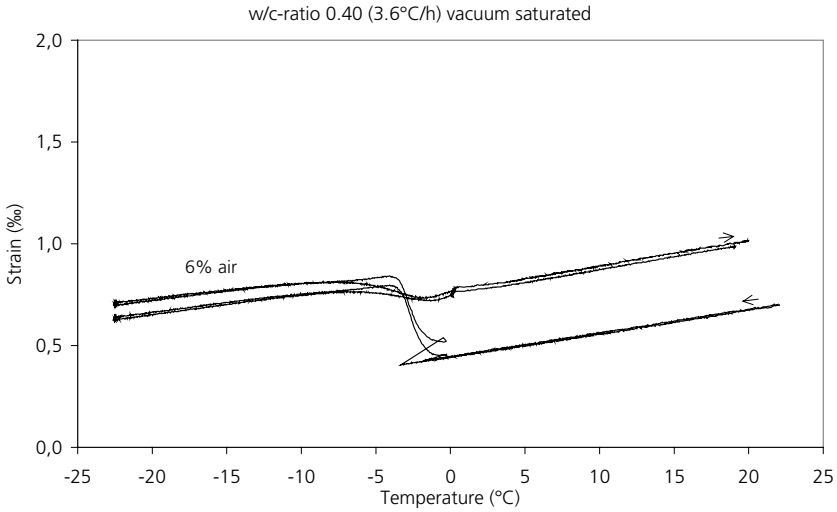

Figure A5.22. Length change versus temperature of vacuum-saturated samples with a 0.40 w/c-ratio and a 6% air content (starting point 0.7 ‰ strain) when exposed to a 'normal' cycle.

A5.3 Test series 3 - Pre-dried, re-saturated specimens with adjusted degree of saturation

Contents

Table A5.4: Damage parameters for all experiments in Test series 3

w/c-ratio	Air content (%)	S_A/S_B	u (%)	$d\theta/dt$=3.6°C/h RF²	Perm.dil. (‰)	dil. at sc/ dil. at -20°C (‰)	$d\theta/dt$=7.8°C/h RF²	Perm.dil. (‰)	dil. at sc/ dil. at -20°C (‰)
0.60	4	-/0.96	9.13	0.32	0.81	0.38/1.54			
0.60	4	-/0.98	9.37	0.37	0.79	0.31/1.52			
0.60	4	-/0.96	9.43				0.44	0.91	0.52/1.56
0.60	4	-/0.91	9.00				0.72	0.50	0.25/0.85*
0.60	6	-/0.97	9.98	0.62	0.52	0.11/0.92			
0.60	6	-/0.94	9.76	0.69	0.44	0.10/0.86			
0.60	6	-/0.91	9.24				0.85	0.4	0.23/0.70
0.60	6	-/0.95	9.70				0.52	0.81	0.25/1.39
0.40	6	-/0.86	8.69	0.96	0.08	0.10/0.05			
0.40	6	-/0.93	9.23	0.69	0.40	0.28/0.73			
0.40	6	-/0.97	9.08				0.90	0.17	0.12/0.20
0.40	6	-/0.94	8.86				0.86	0.08	0.04/0.03
0.45	4	-/0.98	9.92	0.50	0.66	0.32/1.21			
0.45	4	-/0.95	9.29	0.53	0.71	0.53/1.13			
0.45	4	-/0.94	8.93				1	0.10	0.06/0.07
0.45	4	-/0.97	9.26				0.92	0.173	0.06/0.24
0.45	10	-/0.85	9.95	0.96	0.03	0.05/-0.05			
0.45	10	-/0.93	10.95	0.90	0.14	0.06/0.17			
0.45	10	-/0.96	9.51				0.92	0.07	0.05/0
0.45	10	-/0.92	9.48				1	0.07	0.05/-0.07
0.45	6	-/0.86	7.66	0.90	0.1	0.12/1.10			
0.45	6	-/0.93	8.57	0.64	0.50	0.31/0.90			
0.45	6	-/0.94	8.15				0.83	0.33	0.18/0.55
0.45	6	-/0.97	8.34				0.76	0.44	0.13/0.73

RF² is the relative resonance frequency before and after freeze/thaw, squared. Perm. dil. is the permanent dilation. dil. at sc. is the dilation at super-cooling. dil at -20°C is the dilation at -20°C. Dilation is defined in Figure 4.4.4. S_A and S_B are the degrees of saturation, see Equations (4.5.3) and (4.5.5), u is the moisture content, see Equation (4.5.2).

Figures A5.23-A5.25: Length change diagrams. Test series 3

All length change curves have the same starting point. The curves represent the total response of the specimens including the measuring frame and the sensor. The thermal movements of the frame and sensor are small compared to the specimen and are completely linear. Therefore they have only a minor influence on the results and can be neglected.

Only results for w/c 0.45 are shown below. Results for w/c 0.60 and 0.40 are shown and discussed in Chapter 5, paragraph 5.5.

w/c-ratio 0.45: 4% air

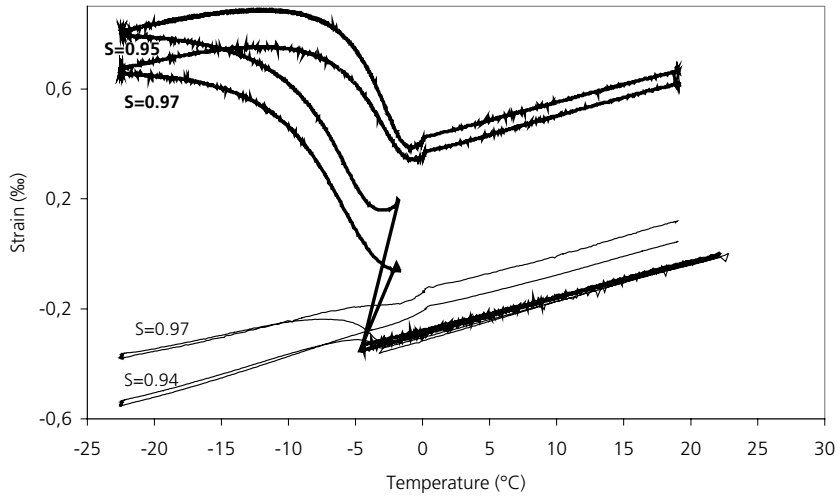

Figure A5.23. Samples with adjusted degrees of saturation with a w/c-ratio of 0.45 containing 4% air. The thick lines derive from samples exposed to a 'normal' cycle.

w/c-ratio 0.45: 6% air

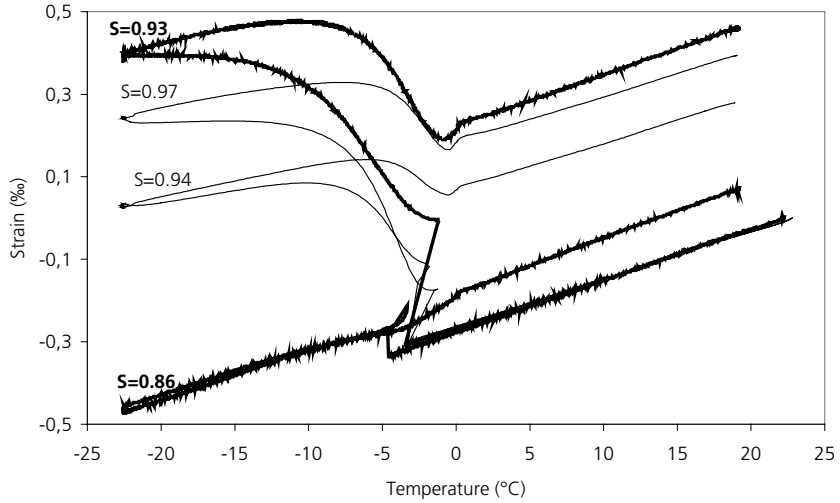

Figure A5.24. Samples with adjusted degrees of saturation with a w/c-ratio of 0.45 containing 6% air. The thick lines derive from samples exposed to a 'normal' cycle.

w/c-ratio 0.45: 10% air

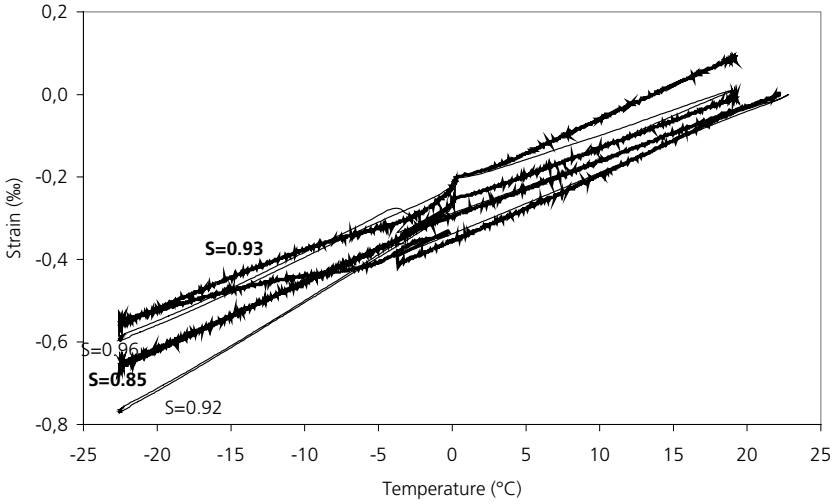

Figure A5.25. Samples with adjusted degrees of saturation with a w/c-ratio of 0.45 containing 10% air. The thick lines derive from samples exposed to a 'normal' cycle.

APPENDIX to Chapter 6

A6.1 Test series 4 - Never-dried specimens with 'natural' water content

Contents

Table A6.1: Damage parameters for all experiments in Test series 4

	dϕ/dt=3.6°C/h		3h duration of constant temperature				
w/c-ratio	Nom. air content (%)	S_A/S_B	u (%)	RF^2	Permanent dilation (‰)	dil. at sc (‰)	max dil1/ maxdil2 (‰)
0.60	Natural	-/0.94	8.34	0.71	0.51	0.38	0.50/1.04
0.60	Natural	-/0.95	8.23	0.71	0.43	0.23	0.41/0.93
0.60	4	-/0.90	9.10	0.86	0.04	0.11	-0.06/-0.02
0.60	4	-/0.97	9.31	0.79	0.06	0.04	-0.07/0.03
0.60	6	-/0.86	9.14	0.94	0.02	0.03	-0.08/-0.10
0.60	6	-/0.88	9.16	0.96	0.01	0.04	-0.09/-0.12
0.40	Natural	-/1	8.01	0.90	0.31	0.06	0.28/0.60
0.40	Natural	-/0.99	7.77	0.92	0.23	0.04	0.21/0.48
0.40	4	-/0.93	9.85	1	0.09	0.02	0.11/0.11
0.40	4	-/0.97	9.11	1	0.08	0.01	0.07/0.03
0.40	6	-/0.91	9.43	1	0.05	0.02	-0.002/-0.07
0.40*	6*	-/0.93*	9.43*	1*	0.09*	0.04*	0.23*/0.15*
0.45	Natural	-/0.91	5.38	0.74	0.37	0.03	0.33/0.81
0.45	Natural	-/0.96	7.99	0.86	0.23	0.003	0.20/0.50
0.45	6	-/0.91	8.94	0.85	0.08	0.02	-0.002/-0.04
0.45	6	-/0.90	8.92	0.98	0.06	0	-0.008/-0.06
0.45	10	-/0.81	9.63	0.65	0.03	0	-0.07/-0.12
0.45	10	-/0.80	9.84	0.94	0.03	0.02	-0.05/-0.09

**)The LVDT-sensor malfunctioned.*

RF^2 is the relative resonance frequency before and after freeze/thaw, squared. Perm. dil. is the permanent dilation. Dil. at sc. is the dilation at super-cooling. Dil at -20°C is the dilation at -20°C. These dilations are defined in Figure 4.4.4. Max. dil. 1 is the maximal dilation occurring at –15°C. Max. dil. 2 is the maximal dilation occurring at -30°C. S_A and S_B are the degrees of saturation, see Equations (4.5.3) and (4.5.5), u is the moisture content, see Equation (4.5.2).

Figures A6.1-A6.6: Length change diagrams. Test series 4

Each curve represents a single specimen. All samples of the same concrete type, have the same starting point in the figures (not necessarily at zero ‰ strain). The starting points of the various curves have been so placed as to allow all specimen of the same w/c-ratio to be shown in the same figure. Specimens with the lowest air content have the highest starting point, and specimens with the highest air content the lowest starting point. The surface temperature versus time for of one of the samples is also shown. The curves represent the total response of the specimens, including the measuring frame and the sensor. The thermal movements of the frame and sensor are small compared to the specimen and are completely linear. Therefore they have only a minor influence on the results and can be neglected.

The results in Figure A6.5 and Figure A6.6 for one of the specimens with 6% air indicate that something was probably wrong with the LVDT-gauge. This specimen showed a very large momentary dilation when the super-cooling was overcome, whereas neither any large decrease in the resonance frequency nor any high degree of saturation were found. The length change measurements for that sample were thus disregarded.

w/c-ratio 0.60

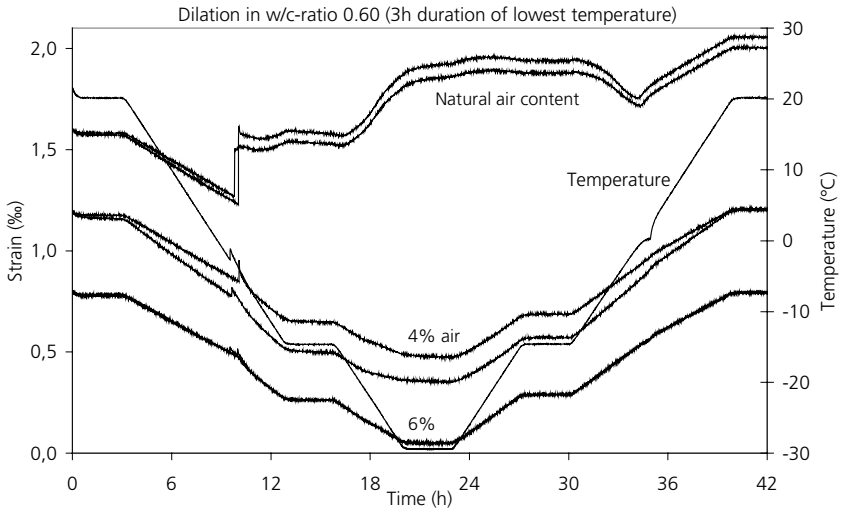

Figure A6.1. Length-change and temperature versus time for samples with w/c-ratio 0.60 and natural, 4 or 6% air content, exposed to two different temperature levels.

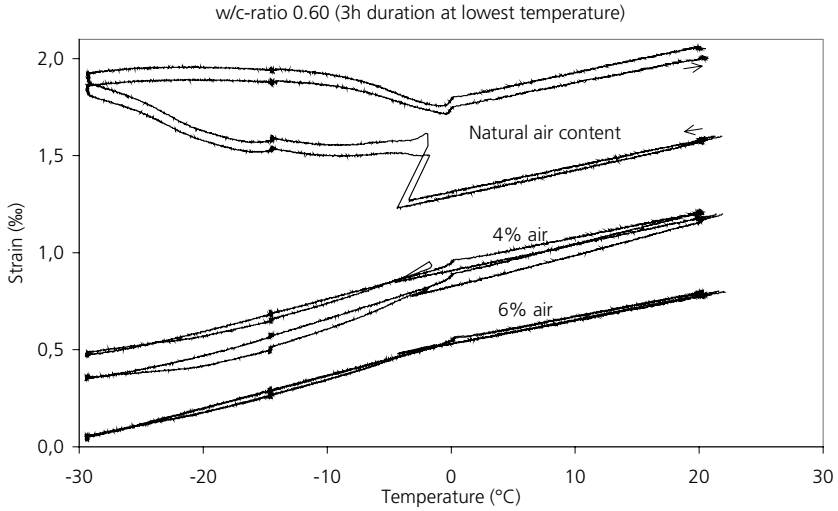

Figure A6.2. Length-change and temperature versus time for samples with w/c-ratio 0.60 and natural, 4 or 6% air content, exposed to two different temperature levels.

w/c-ratio 0.45

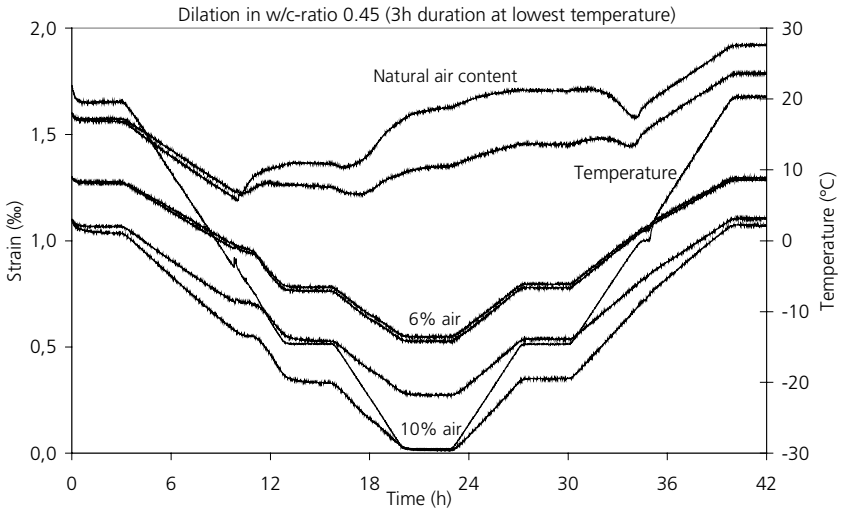

Figure A6.3. Length-change and temperature versus time for samples with w/c-ratio 0.45 and natural, 6 or 10% air content, exposed to two different temperature levels.

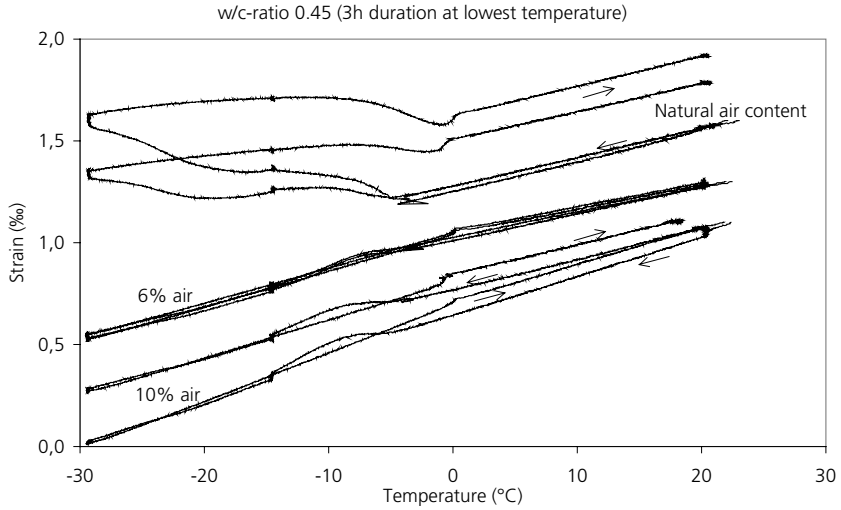

Figure A6.4. Length-change and temperature versus time for samples with w/c-ratio 0.45 and natural, 6 or 10% air content, exposed to two different temperature levels.

w/c-ratio 0.40

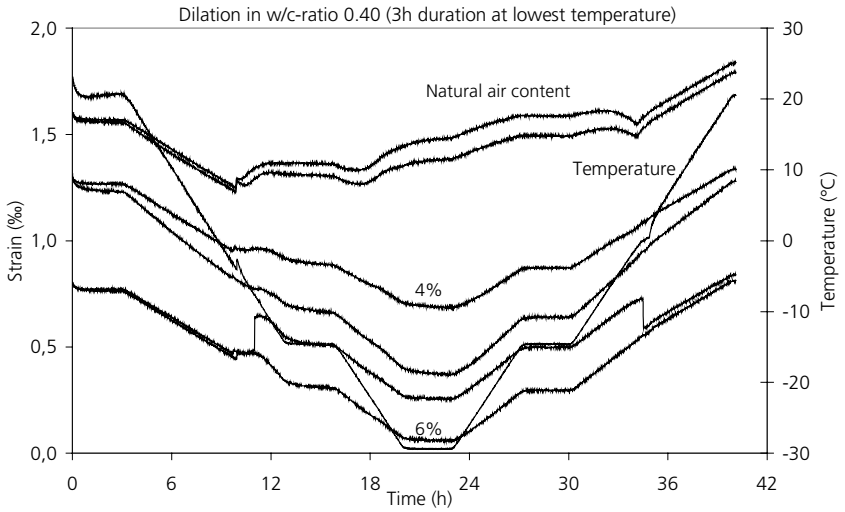

Figure A6.5. Length-change and temperature versus time for samples with w/c-ratio 0.40 and natural, 4 or 6% air content, exposed to two different temperature levels.

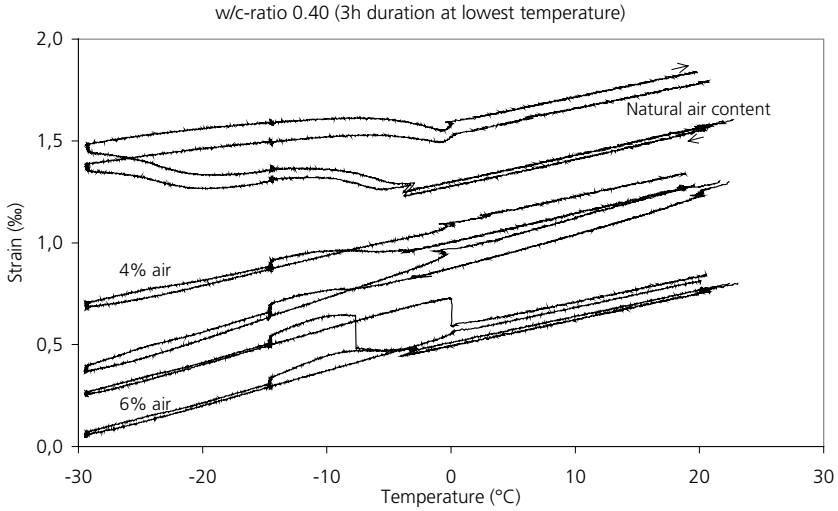

Figure A6.6. Length-change and temperature versus time for samples with w/c-ratio 0.40 and natural, 4 or 6% air content, exposed to two different temperature levels.

A6.2 Test series 5 - Never-dried specimens with adjusted degrees of saturation

Contents

Table A6.2: Damage parameters for all experiments in Test series 5

	dϕ/dt=3.6°C/h		3h duration of constant temperature				
w/c-ratio	Nom. air content (%)	S_A/S_B	u (%)	RF²	Perm.dilation (‰)	dil at sc (‰)	Maxdil 1/ Maxdil 2(‰)
0.60	4	-/0.92	9.30	0.45	1.03	0.52	1.65/2.05
0.60	4	-/0.87	8.37	0.72	0.275	0.33	0.43/0.50
0.60	6	-/0.93	9.89	0.72	0.50	0.64	0.78/1.0
0.60	6	-/0.87	9.10	0.86	0.30	0.22	0.41/0.57
0.40	4	-/0.92	9.76	0.50	1.11	0.97	1.61/1.77
0.40	4	-/0.90	8.46	0.86	0.348	0.26	0.48/0.54
0.40	6	-/0.95	9.85	0.49	1.10	0.96	1.56/1.76
0.40	6	-/0.89	9.02	0.71	0.50	0.39	0.64/0.70
0.45	6	-/0.95	9.31	0.58	0.84	0.70	1.32/1.57
0.45	6	-/0.90	8.91	0.90	0.31	0.32	0.45/0.53
0.45	10	-/0.94	11.15	0.62	0.59	0.23	0.82/0.94
0.45	10	-/0.91	11.15	0.64	0.71	0.40	0.99/1.10

RF² is the relative resonance frequency before and after freeze/thaw, squared. Perm. dil. is the permanent dilation. Dil. at sc. is the dilation at super-cooling. Dil at -20°C is the dilation at -20°C. These dilations are defined in Figure 4.4.4. Max. dil. 1 is the maximal dilation occurring at –15°C. Max. dil. 2 is the maximal dilation occurring at -30°C. S_A and S_B are the degrees of saturation, see Equations (4.5.3) and (4.5.5), u is the moisture content, see Equation (4.5.2)

Figures A6.7-A6.12: Length change diagrams. Test series 5

Each curve represents a single specimen. All samples of the same concrete type, have the same starting point in the figures (not necessarily at zero ‰ strain). The starting points of the various curves have been so placed as to allow all specimen of the same w/c-ratio to be shown in the same figure. Specimens with the lowest air content have the highest starting point, and specimens with the highest air content the lowest starting point. The surface temperature versus time for of one of the samples is also shown. The curves represent the total response of the specimens, including the measuring frame and the sensor. The thermal movements of the frame and sensor are small compared to the specimen and are completely linear. Therefore they have only a minor influence on the results and can be neglected.

w/c-ratio 0.60

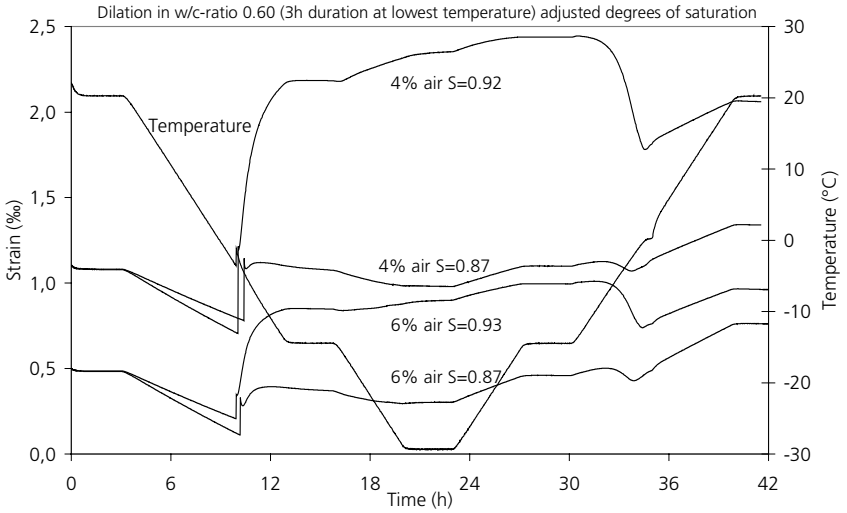

Figure A6.7. Length-change and temperature versus time for samples with w/c-ratio 0.60, and air content 4 and 6%, adjusted to different degrees of saturation, and exposed to two temperature levels.

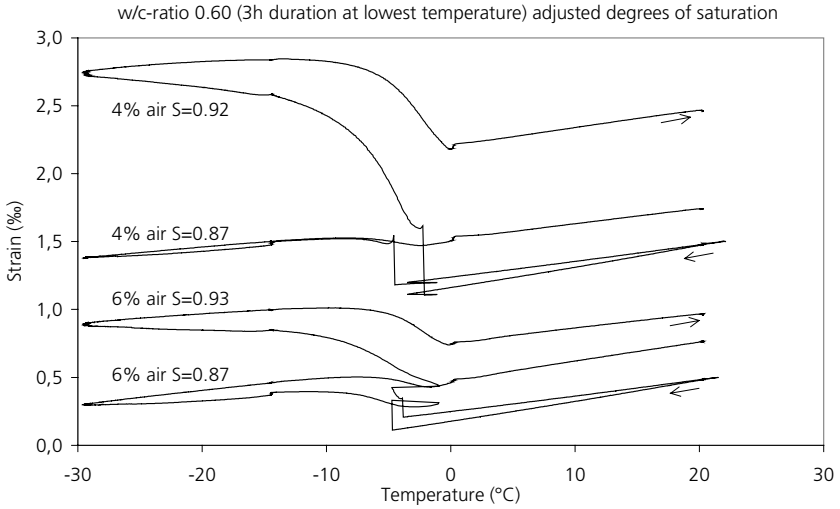

Figure A6.8. Length-change and temperature versus time for samples with w/c-ratio 0.60, and air content 4 and 6%, adjusted to different degrees of saturation, and exposed to two temperature levels.

w/c-ratio 0.45

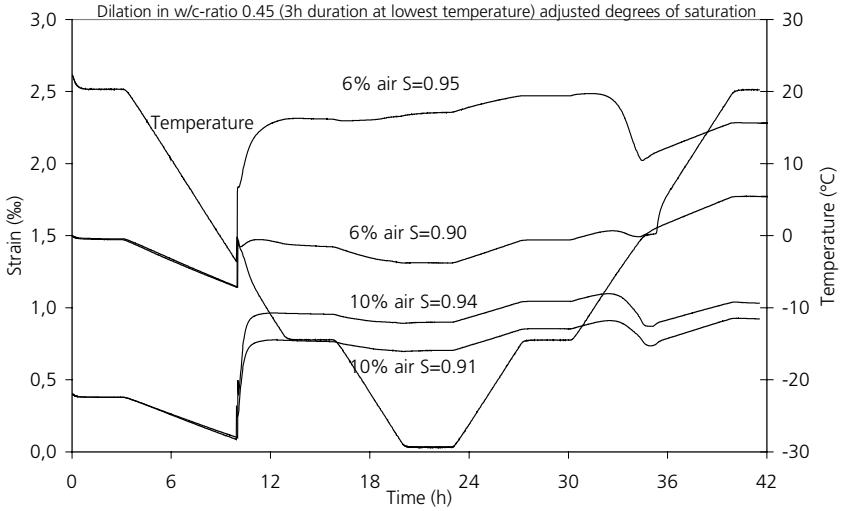

Figure A6.9. Length-change and temperature versus time for samples with w/c-ratio 0.45, and air content 6 and 10%, adjusted to different degrees of saturation, and exposed to two temperature levels.

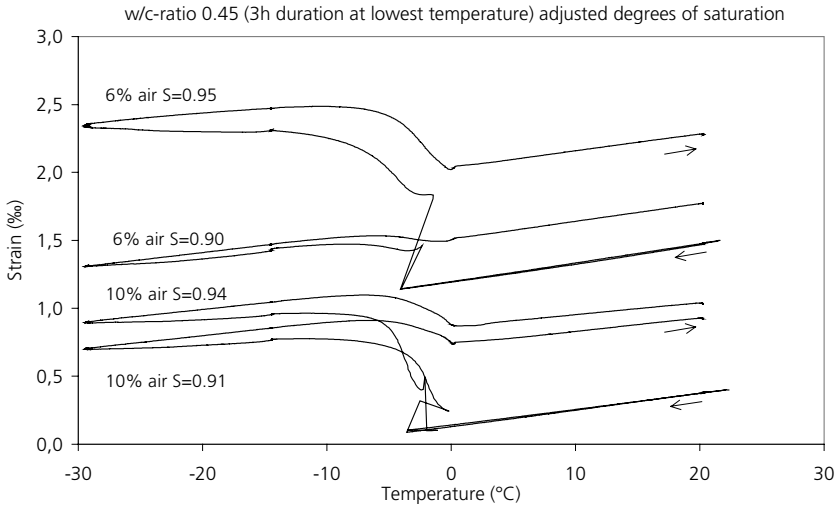

Figure A6.10. Length-change and temperature versus time for samples with w/c-ratio 0.45, and air content 6 and 10%, adjusted to different degrees of saturation, and exposed to two temperature levels.

w/c-ratio 0.40

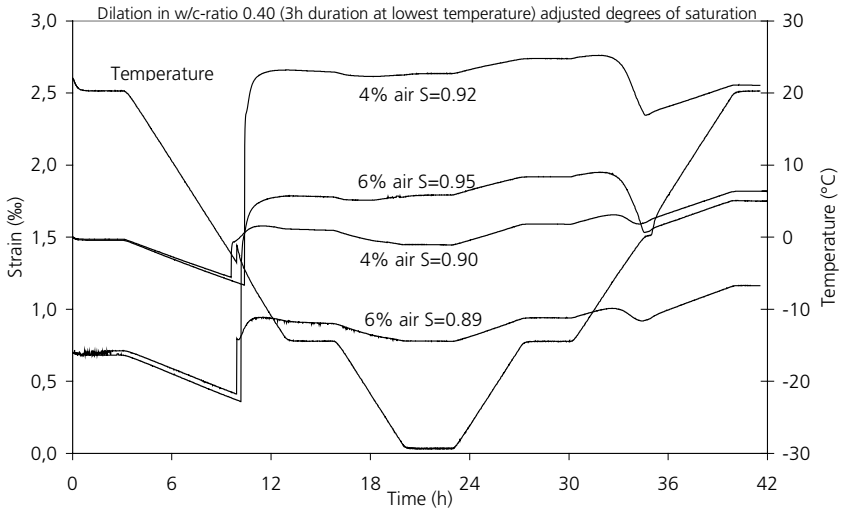

Figure A6.11. Length-change and temperature versus time for samples with w/c-ratio 0.40, and air content 4 and 6%, adjusted to different degrees of saturation, and exposed to two temperature levels.

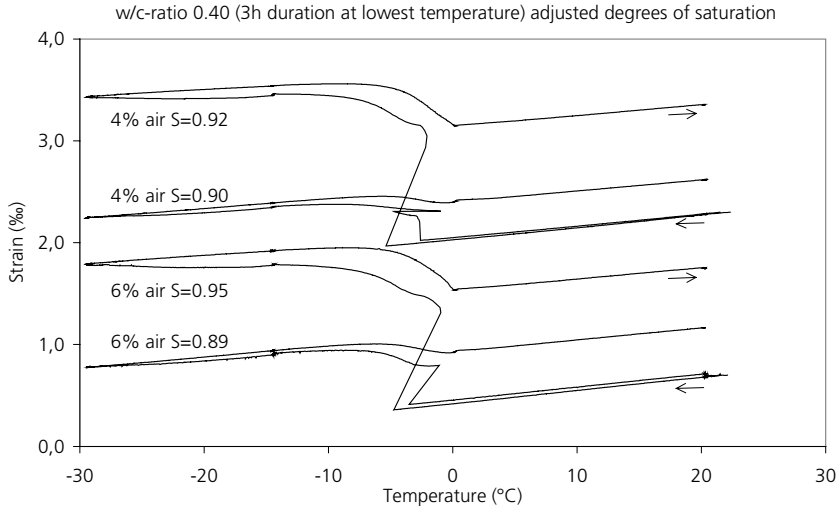

Figure A6.12. Length-change and temperature versus time for samples with w/c-ratio 0.40, and air content 4 and 6%, adjusted to different degrees of saturation, and exposed to two temperature levels.

APPENDIX to Chapter 7

A7.1 Test series 6 - Never-dried specimens with ‘natural’ water content

Contents

Table A7.1: Damage parameters for all experiments in Test series 6

		dϕ/dt=3.6°C/h		12h duration of constant temperature				
w/c-ratio	Air content (%)	S_A/S_B	u (%)	RF^2	Perm.dilation (‰)	Dil at sc (‰)	Dil at -15°C (‰)	Dil at -30°C (‰)
0.60	Natural	1/-	8.10	0.69	0.35	0.21	0.38/0.36	0.87/0.90
0.60	Natural	1/-	8.26	0.69	0.35	0.23	0.38/0.35	0.81/0.85
0.60	4	0.85/-	8.23	0.76	0.10	0.04	-0.05/-0.06	0.02/0
0.60	4	-/-	8.70	0.96	0.048	0.02	-0.07/-0.08	-0.02/-0.04
0.60	6	0.85/-	8.46	0.90	0.02	0.02	-0.09/-0.09	-0.12/0.12
0.60	6	0.88/-	8.81	0.90	0.01	0.03	-0.08/-0.081	-0.10/-0.10
0.40	Natural	0.86/-	8.03	0.77	0.34	0.08	0.37/0.35	0.63/0.67
0.40	Natural	0.84/-	8.18	0.77	0.32	0.08	0.31/0.29	0.59/0.62
0.40	4	0.98/-	8.33	0.85	0.05	0.04	0.07/0.02	0.01/-0.01
0.40	4	0.92/-	8.91	0.92	0.05	0.09	0.09/0.04	0.02/0.01
0.40	6	0.94/-	8.92	0.98	0.07	0.01	0.02/-0.02	-0.05/-0.06
0.40	6	0.93/-	9.19	0.88	0.08	0.02	0.06/0.03	0.01/-0.01
0.45	Natural	0.91/-	8.80	0.77	0.42	0.03	0.37/0.34	0.78/0.84
0.45	Natural	0.91/-	8.71	0.74	0.35	0.03	0.33/0.31	0.70/0.75
0.45	6	0.94/-	8.70	0.98	0.05	0.212	-0.05/-0.06	-0.09/-0.09
0.45	6	0.93/-	9.13	0.90	0.05	0.02	-0.02/-0.03	-0.07/-0.07
0.45	10	0.85/-	9.49	0.96	0.05	0.01	-0.05/-0.06	-0.106/-0.106
0.45	10	0.81/-	9.20	0.86	0.05	0.02	-0.05/-0.05	-0.09/-0.09
0.45	4	0.91/-	8.44	0.88	0.08	0.02	0.07/0.02	0.07/0.04
0.45	4	-/-	8.15	0.94	0.12	0.03	0.11/0.05	0.12/0.07

S_A and S_B are degrees of saturation, see Equations (4.5.3) and (4.5.5). u is the moisture ratio, see Equation (4.5.2). Dil. at -15°C and -30°C give the strain levels at the beginning and the end of the isothermal periods. Perm. dilation is the permanent dilation, see Figure 4.4.4. RF^2 is the relative resonance frequency after and before freeze/thaw squared. dil.at sc. is the dilation at supercooling, see Figure 4.4.4.

Figures A7.1-A7.6: Length change diagrams. Test series 6

Each curve represents a single specimen. All samples of the same concrete type, have the same starting point in the figures (not necessarily at zero ‰ strain). The starting points of the various curves have been so placed as to allow all specimen of the same w/c-ratio to be shown in the same figure. Specimens with the lowest air content have the highest starting point, and specimens with the highest air content the lowest starting point. The surface temperature versus time for of one of the samples is also shown. The curves represent the total response of the specimens, including the measuring frame and the sensor. The thermal movements of the frame and sensor are small compared to the specimen and are completely linear. Therefore they have only a minor influence on the results and can be neglected.

w/c-ratio 0.60

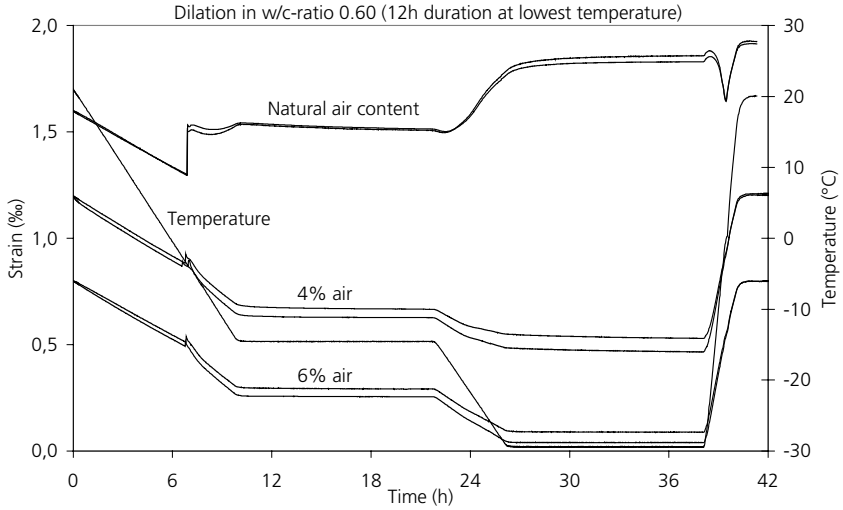

Figure A7.1. Length change and temperature versus time for samples with w/c-ratio 0.60.

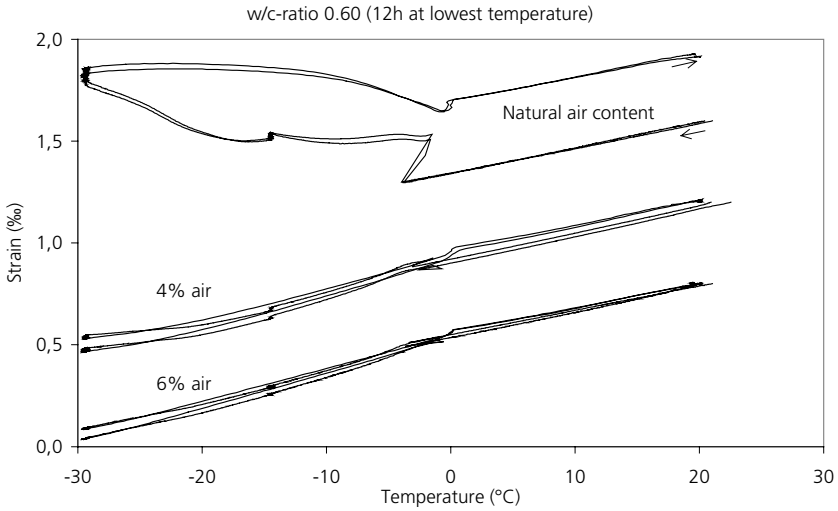

Figure A7.2. Length change versus temperature for samples with w/c-ratio 0.60.

w/c-ratio 0.45

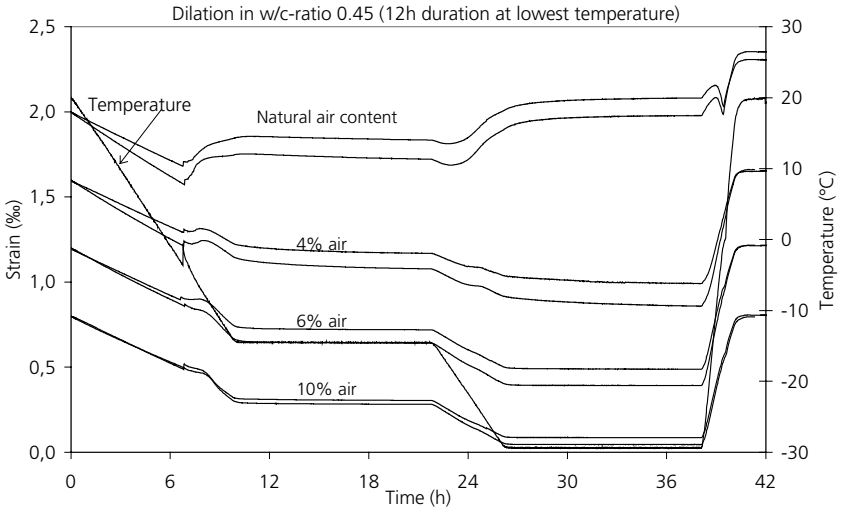

Figure A7.3. Length change and temperature versus time for samples with w/c-ratio 0.45.

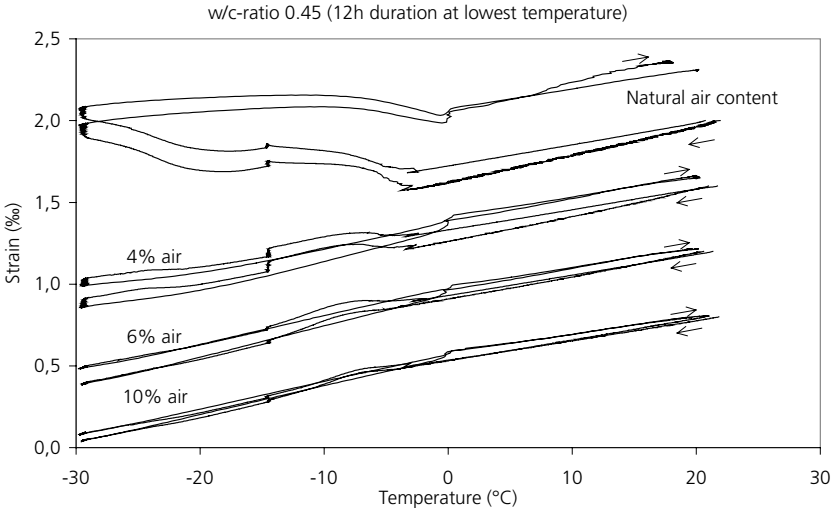

Figure A7.4. Length change versus temperature for samples with w/c-ratio 0.45.

w/c-ratio 0.40

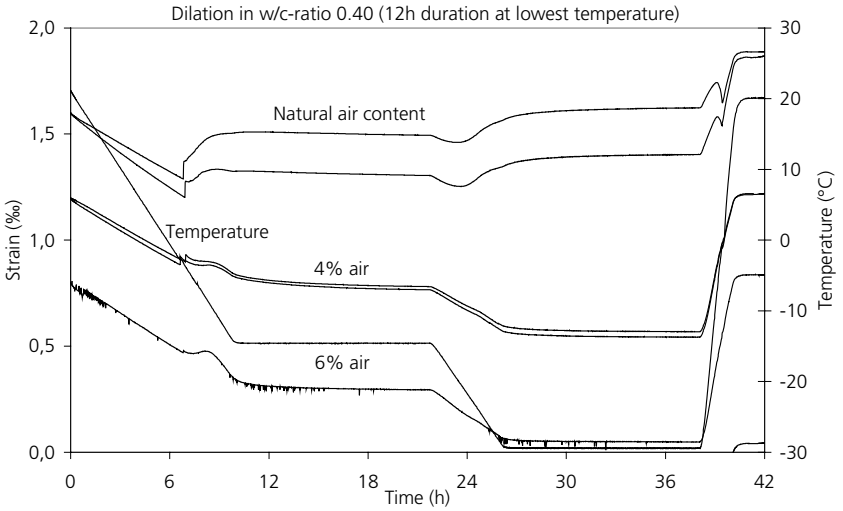

Figure A7.5. Length change and temperature versus time for samples with w/c-ratio 0.40.

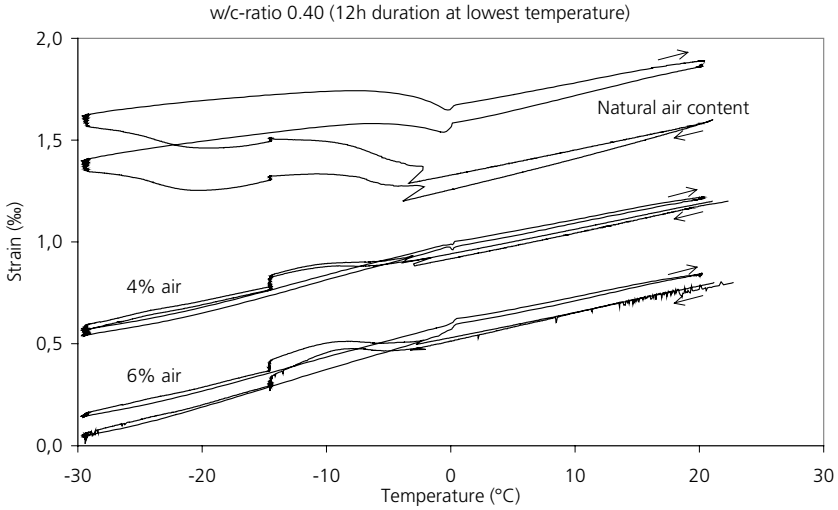

Figure A7.6. Length change versus temperature for samples with w/c-ratio 0.40.

A7.2 Test series 7 - Pre-dried, re-saturated samples with adjusted degree of saturation

Contents

Table A7.2: Damage parameters for all experiments in Test series 7

		dϕ/dt=3.6°C/h			12h duration of constant temperature			
w/c-ratio	Air content (%)	S_A/S_B	u (%)	RF²	Perm. dilation (‰)	Dil at sc (‰)	Dil at -15°C (‰)	Dil at -30°C (‰)
0.60	4	-/0.93	8.81	0.55	0.66	0.50	0.97/0.94	1.26/1.29
0.60	4	-/0.88	8.58	0.72	0.32	0.35	0.50/0.45	0.61/0.61
0.60	6	-/0.86	8.68	0.81	0.24	0.34	0.34/0.30	0.43/0.42
0.60	6	-/0.93	9.75	0.60	0.62	0.17	0.96/0.94	1.22/1.24
0.40	4	-/0.87	7.76	0.96	0.07	0.04	0.04/0.01	0.01/-0.01
0.40	4	-/0.92	8.24	0.71	0.27	0.07	0.39/0.36	0.41/0.38
0.40	6	-/0.86	8.49	0.84	0.22	0.20	0.28/0.24	0.27/0.25
0.40	6	-/0.93	9.27	0.79	0.35	0.13	0.49/0.45	0.48/0.46
0.45	4	-/0.94	9.01	0.82	0.37	0.20	0.53/0.48	0.70/0.70
0.45	4	-/0.85	8.46	1	0.08	0.03	-0.05/-0.06	-0.07/-0.09
0.45	10	-/0.84	10.11	0.97	0.11	0.08	0.05/0.03	0.02/0.01
0.45	10	-/0.92	11.22	0.91	0.26	0.18	0.27/0.24	0.26/0.25
0.45	6	-/0.86	7.84	0.98	0.18	0.08	0.12/0.08	0.14/0.12
0.45	6	-/0.92	8.10	0.67	0.54	0.17	0.77/0.74	0.92/0.91

S_A and S_B are degrees of saturation, see Equations (4.5.3) and (4.5.5). u is the moisture ratio, see Equation (4.5.2). Dil. at -15°C and -30°C give the strain levels at the beginning and the end of the isothermal periods. Perm. dilation is the permanent dilation, see Figure 4.4.4. RF² is the relative resonance frequency after and before freeze/thaw squared. dil.at sc.is the dilation at supercooling, see Figure 4.4.4.

Figures A7.7-A7.12: Length change diagrams. Test series 7

Each curve represents a single specimen. All samples of the same concrete type, have the same starting point in the figures (not necessarily at zero ‰ strain). The starting points of the various curves have been so placed as to allow all specimen of the same w/c-ratio to be shown in the same figure. Specimens with the lowest air content have the highest starting point, and specimens with the highest air content the lowest starting point. The surface temperature versus time for of one of the samples is also shown. The curves represent the total response of the specimens, including the measuring frame and the sensor. The thermal movements of the frame and sensor are small compared to the specimen and are completely linear. Therefore they have only a minor influence on the results and can be neglected.

w/c-ratio 0.60

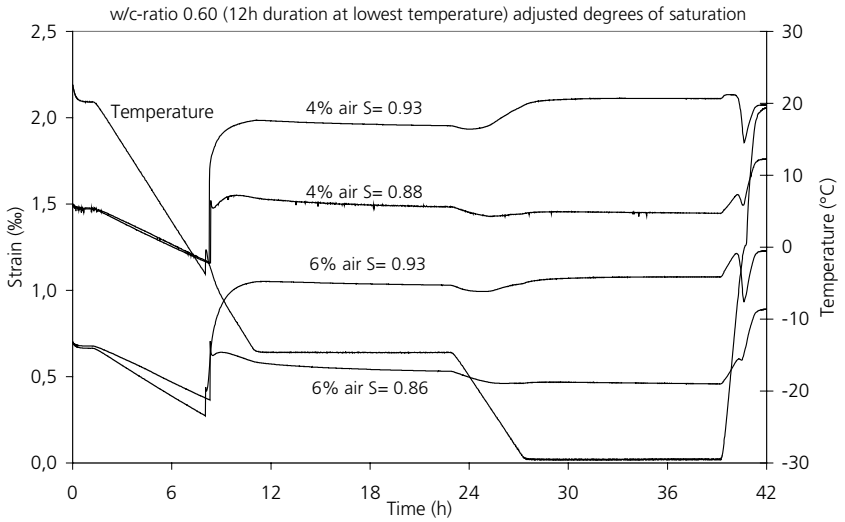

Figure A7.7. Length change and temperature versus time for samples with w/c-ratio 0.60, containing 4% or 6% air, prepared to different degrees of saturation.

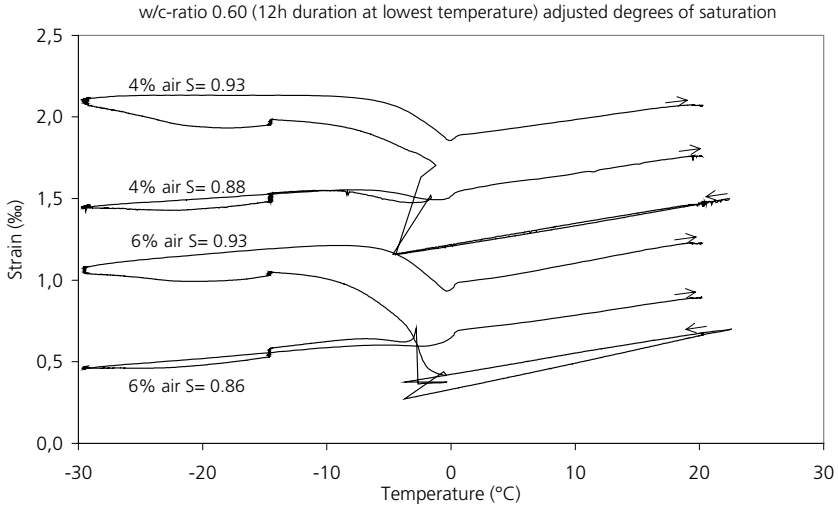

Figure A7.8. Length change versus temperature for samples with w/c-ratio 0.60, containing 4% or 6% air, prepared to different degrees of saturation.

w/c-ratio 0.45

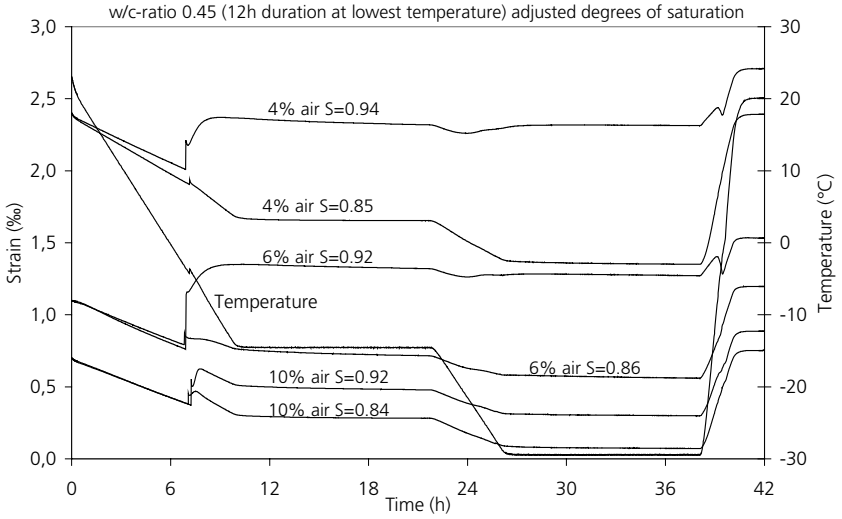

Figure A7.9. Length change and temperature versus time for samples with w/c-ratio 0.45, containing 4% or 6% air, prepared to different degrees of saturation.

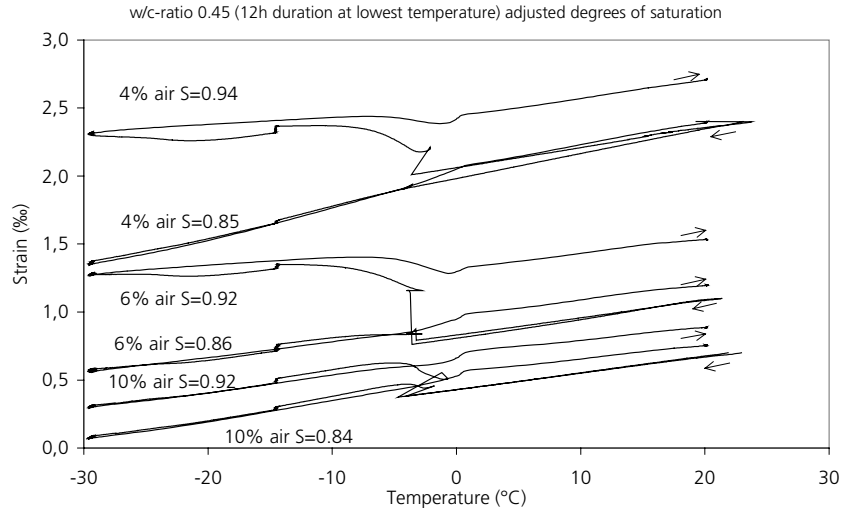

Figure A7.10. Length change versus temperature for samples with w/c-ratio 0.45, containing 4% or 6% air, prepared to different degrees of saturation.

w/c-ratio 0.40

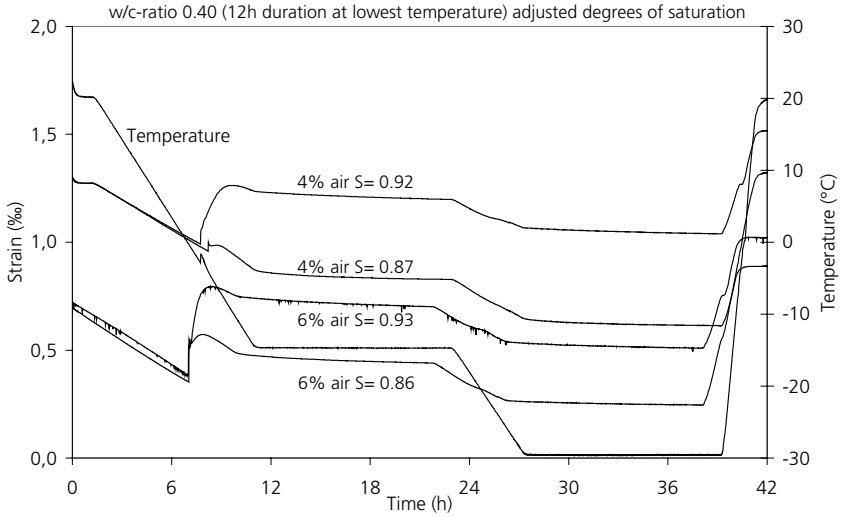

Figure A7.11. Length change and temperature versus time for samples with w/c-ratio 0.40, containing 4% or 6% air, prepared to different degrees of saturation.

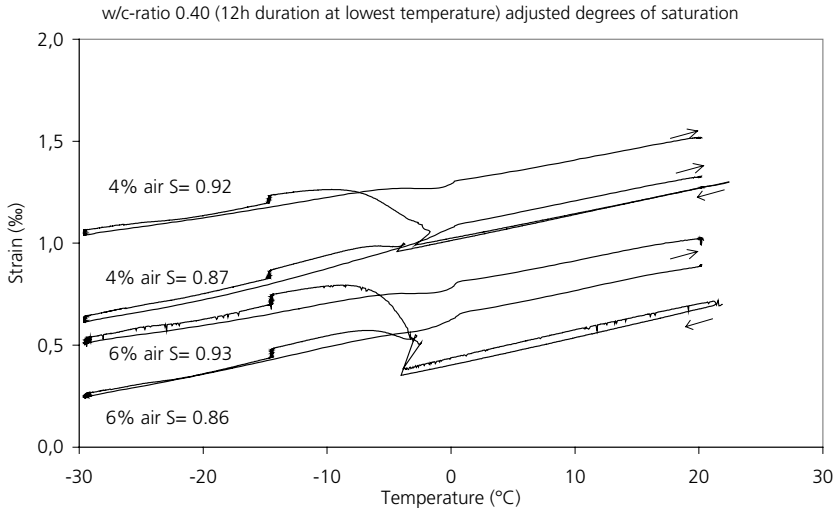

Figure A7.12. Length change versus temperature for samples with w/c-ratio 0.40, containing 4% or 6% air, prepared to different degrees of saturation.

APPENDIX to Chapter 11

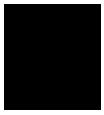

A11.1 Mix proportions. Properties of the fresh concrete. Concrete strength. Chapter 11

Casting period: spring 2001

Specimens: 1 block, 400x400x150 mm, 3 cubes, 150 mm

The mix proportions, the density of the fresh concrete, the air content of the fresh concrete, and the 28-day cube strength are listed in Table A11.1.

Table A11.1: Mix composition. Properties of the fresh concrete. 28-days compressive strength

w/c	Nominal air content (%)	Cement (kg/m^3)	Water (kg/m^3)	Sand 0-3 mm (kg/m^3)	Gravel 4-8 mm (kg/m^3)	AEA [1] (kg/m^3)	Fresh air content (%)	Density of fresh concrete (kg/m^3)	Cube strength (MPa)	Slump (mm)
0.40	non-AE	525	215	816	816	0	2.45	2383	73.3	10
	4	525	215	763	763	1.2	4.9	2303	67.4	35
	6	525	215	736	763	1.7	6.4	2263	62.7	65
0.6	non-AE	350	210	897	897	0	1.9	2377	44.2	20
	4	350	210	844	844	0.56	5.0	2299	39.2	35
	6	350	210	817	817	1.5	6.7	2228	31.4	120

[1] Neutralized Vinsol Resin 10% strength. Water in the admixture is not included in the w/c-ratio.

A combined temperature scanning calorimeter and dilatometer for studies of freeze/thaw effects in porous materials

Katja Fridh
MSc.
Building Materials, Lund Institute of Technology
Box 118, 221 00 Lund
E-mail: katja.fridh@byggtek.lth.se

Sture Lindmark[1]
Dr.
Building Materials, Lund Institute of Technology
Box 118, 221 00 Lund

Lars Wadsö
Dr.
Building Materials, Lund Institute of Technology
Box 118, 221 00 Lund
E-mail: lars.wadso@byggtek.lth.se

ABSTRACT

In this paper we present a new combined temperature scanning calorimeter and dilatometer for the study of frost damage in relatively large samples (length 150 mm, diameter 40 mm) of cement-based materials. The two measuring techniques have been calibrated and tested both separately and combined. Measurements performed for testing the equipment show a satisfactory accuracy. The equipment is suitable for studies of frost deterioration mechanisms.

Key words: temperature scanning calorimeter, dilatometer, calibration, mortar, concrete.

1. INTRODUCTION

Frost damage of concrete and other porous materials is a major problem in outdoor structures, e.g. facades, bridges, dams and roads. Frost damage occurs both as surface scaling in which layers of the material are gradually scaled off from the material, and as internal deterioration in which ice formation creates hydraulic pressure and ice pressure on pore walls inside porous materials.

In the field of salt frost scaling substantial research was done in the 1980's and 1990's. Much of the research was performed within the RILEM TC 117 FDC 'Freeze Thaw and

[1] Presently at Icopal AB, Box 848, 201 80 Malmö, Sweden. E-mail: sture.lindmark@icopal.se.

De-icing Salt Resistance'. Recently, damage hypotheses of surface scaling were presented by Lindmark [1] and by Jepsen [2], both hypotheses were based on the theory of ice lens growth [3]. Jacobsen [4] performed extensive experimental research on ordinary Portland cement concretes and on concrete containing silica fume. Kaufmann [5] made extensive studies on the basis of which a qualitative discussion of destruction mechanisms was made. Rønning [6] carried out a large investigation about moisture uptake during freeze/thaw experiments and on the connection between laboratory testing and field exposure. A theoretical analysis of this water uptake process has been reported by Setzer [7].

The deterioration mechanisms responsible for surface and internal attack are fundamentally the same: water is transformed into ice, a process causing stresses in the material, as a consequence of which micro-cracking and reduced strength can occur [8]. The materials ability to accommodate the ice, to transport excess water and to hold unfrozen water decides how well it will perform during sub-zero temperatures. A major factor for frost damage is of course the water content in the material [9].

The mechanisms behind frost damage are complex, and the most important influencing factors can be divided into two groups, external and internal factors. The external factors are the freeze-thaw cycle (lowest temperature, duration, freezing rate) and the outer salt concentration. Among the internal factors the most important are pore size distribution, permeability and degree of saturation.

To explain the mechanism of internal frost attack several measuring equipments have been developed, many of them for the study of dilation (length changes) e.g. Valore [10]. Powers and Helmuth [3] formulated the theory of ice lens growth that not only explained observed phenomena but also provided the theory on which the salt frost scaling deterioration process by Lindmark [1] is based. Large investigations regarding length-change during freezing and thawing have also been carried out by Fagerlund [9] and Vourinen [11].

The study of ice-formation and melting using sensitive differential temperature scanning calorimeters was first carried out by Bager and Sellevold [12,13,14]. Their work was followed by studies of Fontenay [15], Matala [16], Kaufmann [5] and others.

As internal frost damage is caused by the phase transition of water to ice and possibly also ice to water, the combination of dilation and ice formation/melting (calorimetry) measurements is a very powerful way to investigate frost damage mechanisms. Verbeck and Klieger [17] presented the first equipment of this kind in 1958. Fagerlund [18] presented his combined measurement equipment in 1973. Penttala [19,20] placed strain gauges on samples tested in a temperature scanning calorimeter manufactured by Setaram.

In this paper the design of a new equipment for simultaneous measurements of ice formation/melting and expansion/contraction will be presented together with some test results. The calorimeter gives information on how much ice that forms (and at which temperature) in a concrete with a certain degree of saturation. The dilatometer gives information on to what extent this ice formation effects the material and how large

damage it causes. This is very important information for the modelling of the relation between ice formation and loss of strength.

A problem with using the available temperature scanning calorimeters is the small specimen sizes (typically d=14 mm, l=60mm). Our instrument can handle specimens with a diameter of 40 mm and a length of 150 mm. This makes it possible to study concrete samples. The preparation of the specimens is also uncomplicated and rapid which is important with regards to minimizing the moisture loss.

The equipment will be used to study the effect of different freezing rates, lowest temperatures, durations and degrees of saturation on the internal frost resistance of micro-concrete. The objective with this work is to explain the mechanisms behind internal frost deterioration.

2. INSTRUMENT

The instrument is a combination of a temperature scanning calorimeter of the heat-conduction type and a LVDT (Linear Variable Differential Transducer) dilatometer. It simultaneously measures heat production/consumption during freezing and thawing and the associated length changes. Figures 1 and 2 show cross sections of the instrument.

The heat-flow is measured with eight thermo-couple plates (CP 1-127-08, Melcor, Trenton NJ, USA) surrounding the aluminium vessel holder (a total of 1016 semi-conductor thermo-couples). The sample (height 150 mm, diameter 40 mm) is placed in a cylindrical Invar vessel that is placed in the vessel holder (Fig. 2). Invar, a metal alloy containing 36% Ni and 64% Fe, has a low coefficient of thermal expansivity ($2 \cdot 10^{-6}$ 1/K). The sample is placed between a cylindrical stud (diameter 2 mm) on the bottom and the LVDT dilatometer (see section 3.1) at the top.

The instrument is a twin calorimeter with a reference sample placed in an identical calorimeter (Fig. 1). The reference should have approximately the same thermal properties as the sample, but not show any phase transitions in the temperature region of the measurement. The sample and the reference calorimeters are connected differentially so that disturbances that enter both calorimeters will be compensated for.

Each calorimeter has two aluminium heat sinks and the whole instrument is housed in a box made of 2 mm aluminium. Most empty volumes in the instrument are filled with insulation of extruded polystyrene.

The instrument is placed in a programmable low-temperature freezer with an internal fan (305/80-180 DU, Weiss Umwelttechnik GMBH, Lindenstruth, Germany). It is the temperature surrounding the calorimeter that controls its temperature. Normally the temperature is scanned quite slowly, e.g. 3 K/h.

The LVDT dilatometers are fastened in the lids of the Invar vessels (Fig. 2). Temperature is measured at five points inside the calorimeter with thermo-couples type

K. The points are; sample, vessel holder, sample heat sink, reference vessel holder, and reference heat sink (the locations are shown in Fig. 2).

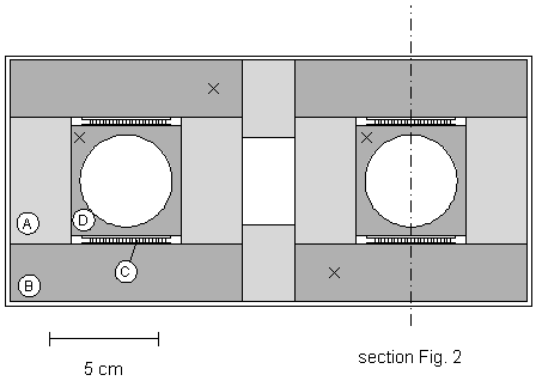

Figure 1 - Schematic drawing of instrument (horizontal cross section). (A) Insulation, (B) Heat sink, (C) Heat flow sensor, (D) Vessel holder. The sample is placed in the left vessel holder and a reference sample is placed in the right vessel holder. The x:s indicates the positions of the thermocouples for temperature measurement. The empty space in the center of the calorimeter houses the electrical wiring.

3. CALIBRATION

3.1 Measurements of length changes

The LVDT dilatometer (GTX2500, RDP Electrosense Inc., Pottstown PA, USA) has a linear stroke of ±2.5 mm and a stated repeatability of 0.15 μm. It is placed on top of the sample in the calorimeter (Fig. 2). The output from the dilatometer, a length L (mm), can for the present set-up be written as a function of the reference length L (mm) and thermal expansivity α (1/K) of a sample (subindex 1) and the sample holder (subindex 2):

$$\frac{dL}{dT} = L_1\alpha_1(T) - L_2\alpha_2(T) + K(T) \qquad \text{(Eq. 1)}$$

Here, K (mm/K) is the thermal expansion of the dilatometer itself. Note that α_1, α_2 and K are functions of the temperature. The expansion properties of the sample holder and the dilatometer are not well known, and are therefore grouped together as one calibration parameter β (mm/K). Thus, Eq. 1 can be rewritten as:

$$\frac{dL}{dT} = L_1\alpha_1(T) + \beta(T) \qquad \text{(Eq. 2)}$$

To calibrate the equipment, a measurement with a sample with known L_1 and α_1 is made and $\beta(T)$ is calculated. This β is then used to calculate $\alpha_1(T)$ of a sample after a measurement:

$$\alpha_1(T) = \frac{dL/dT - \beta(T)}{L_1} \qquad \text{(Eq. 3)}$$

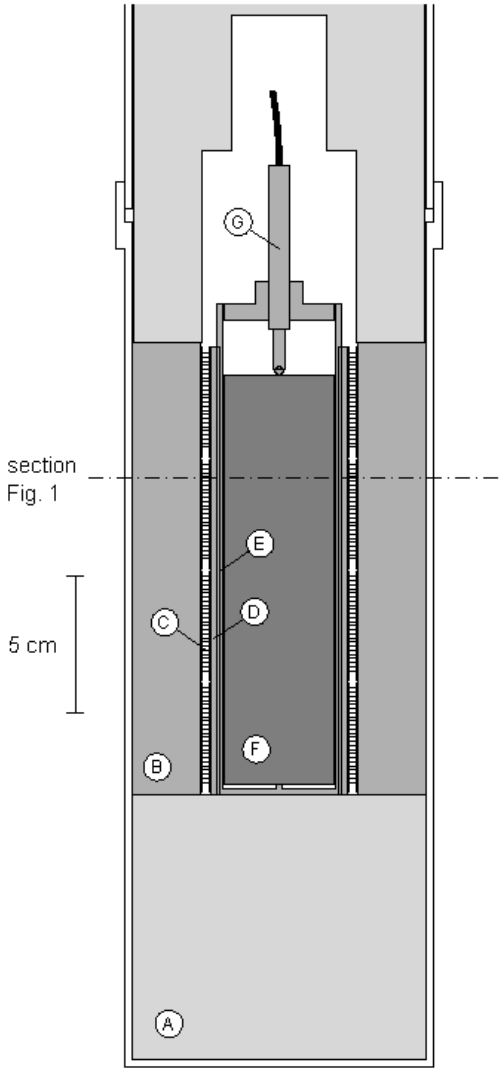

Figure 2 - Schematic drawing of instrument (vertical cross section). (A) Insulation, (B) Heat sink, (C) Heat flow sensor, (D) Vessel holder, (E) Vessel, (F) Sample, (G) LVDT Dilatometer. The top part of the calorimeter (with insulation) is not shown.

The dilatometer was calibrated with a 152 mm borosilicate glass square rod (Standard Reference Material 731L3, NIST, Gaithersburg MD, USA) using the thermal expansivity provided by NIST as a third order equation in the temperature range -173 - +20°C. In the calibration, β was found to be rather constant in the temperature range –60°C-+20°C, with a value of $3.4 \cdot 10^{-4}$ mm/K.

3.2 Heat flow

The calibration of the calorimeter was made electrically while the calorimeter was kept at three temperatures, +21°C, -18.3°C and –57.5°C. At each temperature a heat pulse was made and the resulting output signal was observed. For the calibration, we used a precision resistor of 100.0±0.1 Ω centrally placed in a sample made from polyoxymethylene (POM) polymer that has similar thermal properties as cement mortar. The resistance of the heater did not change by more than 0.04 Ω when the temperature changed from +20°C to -60°C.

The heat Q (J) released in each calibration pulse is:

$$Q = I^2 R \Delta t \qquad \text{(Eq. 4)}$$

Here, I (A) is the current through the heater, R (Ω) is the resistance of the heater, and Δt (s) is the duration of each pulse. The corresponding output from the calorimeter is the integral in units of (Vs) of the signal U (V) from the heat flow sensors. The calibration coefficient ε (W/V), used to convert the signal from the calorimeter to heat flow, is the ratio of Q and the integral of the signal from the heat flow sensors:

$$\varepsilon = \frac{Q}{\int U dt} \qquad \text{(Eq. 5)}$$

Figure 3 shows the result of the calibration of the calorimeter. Note that the calibration coefficient is temperature dependent.

4. TEST MEASUREMENTS

To test the length-change equipment a test measurement was performed on a bar of aluminium alloy with a diameter of 40 mm and a length of 145 mm (unknown type of alloy). The coefficient of thermal expansion directly obtained by the dilatometer is seen in Fig. 4 as a thin line. This signal was then adjusted with β and the thick line was obtained. This calculated coefficient of thermal expansion is somewhat higher than handbook values for pure aluminium. However, freeze/thaw dilations are substantially larger than those of aluminium and will be easy to detect (cf. Fig. 6).

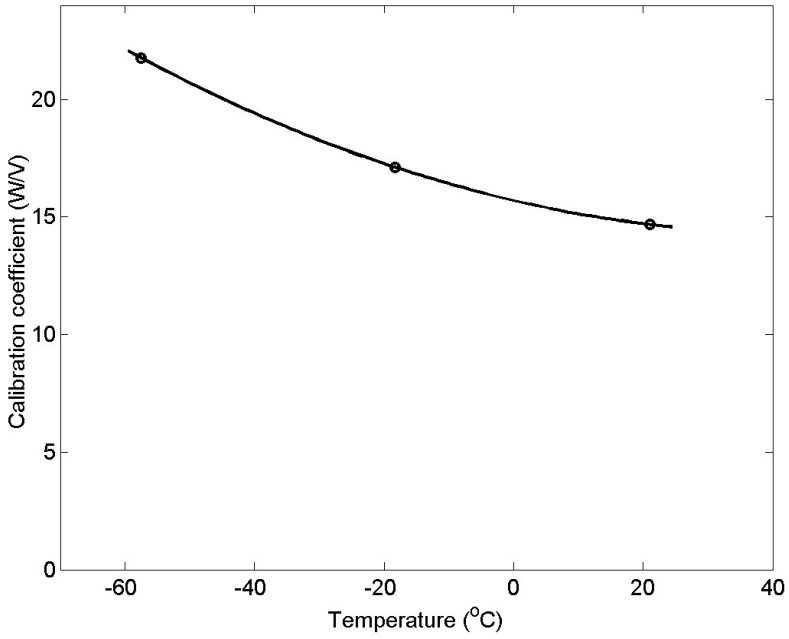

Figure 3 - Result of calibration of the calorimeter.

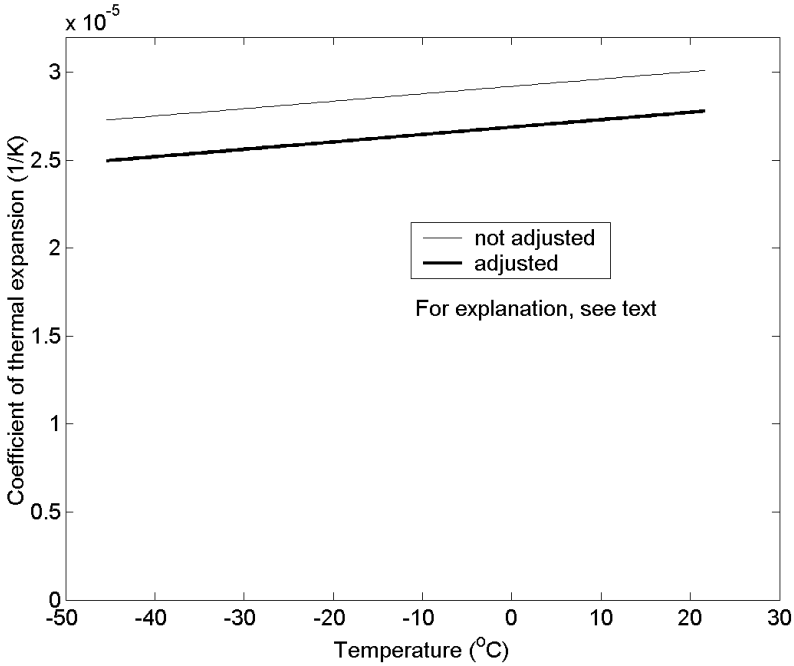

Figure 4 - Coefficient of thermal expansion at test measurement on a rod of aluminium alloy. Comparison between direct measured value and value corrected for the thermal expansivity of the equipment.

A measurement with a sample of 10.82 g of water placed in a plastic vessel was also made. The result is shown in Fig. 5. It is seen that the shape of the freezing peak is different from the shape of the melting peak. This test experiment is further discussed in the next section of the paper.

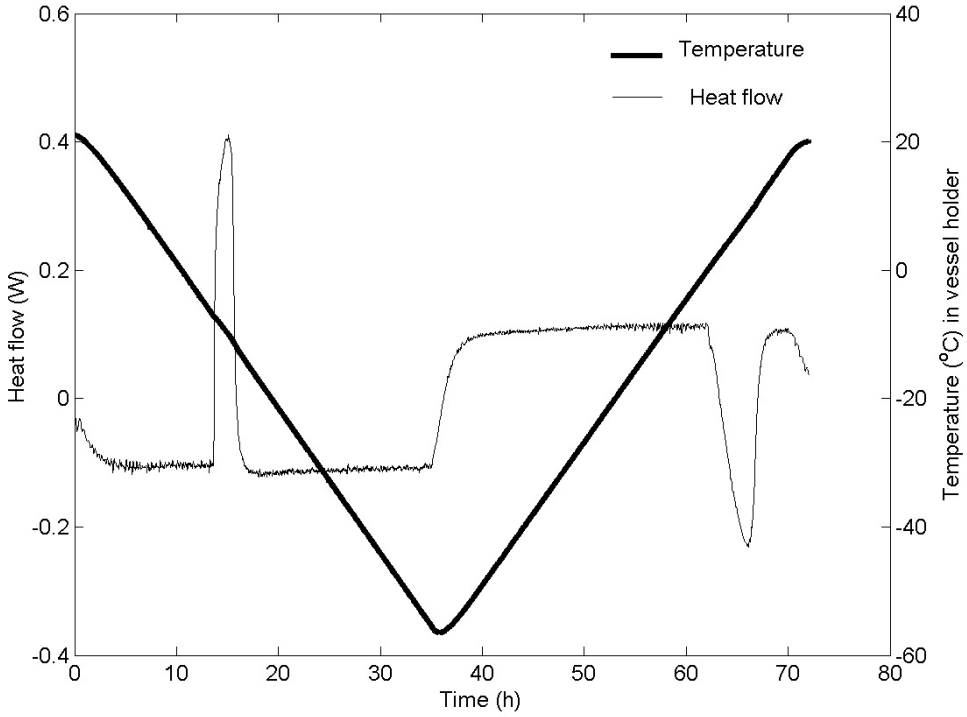

Figure 5 - Test measurement on 10.82 g of water: heat flow and temperature in vessel holder.

The equipment was made for the study of ice formation and length-change in cement-based materials. A first result of this type of measurement is presented in Fig. 6. A cylinder of micro-concrete, w/c-ratio 0.45 with an air content of 6% was dried at +105°C and thereafter vacuum saturated with water. A hole for the thermocouple had been made so the temperature could be measured in the center of the specimen. Before the start of the measurement the sample was wrapped in plastic foil to keep the moisture inside the specimen. There is no way to stop the water from moving from the inside of the specimen to the surface during freezing, but the plastic foil makes sure that most of the water goes back into the sample again during thawing. A piece of glass was glued on the top of the specimen to ensure free movement of the LVDT dilatometer. The sample was placed in the calorimeter and tested during a freeze-thaw cycle from +20°C to –70°C with a temperature scanning rate of 4.2 K/h and an isothermal period of seven hours at the lowest temperature.

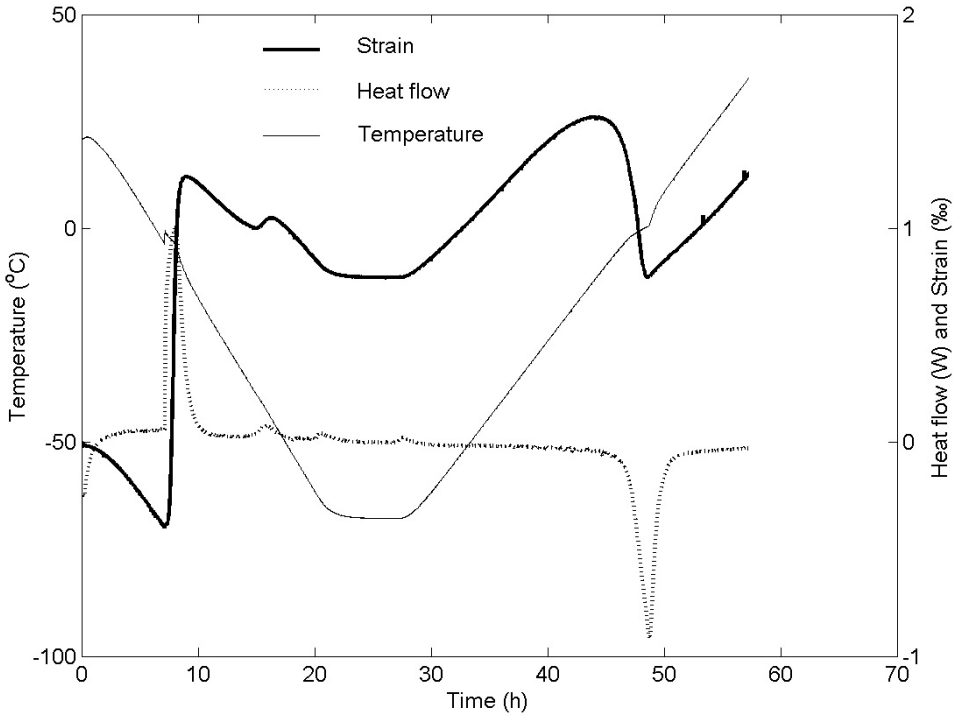

Figure 6 - Test measurement on micro-concrete. The temperature was measured in the center of the sample.

The length measurement shows that during the first large ice formation occurring at –4°C a large expansion takes place simultaneously with the large heat flow (ice formation). The smaller second peak in the heat flow measurement results in a minor expansion. Just before and after the isothermal period at –70°C small variations in the heat flow can be seen, but they are artefacts of the temperature cycle and do not result in any expansion. A large expansion during temperature increase, probably caused by the difference in thermal expansivity between the micro-concrete and the ice, is seen before the large contraction that occurs when the ice melts at about 0°C. When the temperature in the sample returns to +20°C, a permanent length change of about 1% indicates that the sample has suffered internal damage.

Even if there is still work to do to increase the sensitivity and to improve the calibration coefficients it is already possible to study the different phenomena that occur during freezing and thawing of micro-concrete and their consequences.

5. COMPUTER SIMULATIONS

A thermal model of the calorimeter with heat capacities connected by thermal conductances was developed. It is a simple model that only includes the essential

factors to model the overall temperature development during a measurement. The sample is modelled as two (isothermal) heat capacities and the reference is modelled as one (Fig. 7). The heat capacities used in the model were calculated from the geometry, density and specific heat capacities of each part (Table 1).

The thermal conductances are more difficult to assess as they depend on thermal conductivities of the materials and their contact zones, air gap geometries, radiation, possible convective heat flow etc. For the present case initial parameters were calculated. Some of these were modified to get a better fit between simulation and measurement for the freezing peak (Table 2).

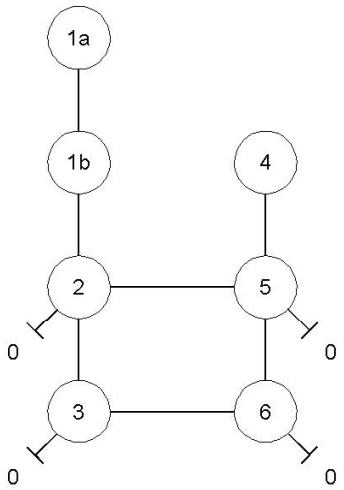

Figure 7 - The thermal model of the calorimeter. Each circle is a heat capacity (J/K) of a part of the calorimeter: sample and vessel (1a and 1b), vessel holder (2), sample side heat sink (3), reference and vessel (4), reference vessel holder (5) and reference side heat sink (6). The lines connecting the circles are thermal conductances (W/K). The short lines ending with a short perpendicular line are thermal conductances to the surrounding (0, the air of the freezer).

A simulation was made of the behaviour of the calorimeter during the measurement with 10.82 g water being cooled from +20°C to –60°C and back again. In the simulation the temperature at which water freezes was set to –7°C (the super-cooling freezing temperature observed during the measurement). The melting temperature was set to 0°C.

The simulation was made with forward differences in which at each time step the heat flow q_{ij} (W) between two heat capacities i and j are calculated with:

$$q_{ij} = k_{ij}(T_i - T_j) \qquad \text{(Eq. 6)}$$

Here, k_{ij} (W/K) is the thermal conductance between i and j. The temperature in heat capacity i is then updated with:

$$T_{i,new} = T_{i,old} + \frac{\Delta t}{C_i} \sum q \qquad \text{(Eq. 7)}$$

Here, Σq is the sum of all heat flows to heat capacity i, Δt (s) is the time-step in the simulation and C_i (J/K) is the heat capacity of i. In the present simulation a time step of 10 s was used and the ambient temperature was taken from the measurement file.

The freezing was modelled by checking if the temperature was below freezing temperature (-7°C) at the same time as 1a or 1b contained liquid water. If this was the case, an amount of water corresponding to the temperature decrease below the freezing temperature was frozen and the temperature was set back to the freezing temperature. The temperature thus stayed constant (at -7°C) during the freezing period. Melting was modelled in a similar way. The following data was use for the water: specific heat capacity (liquid): 4.18 J/g/K, specific heat capacity (ice): 2.2 J/g/K, and heat of fusion: 334 J/g.

As it has been difficult to theoretically calculate the thermal conductivities of the calorimeter (except for the conductivities of the thermo-couple plates) these were fitted to the experimental data in two steps. First the external conductances between air of freezer and heat sinks (0-3 and 0-6, cf. Fig. 7) were fitted so that the simulation results agreed with the temperature measured in the heat sinks. After that the internal conductances between the sample and the sample vessel holder (1a-1b and 1b-2) and between the reference and the reference vessel holder (4-5) were fitted to get a good agreement between the simulation results and the experimentally measured freezing peak.

Figure 8 shows the result of the simulation together with the result of the measurement. The double peaks in the simulation results are artefacts of that the sample is modelled in two parts. The outer part (1b) has to freeze first and stays at the freezing temperature until all water has frozen. It then takes some time before the freezing of the inner part (1a) takes place at the same rate. A similar phenomenon takes place during melting in the simulation.

It is seen that the whole process is modelled quite well by the simulation model, except the melting that is slower than the freezing, i.e. that melting cannot be modelled with the same simulation parameters as the freezing. Integration of the peaks gives:

- Freezing simulation: 3440 + 150 = 3590 J → 10.7 g water
- Freezing measurement: 3423 + 150 = 3573 J → 10.7 g water
- Melting simulation: 3540 J→ 10.6 g water
- Melting measurement: 3732 J→ 11.2 g water

Here the mass of water has been calculated with the heat of fusion at 0°C of 334 J/g, and the correction of 150 J for the freezing was calculated as:

$$(c_l - c_s)(T_m - T_f)m \qquad \text{(Eq. 8)}$$

Here c_l and c_s (J/g/K) are the specific heat capacities of liquid water and ice, T_m and T_f (K) are the temperatures of melting and freezing, and m (g) is the mass of water. This

corrects for that the freezing peak is smaller than the melting peak because heat has been used to supercool liquid water from T_m to T_f (from 0 to -7°C).

The use of a model such as this is mainly to increase the understanding of how the instrument works. It can for example be used to simulate the calorimeter output from a calibration pulse or a freezing process. More detailed descriptions of the sample, e.g. for a mortar sample, can be developed and used to test phase-change models. The model can also give information on which factors that we need to investigate more closely, e.g. in the present model all parameters seems physically relevant except the surprisingly low thermal conductivities between sample/reference and the sample/reference vessel holders. The fact that the present model accurately models freezing, but not thawing is an indication that the model cannot handle cases both with and without supercooling. Fitting the result to the equilibrium thawing instead of the non-equilibrium freezing (as was done in the present paper) will only give even lower thermal conductivities between sample/reference and the sample/reference vessel holder. The modelling of the freezing of supercooled water could probably also be improved. Here further investigations are needed.

Table 1 - Heat capacities C (J/K) used in the simulation model of the calorimeter. The figures have been calculated from the volumes and heat capacities of the different parts.

		C / J/K
1a	inner part of sample	75[1]
1b	outer part of sample and vessel	75[1]
2	sample vessel holder	450
3	sample side heat sink	2600
4	reference and vessel	320[2]
5	reference vessel holder	450
6	reference side heat sink	2600

1. For 10.82 g water used in experiment and simulation (no mortar sample).
2. For the plastic reference used during test measurement with 10.82 g water.

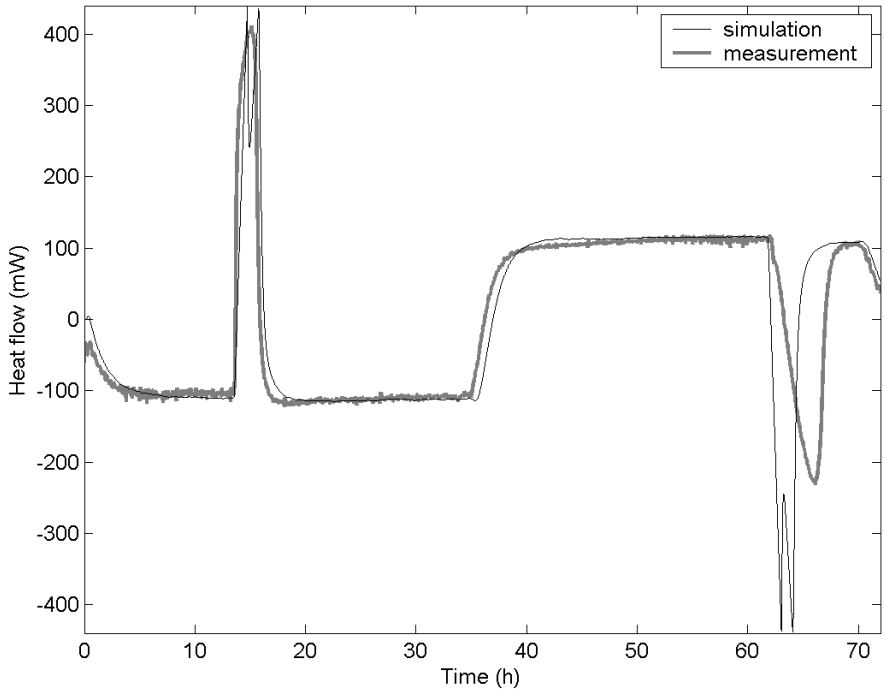

Figure 8 - Results from measurements with 10.82 g of water placed in a plastic container in the vessel. The double peaks seen in the simulation results are artefacts of the two-compartment model of the sample.

Table 2 - Thermal conductances k (W/K) used in the simulation model. The numbers refer to the different parts of the calorimeter (cf. Fig. 7). Most figures have been calculated from the thermal conductivity and geometry of the insulation (cf. table footnotes).

		k / W/K
1a-1b	in sample[1]	0.29
1b-2	sample and vessel to sample vessel holder[1]	0.29
2-3	heat flow sensors[2]	1.70
2-5	through insulation	0.005
3-6	through insulation	0.013
4-5	reference and vessel to reference vessel holder[3]	0.14
5-6	heat flow sensors[2]	1.70
0-2	through insulation	0.010
0-3	through boundary layer[4]	1.1
0-5	through insulation	0.010
0-6	through boundary layer[4]	1.1

1. Fitted parameter.
2. Calculated from data from manufacturer (Thermoelectric Handbook 2002 [21]).
3. Fitted parameter.
4. Calculated with an apparent heat transfer coefficient of 25 $W/m^2/K$ between the heat sinks and the air of the freezer.

As seen in Table 2 some conductances are much lower than the others (0-2, 0-5, 2-5, and 3-6) and can probably be set to zero in a future simulation model.

6. CONCLUSIONS

A combined scanning calorimeter and dilatometer has been developed. At this early stage it shows promising results and can be used to study different phenomena occurring during freezing and thawing of cement based materials and other porous materials. The advantages with this instrument are the relatively large sample size, the simultaneous measurement of heat flow and dilation, and the easy and fast preparation of the specimens. This paper also contains construction details and calibration data.

7. FUTURE WORK

The combined scanning calorimeter and dilatometer will be used for measurements on mortar and concrete samples. Comparison with earlier measurements will also be made but these may be difficult as different measurement techniques and sample sizes have been used.

The following factors could be further investigated to improve the equipment:

- Electrical calibrations and measurements on water to more accurately determine the calorimetric calibration coefficients.
- Further work to investigate the discrepancy in the dilation measurements (discussed in connection with Fig. 4).
- Further work to improve the thermal model of the calorimeter.

- Developing a thermal model for mortar samples with which we can test phase-change models.

REFERENCES

1. Lindmark, S., 'Mechanisms of salt frost scaling of Portland cement-bound materials: Studies and hypothesis', Doctoral thesis, Division of Building Materials, Lund Institute of Technology, 1998.

2. Jepsen Tange, M., 'Salt frost scaling – interaction of transport mechanisms and ice formation in concrete', Doctoral thesis, Building Technology, Danish Technological Institute and Aalborg University, 2002.

3. Powers, T.C and Helmuth, R.A., 'Theory of volume changes in hardened Portland-cement paste during freezing', Proceedings, Highway Research Board 32, Bull. 46 1953.

4. Jacobsen, S., 'Scaling and cracking in unsealed freeze/thaw testing of Portland cement and silica fume concretes', Doctoral thesis, Division of Structural Engineering, Concrete section, The Norwegian Institute of Technology, 1995.

5. Kaufmann, J., 'Experimental Identification of Damage Mechanisms in Cementitious Porous Materials on Phase Transition of Pore Solution under Frost De-Icing Salt Attack', École Polytechnique Fédéral de Lausanne, Thése No 2037, 1999.

6. Rønning, T., 'Freeze-thaw resistance of concrete, effect of: curing conditions moisture exchange and materials', Doctoral thesis, Department of Structural Engineering, Faculty of Civil and Environmental Engineering, Norwegian University of Science and Technology, Trondheim 2001.

7. Setzer, M.J., 'Development of the micro-ice-lens model', Frost Resistance of Concrete, Proceedings, Editors, Setzer, M.J., Auberg,R., Keck,H-J., Rilem Publications S.A.R.L, Canchan, 2002.

8. EU-project CONTECVET. Manual for assessing concrete structures affected by frost. Annex E: Effect of internal frost damage on mechanical properties of concrete, Div. of Building Materials, Lund Institute of Technology 2001.

9. Fagerlund, G., 'Critical degrees of saturation at freezing of porous and brittle materials', Doctoral thesis, Division of Building Material, Lund Institute of Technology, report 34, 1972.

10. Valore, R.C., 'Volume changes in small concrete cylinders during freezing and thawing', Journal of American Concrete Institute, vol 21, no 6, 1950.

11. Vourinen, J., 'On the behaviour of hardened concrete during freezing', The State Institute for Technical Research, Finland 1969.

12. Bager, D.H. and Sellevold, E.J., 'Ice Formation in Hardened Cement Paste, Part I – Room Temperature Cured Pastes With Variable Moisture Contents' Cement and Concrete Research, vol 16, pp. 709-720, 1986.

13. Bager, D.H. and Sellevold, E.J., 'Ice Formation in Hardened Cement Paste, Part II – Drying and Resaturation on Room Temperature Cured Pastes' Cement and Concrete Research, vol 16, pp. 835-844, 1986.

14. Bager, D.H. and Sellevold, E.J., 'Ice Formation in Hardened Cement Paste, Part III – Slow Resaturation of Room Temperature Cured Pastes' Cement and Concrete Research, vol 17, pp. 1-11, 1987.

15. Le Sage de Fontenay, C., 'Isdannelse i hærdnet Cementpasta', Building Materials Laboratory, Department of Civil Engineering, Technical University of Denmark, 1982.

16. Matala, S. 'Effects of carbonation on the pore structure of granulated blast furnace slag concrete', Concrete Technology, Faculty of Civil Engineering and Surveying, Helsinki University of Technology, 1995.

17. Verbeck, G. & Klieger,P, 'Calorimeter-Strain Apparatus for Study of Freezing and Thawing Concrete', Bulletin 176, Highway Research Board, Washington, 1958.

18. Fagerlund, G., 'Significance of critical degree of saturation at freezing of porous and brittle materials', ACI Symposium "Durability of concrete", Ottawa 1973, ACI Special publications, Detroit 1975.

19. Penttala, V., 'Freezing-Induced Strains and Pressures in Wet Porous Materials and Especially in Concrete Mortars', Advanced Cement based Materials, vol 7, nr 1, 1998, pp 8-19.

20. Penttala, V., 'Strains and Pressures Induced by Freezing Mortars Exposed in Sodium Chloride Solution', Concrete Science and Engineering, vol 1, pp 2-14, 1999

21. Thermoelectric Handbook 2002, www.melcor.com